THE FAILURE OF REINFORCED CONCRETE BEAMS AND SLABS SUBJECTED TO FIRE

by

Arastou Armaghani, M.Sc.

A thesis submitted for the Degree of

Doctor of Philosophy

in the Faculty of Engineering of the University

of London

Imperial College of Science and Technology

London

September 1976

ABSTRACT

Nonlinear behaviour of reinforced concrete beams and slabs are presented under high temperature using a layered finite element technique.

The equation of heat conduction is solved for two and three dimensional rectangular bodies under steady and non-steady state temperature with the use of a particular solution of the partial differential of the heat equation. This solution is then employed with the help of the Fourier's sine series to obtain the temperature equations within the beams and slabs for various practical surface temperatures. To save on computational time, the ensuing series in the temperature equations were reduced to a single term.

Two reinforced concrete beams were analysed under the service loads and then subjected to fire up to failure. The analytical results were in good agreements with the corresponding experimental data. The behaviour of one of the beams was also studied when it was subjected to fire only.

A simply supported rectangular reinforced concrete slab was designed and then analysed under the design load and increasing surface temperature. The effect of the varying magnitude of the external load (below and above the design load) is given when the slab is subjected to the same surface temperature.

Two computer programs were developed for the analysis of the beams and slabs which include non-linear material relationships, cracking or crushing of concrete and yielding of the reinforcement.

ACKNOWLEDGEMENTS

The author thanks professor A. J. Harris for the opportunity to undertake this work in the concrete structure and technology section of the departement of civil engineering at Imperial College.

The author wishes to thank Dr. P. J. E. Sullivan for supervising the project. His constant encouragement, utmost concern and valuable advice throughout the research work especially at the final stage is very gratefully acknowledged.

The author would like to express his appreciation to his wife for her unending patience, care and sympathy during the research period.

The author remembers and sincerely thanks his friend Dr. F. Labib, who helped at various stages of the work.

CONTENTS

	Page
ABSTRACT	2
ACKNOWLEDGEMENT	3
CHAPTER ONE: I-Introduction	
1.1-General Remarks	10
1.2-Arrangement Of The Thesis	12
CHAPTER TWO: II-Review Of Past Work	
2.1-Introduction	15
2.2-Concrete Material	15
2.2.1-Stress-Strain Relationship At Constant Room Temperature	15
2.2.2-Stress-Strain Relationship At Elevated Temperature	22
2.2.3-Thermal Properties of Concrete	25
2.2.3-A- Thermal Conductivity	25
2.2.3-B- Density	27
2.2.3-C- Specific Heat	27
2.2.3-D- Diffusivity	28
2.3-Behaviour Of Steel	29
2.4-Non-linear Technique	31
2.5-Finite Element Technique	33
2.6-Cracking In Reinforced Concrete Members	36

		Page
CHAPTER THREE:	III-Material Properties And Nonlinearity	44
	3.1-Introduction	44
	3.2-Concrete	45
	3.2.1-Biaxial Behaviour Of Concrete	46
	3.2.2-Biaxial Stress-Strain Relationship Of Concrete	47
	3.2.3-Effect Of High Temperature On The Properties Of Concrete	53
	3.2.3.1-Mechanical Properties	54
	3.2.3.2-Physical Properties	56
	3.3-Steel Reinforcement	59
	3.3.1-Effect Of Temperature On Properties Of Steel	60
	3.4-Numerical Solution Of Material Nonlinearity	61
CHAPTER FOUR:	IV-Layered Finite Element Technique	85
	4.1-Introduction	85
	4.2-The Finite Element Method	86
	4.3-General Technique	88
	4.4-Nonlinear Analysis of Reinforced Concrete Beams	96
	4.5-Reinforced Concrete Slabs	112
	4.5.1-A Brief Description Of Plate Formula	113

Page

CHAPTER FOUR: (CONT.)

4.5.2-Layered Method Analysis Of Reinforced Concrete Slabs 121
4.5.3-General Assumptions 122
4.5.4-General Formula 124
4.5.5-Displacement Functions 129
4.5.6-Strain-Displacement Relationship 136
4.5.7-Stress-Strain Relationship 140
4.5.8-Stress-Displacement Relationship 141
4.5.9-Stiffness Matrix 141

CHAPTER FIVE: V-Conduction Of Heat 158
5.1-Introduction 158
5.2-Heat Transfer 158
5.3-Temperature Equation 161
5.4-Heat Equation 164
5.5-Boundary And Initial Conditions 166
5.6- A Particular Solution 168
5.7- A Numerical Solution 171

CHAPTER SIX: VI-Analytical Solution Of Heat Equation 180
6.1-Introduction 180
6.2-One Dimensional Body 181
6.3-Two Dimensional Body 181
6.3.1-Finite Depth Body 182
6.3.2-Semi-infinite Depth Body 184

Page

CHAPTER SIX: (CONT.)

6.3.3-Practical Forms Of Surface Temperature 185

6.3.4-Type One 185

6.3.5-Type Two 193

6.3.5.1-General Form 194

6.3.6-Sine Equation Surface Temperature 201

6.3.7-Reducing The Computer Time 202

6.4-Three Dimensional Body 203

6.4.1-Semi-infinite Depth Body 203

6.4.2-Finite Depth Body 205

6.4.3-Reducing The Computer Time 208

6.5-Non-steady State Temperature 211

6.5.1-One Dimensional Body 211

6.5.2-Two Dimensional Body 213

6.5.3-Treatment Of Boundary Conditions 218

6.5.4-Three Dimensional Body 218

6.6-A Comparison With Numerical Solution 222

CHAPTER SEVEN: VII-Analysis Of Beams 229

7.1-Object And Scope 229

7.2-Experimental Investigation 230

7.3-Analytical Models Of The Beams 231

7.4-Heat And Loading Condition 234

7.5-Behaviour Of Beams Under Service Load 235

		Page
CHAPTER SEVEN:	(CONT.)	
	7.6-Behaviour Of Members Subjected To Fire And Comparison With The Experimental Results	237
	7.7-Behaviour Of Unloaded Beam Subjected To Fire	243
	7.8-Behaviour Of Unreinforced And Unloaded Concrete Beam Subjected To Fire	245
CHAPTER EIGHT:	IIX-Analysis Of Slabs	281
	8.1-Object And Scope	281
	8.2-Analytical Model Of The Slab	282
	8.3-Behaviour Of The Slab Under The External Load	284
	8.4-Behaviour Of The Slab Subjected To Fire	286
	8.5-Effect Of External Load On The Behaviour Of The Slab Subjected To Fire	290
CHAPTER NINE:	IX-Computer Programs	318
	9.1-Introduction	318
	9.2-Failure Criteria Of Materials	319
	9.3-The Convergence Criteria	320
	9.4-The Main Sequence Of Operations	321
	9.5-A Brief Description Of The Subroutines	327

Page

CHAPTER TEN: X-Conclusions 334

10.1-General Conclusions 334

10.2-Conclusions From The Analytical Results Of The Beams And Slabs 335

10.3-Recommendation For Future Work 338

REFERENCES: 339

APPENDIX I: 354

APPENDIX II: 356

APPENDIX III: 359

CHAPTER ONE

I-Introduction

1.1-General Remarks

Structural engineering, particularly in the realm of statically indeterminate structures, has always been associated with a vast amount of laborious calculations. The electronic computer offers means of reducing this work as well as opening larger areas of investigation to the structural designer.

The development of computer and sophisticated programs has extended the scope of concrete as a structural material for many useful purposes. Although a considerable amount of research work has been done and much more is now in progress, the behaviour of reinforced concrete members under high temperature can not be said to be fully understood. This is not only because the structural behaviour of reinforced concrete members at room temperature is not entirely clear, but also because many more factors influence its behaviour at high temperatures than at constant room temperature. Some factors which under normal condition are independent become interdependent under high temperatures, and time factor particularly plays an important role.

The object of this research is to develop a mathematical model which will predict the behaviour of reinforced concrete beams and slabs when subjected to fire conditions. Classical solution of conduction of heat equation is used to compute the temperature distribution at various times and is

introduced into the compatibility equation by a layered finite element approach for the structural analysis. The beam and slab are assumed to be composed of rectangular elements, which are divided into a finite number of layers. Temperature dependent material properties are considered together with temperature dependent stress-strain laws.

Computer programs have been developed and the results of the thermal analysis are in the form of temperature continuous passing through the centroids of the layers. Some of the models are intended to be applied for reinforced concrete beams as well as slabs. The structural behaviour of reinforced concrete, under high temperature or otherwise, has different characteristics from that of homogeneous material, since a particular level of stress does not necessarily correspond to a unique value of strain. To find a unique relation between stress and strain, other factors such as loading period, loading history, loading ratio and boundary condition must be taken into account.

Under high temperature case, a number of factors become so closely interwoven that it is difficult to seperate a dominant one at any given time. Therefore it is difficult to find a close similarity between stress and strain characteristics in the result of many research works, even though the concrete is similar.

It is sometimes difficult to compare in a systematic way the results of different experiments on the structural behaviour of concrete under high temperature. Notwith-

standing the many studies of concrete under high temperatures, very little work has been done which combines that results with a study of the behaviour of structural element in the practice.

The main problem in this field is that there are a large number of variables and most of these are time dependent. Once the time variable becomes important, the equations become complex and often mathematically insoluable, but the practical solution available can be carried out by an approximate step-by-step iterative technique.

However, when a logical system to solve the problem is set up in structural mechanics, the equilibrium equations can be derived from Newton's first law and the first law of thermodynamics (conservation of energy).

It is known that the solution of the equilibrium equations with the compatibility criteria produce the unique answer when the boundary conditions and constitutive relations are defined. However, these equations generally contain no terms for sequence and time.

The whole process is divided into time intervals under the assumption that within the interval, time effect is constant or negligible. The time steps are accompanied by a feed-back which inputs the results calculated at the end of a given time into the beginning of the next time step.

1.2-Arrangement Of The Thesis

The discussions of the next nine chapter of the present thesis can be divided into two seperate problems.

Firstly, the conduction of heat equation for an isotropic homogeneous body which is a linear partial differential equation is solved with the help of a particular solution of this equation. The temperature distributions within one, two and three dimensional rectangular bodies, heated from boundary surfaces are given. This study also can be divided into two parts;

1-The analytical solutions of heat equation and distributions of temperature within the bodies under steady state temperature case with various boundary conditions are given in chapter five and some results are compared with a numerical method of solution.

2-In chapter six, classical solution of heat equation is examined under non-steady state temperature in which the boundary temperature can be constant or time dependent. For the second condition when the surface temperature varies with time, it is assumed that the boundary temperature is constant within each incremental time.

Since this part of work is purely mathematical, it is discussed seperately, and the results are used in the analysis of reinforced concrete beams and slabs, in the corresponding chapters.

A numerical method of analysis of reinforced concrete members, called the layered finite element method is discussed in chapter four, while in chapter three the behaviour of steel and concrete under service load and high temperature and also non-linearity of the materials are discussed.

With the help of two seperate computer programs, which are explained briefly in chapter nine, reinforced concrete beams and slabs are analysed under external loads (distributed or/and concentratdedloads) and high temperature in chapter seven and chapter eight, respectively and some results are compared with experimental works.

However, the standard form of each chapter comprises two parts, the text and figures in the order named. In the numerals of references, following the authors' names, and these of equations such as [Ref. 12]. The equations are quoted such as (4.26), the former is for chapter number, and the latter for the consecutive number in a chapter.

Each notation is explained when it appears first. However, in general, a row vector is shown by $\{\ \}$, even when coefficients are written horizontally between the brackets and other wise a tilde ($\sim$) appearing under a single letter such as $\underset{\sim}{a}$ represents a row vector. A column vector is shown by transpose of a row vector to save space, for example;

$$\underset{\sim}{a}_8 = \left\{ a_1 \quad a_2 \quad a_3 \ \cdots \ a_8 \right\}^t$$

A matrix is shown by $[\ ]$, even when coefficients have to be shown between the brackets and in other case a bar (-) under a single letter denotes the matrix such as $\underline{D}$. Finally the inverse of a square matrix is shown by $[\ ]^{-1}$ or $\underline{D}^{-1}$.

CHAPTER TWO

II- Review Of Past Work

2.1- Introduction

Structural mechanics has been developing for centuries to achieve the present system, which is based on relatively simple equations describing the structural behaviour of idealized materials. Under this simplified assumption, theoretical analysis of the structural behaviour of continua is still often complicated and its solution complex. However, in the last two decades, the gap between the idealized and the actual fundamental behaviour of the material has been reduced by the use of digital computer to give more realistic solutions. Although the study of the actual material behaviour has been carried out from various aspects, many problems are still unresolved in structural engineering, even when these materials are assumed isotropic homogeneous and subject to simple conditions.

In this chapter the past research work on the behaviour of concrete and steel materials will be discussed.

2.2- Concrete Material

2.2.1- Stress-Strain Relationship At Constant Room Temperature.

Although the procedure of testing under uniaxial test is simple, the actual mechanical processes within the specimens can be complex, especially for concrete materials

since many parameters can influence the results. For mild heating of concrete (10 to 30 ^{o}C), recent research works are aimed at giving an overall view of the stress - strain relationship. Experimental investigators have succeeded in obtaining typical shapes of stress - strain curves. A typical curve as in figure (2.1), starts out with a nearly linear portion up to about 30% of ultimate load called the proportional limit, beyond which, the stress-strain curve deviates gradually from the straight line, reaches a peak depending on the stiffness of material and exhibits a falling branch. Since the material of most aggregate particles exhibits a reasonably linear stress-strain relationship the departure from linearity is primarily due to the cement phase [Ref. 87] and the interface between aggregate and cement and the possible development of internal microcracking. Thus the shape of the stress-strain curve and failure of concrete is due to progressive internal microcracking.

A summary of the investigations into the compressive stress-strain response under uniaxial monotonic and cyclic loading is given in [Ref. 1] . Among the various mathematical expressions Hognestad [Ref. 2] proposed that the stress-strain characteristic can be determined by a combination of a linear equation and a second degree polynomials as shown in figure (2.2). His work simulated research into the analysis of the structural behaviour of beams derived from the properties of concrete. This work helped to develop the inelastic theories associated with the design of reinforced concrete, which befor depended on the modular ratio and the

permissible stress concept.

Hognestad [Ref. 3] also carried out series of test on concentrically loaded cylinders and eccentrically loaded prisms and derived stress-strain curves, which were found to be similar in form for both concentric and eccentric specimens. A few simple stress-strain curves for concrete have been represented by Smith [Ref. 4] and Brock [Ref. 5] in compression.

Smith pointed out the significant effect of strain distribution on the moment capacity of the member, and he suggested that the flexural stress-strain curves should be obtained by simulating the sectional condition of the member subjected to bending moment.

Brock proposed a simple technique which enabled the use of the stress-strain curve obtained by a normal testing machine for strain controlled tests in order to analyse the behaviour.

Kirtz and Lee [Ref. 6] assumed a concrete stress - strain relationship in the form of a second degree polynomial as follows;

$$\sigma^2 + a_1\epsilon^2 + a_2\epsilon\sigma + a_3\sigma + a_4\epsilon = 0 \qquad (2.1)$$

where, coefficients a_1 to a_4 were determined from a statical analysis from Hognestad's experimental curves [Ref. 3], for six grades of concrete, ranging from 7.0 to 52.0 N./mm^2 as shown in figure (2.3).

Rusch [Ref. 7] investigated the validity of the

strength and deformational properties of concrete with loading time. A broad range of straining rates and sustained loading were obtained for the stress-strain curves and flexural stress-strain curves were derived from concentric compressive test results by assuming that;

A- In flexure the strain rate of each fibre in a section is proportional to its distance from the neutral axis.

B- Any differences in the behaviour of sections, concentrically and eccentrically loaded are due to the presence of a differential strain rate for different fibres in the eccentrical loading.

Finally, the following simple stress-strain relationships were derived;

$$\sigma = \sigma_o\left(2 - \frac{\epsilon}{\epsilon_o}\right).\frac{\epsilon}{\epsilon_o} \qquad \text{for} \qquad \epsilon \leq \epsilon_o \qquad (2.2\text{-a})$$

$$\sigma = \sigma_o \qquad \text{for} \qquad \epsilon_o \leq \epsilon \leq \epsilon_m \qquad (2.2\text{-b})$$

where, $\epsilon_o = 0.002$, $\epsilon_m = 0.0035$ and $\sigma_o \doteq f'_c$ is the uniaxial compressive strength.

In the equation suggested by Desayi and Krishnan [Ref. 8], the ratio of E/E' is fixed, where E is the initial tangent modulus and E' is the secant modulus. The improved version was proposed by Saenz [Ref. 9] which takes account of the secant modulus. E/E' varies from nearly 4 for normal concrete with an ultimate strength of 1000 PSI (7 N./mm^2) to about 1.3 for high quality concrete of 10,000 PSI (70 N./mm^2).

Sturman et al [Ref. 10] investigated stress-strain relationships of concrete under concentric and eccentric loading and the relationship between microcracking inelasticity. It was concluded that the shape of the stress-strain curves at high stresses were related to microcracking. The apparent ductivity of concrete is due to a cumulative effect of brittle fracture in micro-regions and the presence of strain gradient retarding microcracking. A comparison between concentric and eccentric stress-strain curves revealed that the maximum stress and the correspondin strain were 20 per cent and 50 per cent higher, respectively in an eccentric loading.

Most workers, since Hognestad, are in reasonable agreement as to the shape of the stress-strain characteristic befor the ultimate strain although the ultimate strength differs considerably depending on many factors. It is also known that, the curvature of the various diagram may differ considerably due to the properties of the mix, for instance, the lower the cement content, the more curved in the diagram. The other factors influencing the shape of the stress-strain are, the type of the aggregate, age, testing condition, rate of loading, etc. The limits of validity and degree of approximation of the various formulas proposed with an emphasis on simplicity are restricted.

The investigation into biaxial loading of concrete are usually divided into the groups based on the shape of the specimen used. A review of the investigations on the type of the specimen is given by Kupfer an Hilsdorf [Ref. 11].

The problem facing the investigator is how to induce the desired state of stresses or strains into the particular specimen. Concrete plates or cubes, used for studies of biaxial compressive strength were confined along the loaded faces due to the friction between the bearing platens of the testing machine and the concrete. These results indicate that the biaxial compressive strength is higher than the uniaxial compressive strength.

Biaxial compressive stresses were also generated by subjecting a cylindrical specimen to hydrostatic pressure in radial direction. Hollow cylinders have been subjected to torsion and axial compression and the results reported by a number of investigators [Ref. 12 and 13].

McHenry [Ref. 14] tested hollow cylinders under axial compression and internal hydrostatic pressure. As the tests were conducted on a variety of specimen with different type of concrete and subjected to various loading conditions and machine testing effects the overall results can not express a consistent behaviour. The comparison of the various test results [Ref. 15]indicates that, in general the strength in uniaxial tension is about 8-10 times larger than the strength in uniaxial tension and the strength in biaxial compression is about 10-25 per cent greater than the strength in uniaxial compression.

Kupfer [Ref. 11 and 16] presented a relatively comprehensive strain measurements of various concrete under predefined ratio of stresses in biaxial direction. The concrete specimen of $20\times20\times5$ mm^3 was tested by the new test

apparatus developed by Hilsdorf [Ref. 17]. Restraint of the test specimen was avoided by using brush-like load bearing platens. A series of stress-strain curves in biaxial compression, tension compression and biaxial tension were reported and concluded that for the case of biaxial compression in two principal directions the strength of concrete may be up to 27% higher than the uniaxial strength.

Buyukozturk et al [Ref. 18] investigated the biaxial behaviour of concrete in an experimental model consisting of preselected circular discs of aggregates with radius (r) set in a square array with average clear distance of 0.2r and 0.5r. They also used test arrangement originally proposed by Hilsdorf [Ref. 17]. Formation and propagation of microcracking as a significant cause of non-linear response were followed by x-ray in the uniaxial loading. A plane stress finite element model representing the experimental model was used for an analytical study. Liu [Ref. 20] tested real concrete specimens and idealized models (aggregate discs of three different sizes randomly embedded in a mortar matrix) under the same test arrangement used by previous investigators [Ref. 11 and 18]. Based on the results of the real concrete specimens a general stress-strain relationship for concrete in uniaxial and biaxial compression was proposed which also aggreed with test results obtained by Kupfer [Ref. 11]. The proposed relationship which satisfies the boundary conditions at zero stress and peak stress, also includes the ratio of stresses in the two orthogonal directions. The relation reduces to the equation

proposed by Desyi [Ref. 8] and Saenz [Ref. 9] under special case in uniaxial direction. An emperical failure envelope for concrete under biaxial compression was presented by the same outhors in [Ref. 21].

2.2.2- Stress-Strain Relationship At Elevated Temperature.

The limitation of using uniaxial compression to derive the strength of the structure is further accentuated at elevated temperatures. Further, the technical difficulties of testing at high temperatures have also been a hindrance, and there is even less investigated information than that obtained at constant room temperature. In this study, the expansion is treated as part of the basic information for the stress-strain relationship at high temperatures.

Befor 1956 most investigations into the thermal behaviour were directed at the thermal expansion during the heating and the permissible stress after cooling.

Willis and Dereus [Ref. 22] showed that the coefficient of thermal expansion was dependent on the type of the aggregate, and for gravel concrete was almost the same as that for steel between 5 ^{o}C and 60 ^{o}C.

Malhotra [Ref. 23] investigated the effect of high temperatures from 20 ^{o}C to 700 ^{o}C on the compressive strength of concrete under constant high temperature as well as after cooling. Malhotra tested 2 in.(51 mm) diameter cylindrical specimens by 4 in. (102 mm) height, using 3/8 in. (10 mm) maximum size coarse flint aggregates. The three aggregates

cement ratios were 3.0, 4.5 and 6.0. Temperatures were measured at the centre and at the surface of the specimen, and the mean was taken as the average of overall temperature allowing an error range of 10 °C.

Harmathey [Ref. 24] investigated the temperature effects on the uniaxial stress-strain relationships of mortar and light weight aggregate concrete. He tested 1.75 in. (44.5 mm) diameter cylindrical specimens by 3.5 in. (89 mm) height, at temperatures up to 700 °C, and derived stress - strain temperature relationships as shown in figure (2.4), and the conclusions were as follows;

A- There are marked individual differences in the characteristics of seemingly identical specimens under similar environmental conditions.

B- There is little change in the properties of both materials up to about 200 °C.

C- Above 260 °C there is a general decreases on the modulus of elasticity and ultimate strength, and an increase in the deformation at failure with increase in temperature.

Furmura [Ref. 25] also measured the stress-strain relationship of concrete at high temperature (30 to 700 °C) of 50 mm diameter cylindrical specimens made of 10 mm maximum size gravel and ordinary cement. Specimens were heated for about two hours at a specific temperature befor applying cyclic loads, and the stress-strain characteristics were plotted.

Sullivan [Ref. 26] investigated the structural properties of concrete and mortar beams in flexure, their

reversible and irreversible components of strain due to temperature effects, and their time dependent characteristics. It indicates a continuous decrease in f'_u of mortar with the rate of drop increasing with temperature in both their upper and lower boundary curves, as shown in figure (2.5). The size of the beam specimen was 51×76×83 mm^3, and flint aggregate was used. Some of conclusions on the stress-strain-temperature were as follows;

A- The longitudinal movements curve shows two linear portions, as shown in figure (2.6). For test temperatures above 350 ^oC there appeared to be a residual non-recoverable expansion due to the development of microcracks, around the flint, which did not completely close up when the beam was cooled.

B- The values of modulus of elasticity dropped as temperature increased. The ratio of modulus during heat treatment to the modulus befor heat treatment decreased quite rapidly between 20 and 100 ^oC, was sensibly constant between 100 and 300 ^oC and then decreased again above 300 ^oC.

C- At 400 ^oC the creep rate for the concrete specimen reached the plastic stage and was creeping rapidly at very low load.

Takeda [Ref. 27] studied the effects of curing temperature (20 to 80 ^oC) on the strength and modulus of elasticity of concrete incorporating gravel aggregate and portland or other types of cement. He showed that even at low temperature (20 to 80 ^oC), when heated for long periods, compressive strength had a tendency to reduce.

Bizri [Ref. 28] applied the finite element method to analyse column behaviour at elevated temperatures. In his literature survey, he reviewed the information on the upper and the lower limit of various relationships, e.g. stress-temperature, modulus of elasticity versus temperature and coefficient of thermal expansion, conductivity and some of them have been used in the present study by making mathematical models of these relationships.

Akhtaruzzaman [Ref. 29] investigated the thermal effects of both transient and steady temperature conditions on concrete. He tested beam specimens ($50\times75\times840$ mm^3) made from flint aggregate and derived expressions connecting the modulus of elesticity under transient heating to that at steady state temperature.

2.2.3- Thermal Properties of Concrete

In order to calculate the temperature distribution within the concrete members under non-steady state temperature, the thermal conductivity, density and specific heat are required for the solution of conduction of heat equation. These are reviewed seperately in this section leading to the derivation of the diffusivity of concrete.

2.2.3-A- Thermal Conductivity

It has been claimed that the conductivity of concrete can be determined by that of its constituents. Campbell-Allen [Ref. 30] presented the following formula using an idealized model of concrete in order to obtain the theoretical valuc

in terms of the thermal conductivities of the constituents;

$$k = k_m\left[\, 2a - a^2 + \frac{k_a(1-a)^2}{k_a a + k_m(1-a)}\right],$$

where,

$a = 1 - (1 - b)^{\frac{1}{3}}$, and;

b = volume of mortar per unit volume of concrete,

k_m= thermal conductivity of mortar,

k_a= thermal conductivity of aggregate.

Harada [Ref. 31] measured conductivity of gravel concrete composed of varying constituents and the mortar content using cylindrical specimens of 50 mm diameter by 240 mm height. He presented the following values of the conductivity of concrete;

$k = 1.584$ kcal./m-hr-^{o}C when $T \leq 100\ ^{o}$C,

$k = 1.584\text{-}0.001(T\text{-}T_o)$ kcal./m-hr-^{o}C when $T \geq 100\ ^{o}$C,

where, T is the temperature of material and T_o is the constant room temperature.

Harada and Shiina [Ref. 32] using 200 mm diameter 20 mm thick disk specimens made from various concrete, found a considerable drop in thermal conductivity at around 100 ^{o}C and 430 ^{o}C due to the latent heat and phase change in concrete.

Odeen [Ref. 33] derived the following relationship for conductivity of concrete by plotting several worker's data;

$k = 1.4\mathrm{Exp}(-0.001T)$ kcal./m-hr-^{o}C,

where, T is temperature of the material (^{o}C).

2.2.3-B- Density

Density of concrete at a given temperature is clearly a function of both weight loss and the thermal expansion which can be shown to be;

$$\frac{\rho}{\rho_o} = \frac{1 - \epsilon_T}{(1 + \alpha)^3} \qquad (2.3)$$

where, ρ = density at temperature T,

ρ_o = density at constant room temperature,

ϵ_T = thermal strain in a given condition.

Equation (2.3) can be written approximately in the following form;

$$\rho = (1-\epsilon_T)(1-3\alpha)\rho_o$$

or;

$$\rho = (1-3\alpha-\epsilon_T)\rho_o$$

Phillеo [Ref. 34] showed that most of the water was lost by 450 °C. He concluded that the weight loss of concrete made from calcareous aggregates was determined by the chemical change at high temperature.

Akhtaruzzaman [Ref. 29] plotted the moisture loss in flint aggregate concrete with increasing temperature.

The change in density of concrete with temperature has been taken from [Ref. 28] and has been used to derive the diffusivity of concrete which is given in chapter three.

2.2.3-C- Specific Heat

Although it is easy to find the values of specific heat of concrete at room temperature in most text books on

heat transfer, the specific heat of various concretes at high temperature is not available. Harmathy [Ref. 35] and 36 derived graphs for the volumetric capacity, $\rho.c$, versus temperature (up to 900 °C) and showed that above 100 °C it is approximately constant. Kishitani [Ref. 37] tabulated the values, quoting experimental results from Harada [Ref. 38] and Orchard [Ref. 39]. According to his table, the specific heat values of concrete are as follows;

0.22 to 0.24 kcal./kg.-°C for $10 \leq T \leq 30$ °C

depending on aggregate and;

0.13 to 0.20 kcal./kg.-°C when temperature is at around 300 °C.

2.2.3-D- Diffusivity

Summing up the value of diffusivity for concrete, $h=\frac{k}{\rho c}$, can range as follows;

A- At normal temperature (10 to 30 °C),

1- Aggregate of higher conductivity (e.g. sand stone) =0.0045 to 0.0062 m^2/hr.

2- Aggregate of lower conductivity (e.g. lime stone) =0.0030 to 0.0050 m^2/hr.

3- Some type of river sand aggregate = 0.0025 to 0.0028 m^2/hr.

4- Some type of light weight aggregate = 0.0013 to 0.0018 m^2/hr.

B- At elevated temperature (200 to 400 °C),

1- Ordinary weight aggregate = 0.0024 to 0.0054 m^2/hr

2- Some type of light weight aggregates = 0.0004 to 0.0016 $m^2/hr.$

2.3- Behaviour Of Steel

Although the number of reported papers on the properties of steel are much more than those for concrete, the sensitive response of steel to the change of factors such as composition, processing variables, heat treatment, makes it difficult to find accurate data for a given reinforcing bar in concrete.

The stress-strain curves of steel used in rein - forced concrete usually exhibit an initial linear elastic portion, a yield plateau, a strain hardening and a final stage until rupture occurs. The stress at yield point as yield strength is an important property of the reinforcement. The yield strength is generally taken as the stress corresponding to a particular strain. The stress-strain curves for steel in tension and compression are assumed to be identical.

The British Iron and Steel Research Association [Ref. 40] produced tables, derived from tests carried out by the National Physics Laboratory, London, which give the composition and heat condition of steel and also mean coefficient of thermal expansion. Simmons [Ref. 41] showed a graphical summary of the high temperature strength data for carbon steel, including summaries for tensile strength, 0.2 per cent offset yield strength, per cent elongation, and reduction of area when extended. The joint conference of

B.I.S.R.A and I.S.I [Ref. 42] published their proceedings which contained comprehensive information on high temperatures properties of steels.

Johnson [Ref. 43] gave a statical procedure for the analysis and assesment of yield stress in terms of confidence limits. He suggested the use and interpretation of the lower confidence limit for the definition of minimum values of high temperature yield or proof stress.

Todeschini [Ref. 44] and Pfrang [Ref. 45] and other workers each used complete stress-strain relationships to derive a general failure criterion, i.e. failure function in given conditions without numerous simplifying assumptions. Sargin [Ref. 46] proposed a functional relationships between the stress block parameters and given conditions of the material and structure. He also gave a clear review on the sectional theories, dividing them into two following catagories;

1- Ultimate strength theory, which assumed that sectional failure is decided by the material used.

2- General theory, which assumed that sectional failure is related to the material as well as to the expected deformation of the section. During heating, this general theory can be extended to include the change of material properties with respect to position and time, by normal principles of mechanics.

2.4- Non-linear Technique

In the last two decades, the solution of structural non-linearity has been tackled in many ways by various investigators, and several techniques have been proposed for the solution of non-linear material problems. The non-linear behaviour in structural system is usually in one of the following catagories;

A- Material non-linearity, which arises from the stress-strain relationship which departs from linear behaviour.

B- Geometrical non-linearity due to nonlinear strain-displacement relationship arises from large strains and large displacements.

However, the solution of non-linear material problems can be broadly classed into two following methods;

1- The same elastic problem is repeatedly solved and successive corrections applied to reproduce finally the appropriate constitutive law.

2- Different linear elastic problems are successively solved to achieve the same objective, which are explained in chapter three.

However, hybrid varieties can be obtained by a combination of the two approaches. In general mathematical techniques that can be used successfully to treat one type of non-linearity are with the modification applicable to the other type. An extensive review of the finite element applications to non-linear structural system is given by

Oden [Ref. 47].

Argyris [Ref. 48] used initial strain method to solve elastoplastic problems by the finite element method. The increase of plastic strain was compared and treated as an initial strain with no change in stress. This method fails if ideal plasticity exists or if the degree of the hardening is small. Nilson [Ref. 49] and Franklin [Ref. 50] employed linear incremental procedure to trace the non-linearity of the material. Marcal [Ref. 51] used variable elasticity technique which would successfully treat any elastoplastic and perfectly plastic material. The method suffer the disadvantage that the stiffness of the structure is changed at each iteration and from the computational point of view is an expensive operation.

Zienkiewicz [Ref. 52] developed a method called stress transfer process to deal with no tension materials using finite element approach. The calculated principal tensile stress was eliminated in the element, and the structure was equilibrated by equivalent applied nodal forces. A similar approach was later applied to plasticity problems by Zienkiewicz and Valliappan [Ref. 53] as an initial stress method with an advantage to initial strain method for perfectly plastic material and an advantage to variable elasticity technique as the stiffness of the structure is kept constant during the successive iterations. Some different approaches and their applicability to different material law is given by Zienkiewicz and Valliappan [Ref. 54].

2.5- Finite Element Technique

The finite element method was first concieved in 1940 by Hrennikoff [Ref. 55, 56 and 57] and Mchenry [Ref. 58] in their Lattice Model approach. Hrennikoff replaced the actual continuum by uni-dimensional members with equivalent stiffness values by making use of equal deformabilities of the original system and the frame work model. However, the development of the finite element method is associated with the growing demand of the aircraft industry for a procedure which could provide a refind solution for extremely complex aircraft configurations and much more literature on the subject appears in the journal of the aeronautical societies.

Although this method has been subsequently developed by others [Ref. 59, 60 and 61] using two dimensional members, it did not receive the attention it deserved for a long time because of the non-availability of big storage computers to solve the large number of equations resulting from the equilibrium conditions.

The finite element method, however, has been applied equally well to problems in structural mechanics from any field, and it is essentially a generalization of standard procedures for stress analysis.

A major breakthrough in the Hrennikoff's Lattice Model approach came in 1954 when Argyris [Ref. 62] replaced the actual structure by two dimensional extensional elements and this approach was further extended to the present recognizable form by Turner, Clough and Martin [Ref. 63] in

1956. However, the basic concept is that any structural member may be considered as an assemblage of individual structural components, or elements, and the body must consist of a finite number of such elements, interconnected at a finite number of nodal points. It is the finite nature of the connectivity which makes possible an analysis by means of simultaneous algebric equations, and which distinguishes such a solution from those of continuum mechanics.

In fact, it was effort to improve Hrennikoff and McHenry lattice analogy, for representing plane stress systems which first led to the development of the finite element concept by Turner [Ref. 63]. An important part of this work was an evaluation of the in-plane stiffness of a two dimensional body (plate) so as to establish a relation between the forces and the displacements of the nodal points, similar to that of one dimensional (bar) members. The method advanced very rapidly with the development of the high speed digital computer. Since 1956, an enormous amount of work has been done and an excellent bibliography on the subject may be found in [Ref. 64, 65 and 66] and the method has been aptly named as the finite element method, and now it permits the determination of stresses and displacements in two and three-dimensional bodies such as plates, shells and other elastic continua by the same techniques that are commonly applied to framed structures. The idealization produces a highly indeterminate structural system.

Clough [Ref. 67] derived the stiffness matrix of triangular and rectangular elements by applying the principal

of virtual displacement. Wilson suggested that the derivation of an element stiffness may be based on energy consideration, and he extended [Ref. 68] the finite element method to non-linear problems. Deherty [Ref. 69] and Wilson [Ref. 70] proposed methods to improve the basic accuracy of low-order finite element when subjected to certain stress gradient.

However, the finite element method of solution for stresses and displacements is greatly facilitated by matrix formulation, coupled with the use of high-speed digital computers. In this method, it is apparent that the body elements are not merely pieces cut from the original structure, but rather are special types of elements constrained to deform in specified patterns such that continuity of the assemblage is maintained, and it has been shown by Wilson [Ref. 71] that, the errors associated with this type of idealization can be reduced to any desired value by reducing the size of the elements, thus increasing the number of nodal points at which continuity is satisfied explicity. Alternatively, Mallett [Ref. 72] has observed that, by using a higher order displacement field within the basic element, a relatively smaller number of elements may give improved accuracy with more rapid convergence.

Details of the finite element method and recent advances can be found in various text books [Ref. 73 and 74].

2.6- Cracking In Reinforced Concrete Members

Early work in finite element study of cracking in reinforced concrete members was initiated by Ngo and Scordelis [Ref. 75] who studied the behaviour of cracked beams by using triangular finite elements. They represented the pre-existing cracks by seperating the concrete elements either side of the crack, and the linkage element was introduced to give steel-concrete interaction. Nilson [Ref. 49] considered crack propagation by allowing crack to follow the element boundaries and progressively twinning the nodal points as the crack propagated between the elements. This method required a change in the topology of the structure continually due to crack propagation, hence it presented some undesirable features as far as programming and predicted behaviour is concerned.

Ngo, Franklin and Scordelis [Ref. 76] tried to overcome this problem by predefining the expected total length of a shear crack, which is observed in the experiment, in their study of reinforced concrate beams. The two sides of the crack were initially held rigidly together by very stiff linkage elements, the crack propagation was simulated without renumbering the nodal points.

If pre-existing cracks are not assumed, then criteria are required for choosing the points where cracks are likely to initiate and for determing the direction and extent of crack propagation. Zienkiewicz [Ref. 73] have proposed that the entire element which has developed tensile stress exceeding the tensile strength should be assumed to

be cracked in the direction perpendicular to the stress. The load sustained by the stress field associated with the crack was then redistributed to the rest of the structure and zero stiffness was assumed for the element perpendicular to the crack.

Villiappan and Nath [Ref. 78] used the same method for cracking and applied the load incrementally. To study plane stress problems Cervenka [Ref. 79] used a constant strain finite element with steel distributed over the element in two orthogonal directions.

In order to study rock structures, Zienkiewicz, Vallippan and King [Ref. 52] presented non-tension model in, which the material was assumed to sustain compression only, all tensile stresses were therefore eliminated in an iterative technique called stress transfer method, and equivalent nodal forces were applied to the surrounding materials.

Recently the problem of crack propagation has been tackled by using various iterative techniques. The considerable merit of these procedures lies in the fact that, it reduces the computational effort by making revisions to load vector rather than the stiffness matrix. The initial stress method introduced by Zienkiewicz [Ref. 53] for elasto-plastic solutions was further extended by Valliappan and Doolan [Ref. 80] for determing the stress distribution in reinforced concrete structures due to cracking of concrete and elasto-plastic behaviour of steel. The load was applied incrementally if the principal stress in any concrete element exceeded the tensile strength of concrete in any iteration, the tensile

stress was released and equivalent nodal forces applied. The prescribed tension for the cracked element was then assumed to be zero. The original stiffness matrix of the structure was however, kept constant throughout the loading.

On a discussion of reference (80), Shnorbich et al [Ref. 81] stated that, the pure initial stress approach, always using the original elastic matrix of structure as the basic for solution and interacting with pseudo stresses to correct the stress state may not be the most economical approach. They suggested that, periodically updating the stiffness matrix is desirable. Cracking was considered as the changing of the material properties of concrete from isotropic to orthotropic, i.e. a change in the stiffness matrix of the element. This manner of introducing cracking, allows some shear capacity to be retained in the crack element. This allowance for shear corresponds for taking into account the concept of aggregate interlock across the cracked surface.

Nam and Salman [Ref. 82] using isoparametric elements demonstrated that, constant stiffness method (keeping the same original stiffness matrix) provides neither an efficient nor correct solution for evaluating non-linear behaviour of concrete due to cracking in flexural members. Variable stiffness method was shown to be an effective method for prediction of cracking in concrete flexural members.

Hand et al [Ref. 83] in a non-linear layered analysis of reinforced concrete plates and shells retained some shear stiffness in the cracking plane to account for aggregate

interlock which resulted in a good correlation with the test results.

Suidan and Schnobrich [Ref. 84] used a three dimensional isoparametric 20-node rectangular elements for analysis of reinforced concrete structure which included a factor of shear retension in the cracked plane of concrete.

Colville and Abbasi [Ref. 85] presented a plane stress reinforced concrete finite element using models in which the steel and concrete are considered as one element so as to make the idealization of the structure independent of the geometry of the reinforcement.

Lin and Scordelis [Ref. 86] used triangular layered elements idealization for the analysis of reinforced concrete shells in which the steel was presented as smeared layer. While assuming zero modulus of cracked concrete elements perpendicular to the crack direction, the tensile stress was released step wise gradually according to a specified loading curve.

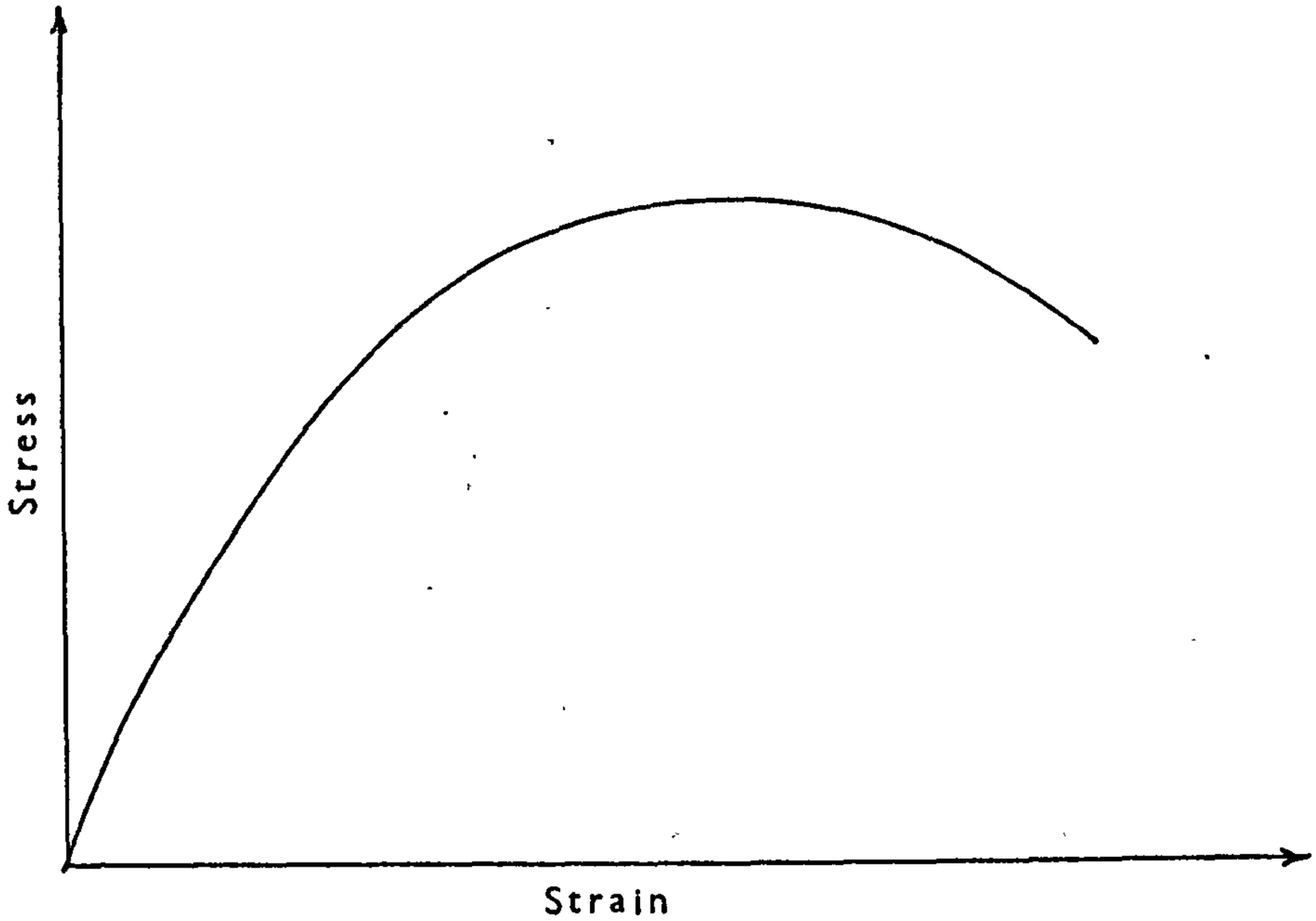

Fig. 2.1_ A Typical Stress_Strain Relationship Of Concrete Material.

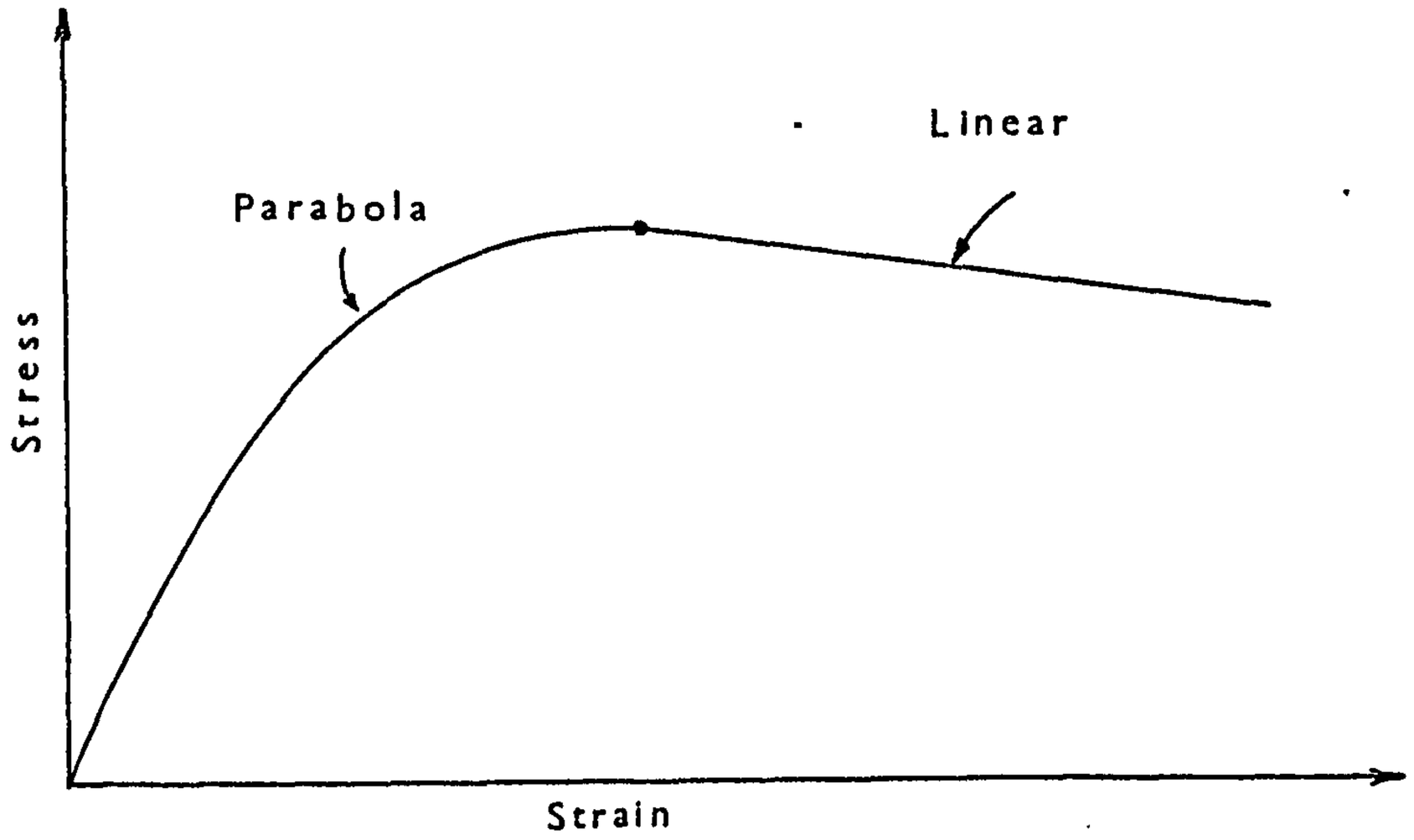

Fig. 2.2_ Stress_Strain Curve For Concrete In Compressive; Ref. 2.

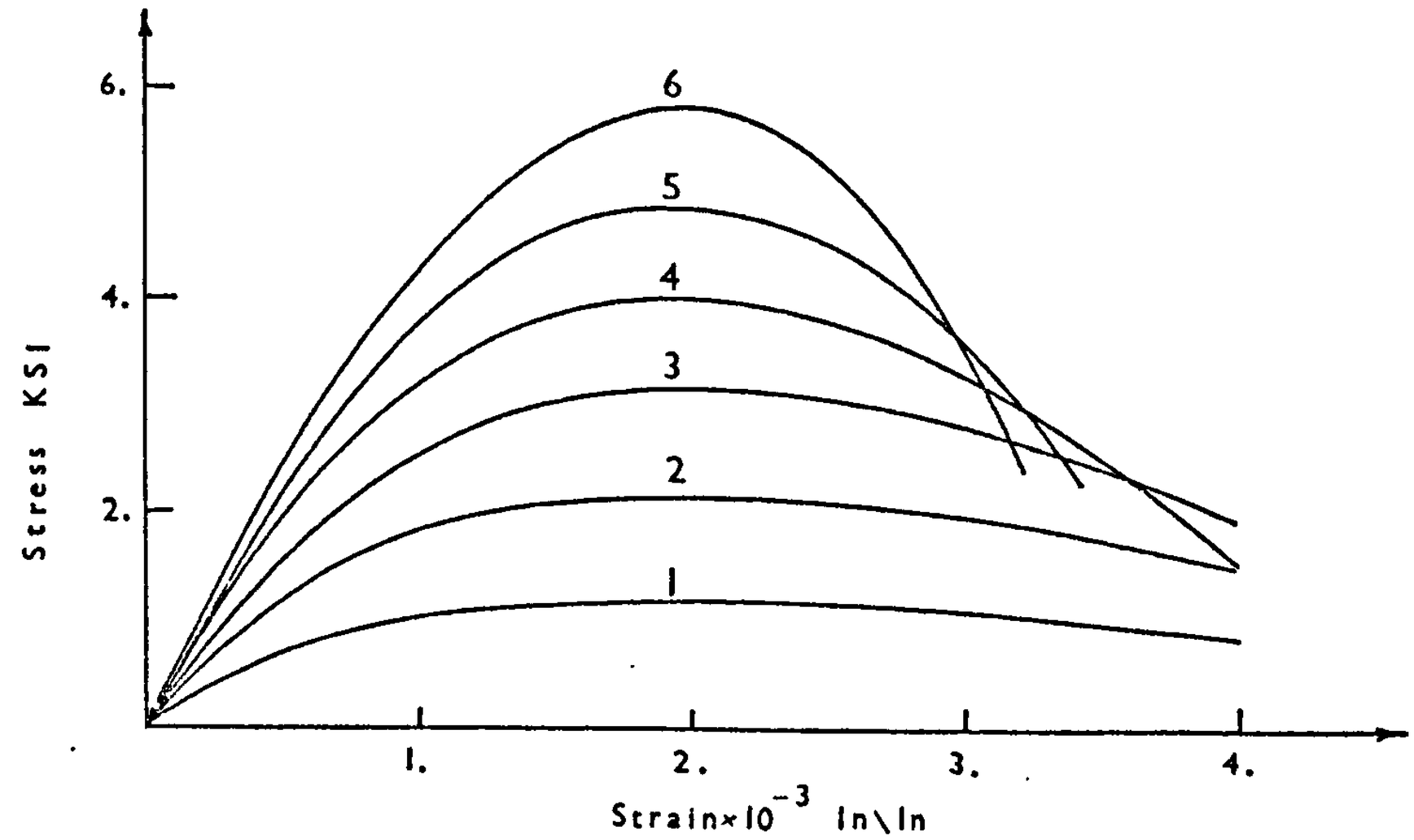

Fig. 2.3_ Stress_Stain Relationship Of Concrete In Flexure; Reference 3.

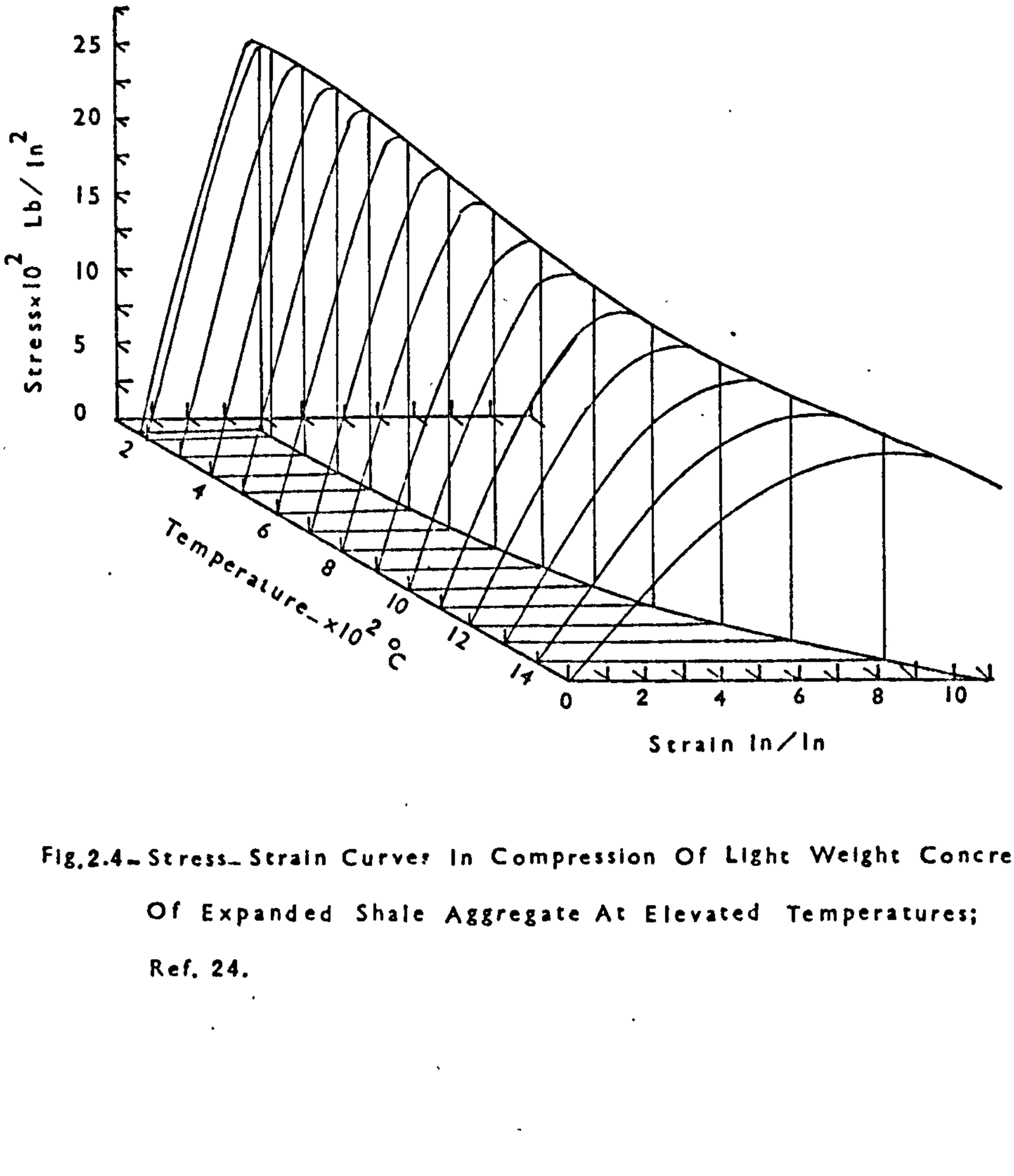

Fig. 2.4_ Stress_ Strain Curves In Compression Of Light Weight Concrete Of Expanded Shale Aggregate At Elevated Temperatures; Ref. 24.

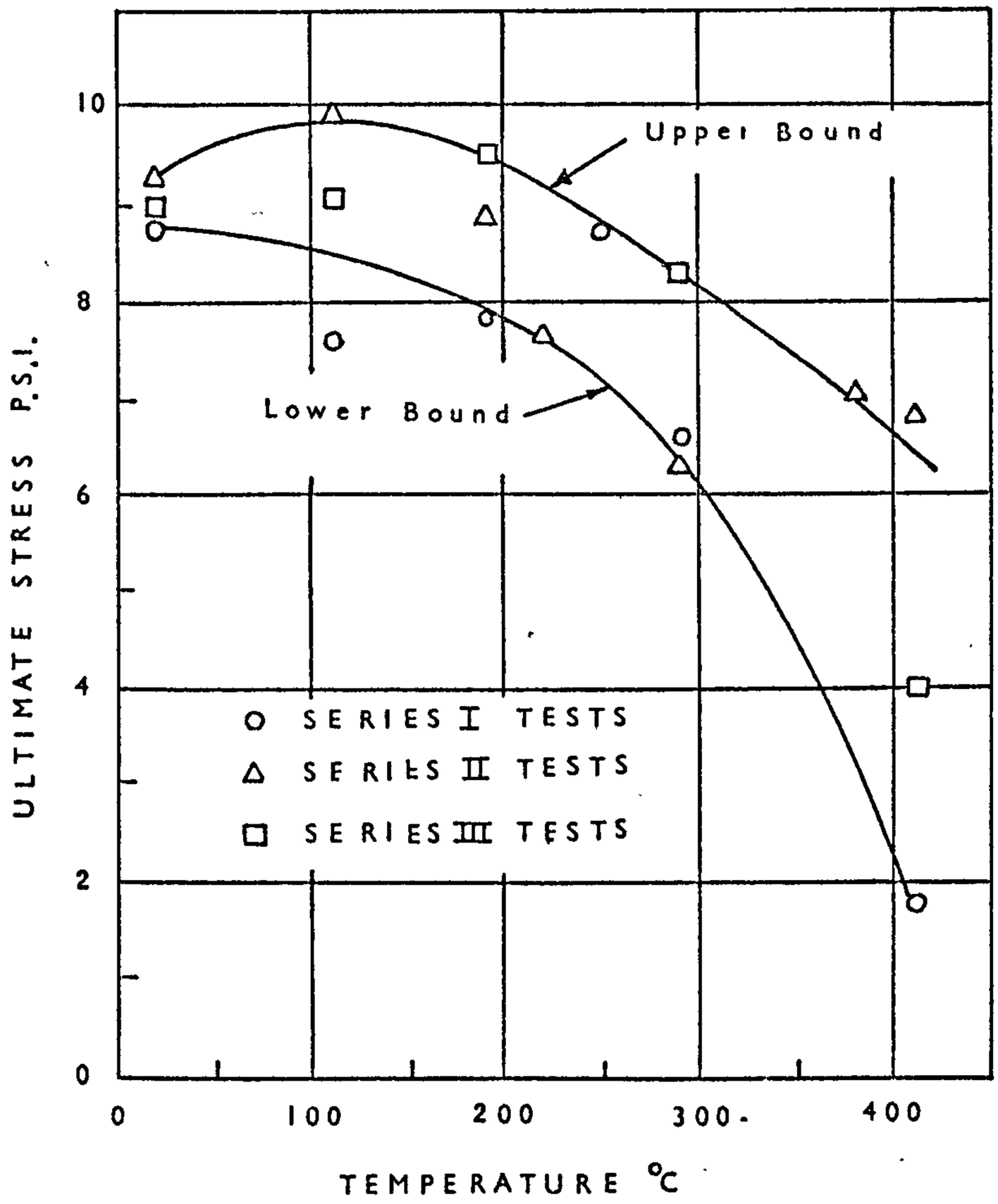

Fig. 2.5 - Effect Of Temperature On Ultimate Stress Of Mortar Beams; Ref. 26.

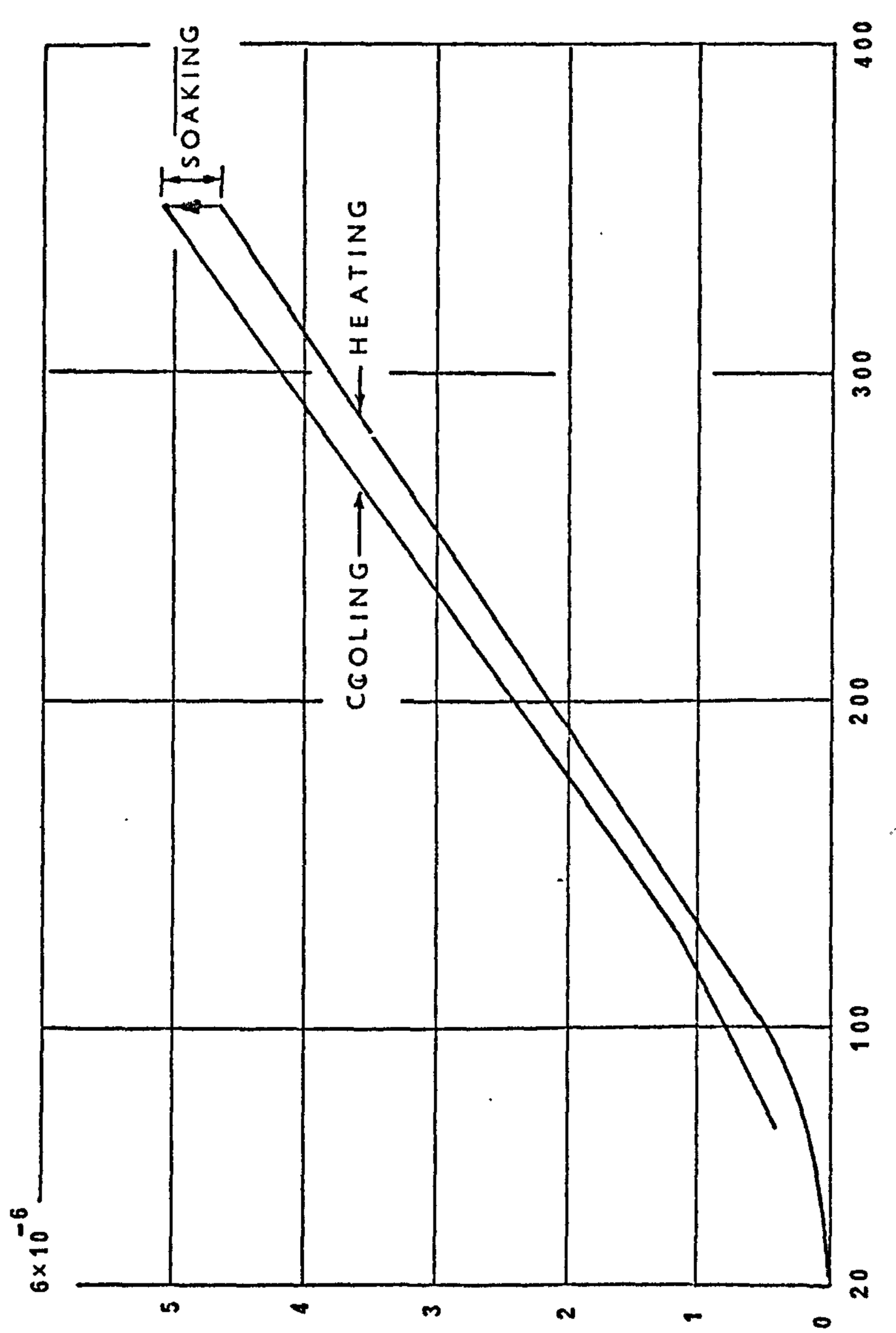

Fig.2.6- Effect Of Temperature On Longitudinal Movement; Reference 26.

CHAPTER THREE

III- Material Properties And Nonlinearity

3.1- Introduction

The purpose of this chapter is;

A- to discuss the behaviour of reinforced concrete structures and,

B- to present a numerical technique for describing this behaviour.

The concrete properties are discussed both in terms of the role of internal microcracking and of its response at an engineering level.

Concrete and steel materials subjected to higher temperatures are reviewed and some mathematical relationships between temperature and physical and mechanical properties of both materials are given, which are then used to analyse beams and slabs under high temperatures.

Numerical techniques for material nonlinearity are introduced in incremental form, which reduce a non-linear solution into the solution of a series of linear problems. At the final iteration the appropriate nonlinear conditions are satisfied.

It should be mentioned here that, a non-linear structural problem must obey the fundamental conditions of continuum mechanics, e.g. equilibrium, compatibility and the constitutive relations of the material.

3.2- Concrete

The physical property of normal concrete as a composite material depends on the properties of the constituents and mechanism of interaction (chemical and mechanical interaction between the aggregates and cement) in which stiffer and stronger particles (aggregates) are embedded in a softer and weaker cement paste. The property of the hardened cement paste which bonds the aggragates of different sizes depends primarily on the initial water-cement ratio and the degree of the hydration.

The stress-strain relationships of concrete obtained experimentally are dependent upon the size of the specimen, the induced states of stress and strain in the specimen, moisture condition and temperature and loading conditions.

The formation and propagation of microcracks are now accepted as the causes of fracture and failure of concrete. Microcracks may exist in the material prior to loading due to shrinkage; thermal effects, etc. Research carried out at Imperial College has shown that there are at least four stages in the process of crack initiation and propagation under all stress states [Ref. 94 and 95].

The crack propagations path may occur [Ref. 15];

A- at the aggregate paste interface,

B- within the cement paste or mortar matrix,

C- in the particles of aggregate.

The overal effect of microcracks reflected in the shape of the stress-strain curves observed experimentally is still necessary to describe the behaviour of concrete in

uniaxial, biaxial and triaxial states of stress. The stress-strain curves can then be expressed by various emperical formulae to be used in the numerical analysis, but to produce a criterion of failure for concrete has proved to be a difficult task for the investigator. The principal reasons that no simple criterion of failure is applicable to concrete and mortar at the present are as follows;

1- The complex and variable structure of many different types of concrete.

2- The complicated mechanisms of crack initiation and propagation up to failure under different states of stress.

3- The significant influence of loading conditions, the specimen size, moisture condition, temperature, etc., on the deformational and ultimate strength of concrete.

3.2.1- Biaxial Behaviour Of Concrete

Many workers investigated the behaviour of concrete under biaxial states of stress, using a variety of loading and testing conditions and several studies have been reported [Ref. 11, 16, 18, 20 and 96 to 99].

The overall behaviour of a test specimen under biaxial states of stress gives the following results;

1- Significantly higher strength is attainable for a given concrete in biaxial loading than uniaxial loading, [Ref. 11, 16 and 20]. The strength increase depends on the ratio between the applied stresses. It appears to be a

maximum (up to 27% higher than the uniaxial value) at a stress ratio of about 0.5 [Ref. 11 and 16] and diminishes at the ratio is increased to unity (up to about 16% higher than the uniaxial value), as in figure (3.1).

2- For primary study the stress-strain relationship of concrete under biaxial compression may be considered linear up to 30-35 per cent of the ultimate strength,

3- The concrete strain in the direction of the maximum principal compressive stress corresponding to the ultimate stress conditions varies from 0.002 (uniaxial) to 0.003 (biaxial), [Ref. 11].

4- The variation of Poisson's ratio from biaxial tension (0.18) to biaxial compression (0.20) is negligible.

A typical stress-strain relationship of concrete under biaxial compression for various ratio of stresses obtained by Kupfer [Ref. 11] and Liu Ref. 20 are given in figures (3.1) and (3.2), respectively.

3.2.2-Biaxial Stress-Strain Relationship Of Concrete

In this section the stress-strain relationship of concrete for numerical analysis at constant room temperature is given followed by the effect of high temperature on this relationship. A mathematical model derived for use in the analysis of reinforced concrete beams and slabs at high temperatures.

Experimental results on the behaviour of concrete confirm approximately linear behaviour in tension up to

30-35% of the ultimate strength at room temperature. As the state of stress is almost tensile in the tension elements, concrete can be assumed to be an elastic linear material and the crack occurs perpendicular to the direction of the major principal stress at the ultimate tensile strength of concrete [Ref. 88, 89 and 90].

The stress-strain relationships in the principal directions of a linear elastic, isotropic body can be written in the following form;

$$\underset{\sim}{\sigma}_p = \underline{D}_p \cdot \underset{\sim}{\epsilon}_p \qquad (3.1)$$

where, $\underset{\sim}{\sigma}_p$ and $\underset{\sim}{\epsilon}_p$ are principal stress and strain column vectors, respectively in which,

$$\underset{\sim}{\sigma}_p = \left\{ \sigma_1 \quad \sigma_2 \quad 0 \right\}^t$$

$$\underset{\sim}{\epsilon}_p = \left\{ \epsilon_1 \quad \epsilon_2 \quad 0 \right\}^t$$

and $\underline{D}_p$ is the elasticity matrix in principal directions given by;

$$\underline{D}_p = \frac{E}{1-\mu^2} \begin{bmatrix} 1 & \mu & 0 \\ \mu & 1 & 0 \\ 0 & 0 & \frac{1-\mu}{2} \end{bmatrix}_p \qquad (3.2)$$

where, E and μ are the modulus of elasticity and Poisson's ratio of material, respectively.

Liu et al [Ref. 21] developed a mathematical model of stress-strain relationship concerning the non-linear

behaviour of concrete under biaxial compression as follows;

$$\sigma = a_1 \cdot \frac{\epsilon E + a_2}{(1 - a\mu)(1 + \epsilon a_3 + \epsilon^2 a_4)} \qquad (3.3)$$

where, σ is the stress in the considered direction and ϵ is the corresponding strain. a is the ratio of principal stress in the direction considered. E and μ are the initial tangent modulus and Poisson's ratio in uniaxial loading and a_1 to a_4 are arbitrary constants which can be found by the following boundary conditions;

$$1- \quad \sigma = 0 \quad \text{and} \quad \frac{\partial \sigma}{\partial \epsilon} = \frac{E}{1 - a\mu}, \quad \text{when} \quad \epsilon = 0,$$

$$2- \quad \sigma = \sigma_m \quad \text{and} \quad \frac{\partial \sigma}{\partial \epsilon} = 0, \quad \text{when} \quad \epsilon = \epsilon_m.$$

where, σ_m and ϵ_m are the peak stress and corresponding strain in biaxial compression, respectively which are obtained from experiments.

By substituting the above boundary conditions and assuming $E' = \sigma_m / \epsilon_m$ as secant modulus, the equation (3.3) gives;

$$\sigma = E/(1 - a\mu)\left[1 + \frac{\epsilon}{\epsilon_m}\left(\frac{E}{E'} \cdot \frac{1}{1 - a\mu} - 2\right) + \left(\frac{\epsilon}{\epsilon_m}\right)^2\right] \qquad (3.4)$$

which is the general stress-strain relationship for concrete in biaxial compression given by Liu.

By substituting $a = 0$, equation (3.4) reduces to the equation proposed by Saenz [Ref. 9], and also by assuming $E = 2E'$ the reduced equation gives the stress-strain relationship suggested by Desayi [Ref. 8].

The mathematical expression (3.4) compares satis-

factorily with the experimental results obtained by Kupfer [Ref. 11] and Liu [Ref. 21] as in figures (3.3) and (3.4).

When dealing with material nonlinearity using numerical analysis, such as the finite element technique, the ratio of two principal stresses α, is required, in order to obtain stress σ_p, in principal direction from the strain ϵ_p in this direction. The initially assumed value α_o, may be far from the correct value of the actual stress ratio α. The newly calculated value α_1 based on the initial value α_o approaches the value α is a function of itself;

$$\alpha = f(\alpha) \qquad (3.5)$$

The convergence of solution depends on the shape of the equation (3.5), which is a simple mathematical problem. To avoid certain difficulties in the solution of equation (3.5) a formulation based on the strain ratio, rather than the stress ratio can be adopted as described below;

If concrete is assumed to be elastic, homogeneous and isotropic material, the biaxial stress-strain relationships in principal directions can be written as follows;

$$\sigma_1 = \frac{E}{1-\mu^2}(1+\mu\beta_1)\cdot\epsilon_1$$

$$\sigma_2 = \frac{E}{1-\mu^2}(1+\mu\beta_2)\cdot\epsilon_2 \qquad (3.6)$$

which can be expressed in the following form;

$$\sigma = \frac{E}{1-\mu^2}(1+\mu\beta)\cdot\epsilon \qquad (3.7)$$

where, σ_1, ε_1 and σ_2, ε_2 are the stresses and strains in the two principal directions, σ and ε are stress and strain both in a direction considered and β is the ratio of strain in the orthogonal direction to the strain to the strain in the direction considered, i.e.;

$$\beta_1 = \frac{\varepsilon_2}{\varepsilon_1} \quad , \quad \beta_2 = \frac{\varepsilon_1}{\varepsilon_2}$$

To obtain the biaxial stress-strain relationship, a similar mathematical expression to equation (3.3) is introduced as follows;

$$= a_1 \frac{\varepsilon E + a_2}{1 + a_3 \varepsilon + a_4 \varepsilon^2} (1 + \mu\beta) \qquad (3.8)$$

which must be satisfied the following boundary conditions;

$$1- \quad \sigma = 0 \quad \text{and} \quad \frac{\partial \sigma}{\partial \varepsilon} = E\frac{1+\mu\beta}{1-\mu^2} \quad \text{when} \quad \varepsilon = 0,$$

$$2- \quad \sigma = \sigma_m \quad \text{and} \quad \frac{\partial \sigma}{\partial \varepsilon} = 0 \quad \text{when} \quad \varepsilon = \varepsilon_m,$$

where the notations have the same meaning as previously.

By substituting these boundary conditions in the above equation, the biaxial stress-strain relationship of concrete becomes as follows;

$$\sigma = \frac{(1+\mu\beta).E.\varepsilon}{\left[(1-\mu^2)\ 1-(2-\frac{1+\mu\beta}{1-\mu^2}.\frac{E}{E'})\frac{\varepsilon}{\varepsilon_m} + (\frac{\varepsilon}{\varepsilon_m})^2\right]} \qquad (3.9)$$

This stress-strain relationship is similar to the expression (3.4), but expressed in terms of strain ratio.

The instantanous modulus of elasticity is obtained from equation (3.9) as below;

$$E_i = \frac{\partial \sigma}{\partial \varepsilon}$$

or,

$$E_i = \frac{(1+\mu\beta)\left[1-\left(\frac{\varepsilon}{\varepsilon_m}\right)^2\right] . E}{(1-\mu^2)\left[1-\left(2-\frac{1+\mu\beta}{1-\mu^2}\cdot\frac{E}{E'}\right)\frac{\varepsilon}{\varepsilon_m}+\left(\frac{\varepsilon}{\varepsilon_m}\right)^2\right]^2} \qquad (3.10)$$

and the modulus of elasticity in the principal directions (E_1 and E_2) corresponding to strains (ε_1 and ε_2) and their ratio (β_1 and β_2) can easily be determined. Thus the biaxial incremental stress-strain relationships of concrete can be written in a matrix form as follows;

$$\underset{\sim}{\sigma}_p = \underline{D}_p \cdot \underset{\sim}{\varepsilon}_p$$

where, $\underset{\sim}{\sigma}_p$ and $\underset{\sim}{\varepsilon}_p$ are the incremental stress and strain vectors in the principal directions, and;

$$\underline{D}_p = \begin{bmatrix} E_1 & 0 & 0 \\ 0 & E_2 & 0 \\ 0 & 0 & G \end{bmatrix}_p \qquad (3.11)$$

where the shear modulus G not available as experimental data. The special case of orthotropy in which the additional relation exist among the principal elastic constant [Ref. 91] was assumed as follows;

$$G = \frac{E_1^* \cdot E_2^*}{E_1^* + (1+2)E_2^*} \qquad (3.12)$$

As the Poisson's ratio is already considered in the assessment of shear modulus, the values E_1^* and E^*_2 are hence obtained by seperating Poisson's ratio effect from E_1 and E_2 respectively, which gives;

$$E_i^* = \frac{E_i}{F_i} \qquad i= 1, 2$$

where,

$$F_i = \frac{1+ \mu \beta_i}{1- \mu^2} \qquad i= 1, 2$$

It should be observed that, E_1 and E_2 were the assumed modulus of elasticity of concrete in the principal compressive stress directions under biaxial compression. In biaxial tension , $E_1 = E.F_1$ and $E_2 = E \cdot F_2$ were assumed up to failure in the both directions, where E is the initial modulus in uniaxial compression. In tension-compression case $E_1=E$ and $E_2=E_2$ are assumed in the principal tensile stress and principal compressive stress directions.

3.2.3- Effect Of High Temperature On The Properties Of Concrete.

This section includes a brief review of the effect of high temperature on the concrete properties and a series of mathematical expressions are established to use in the numerical analysis of reinforced concrete beams and slabs.

Generally, temperature influences many properties

of concrete including specific density, uniaxial and biaxial compressive strength, flexural strength, elasticity modulus, thermal conductivity, diffusivity and coefficient of thermal expansion. These variations depend on the water-cement ratio, aggregate-cement ratio, aggregate type and age of concrete.

3.2.3.1- Mechanical Properties

The three properties of concrete, compressive and tensile strength and modulus of elasticity decrease with increasing temperature and the rate and decrease are still a matter of controversy. The main factors that influence these properties are moisture, water-cement ratio, curing and age, cement type and aggregate type. The envelope model for the modulus of elasticity against the temperature values Ref. 28 is shown in figure (3.5). Also the stress-strain relationships for a typical concrete at three different temperatures 68 ^{o}F (20 ^{o}C), 600 ^{o}F (300 ^{o}C) and 1200 ^{o}F (650 ^{o}C) are shown in figure (3.6), given by Bizri [Ref. 28], in which, the peak values of stress occur at 0.002 strain. In the present numerical analysis of beams and slabs under service load and high temperature, the equation (3.10) is used for various peak values of stress corresponding to variable strain values as shown in figure (3.7). To obtain a mathematical expression between stress, strain and also temperature, a polynomial of second order (parabola) is used to cover the stress-strain relationships of concrete at any required temperature in the following form;

$$\sigma = a_1.T^2 + a_2.T + a_3 \qquad (3.13)$$

where, T is the temperature, σ is the corresponding value of stress and a_1, a_2 and a_3 are functions of strain. The following initial values are used to calculate the functions a_1, a_2 and a_3;

$\sigma = \sigma_{20}$ when T = 20 °C,

$\sigma = \sigma_{300}$ when T = 300 °C,

$\sigma = \sigma_{650}$ when T = 650 °C,

where, σ_{20}, σ_{300} and σ_{650} are equations of stress-strain which are obtained by substituting the peak values of stress and strain at corresponding temperatures in equation (3.9). By a simple mathematical operation, the three functions a_1, a_2 and a_3 become as follows;

$$a_1 = \frac{1}{8820}(0.05\,\sigma_{20} - 0.09\,\sigma_{300} + 0.04\,\sigma_{650})$$

$$a_2 = \frac{1}{8820}(-47.5\,\sigma_{20} + 60.3\,\sigma_{300} - 12.8\,\sigma_{650})$$

$$a_3 = \frac{1}{8820}(9750\,\sigma_{20} - 1170\,\sigma_{300} + 240\,\sigma_{650})$$

A similar equation to (3.13) can be found for the modulus of elasticity as follows;

$$E = b_1.T^2 + b_2.T + b_3 \qquad (3.14)$$

where,

$$b_1 = \frac{1}{8820}(0.05\,E_{20} - 0.09\,E_{300} + 0.04\,E_{650})$$

$$b_2 = \frac{1}{8820}(-47.5\ E_{20} + 60.3\ E_{300} - 12.8\ E_{650})$$

$$b_3 = \frac{1}{8820}(9750\ E_{20} - 1170\ E_{300} + 240\ E_{650})$$

where, E_{20}, E_{300} and E_{650} are modulus of elasticity equations obtained from equation (3.10), by substituting the peak values of stresses and corresponding strains at temperature T. In the finite element method of analysis, equation (3.9) gives the actual stresses corresponding to the strains, which are availabe from the analysis due to external loads and these values of stress are compared with the stresses obtained from the numerical analysis due to external loads and the differs of these two stress values (unbalanced stresses) are released in terms of nodal forces of elements and this iteration is continued untill the numerical values of stress reach the actual values obtained from equation (3.9). In the case of temperature, the modulus of elasticity is calculated from equation (3.14) and stresses obtained from numerical analysis are compared with equation (3.13) and the unbalanced stresses are released and the iteration is continued.

3.2.3.2- Physical Properties

1- Conductivity

At the normal room temperature different aggregates have different conductivities, but it has been found by many investigators [Ref. 31 and 32] that the conductivity of most concretes decreases with increase in temperature, with a few

exceptions, where the conductivity remains essentially constant. The aggregate type, aggregate cement ratio and water-cement ratio are the main factors influencing the conductivity of concrete. The age of the concrete has a slight effect on the initial value of conductivity but this effect is negligible, especially at higher temperature. The envelope model for conductivity of concrete which has been derived from many experimental results given in [Ref. 28] is shown in figure (3.8), and the conductivity-temperature relationship derived from this envelope model and used in the present numerical analysis is shown in figure (3.9).

2- Specific Heat And Density

The temperature has a slight effect on the values of density and specific heat of concrete. The values of density and specific heat of concrete used in the numerical analysis, which can be found elsewhere [Ref. 28 and 100]; were 150 LB/FT^3 and 0.272 $BTU/LB-^oF$, respectively.

3- Diffusivity

The diffusivity of any material is calculated by;

$$h = \frac{k}{\rho \cdot c} \qquad (3.15)$$

where, k is conductivity, ρ is density and c is the specific heat of material. For concrete material the conductivity is given by figure (3.9), ρ = 150 LB/FT^3 and c=0.272 $BTU/LB-^oF$

used for the present numerical analysis. As the diffusivity of concrete is proportional with conductivity, decreases with increase in temperature, and in a few cases, remains constant. By using the above values, the relationship between temperature and diffusivity becomes as shown in figure (3.10) and give the following values;

$h = 40.47\times10^{-2}$ $cm^2/min.$ when, $0 \leq T \leq 200$ ^oC,

$h = (40.47-0.0406\ T/2295)\times10^{-2}$ $cm^2/min.$ when,

$200 \leq T \leq 870$ ^oC,

$h = 19.2672\times10^{-2}$ $cm^2/min.$, when 870 $^oC \leq T$

4- Coefficient Of Thermal Expansion

Moisture and evaporation of water, the aggregate type and water-cement ratio are the main factors effecting the thermal expansion of concrete, but curing and age have a slight effect have been neglected. Generally, the thermal coefficient of expansion of concrete increases with increase in temperature. An envelope model covering most experimental results given in [Ref. 28], for this coefficient is shown in figure (3.11). A model which used in the present study chosen from the above envelope model is given in figure (3.12) which has the following mathematical expressions;

$\alpha = (0.027T + 10.8)\times10^{-6}$ $/^oC$, when $0 \leq T \leq 200$ ^oC,

$\alpha = (0.144T - 7.20)\times10^{-6}$ $/^oC$, when $200 \leq T \leq 300$ ^oC,

$$\alpha = 36 \times 10^{-6} \ / \ ^{o}C, \quad \text{when} \quad 300 \ ^{o}C \leq T.$$

5-Surface Temperature Coefficient

Investigation of test results show that the surface temperature is always lower than the furnace temperature. From a careful study of the time-temperature curves obtained from fire tests on Double-T units, by Odeen [Ref. 101], and on two symmetrically placed steel frames by Pettersson [Ref. 102] and Kollbrunner [Ref. 103], it appears that the surface to furnace temperature ratio varies approximately from about 0.4 to 0.8 for fires of duration from quarter of an hour to two hours.

For the purpose of the present analysis, a factor dependent on the duration of fire is used. A basic ratio of 0.4 at one minute, and an increase of 0.005 per minute is used for fires up to two hours duration, as shown in figure (3.14). Represented mathematically it is given by;

$$r = 0.4 + 0.005\ t$$

where r is temperature ratio and t is time elapsed in minutes.

3.3- Steel Reinforcement

The stress-strain relationship of the reinforcing steel is taken as linear which is not very far from the experimental data, represented by a mathematical expression.

3.3.1- Effect Of Temperature

On properties of steel

The modulus of elasticity and yield strength of steel usually show an immediate and continueous decrease in value with any temperature rise with some exceptional cases. The stress-strain relationships of steel at three different values of temperature 68 ^{o}F (20 ^{o}C), 600 ^{o}F (300 ^{o}C) and 1200 ^{o}F (650 ^{o}C) used by Bizri Ref. 28 are shown in figure (3.13). As this figure illustrates, the reinforcing steel yields at constant strain (0.0015) at any temperature values. In the present numerical analysis it is assumed that the strains, corresponding to yield stresses are also varied linearly, with temperature as shown in figure (3.15). This variation of steel strength is given by a simple linear equation to cover the stress of steel at any temperatures against the strain values.

The conductivity of steel also decreases with increase in temperature, but it remains constant at higher temperatures.

Temperature has a slight effect on the value of density of steel. The specific heat of steel increases with increase in temperature and remains constant at higher temperature. The temperature-conductivity and specific heat temperature relationships of steel used in the analysis are shown in figures (3.16) and (3.17), respectively.

By the foregoing assumptions the diffusivity of reinforcing steel is calculated by equation (3.15), and the

diffusivity-temperature relationship which is used in the present investigation is given in figure (3.18) by the following mathematical expression;

$$h = 15.7286\,\frac{-7.5T+\ 24750}{20.9T+\ 42075}\ \ cm^2/min.\ \text{when}\ 0 \le T \le 400\ ^{\circ}C$$

$$h = 15.7286\,\frac{-7.0T+\ 23100}{31.9T+\ 29975}\ \ cm^2/min.\ \text{when}\ 400 \le T \le 600$$

$$h = 3.7233\ cm^2/mi.\quad \text{when}\quad 600\ ^{\circ}C \le T.$$

then the diffusivity of steel decreases with increase in temperature.

Finally, the coefficient of thermal expansion of steel increases with increase in temperature as in figure (3.19) and described by the following two mathematical expressions;

$$\alpha = (0.0144T + 10.8)\times10^{-6}\ \ /\ ^{\circ}C,\quad \text{when}\ 0 \le T \le 800\ ^{\circ}C$$

$$\alpha = 21.0\times10^{-6}\ \ /\ ^{\circ}C,\ \text{when}\quad 800\ ^{\circ}C \le T.$$

3.4- Numerical Solution Of Material Nonlinearity

In the finite element method, the solution of the structural problems with nonlinear materials has to satisfy the compatibility condition. This is automatically satisfied at the nodal points of elements, hence the problem is to ensure that the constitutive relation can be made to preserve the equilibrium of the structure.

A series of linear equations is selected to describe the nonlinear equation to a specified degree of accuracy. As the stress-strain relationship at any point of structure is nonlinear, the force-displacement relationship also becomes nonlinear as in figure (3.20), since the stiffness matrix includes the above nonlinear equations. The nodal force-displacement relationship can then be written as follows;

$$\underset{\sim}{F} = \underline{K} \cdot \underset{\sim}{\delta} \qquad (3.16)$$

where, $\underset{\sim}{F}$ and $\underset{\sim}{\delta}$ are nodal force and displacement vectors and $\underline{K}$ is the stiffness matrix. The solution of the non-linear problems can usually be performed in one of three ways;

1- Incremental method.

2- Iteration method.

3- Mixed method.

The mixed method was used in the analysis. This involves the use of the incremental and iterative techniques and the three methods will therefore be described here.

In the incremental method the load is subdivided into many small increments, which are not necessarily equal. The nodal forces are applied incrementally and at each increment the equation (3.16) is assumed to be linear. By solving this equation the incremental nodal displacements are obtained and then added to the previous accumulated displacements to obtain the total displacements of the nodal points. The incremental process is continued until the total load is reached. The stiffness matrix $\underline{K}$ may be taken different values during different load increments.

The incremental strains at any required point of the structure are obtained from the incremental displacements and are added to the previous values to determine the total values of strains of the point. The same technique is used to find the incremental and total values of stresses from incremental strains. The incremental displacements have been calculated from equation (3.16) in which, the stiffness matrix $\underline{K}$ is evaluated at the end of the previous increment, and the relationship of the present stress and strain gives the stiffness matrix of the next increment. A typical nodal force-displacement and stress-strain relationships in the incremental method are shown in figures (3.20) and (3.21), respectively. The accuracy of the incremental method for solution of nonlinear problems can be improved by taking smaller increments of load but this increases the computational time considerably.

The iteration method consists of a sequence of calculations in which the structure is fully loaded in each iteration. Due to the assumed initial constant value of the stiffness matrix the constitutive stress-strain relationship is not necessarily satisfied and a correction is made to satisfy this relationship. The self equilibrating forces due to this correction is evaluated and to maintain the equilibrium, a set of opposite self equilibrating forces, which are called unbalanced forces, are applied to the structure in the next iteration. The process is continued until the unbalanced forces become sufficiently small.

Solution of such a problem can be accomplished in

a number of ways which depend on the method of computation of the stiffness matrix and unbalanced forces.

Generally, the nonlinear relationship between the stresses $\underset{\sim}{\sigma}$ and the strains $\underset{\sim}{\varepsilon}$ can be defined as follows;

$$\underset{\sim}{\sigma} = \underline{D} \cdot \underset{\sim}{\varepsilon} \qquad (3.17)$$

where, $\underline{D}$ is the elasticity matrix. The corresponding linear stress-strain relationship to equation (3.17) can be written in the following form;

$$\underset{\sim}{\sigma} = \underline{D}^{*} \cdot (\underset{\sim}{\varepsilon} - \underset{\sim}{\varepsilon}_{o}) + \underset{\sim}{\sigma}_{o} \qquad (3.18)$$

where, $\underline{D}^{*}$ is a constant linear elasticity matrix, and initial strains $\underset{\sim}{\varepsilon}_{o}$ and stresses $\underset{\sim}{\sigma}_{o}$ are variable of such a magnitude as to make up the difference between two nonlinear and linear equations. The unbalanced forces can be calculated in either initial stresses or initial strains and the choice of the method and also the speed of convergency depend on the constitutive law governing the behaviour of the material.

In the initial strain method the equations (3.18) is reduced to the following equations;

$$\underset{\sim}{\sigma} = \underline{D}^{*} \cdot (\underset{\sim}{\varepsilon} - \underset{\sim}{\varepsilon}_{o}) \qquad (3.19)$$

and this equation is solved by assuming $\underset{\sim}{\varepsilon}_{o} = 0$ initially with an appropriate constant elasticity matrix to obtain a certain level of stress $\underset{\sim}{\sigma}_{1}$ and strain $\underset{\sim}{\varepsilon}_{1}^{*}$ as follows;

$$\underset{\sim}{\varepsilon}_{1}^{*} = \underline{D}^{*-1} \cdot \underset{\sim}{\sigma}_{1}$$

whereas the strain which should have occured is;

$$\underset{\sim}{\varepsilon}_1 = \underline{D}^{-1} \cdot \underset{\sim}{\sigma}_1$$

The difference of strains,

$$\underset{\sim}{\varepsilon}_o = \underset{\sim}{\varepsilon}_1 - \underset{\sim}{\varepsilon}_1^*$$

is now used as an initial strain in equation (3.19) and the corresponding unbalanced forces element are obtained as in below;

$$\underset{\sim}{F}_o = \int \underline{B}^t \cdot \underline{D}^* \cdot \underset{\sim}{\varepsilon}_o \cdot dv$$

where, $\underline{B}$ is the strain matrix and v is the volume of the element. This process is continued until initial strains $\underset{\sim}{\varepsilon}_o$ or unbalanced forces $\underset{\sim}{F}_o$ become negligible.

In the initial stress method the equation (3.18) is simplified to the following form;

$$\underset{\sim}{\sigma} = \underline{D}^* \cdot \underset{\sim}{\varepsilon} + \underset{\sim}{\sigma}_o \qquad (3.20)$$

and similar to the initial strain method, the equation (3.20) is solved by assuming $\underset{\sim}{\sigma}_o = 0$ initially with an appropriate constant elasticity matrix to reach a certain level of strain $\underset{\sim}{\varepsilon}_1$ and corresponding stress $\underset{\sim}{\sigma}_1^*$;

$$\underset{\sim}{\sigma}_1^* = \underline{D}^* \cdot \underset{\sim}{\varepsilon}_1$$

On the other hand the correct stress which should have occured is calculated by;

$$\underset{\sim}{\sigma}_1 = \underline{D} \cdot \underset{\sim}{\varepsilon}_1$$

and the difference of above two stresses;

$$\underset{\sim}{\sigma}_o = \underset{\sim}{\sigma}_1^* - \underset{\sim}{\sigma}_1$$

is now used as an initial stress in equation (3.20) and the corresponding unbalanced nodal forces of element are obtained from;

$$\underset{\sim}{F}_o = \int \underline{B}^t \cdot \underset{\sim}{\sigma}_o \cdot dv$$

and the process is continued until no appreciable change between two successive iteration exist and $\underset{\sim}{\sigma}_o$ or $\underset{\sim}{F}_o$ become negligible. The initial strain or stress method, in the constant stiffness approach, for a required point within an element are shown in figures (3.22) and (3.23), respectively.

In the iterative technique the stiffness matrix may be chosen as a constant or variable. In the former to constant stiffness matrix is used throughout the analysis and the problem is solved by initial stress or strain technique to calculate the unbalanced nodal forces. In the variable stiffness process a linear solution is preformed each time with the elasticity matrix adjusted from stress or strain level reached at the previous iteration and the unbalanced forces are calculated by initial stress or strain method. A typical model of force-displacement relationship using secant modulus to form the stiffness matrix at each iteration is shown in figure (3.24). Figure (3.25) illustrates a typical nodal force-displacement relationship using tangent modulus. The initial strain and stress methods in the secant modulus approach are shown in figures (3.26) and (3.27),

respectively. In the tangent modulus approach the initial strain and stress methods are shown in figures (3.28) and (3.29), respectively.

The mixed procedure combines the incremental and iterative methods, by approaching the load incrementally and successive iterations preformed after each increment.

The advantage of the incremental method of solution of nonlinear problem is that, it provides a relatively complete description of the load deformation behaviour and the results are obtained at each incremental step. On the other hand the disadvantage of this method is the difficulty of knowing in advance what increments of load are necessary for a good approximation to the exact solution.

The incremental method usually needs more computing time than the iterative technique.

The iterative method is more useful when the material has different properties in tension and compression and is easier to use and faster. The constant stiffness process in iterative method needs a greater number of iterations, but as it is not necessary to invert a new stiffness matrix at each step, it saves the computational time considerably. The rapid convergence to the solution is obtained using a variable stiffness, because the stiffness matrix is modified in each iteration but the computational time is high.

However, the limitation of the iterative procedure is that, the displacements, stresses and strains are obtained for only one load increment.

Finally, the mixed method combines the advantages

of both incremental and iterative procedures and minimizes the disadvantages of each method.

Different mixed methods are used in the present study to deal with material nonlinearities of the beam and slab analysis. The unbalanced nodal forces due to residual stress of cracking, crushing and yielding have been evaluated using initial stress method and the initial strain method is used to take into account the effect of temperature. For a strain reached at the end of each iteration, the difference between the stresses obtained by the analysis and the actual stresses from the constitutive law of the material, was used as the initial stresses, and converted into the nodal forces, and these forces were then applied to the structure in the next iteration.

The stiffness matrix of structure was updated according to a predefined condition. For monotonic nonlinear behaviour of concrete and steel materials a mixed procedure using the secant modulus approach was found to be most efficient.

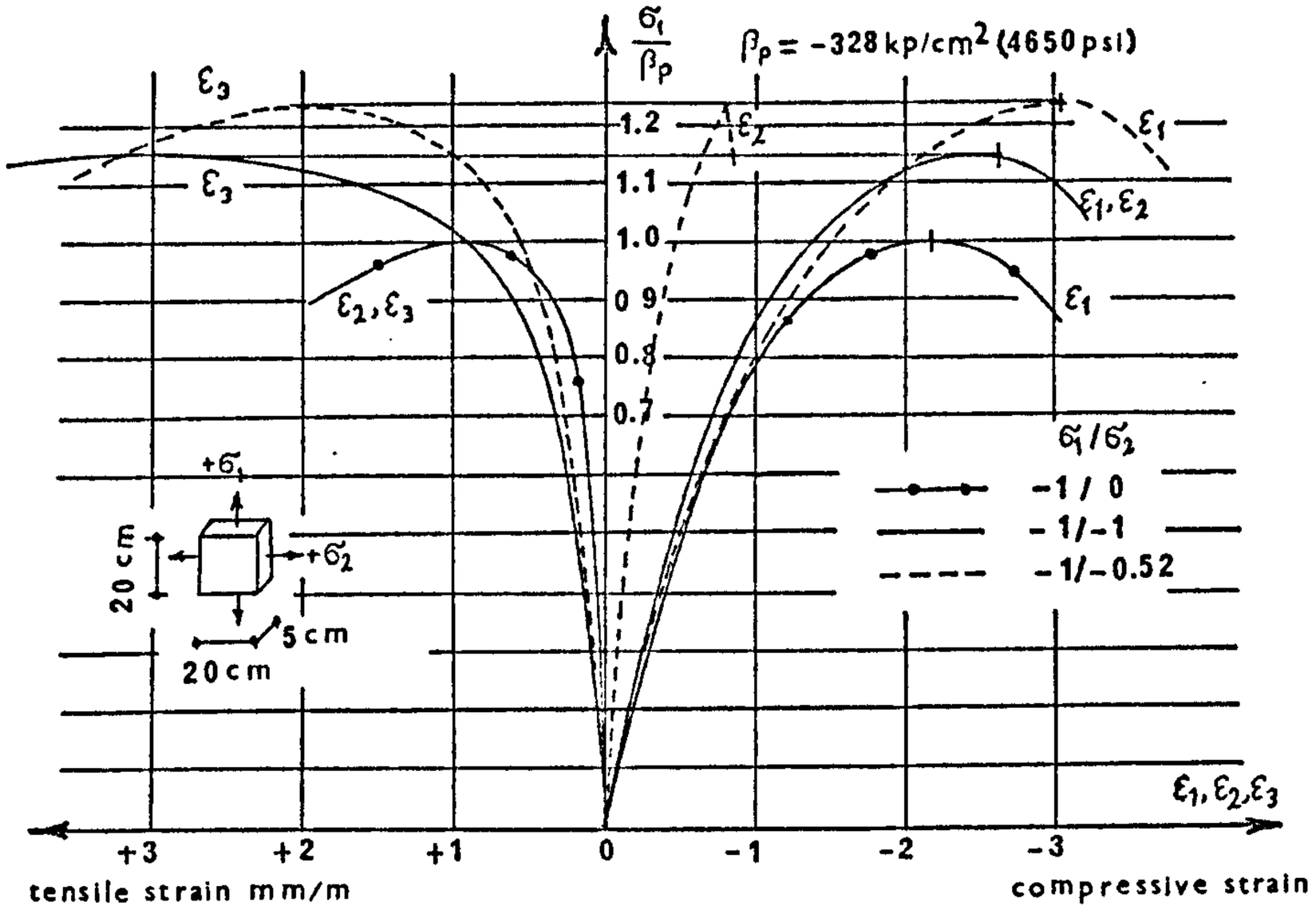

Fig.3.1_Stress-strain relationships of concrete under biaxial compression; Ref.11.

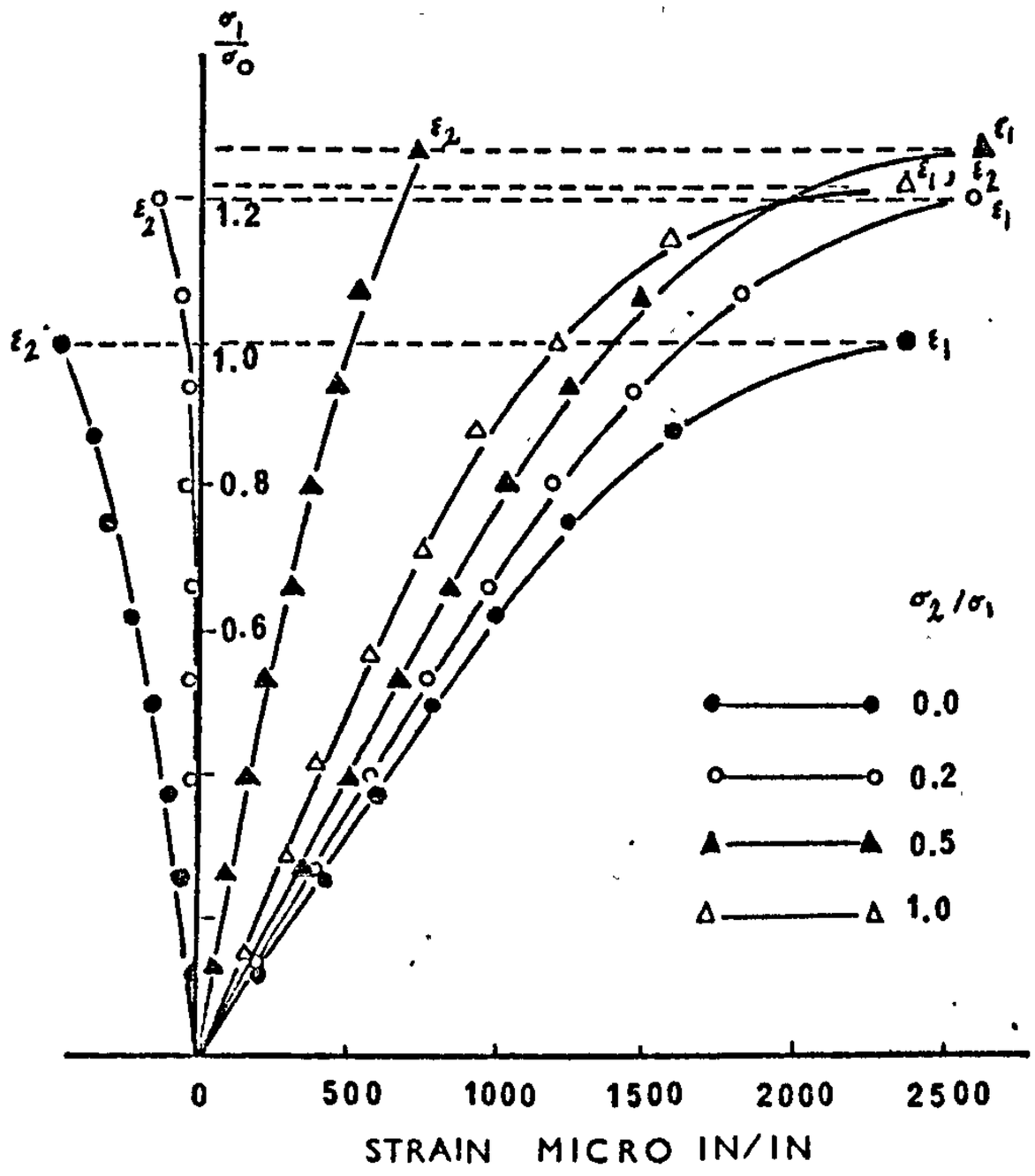

Fig.3.2_Typical stress-strain relation of concrete under biaxial compression; Ref.20.

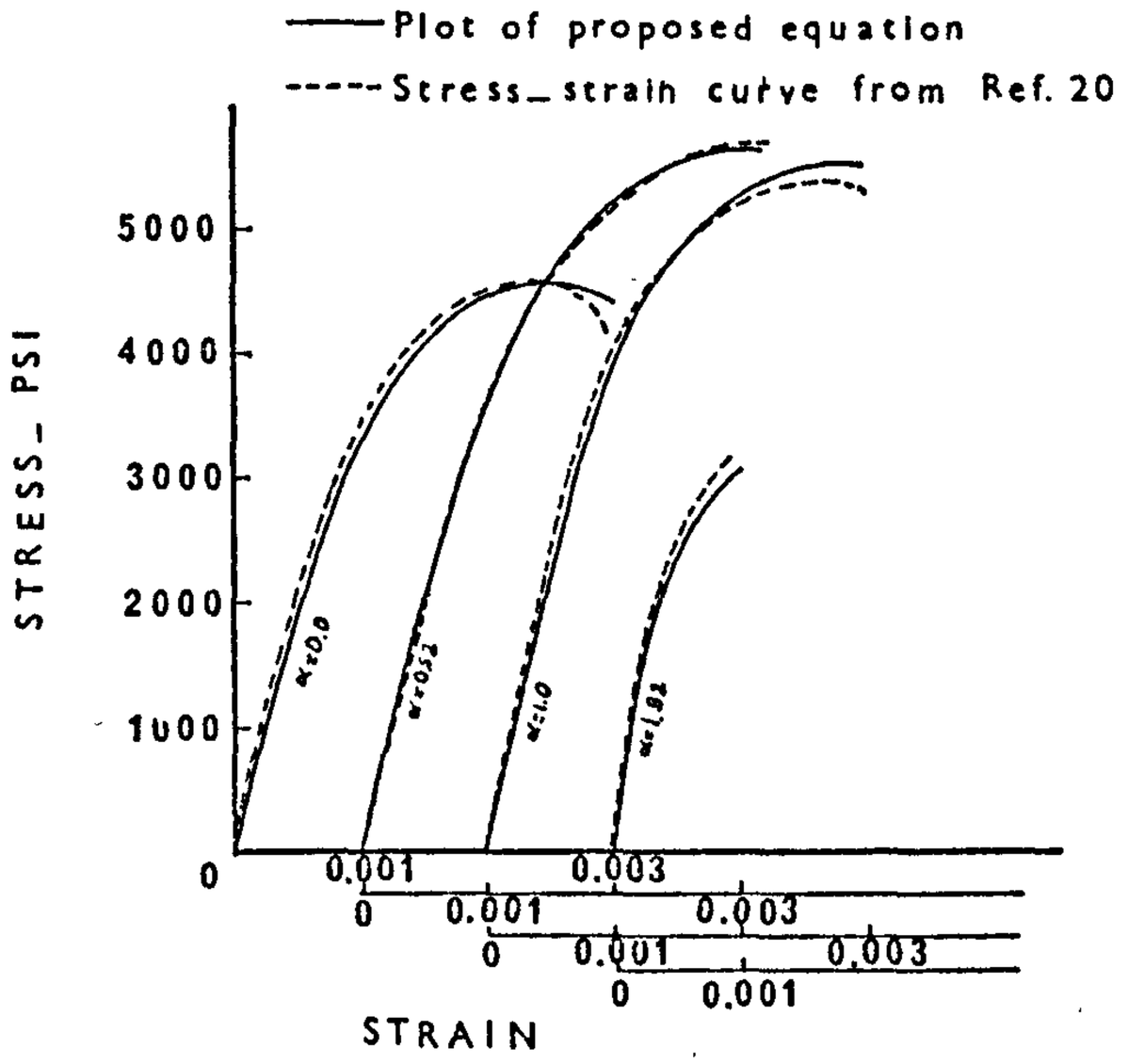

Fig. 3.3_COMPARISON OF PLOT OF PROPOSED EQUATION WITH THOSE OBTAINED FROM BIAXIAL COMPRESSION TESTS (2); Ref. 21

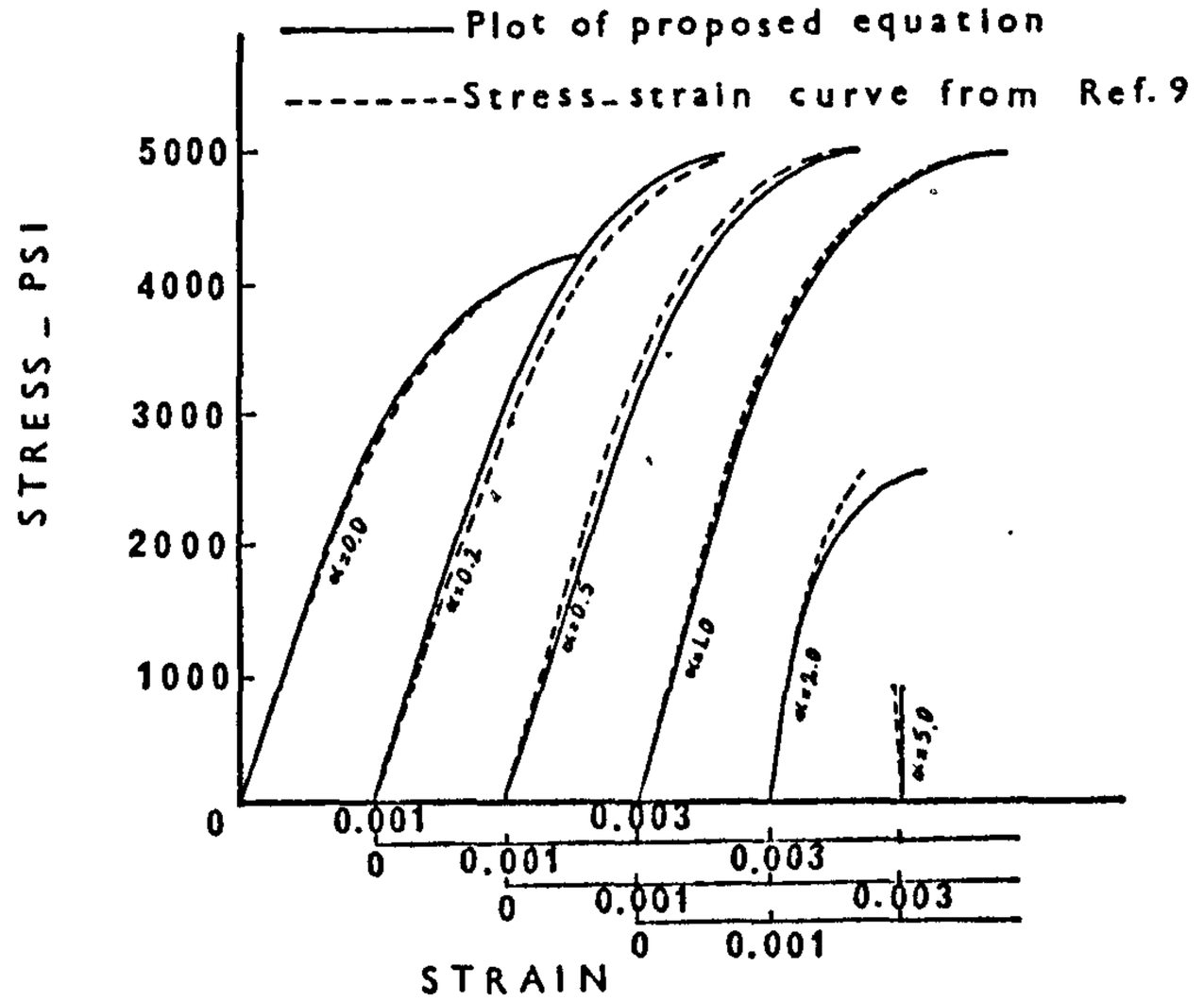

Fig. 3.4_ COMPARISON OF PIOT OF PROPOSED EQUATION WITH THOSE OBTAINED FROM BIAXIAL COMPRESSION TESTS (3); Ref. 21

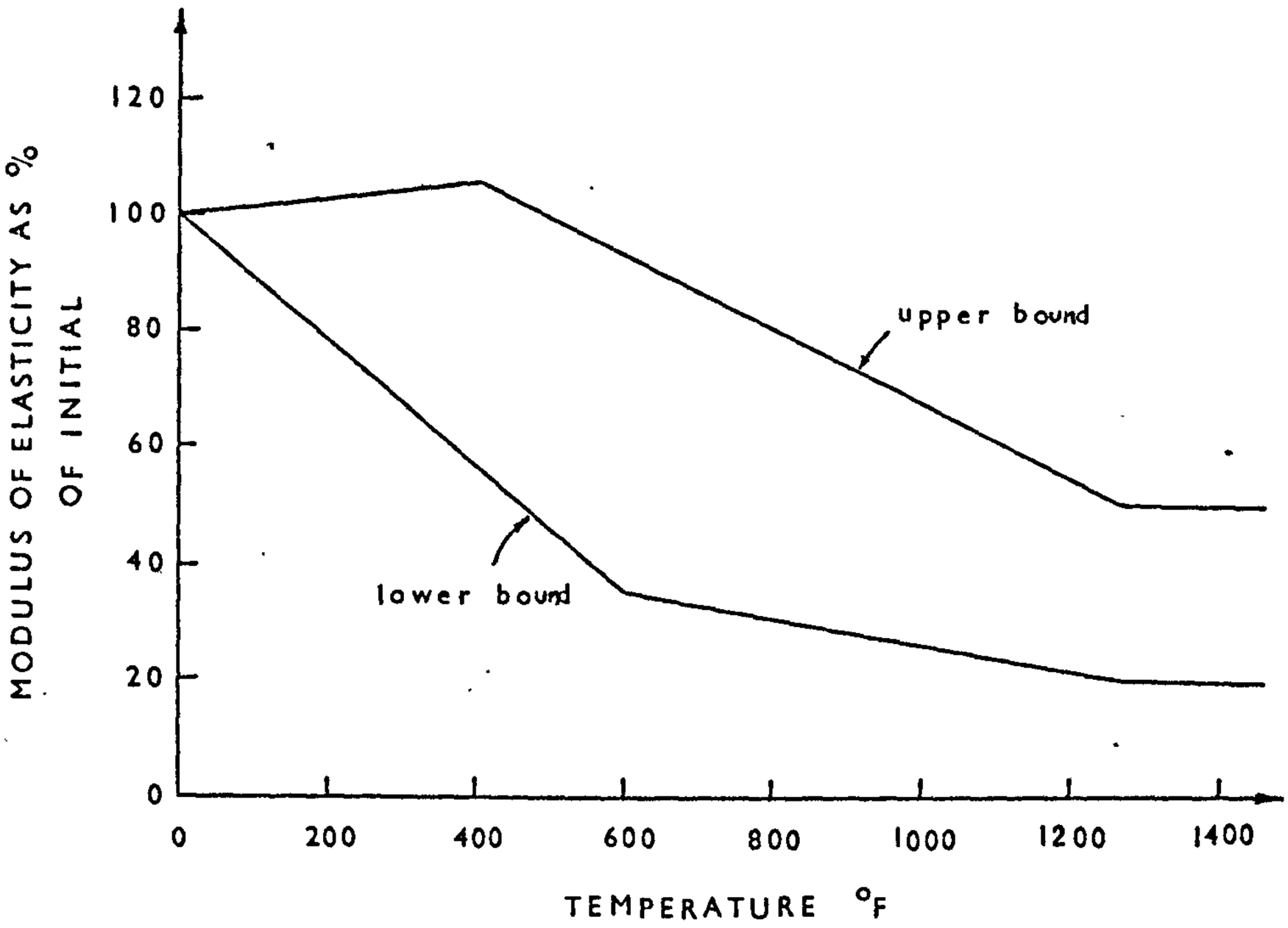

Fig.3.5_ ENVELOP MODEL FOR MODULUS OF ELASTICITY OF CONCRETE; Ref. 28

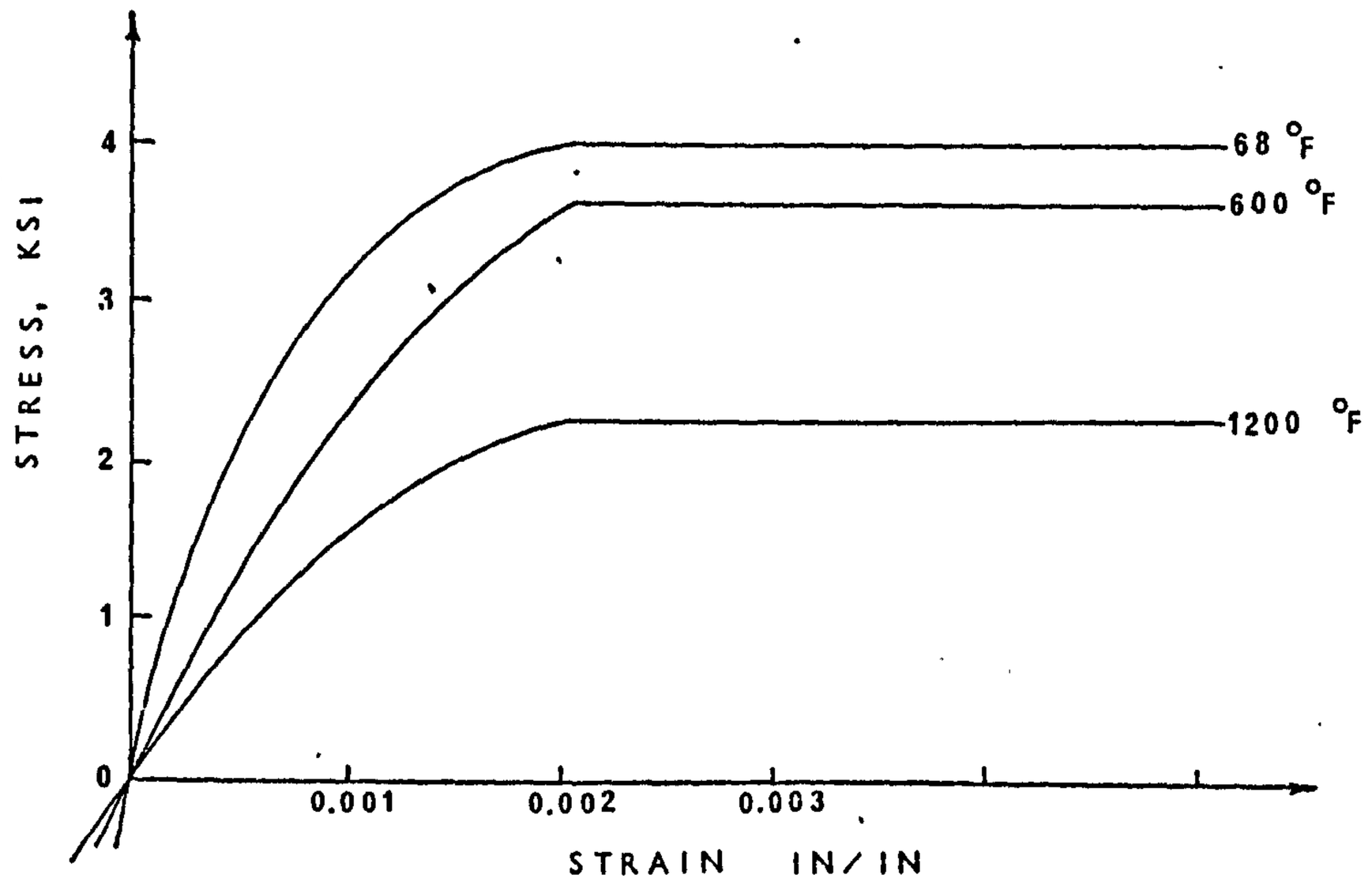

Fig. 3.6_ STRESS_STRAIN RELATIONSHIPS OF CONCRETE AT THREE DIFFERENT TEMPERATURS; Ref. 28

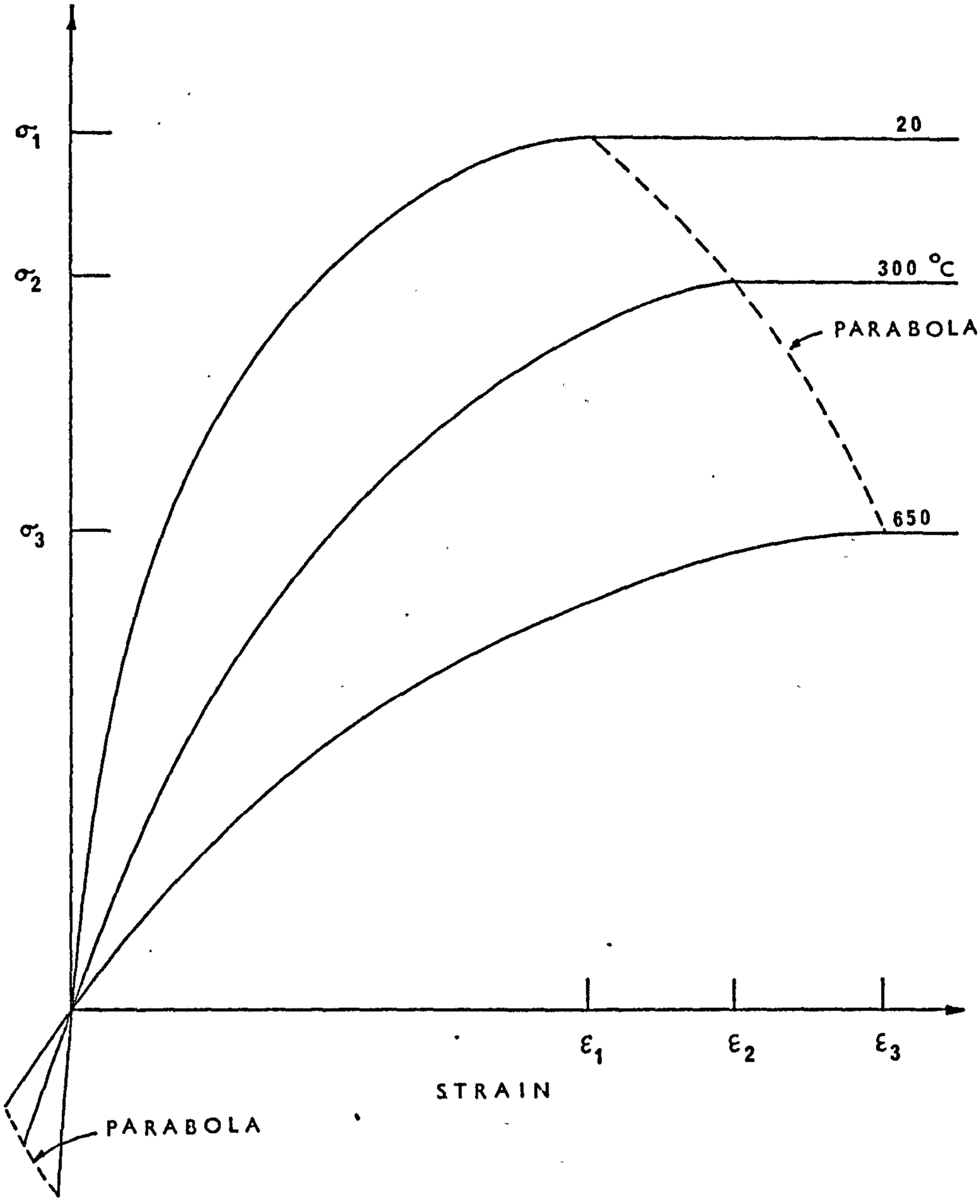

Fig. 3.7_ STRESS_STRAIN CURVES FOR CONCRETE AT THREE DIFFERENT TEMPERATURE VALUES USED IN THE NUMERICAL ANALYSIS.

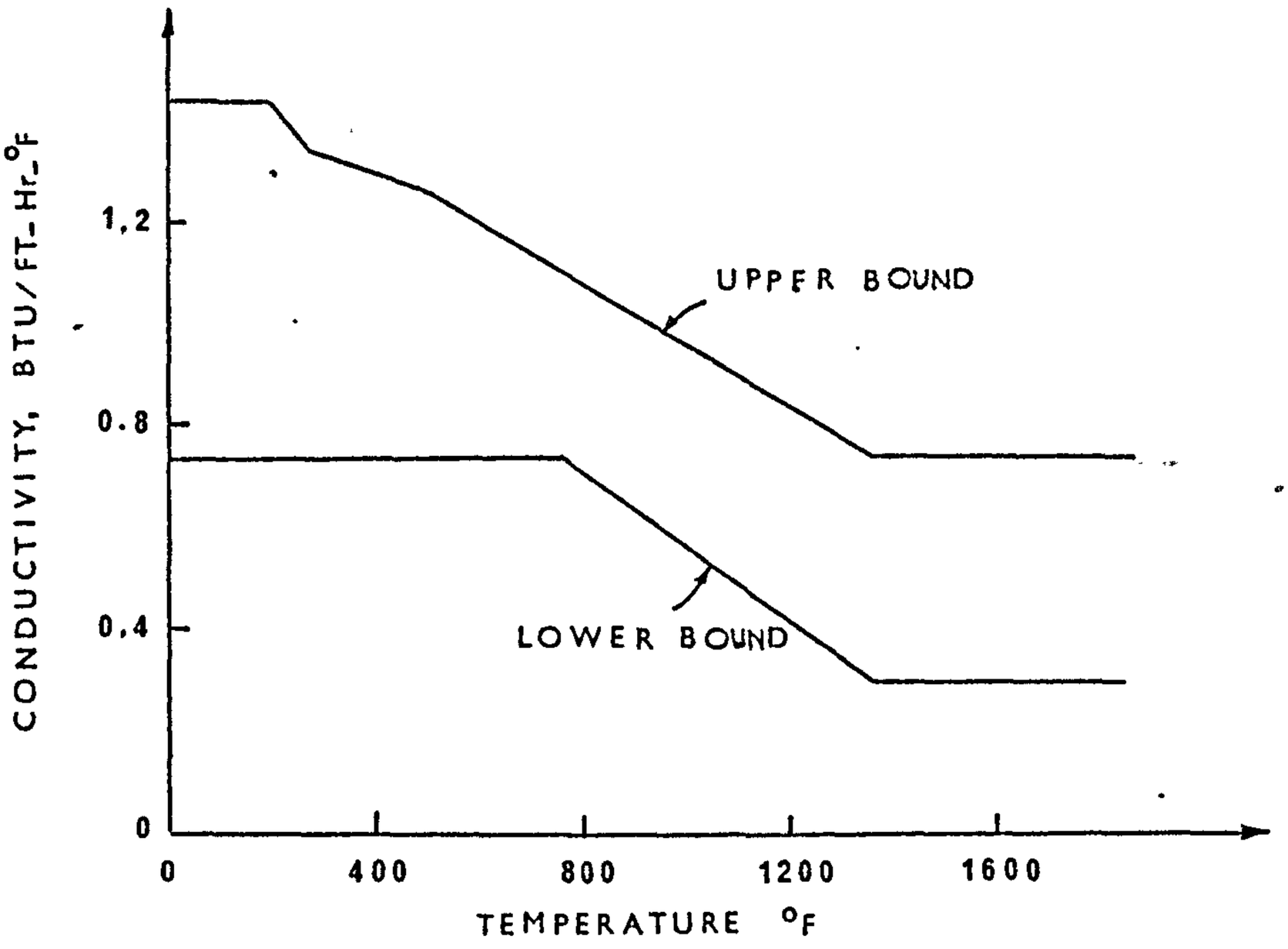

Fig. 3.8 - ENVELOPE MODEL FOR CONDUCTIVITY OF CONCRETE;

Ref. 28

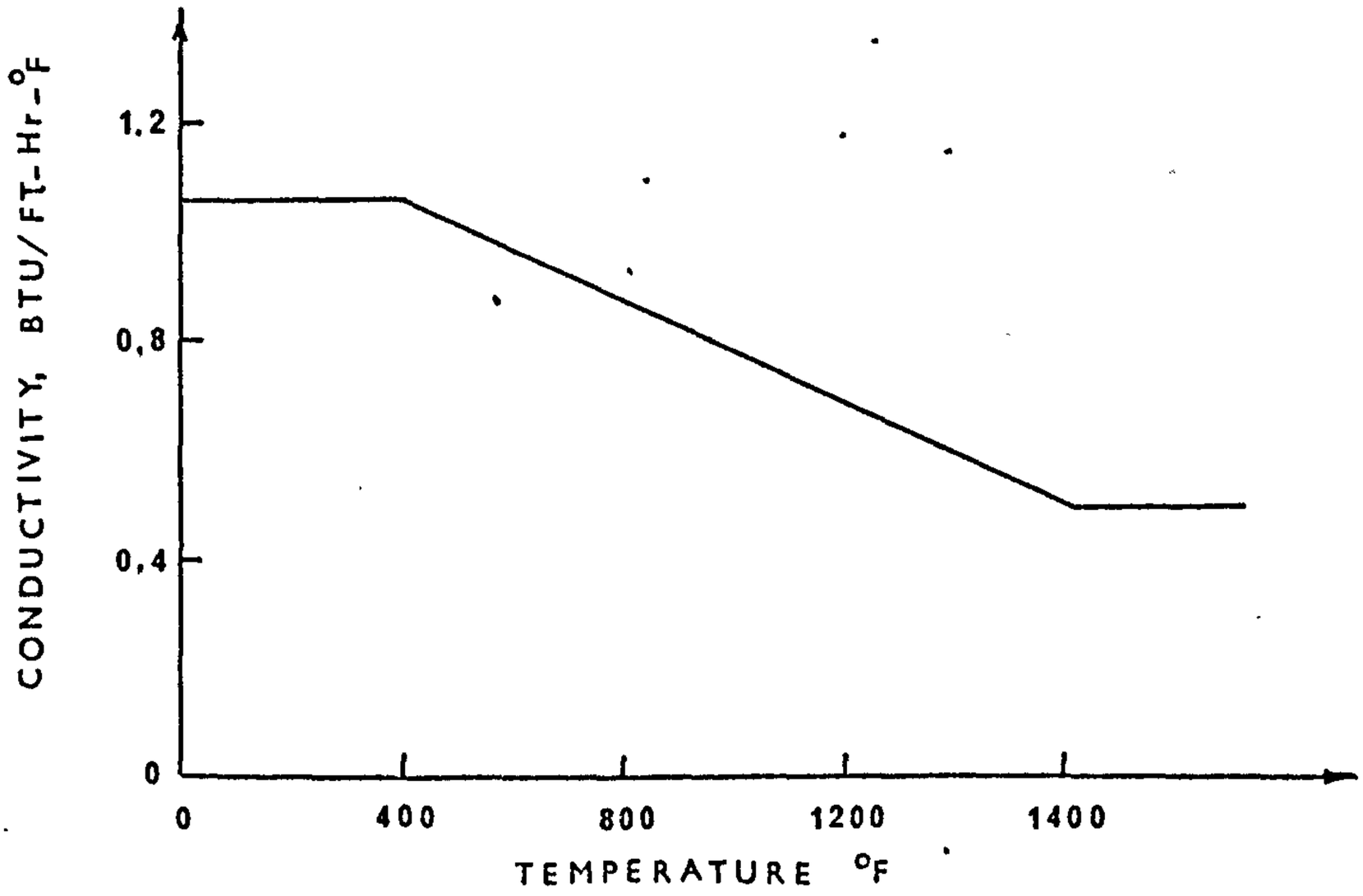

Fig. 3.9 - CONDUCTIVITY-TEMERATURE RELATIONSHIP OF CONCRETE USED IN NUMERICAL ANALYSIS.

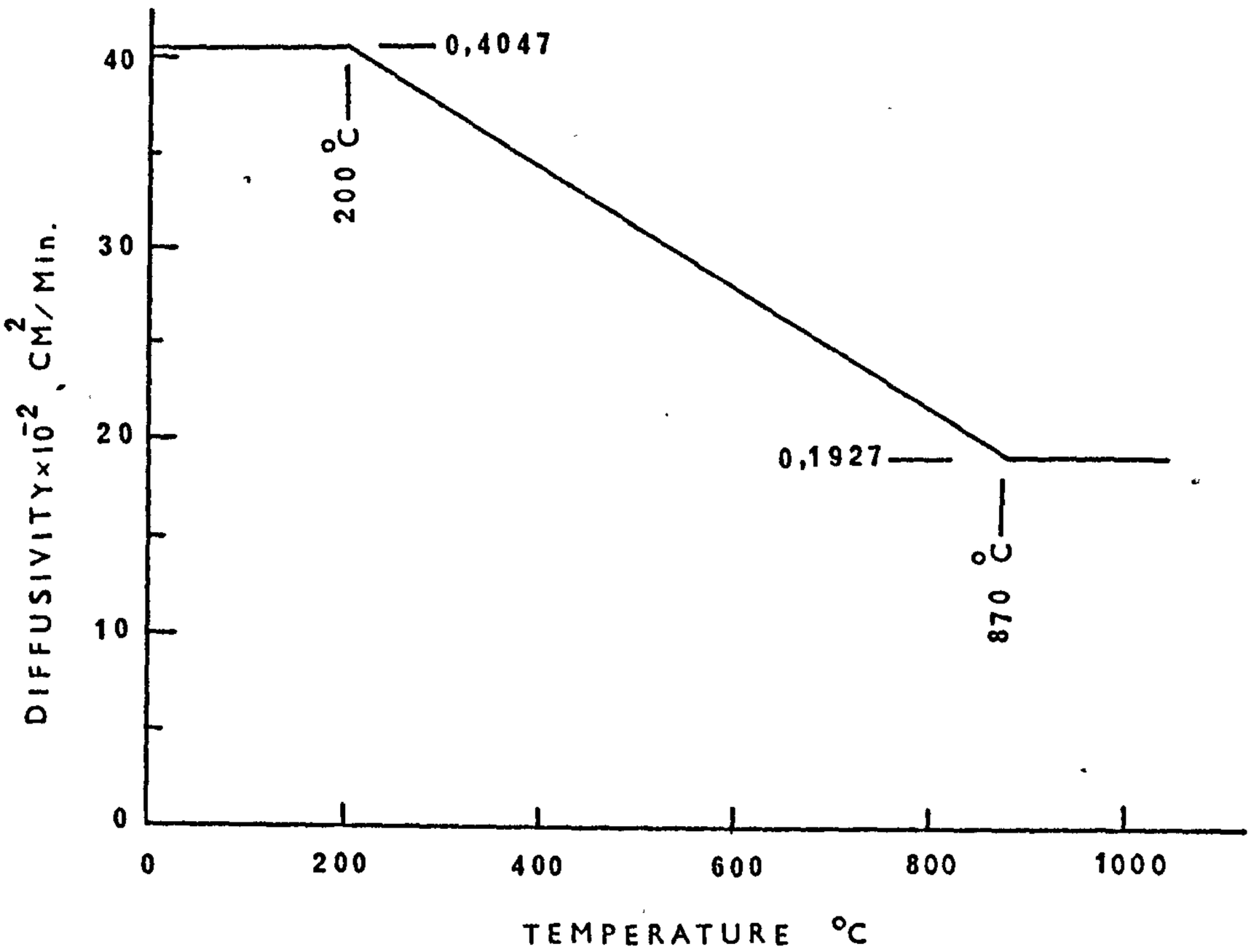

Fig. 3.10- Diffusivity_temperature relationship of concrete used in numerical analysis.

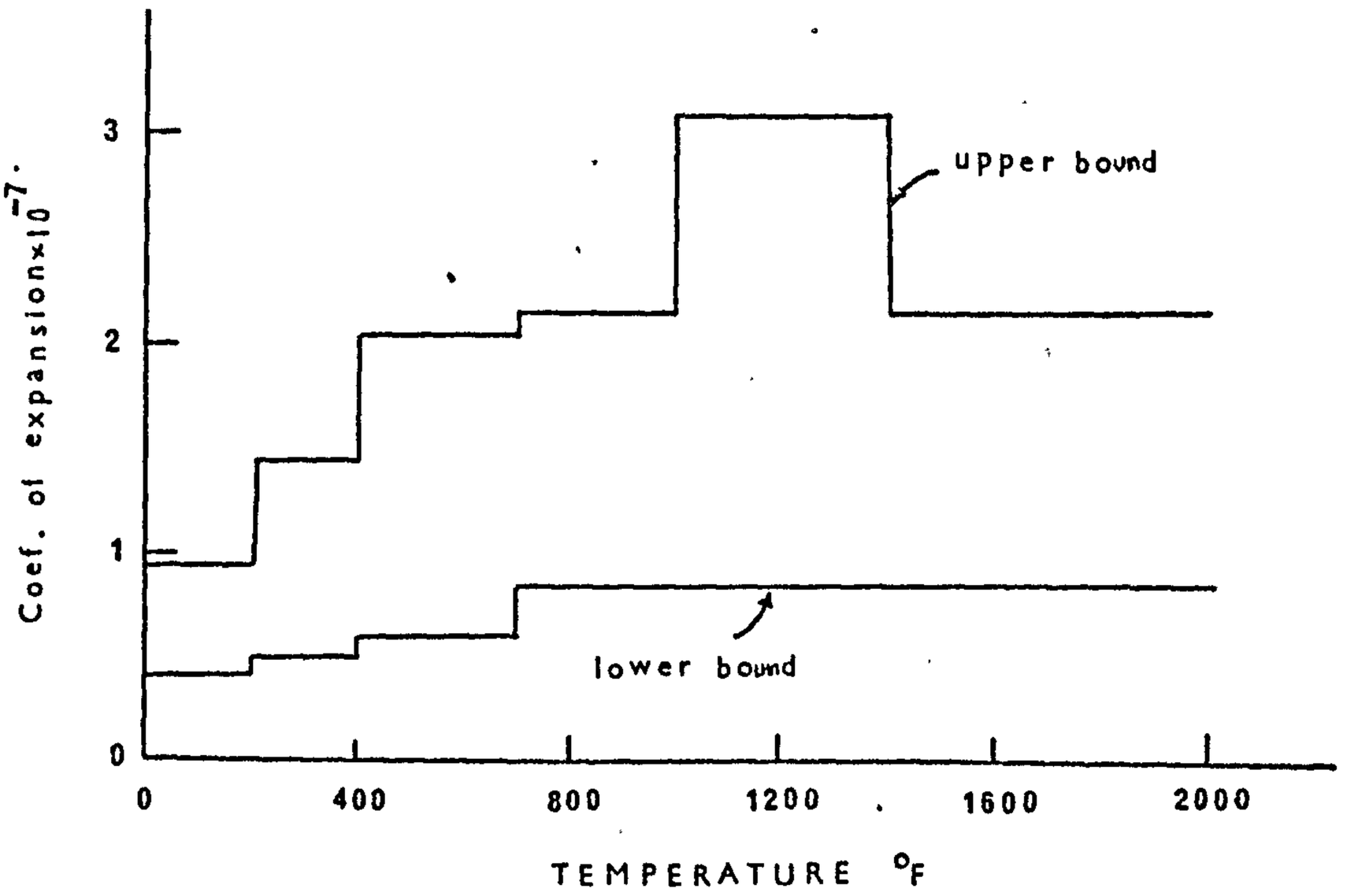

Fig. 3.11_Envelope model for coefficient of therml expansion of concrete; Ref. 28

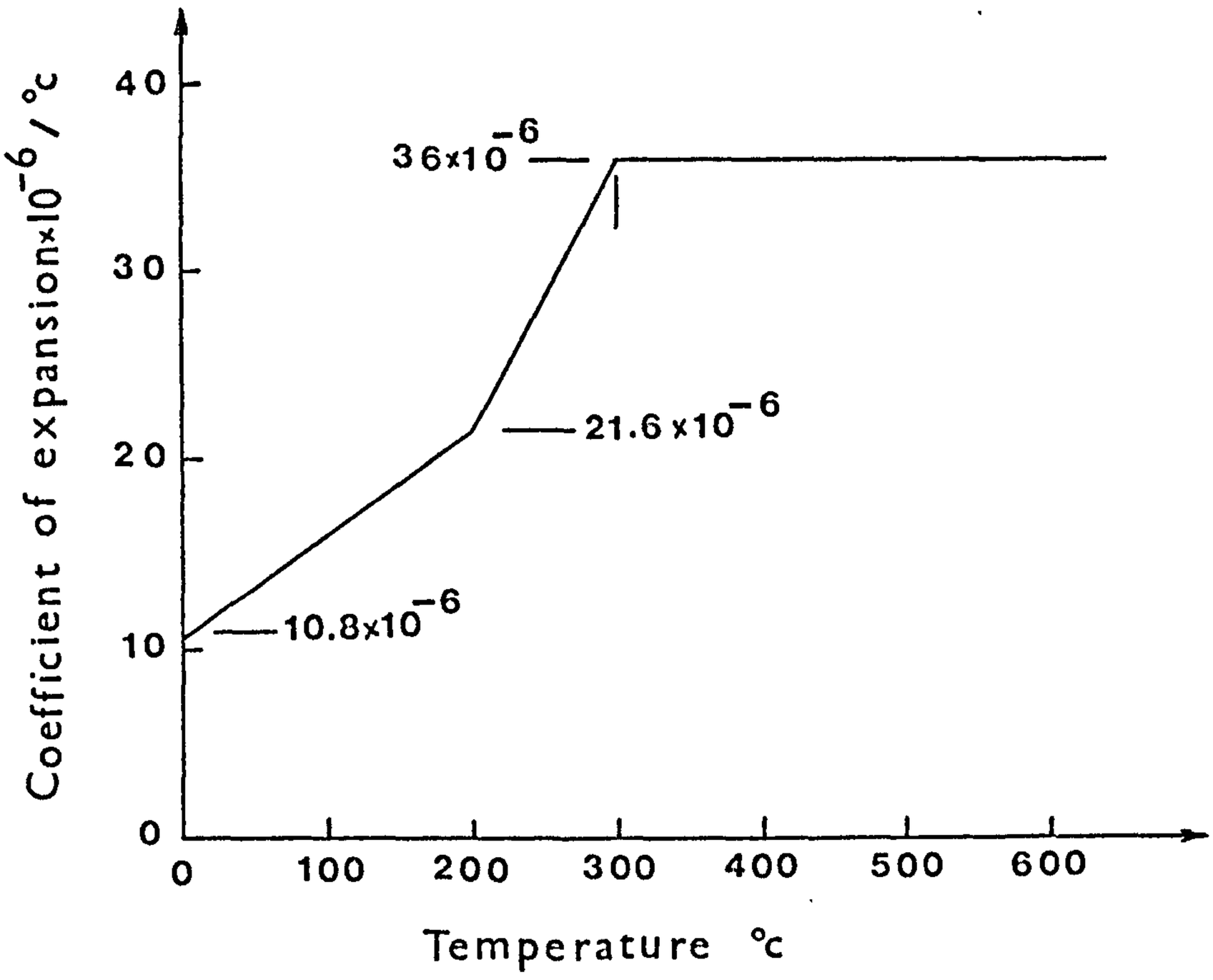

Fig. 3.12_Relationship beween temperatur and the coefficient of expansion of concrete used in the analysis.

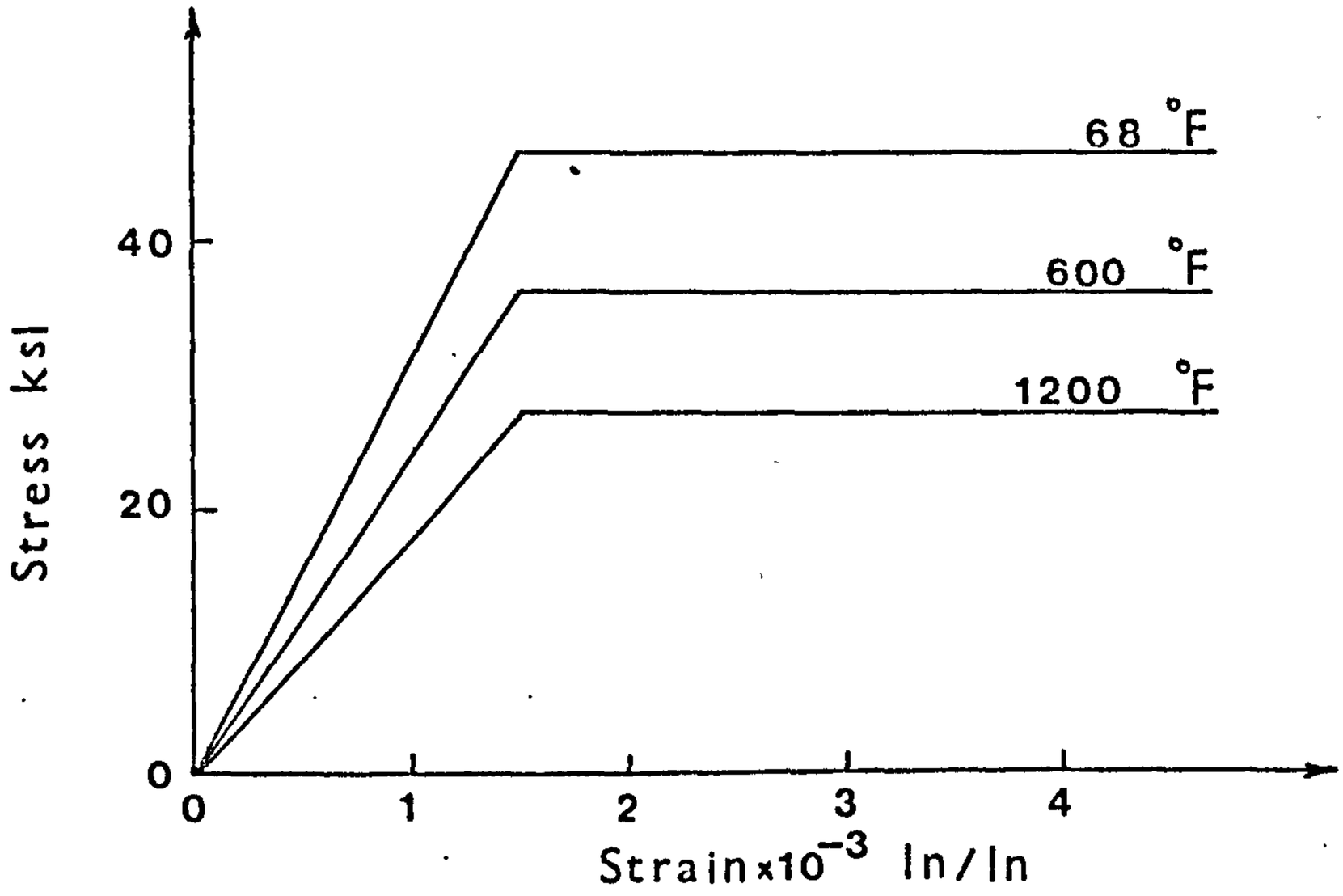

Fig. 3.13_Stress_strain relationship of steel at three different temperatures; Ref. 93

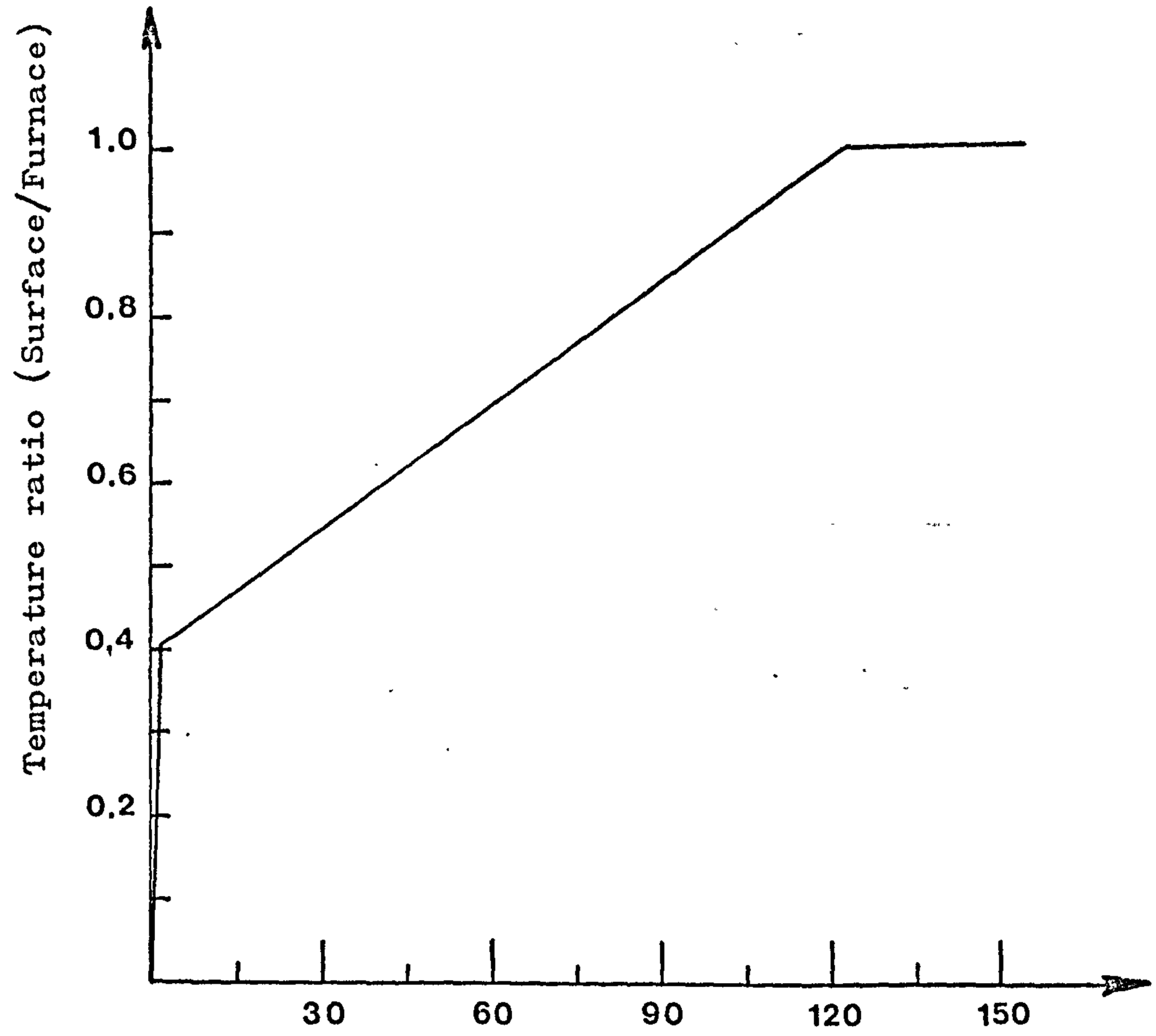

Fig.3.14- Variation of temperature ratio with time, as used in the analysis.

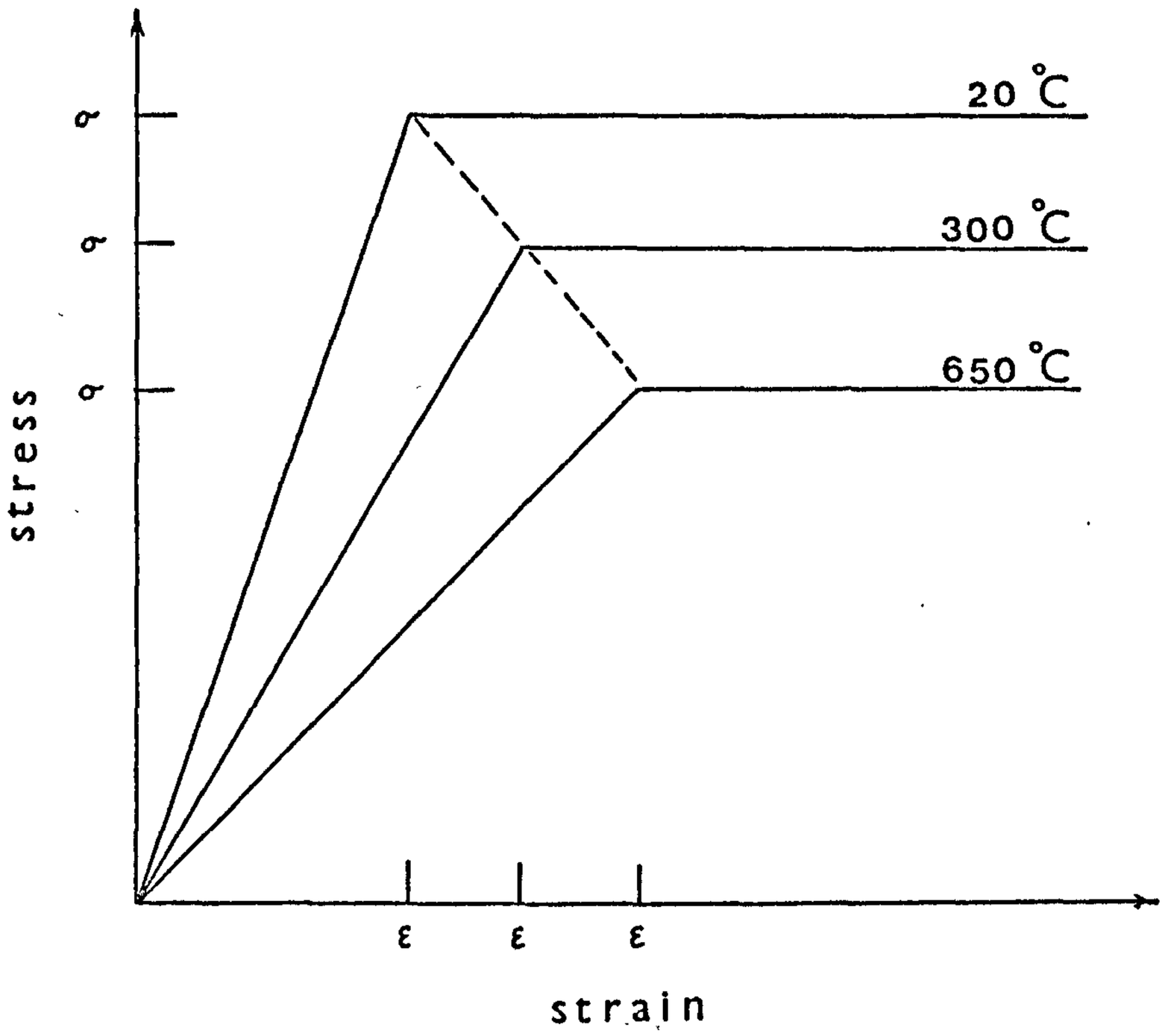

Fig.3.15_Stress-strain curves of steel in three different temperatures.

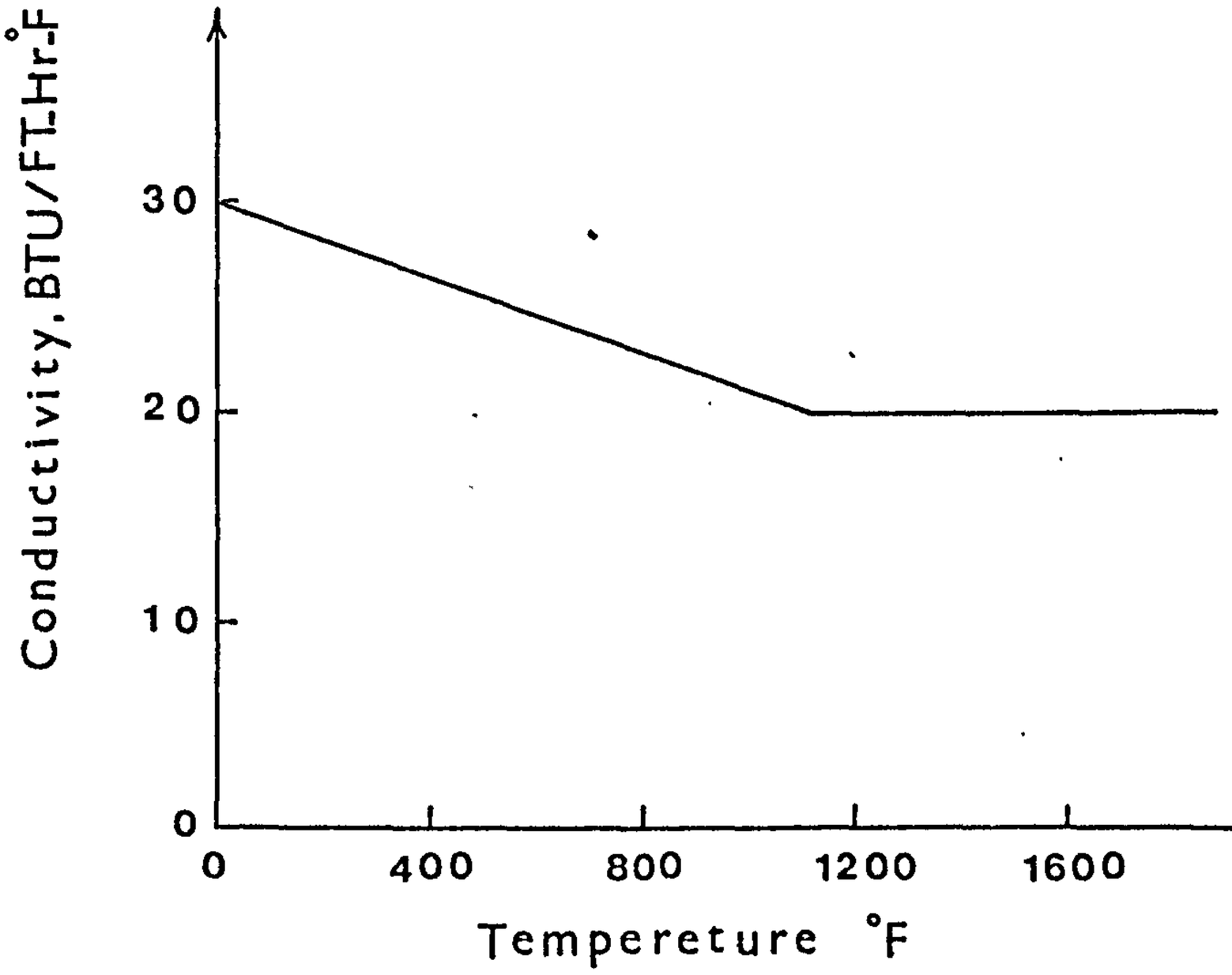

Fig.3.16 - Temperature-conductivity relationship of steel.

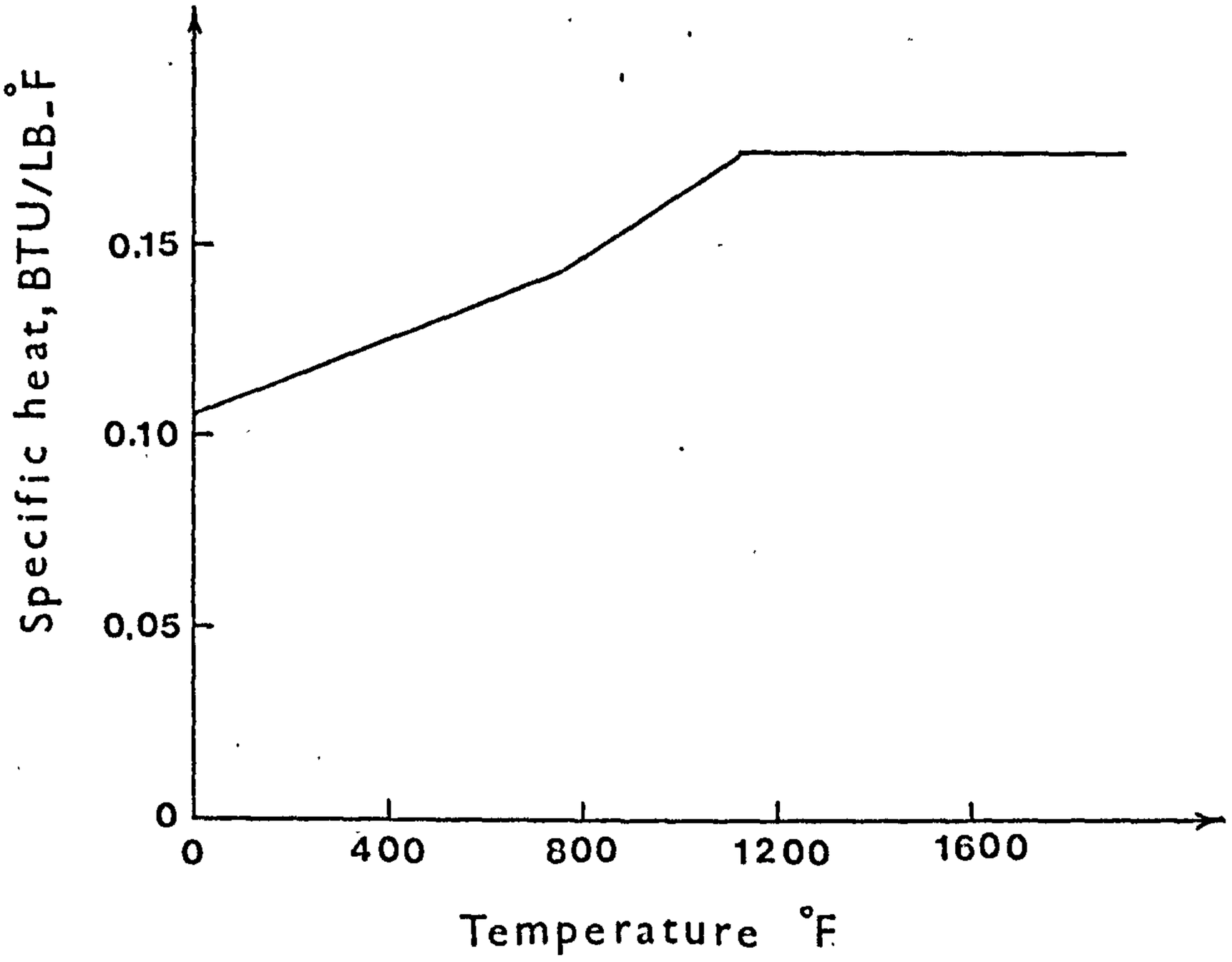

Fig.3.17-Temperature-specific heat relationship of steel; Ref. 93

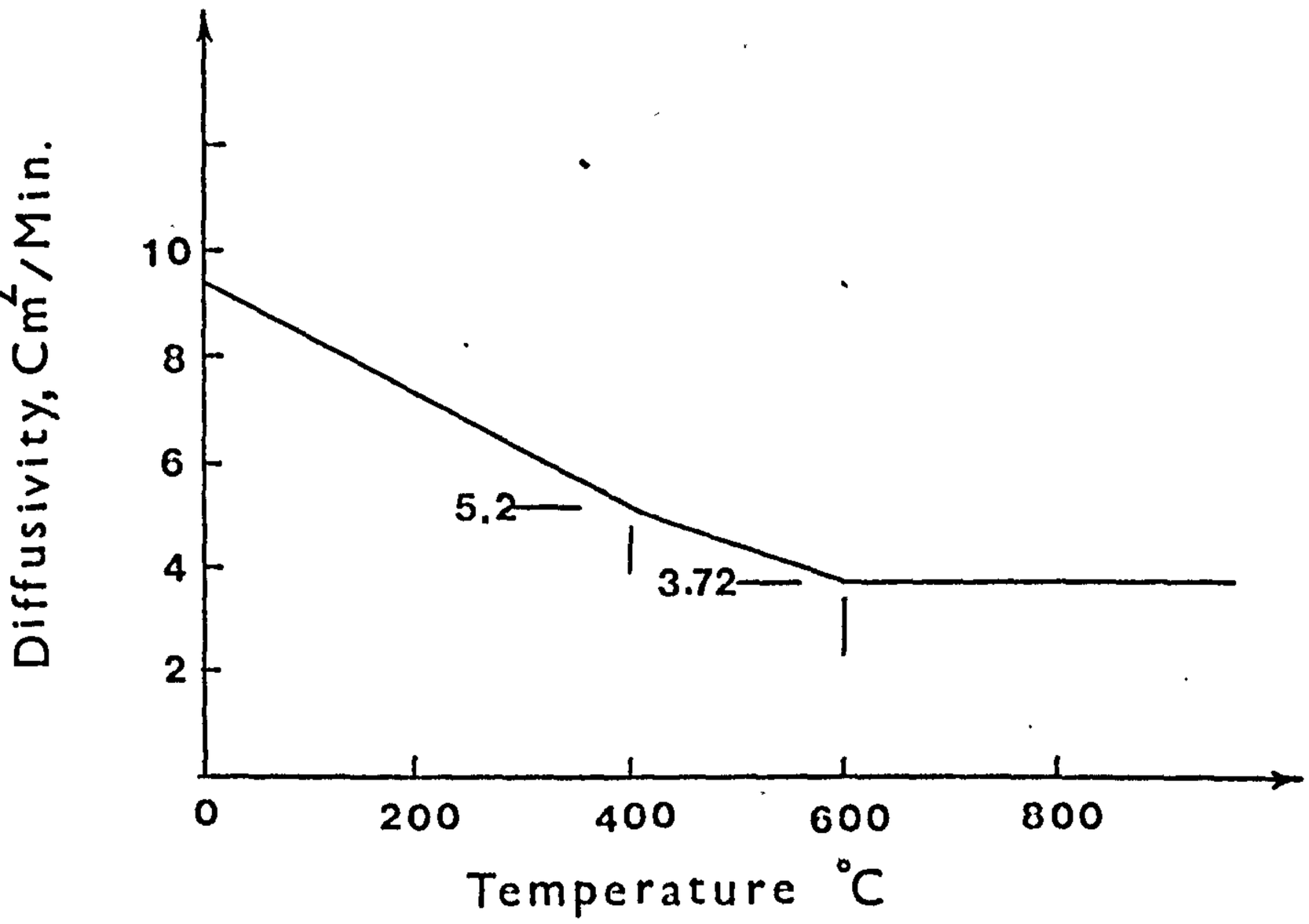

Fig.3.18-Temperature-diffusivity relationship of steel.

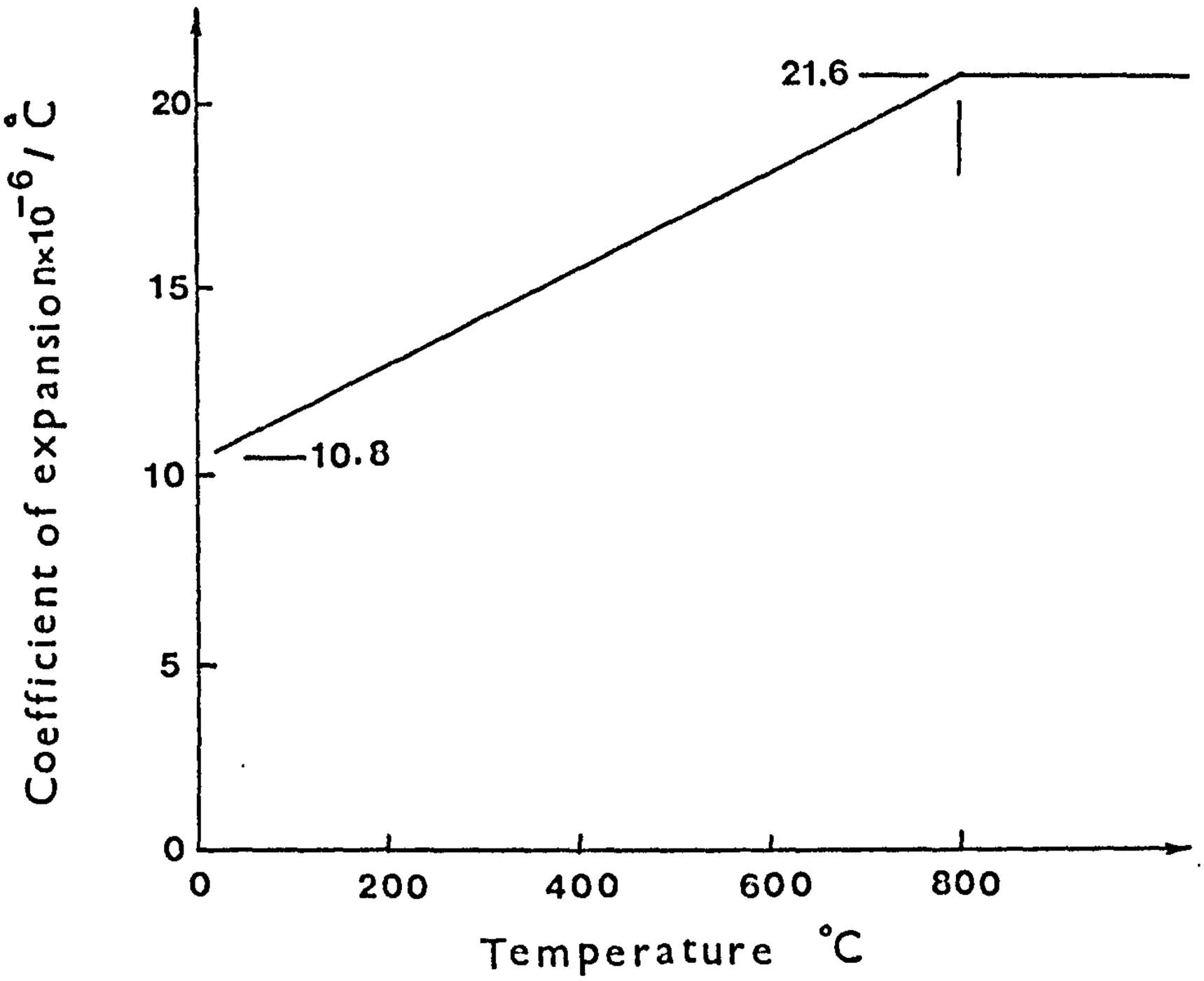

Fig.3.19_ Relationship between temperature and coefficient of expansion of steel.

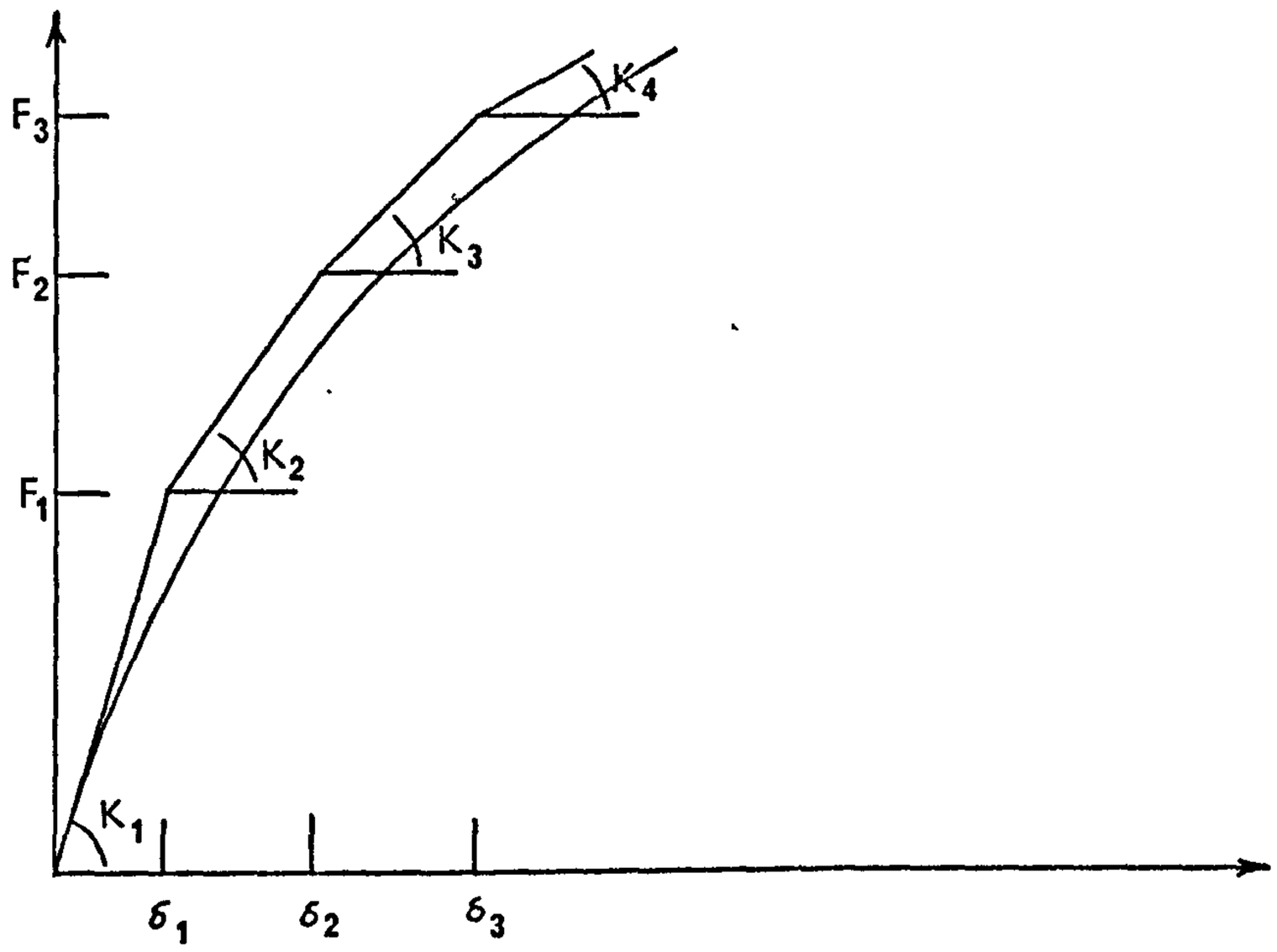

Fig.3.20_ A typical load–displacement relationship at a particular node of structure.

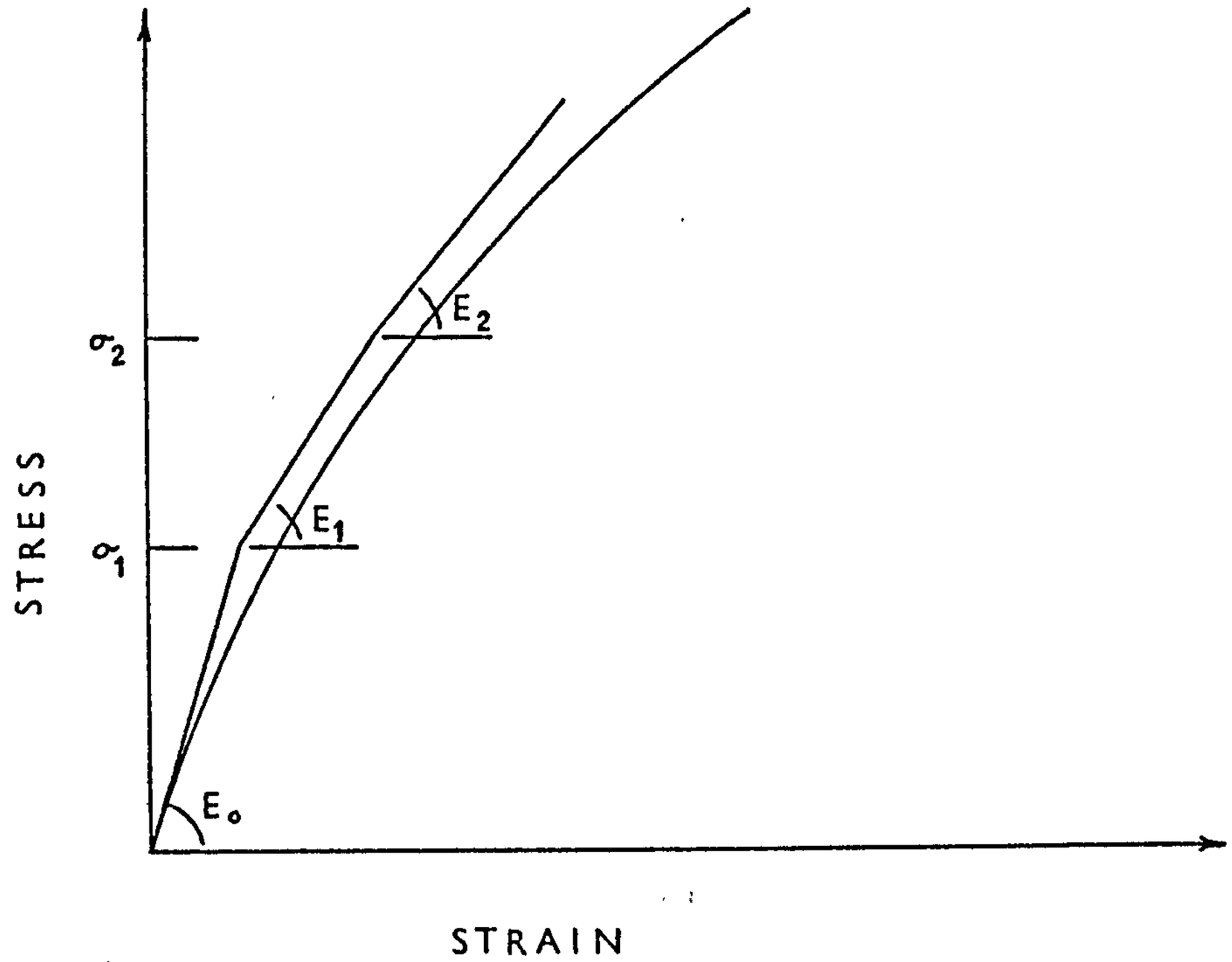

Fig. 3.21 – Stress–strain relationsip in incremental method.

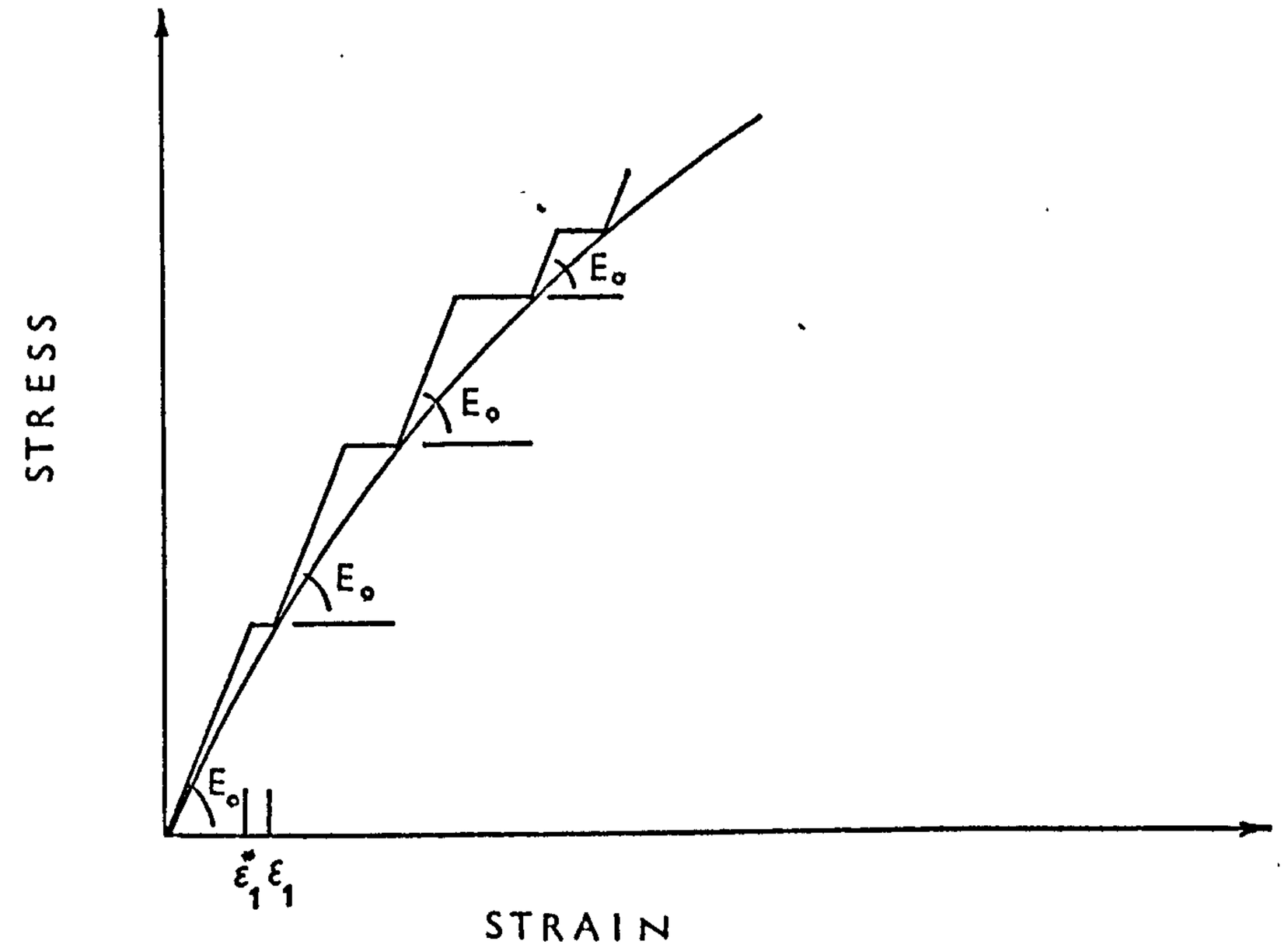

Fig. 3.22 – Stress–strain relationship in initial strain method.

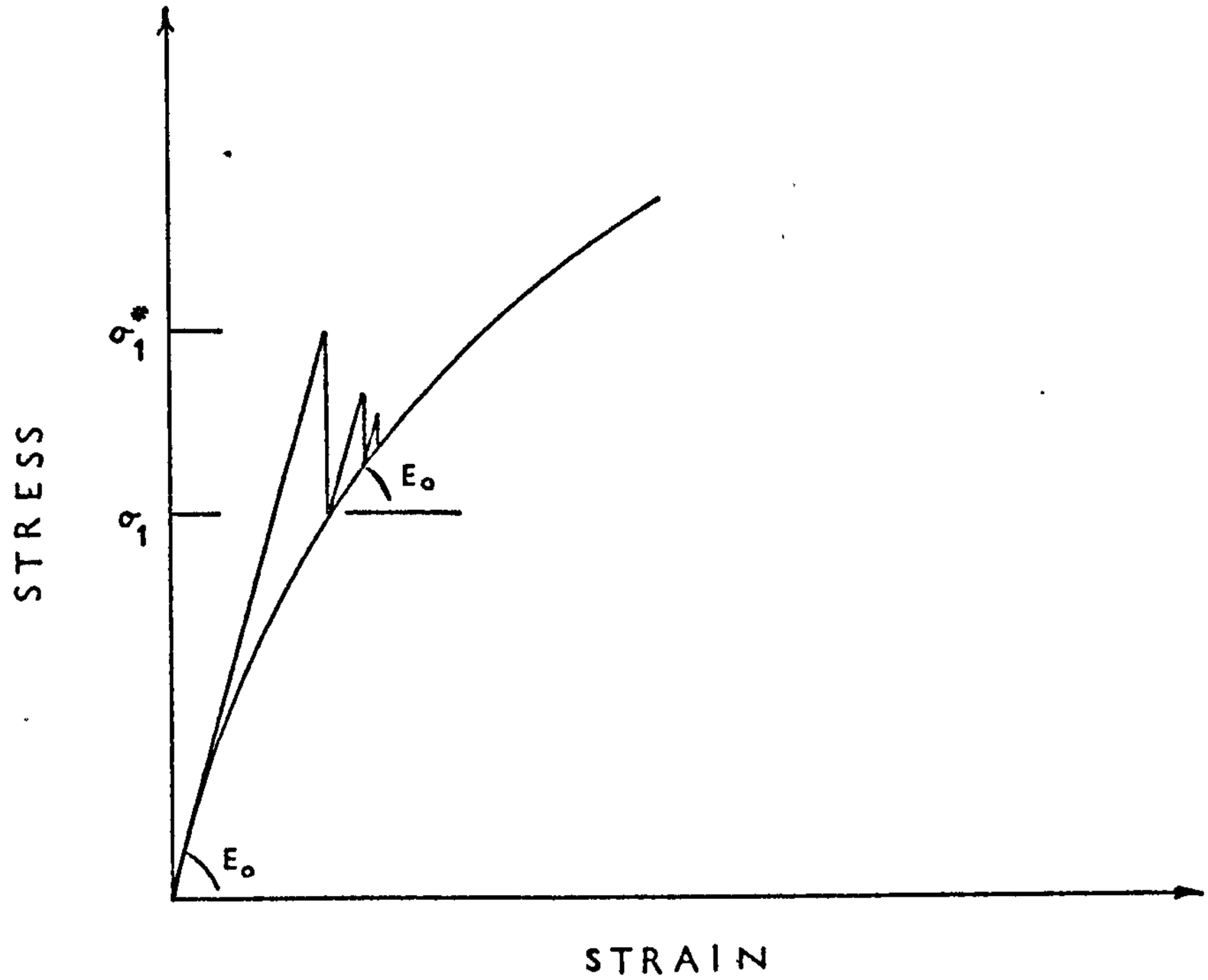

Fig. 3.23 _Stress_strain relationship in initial stress method.

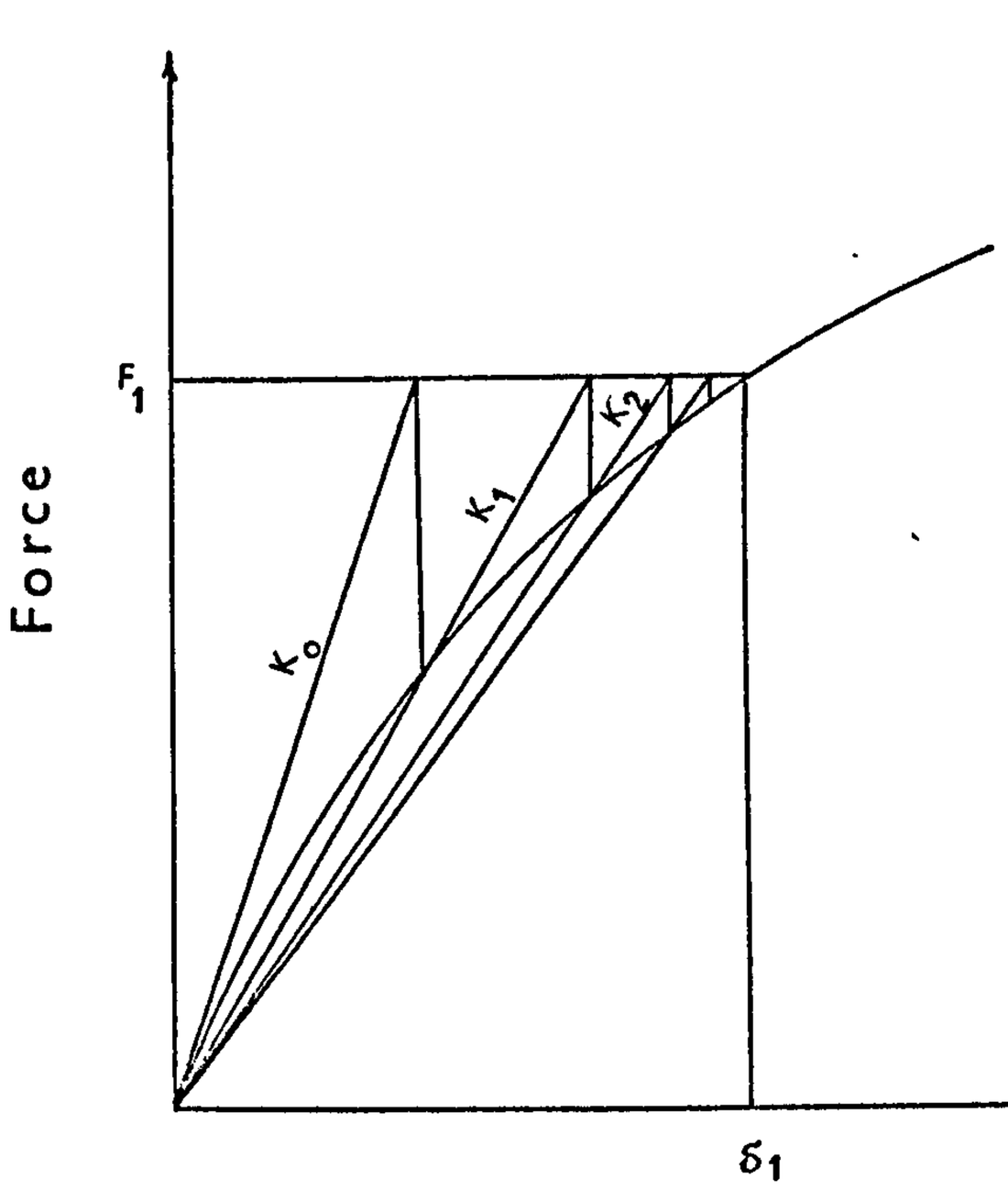

Fig. 3.24_Force_displacement relationship in secant modulus method by variable stiffness Procedure.

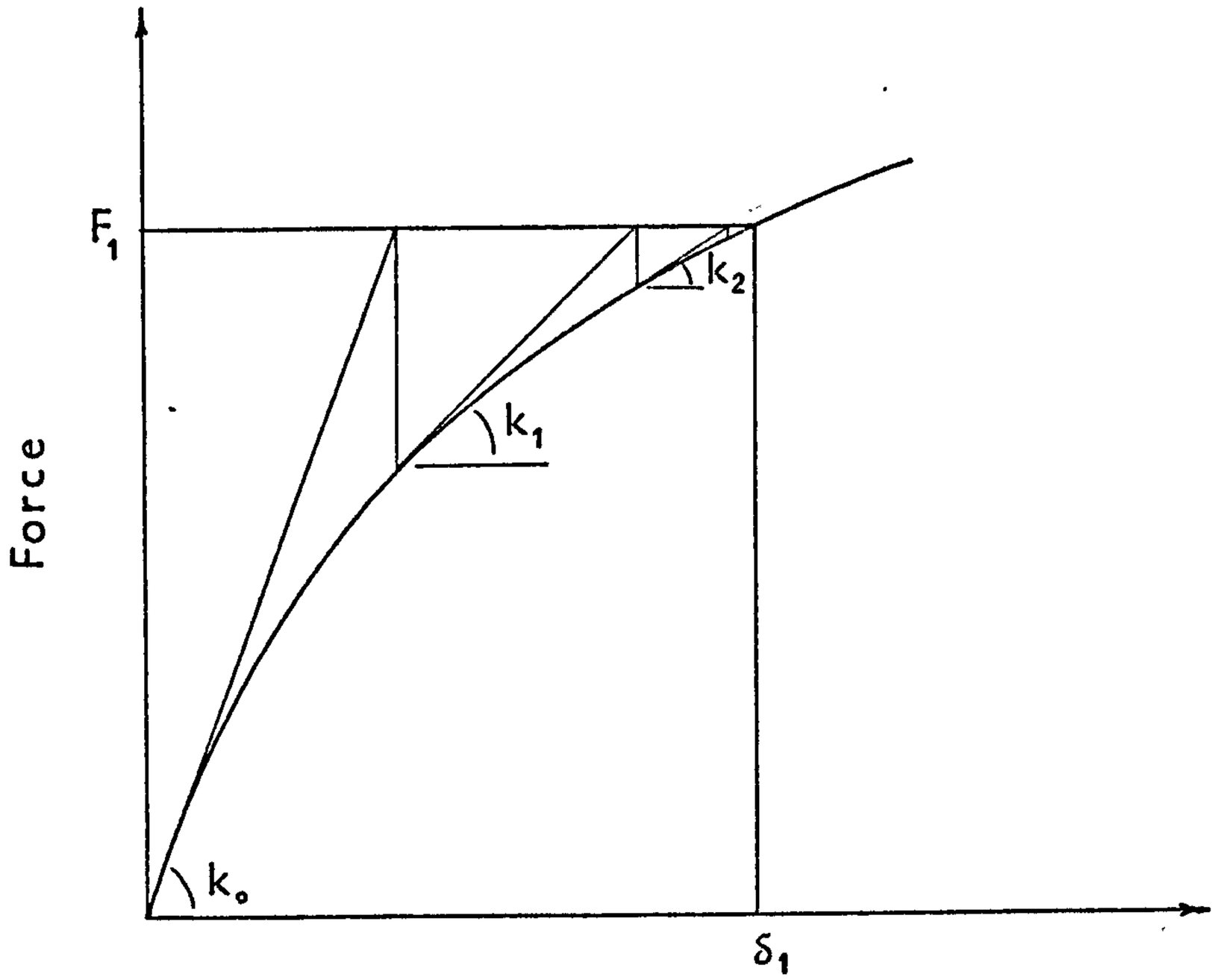

Fig.3.25_Force_displacement relationship in tangent modulus method by variable stiffness Procedure.

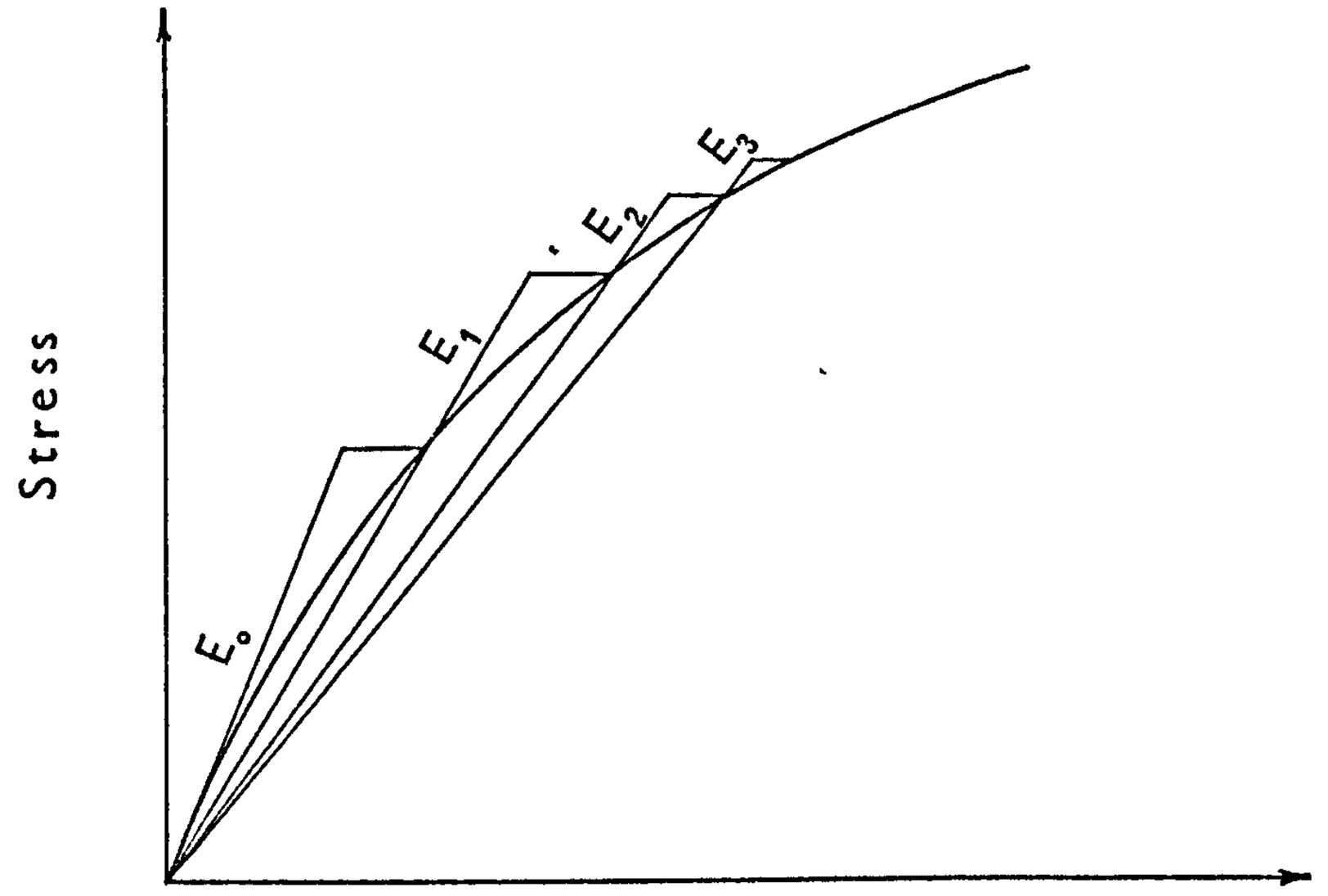

Fig.3.26_Stress_strain relationship in initial strain method by secan modulus approach.

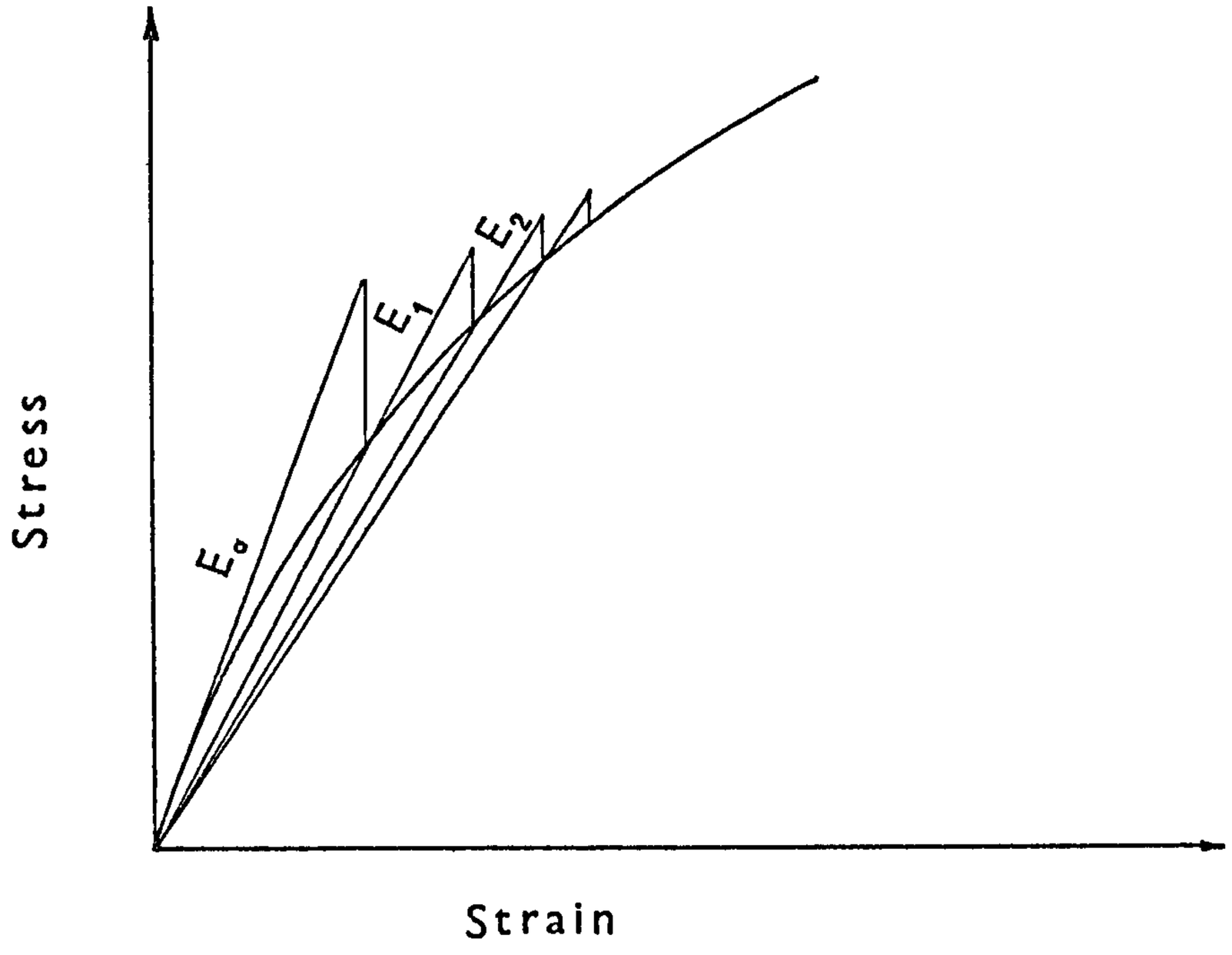

Fig.3.27 _Stress_strain relationship in initial stress method by secant modulus approach.

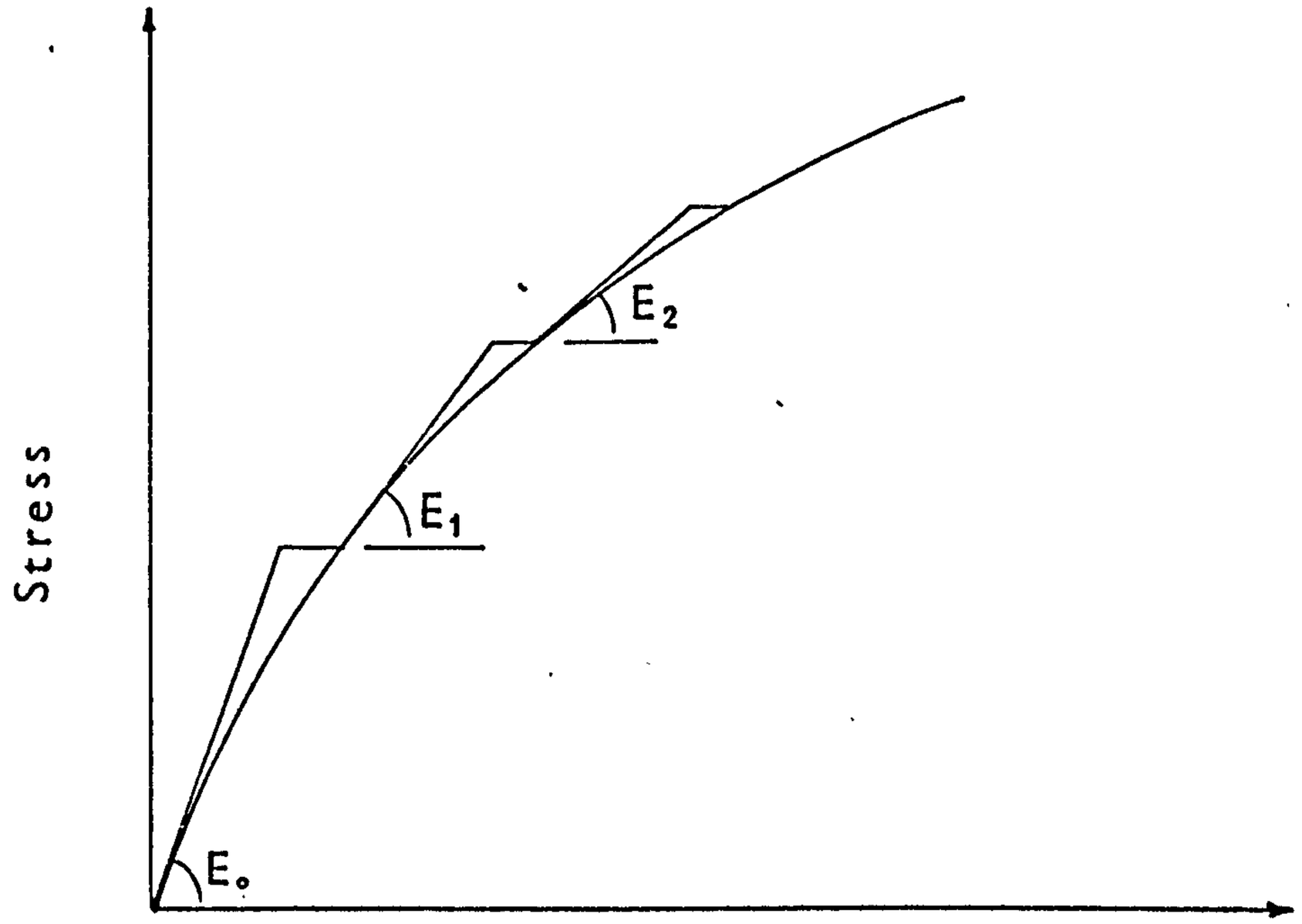

Fig. 3.28_Stress_strain relationship in initial strain method by tangent modulus approach.

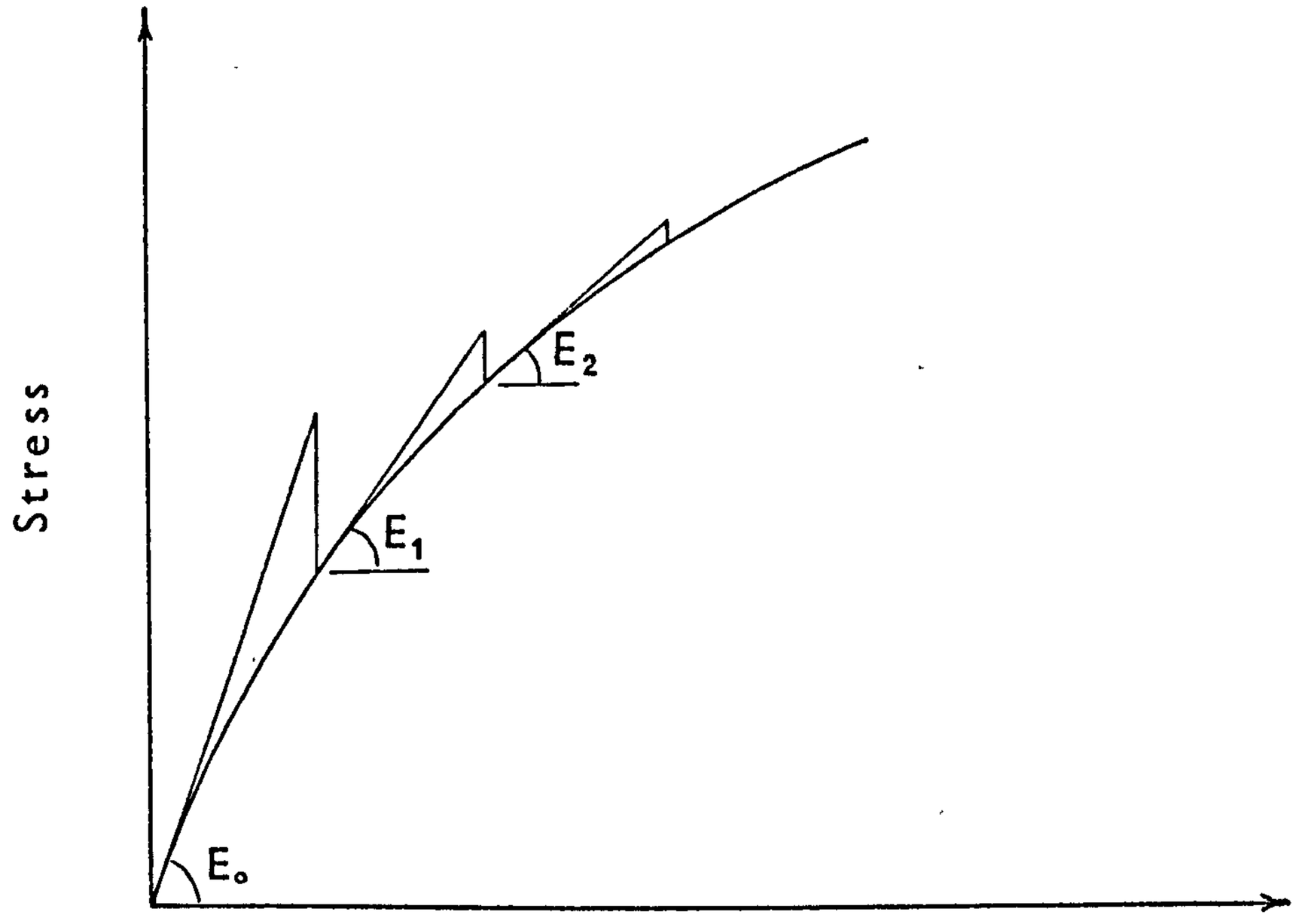

Fig. 3.29 _Stress_strain relationship in initial stress method by tangent modulus approach.

CHAPTER FOUR

IV- Layered Finite Element Technique

4.1- Introduction

The development in methods of structural analysis which has taken place since the war has been due almost entirely to the impact of the digital computer. But it must be realized that, the digital computer is merely a tool for its user, which increases the ability to process information, research and practice, specially in civil engineering.

An example of this development is the finite element technique and its matrix formulation in the analysis of structural elements, and the digital computer has been a prerequisite in achieving a rapid solution. Over the last fifteen years there has been a growing interest in the application of the finite element technique to the analysis of reinforced concrete members particularly with respect to propagation of cracks, [Ref. 52 and 76 to 86].

The finite element technique can treat geometric configuration of any complexity, arbitrary loading and boundary conditions, creep, shrinkage and temperature effects both in the elastic and inelastic range. Although this method has been fully documented elsewhere [Ref. 73, 91 and 92] a brief restatement of its formulation will be given for continuity of presentation and as an introduction to the layered elements used to obtain a solution of problems of reinforced concrete beams and slabs.

The principles of equilibrium and compatibility

and the relationship between forces and displacements, remain basic in the finite element method. It is advantageous to adopt a matrix formulation for convenience of setting out a number of equations for solution by computer as they can be then stored as arrays of numbers. Also the operations of matrix algebra can be provided in the form of standard routines which are rapidly available and can be called into the program by compact instructions. But it must be mentioned that, the matrix method is not usually the best choice for hand calculation. On the other hand some calculations, using matrix formulations are necessary before starting the program.

In the present chapter a numerical method is called, layered finite element method is introduced for the analysis of reinforced concrete beams and slabs, under service load and high temperature which increases within the members. Distribution of temperature within the members, heated on the boundaries, is evaluated from a classical solution of the conduction of heat equation which is given in chapter five and chapter six.

Finally, in the preliminary investigation, the effect of bond between steel and concrete, the influence of creep and shrinkage of concrete are not considered.

4.2- The Finite Element Method

In the finite element method of structural analysis, the structure is first divided into a number of discrete parts in any arbitrary fashion and its mathematical model

formulated such that the body is represented as a assemblage of finite parts which are called "elements" and assumed to be interconnected at a number of nodal points situated on their boundaries. However, such discretization should follow a careful consideration of many types of elements available to represent the states of stress, orientation and magnitude, the degrees of freedom for each node and the number of nodes in each element. The element may, for example, be taken as triangular or quadrilateral plate element, especially to represent an elastic continuum, such as plate. But the actual choice will depend on the geometry of the structure, material properties and the basic assumptions. The force-displacement relationships of each element is derived from the element's geometrical and material properties.

If flexural deformations are to be allowed in reinforced concrete beams or slabs, material variation through the thickness must be taken into account. These deformations can be obtained by a layerring approach, in which, each layer has constant properties throughout the thickness but can have different material properties for different layers. This approach can be applied to two and three dimensional members, and as we will see, in a later section, by employing the layered method and assuming constant material properties for each layer, the real three dimensional problem can be reduced to two dimensions.

The compatibility conditions applying along the interlines or faces depend on the particular distribution of displacements and may or may not be satisfied. Where the

compatibility conditions are not satisfied, a degree of approximation is needed, and the requirements of displacements compatibility along these interlines or faces need to be examined. The displacements occuring within each element are defined by the particular displacement functions or shape functions, which determine whether compatibility is achieved.

The original development of the displacement formulation of the finite element method is based directly on the conditions of equilibrium and compatibility, however, the difficulties encountered to obtain a symmetric element's stiffness matrix for complex elements led to its right characterisation as a generalized form of the Ritz' method in the calculus of variations, with one important difference. Whereas in the Ritz' method the displacement functions prescribe the deformed state over the whole structure, in the finite element technique, prescribed displacements are assigned individually to each element.

4.3- General Technique

In the direct displacement finite element method of stiffness analysis, the nodal displacements are the main unknowns as in the well-known "slope deflection method".

The stress-displacement relationship for each element is determined from the basic applied mechanics rules or by an approximate method in terms of the material properties. Hence, the equilibrium and compatibility conditions at the nodes are achieved.

The displacements within the elements are assumed to follow a pre-defined function in terms of the nodal displacements, and there would be infinite systems of displacements for the compatibility requirements, but the correct pattern of displacements is the one for which the equilibrium exists. Satisfying the compatibility condition within the elements will give the correct set of force system.

For equilibrium, a set of fictitious forces are applied at the nodal points of the elements, which are, in fact representive of the actual stresses acting on the boundaries of the body of the elements. This procedure gives a relationship between the applied forces and displacements, which is known as the stiffness matrix of the element.

By imposing the equilibrium and compatibility conditions at all nodal points of the structure the force-displacement relationship for the whole structure is derived and this procedure gives the stiffness matrix of the whole structure.

The displacement functions within the structure may be defined by a polynomial in a matrix form as follows;

$$\underset{\sim}{U} = \underline{H} \cdot \underset{\sim}{a}_n \qquad (4.1)$$

where, $\underset{\sim}{U}$ is the displacement column vector which gives the displacements of any point of the structure, $\underset{\sim}{a}_n$ is the unknown coefficients column vector, in which, n represents the number of degrees of freedom of the particular element.

Matrix $\underline{H}$ includes the terms of polynomial, such as

$x^m.y^p.z^q$ for a three dimensional element or structure, where x, y and z are the coordinates of any point of the body, and m, p and q are positive integers which are obtained from satisfying the partial differential equation of the problem.

In some cases other properties are added to the foregoing polynomial terms, such as, curvatures of the body for analysis of shells, however the number of the unknown coefficients will depend on the degrees of freedom of the element.

By substituting the properties of any element (e), such as nodal coordinates, curvatures of the element, etc., the displacements of the nodal points can be written as;

$$\underset{\sim}{\delta}_e = \underline{L}_e \cdot a_n \qquad (4.2)$$

where, $\underset{\sim}{\delta}_e$ the nodal displacement column vector of the element has the same order as the unknown coefficient vector, and the shape of square matrix $\underline{L}_e$ depends on the manner of arranging of displacement vector. Two forms are more convenient for calculating the unknown coefficients and also for computer programming and we will intoduce these two forms for a rectangular element in a later section, one for analysis of reinforced concrete beams and the other to obtain the stiffness matrix for slab.

However, from the simultaneous equation (4.2) the unknown coefficient vector can be substituted into equation (4.1) to obtain the displacement functions in terms of the nodal displacements as follows;

$$\underset{\sim}{U} = \underline{H} \cdot \underline{L}_e^{-1} \cdot \underset{\sim}{\delta}_e \qquad (4.3)$$

where, the terms of matrix $\underline{H}.\underline{L}_e^{-1}$ are refered to as the element shape functions.

By considering the strain-displacement relationships at any point of the element (e) we are able to find the relationships between strains at any point within the element and nodal displacements, thus;

$$\underset{\sim}{\epsilon}_e = \underline{B}_e \cdot \underset{\sim}{\delta}_e \qquad (4.4)$$

where, $\underset{\sim}{\epsilon}_e$ is the strain column vector and $\underline{B}_e$, the strain matrix representing the kinematic relationship within the element. The stresses at any point of the element is determined directly from the constitutive stress-strain relation of the material;

$$\underset{\sim}{\sigma}_e = \underline{D}_e \cdot \underset{\sim}{\epsilon}_e \qquad (4.5)$$

where $\underset{\sim}{\sigma}_e$ is the stress column vector and $\underline{D}_e$ the elasticity matrix of element (e) containing the element material properties.

In practice, the elasticity matrix is written in the principal directions of the element, which must transfer into global coordinates. If $\underset{\sim}{\epsilon}_p$ and $\underset{\sim}{\sigma}_p$ represent the strain and stress vectors, respectively, and $\underline{D}_e$ represents the elasticity matrix all in the principal directions, and also $\underset{\sim}{\epsilon}_g$, $\underset{\sim}{\sigma}_g$ and $\underline{D}_g$ represent the strains, stresses and elasticity matrix in global coordinates, the relation between strains in global and local (principal) coordinates may be written as;

$$\underset{\sim}{\epsilon}_p = \underline{T} \cdot \underset{\sim}{\epsilon}_g \qquad (A)$$

or,

$$\underset{\sim}{\epsilon}_p^t = \underset{\sim}{\epsilon}_g^t \cdot \underline{T}^t \qquad (4.6)$$

where $\underline{T}$ is the transformation matrix.

As the work done by stresses is independent of coordinates directions, we have;

$$\underset{\sim}{\epsilon}_g^t \cdot \underset{\sim}{\sigma}_g = \underset{\sim}{\epsilon}_p^t \cdot \underset{\sim}{\sigma}_p \qquad (B)$$

and substituting equation (4.6) into equation (b), we find;

$$\underset{\sim}{\epsilon}_g^t \cdot \underset{\sim}{\sigma}_g = \underset{\sim}{\epsilon}_g^t \cdot \underline{T}^t \cdot \underset{\sim}{\sigma}_p$$

hence;

$$\underset{\sim}{\sigma}_g = \underline{T}^t \cdot \underset{\sim}{\sigma}_p \qquad (4.7)$$

Using equation (4.5) for the principal stresses and by substituting $\underset{\sim}{\epsilon}_p$ from equation (A), we find;

$$\underset{\sim}{\sigma}_p = \underline{D}_p \cdot \underline{T} \cdot \underset{\sim}{\epsilon}_g$$

and finally, by inserting $\underset{\sim}{\sigma}_p$ in equation (4.7), one obtains;

$$\underset{\sim}{\sigma}_g = \underline{T}^t \cdot \underline{D}_p \cdot \underline{T} \cdot \underset{\sim}{\epsilon}_g$$

and since $\underset{\sim}{\sigma}_g = \underline{D}_g \cdot \underset{\sim}{\epsilon}_g$;

$$\underline{D}_g = \underline{T}^t \cdot \underline{D}_p \cdot \underline{T} \qquad (4.8)$$

which transforms the elasticity matrix in the pricipal

directions into global coordinates.

By substituting equation (4.4) into equation (4.5) the stress-displacement relationships become as follows;

$$\underset{\sim}{\sigma}_e = \underline{D}_e \cdot \underline{B}_e \cdot \underset{\sim}{\delta}_e \qquad (4.9)$$

Equation (4.9) for each element or the whole body is determined by imposing the equilibrium and compatibility conditions at all nodal points of each element or structure, respectively. This process in place involves manipulating the stiffness matrix of the individual element in a certain procedure which is a purely mathematical one.

To evaluate the nodal forces $\underset{\sim}{f}_e$ from the element's stresses, the principle of the virtual work is applied to the element, which by assuming all forces at the nodes of the element, this theorem gives;

$$\int_V \underset{\sim}{\bar{\varepsilon}}_e^t \cdot \underset{\sim}{\sigma}_e \cdot dv = \underset{\sim}{\bar{\delta}}_e^t \cdot \underset{\sim}{f}_e$$

where, $\underset{\sim}{\bar{\varepsilon}}_e$ and $\underset{\sim}{\bar{\delta}}_e$ are the virtual strain and displacement vector and v is the volume of the element. Substituting $\underset{\sim}{\bar{\varepsilon}}_e$ and $\underset{\sim}{\delta}_e$ from equation (4.4) and (4.9) the nodal forces in terms of the nodal displacements become as follows;

$$\underset{\sim}{f}_e = \left(\int_V \underline{B}_e^t \cdot \underline{D}_e \cdot \underline{B}_e \cdot dv \right) \cdot \underset{\sim}{\delta}_e \qquad (4.10)$$

which can be shown in the following form;

$$\underset{\sim}{f}_e = \underline{k}_e \cdot \underset{\sim}{\delta}_e$$

where, $\underline{k}_e$ is the element stiffness matrix, which is singular

because of the inclusion of rigid body motion.

Equation (4.10) is in terms of the principal (local) coordinates, and with the help of equation (4.9) can be transformed into global coordinates, which gives the element stiffness matrix as below;

$$\underline{k}_{eg} = \int_V (\underline{B}^t_{eg} . \underline{T}^t . \underline{D}_{ep} . \underline{T} . \underline{B}_{eg}) . dv \qquad (4.11)$$

By assembling the structural elements, the overall stiffness matrix of the structure is derived and is carried out by assuming equilibrium and compatibility at the nodal points.

The total element forces at each node are equated to the applied external forces at this node and for compatibility, the corresponding displacements of the nodes where the element is connected are made equal.

By locating the elements stiffness matrices in the structural stiffness matrix $\underline{K}_g$, the nodal forces components resulting from unit nodal displacements are defined.

The above structural stiffness matrix is singular and hence, boundary conditions must be introduced to obtain a solution, i.e, nodal displacements (main unknown) as;

$$\underset{\sim}{\delta} = \underline{K}^{-1} . \underset{\sim}{F}$$

where, $\underset{\sim}{\delta}$ and $\underset{\sim}{F}$ are the nodal displacement and force vectors, respectively, in global coordinates.

By solving the foregoing simultaneous equations the nodal displacements are calculated and in return, the elements

properties, such as curvatures, slopes, strains and internal forces at any required point within the elements and other required properties are evaluated individually.

The rest of the present chapter describes solution of two different problems by means of the finite element technique, as follows;

A- Analysis of reinforced concrete beams by dividing the body into a finite number of rectangular elements with two degrees of freedom for each node. Each element is divided into a finite number of layers throughout the element thickness by assuming constant material properties for each layer.

B- Analysis of reinforced concrete slabs by dividing into a finite number of layers and a finite number of rectangular elements with twenty degrees of freedom for each element i.e, two rotations and three displacements at each node.

In both problems the body is assumed to be under incremental load up to service load or ultimate load and also under incremental initial strain due to temperature increasing up to failure. All material properties such as conductivity, diffusivity, specific heat, modulus of elasticity and the coefficient of thermal expansion of both steel and concrete materials vary with temperature in a manner described in chapter three.

4.4- Nonlinear Analysis of Reinforced Concrete Beams

The analysis of reinforced concrete members may be considered as a one, two or three dimensional problem. In analysis of members such as reinforced concrete beams which in the uncracked region are long relative the their other dimensions, the maximum stresses are mostly in the direction parallel to the axis, except in the vicinity of supports and at point loads.

On the other hand the state of stress of deep beams is essentially two dimensional. In the case of one dimensional beams, composed of sub-elements each of which may have length and depth of the same order become a two dimensional problem when the members start to crack.

A reinforced concrete beam under inplane forces is in a two dimensional state of stress and the body is divided into a finite number of rectangular elements as in figure (4.1), in which the elements are interconnected together at four corner nodes each with eight degrees of freedom, i.e, two inplane displacements for each node.

In order to obtain the stress resultant relations throughout the thickness of the element particularly in a composite body such as a reinforced concrete beam, it is necessary to obtain each layer's contribution and add them all together.

For each layer the method is independent of the specific type of material properties present, and, as a whole, the sum does not require all layers to have the same material properties. Thus, it is conceivable that a

particular element employing this approach could contain as many different layer material properties as it has layers, which allows for any material property variation through the thickness of the structure.

Thus, each element is divided into a finite number of layers which are interconnected at the surface as in figure (4.2). The cross-section of a I, T and rectangular beams in figure (4.2) have constant geometrical characteristics along the length of the beams and because of cross-sectional symmetry, only half of the beams need be considered.

In order to relate applied forces to corresponding displacements we ahall define the vector;

$$\underset{\sim}{U} = \begin{Bmatrix} u \\ v \end{Bmatrix}$$

as the displacements at any arbitrary point within the beam and;

$$\underset{\sim}{U} = \begin{bmatrix} \underset{\sim}{g} & \underset{\sim}{0} \\ \underset{\sim}{0} & \underset{\sim}{g} \end{bmatrix} \cdot \underset{\sim}{a}_8 \qquad (4.12)$$

where,

$$\underset{\sim}{g} = \{ 1 \quad x \quad y \quad xy \}$$

$$\underset{\sim}{a}_8 = \{ a_1 \quad a_2 \quad a_3 \cdots \quad a_8 \}^t$$

where u and v are inplane displacements of any point within the body in x and y-direction, respectively, and $\underset{\sim}{0}$ is a zero vector. A typical rectangular element with its nodal points i, j, m and n, numbered anticlockwise, in local and global coordinates and also nodal displacements with their positive directions are shown in figure (4.3).

To calculate the eight unknowns coefficients $\underset{\sim}{a}_8$ for a typical element (e) we have the following simultaneuos equations;

$$\Delta\underset{\sim}{\delta}_e = \begin{bmatrix} \underline{A}_e & \underline{0} \\ \underline{0} & \underline{A}_e \end{bmatrix} \cdot \underset{\sim}{a}_8 \qquad (4.13)$$

which are solved by substituting the geometrical properties of element nodal points in equation (4.12), where $\underline{0}$ is a 4×4 zero matrix and the square matrix $\underline{A}_e$ in the global coordinates is;

$$\underline{A}_e = \begin{bmatrix} 1 & x_i & y_i & x_i y_i \\ 1 & x_j & y_j & x_j y_j \\ 1 & x_m & y_m & x_m y_m \\ 1 & x_n & y_n & x_n y_n \end{bmatrix} \qquad (4.14)$$

and the column vector $\Delta\underset{\sim}{\delta}_e$ contains the incremental displacements of nodal points as in below;

$$\Delta\underset{\sim}{\delta}_e = \{ \Delta u_i \quad \Delta u_j \quad \Delta u_m \quad \Delta u_n \quad \Delta v_i \quad \Delta v_j \quad \Delta v_m \quad \Delta v_n \}^t$$

Referring to figure (4.3) the square matrix $\underline{A}_e$ in the local coordinates becomes;

$$\underline{A}_e = \begin{bmatrix} 1 & 0 & 0 & 0 \\ 1 & a & 0 & 0 \\ 1 & a & b & ab \\ 1 & 0 & b & 0 \end{bmatrix} \qquad (4.15)$$

where a and b are the dimensions of the element (e) in the x and y-directions, respectively.

From equation (4.13), the unknown coefficients $\underset{\sim}{a}_8$

become;

$$\underset{\sim}{a}_8 = \begin{bmatrix} \underline{A}_e & \underline{0} \\ \underline{0} & \underline{A}_e \end{bmatrix}^{-1} \cdot \Delta\underset{\sim}{\delta}_e$$

or;

$$\underset{\sim}{a}_8 = \begin{bmatrix} \underline{A}_e^{-1} & \underline{0} \\ \underline{0} & \underline{A}_e^{-1} \end{bmatrix} \cdot \Delta\underset{\sim}{\delta}_e \qquad (4.16)$$

and,

$$\underline{A}_e^{-1} = \begin{bmatrix} s & 0 & 0 & 0 \\ -b & b & 0 & 0 \\ -a & 0 & 0 & a \\ 1 & -1 & 1 & -1 \end{bmatrix} \cdot \frac{1}{s} \qquad (4.17)$$

where s is the area of the element.

By substituting equation (4.16) into equation (4.12) displacements of any point within the element corresponding to the incremental nodal displacements become;

$$\Delta\underset{\sim}{U}_e = \begin{bmatrix} \underset{\sim}{g} & \underset{\sim}{0} \\ \underset{\sim}{0} & \underset{\sim}{g} \end{bmatrix} \begin{bmatrix} \underline{A}_e^{-1} & \underline{0} \\ \underline{0} & \underline{A}_e^{-1} \end{bmatrix} \cdot \Delta\underset{\sim}{\delta}_e \qquad (4.18)$$

thus;

$$\Delta\underset{\sim}{U}_e = \begin{bmatrix} \underset{\sim}{g} \cdot \underline{A}_e^{-1} & \underset{\sim}{0} \\ \underset{\sim}{0} & \underset{\sim}{g} \cdot \underline{A}_e^{-1} \end{bmatrix} \cdot \Delta\underset{\sim}{\delta}_e \qquad (4.19)$$

where the terms of this matrix are refered to as the element shape functions.

The strains at any point (x,y) within the structure are defined from the displacement equations by;

$$\underset{\sim}{\epsilon} = \begin{bmatrix} \partial/\partial x & 0 \\ 0 & \partial/\partial y \\ \partial/\partial y & \partial/\partial x \end{bmatrix} (\underset{\sim}{U}) \qquad (4.20)$$

where $\underset{\sim}{\epsilon}$ is the strain column vector.

Substituting equation (4.18) into equation (4.20) gives the incremental strains at any point of the element in terms of incremental nodal displacements;

$$\underset{\sim}{\epsilon}_e = \left(\begin{bmatrix} \partial/\partial x & 0 \\ 0 & \partial/\partial y \\ \partial/\partial y & \partial/\partial x \end{bmatrix} \left(\begin{bmatrix} \underset{\sim}{g} & \underset{\sim}{0} \\ \underset{\sim}{0} & \underset{\sim}{g} \end{bmatrix} \right) \right) \cdot \begin{bmatrix} \underline{A}^{-1} & \underline{0} \\ \underline{0} & \underline{A}^{-1} \end{bmatrix} \cdot \Delta\underset{\sim}{\delta}_e$$

or;

$$\Delta\underset{\sim}{\epsilon}_e = \underline{C} \cdot \begin{bmatrix} \underline{A}_e^{-1} & \underline{0} \\ \underline{0} & \underline{A}^{-1} \end{bmatrix} \cdot \Delta\underset{\sim}{\delta}_e \qquad (4.21)$$

where,

$$\Delta\underset{\sim}{\epsilon}_e = \{ \Delta\epsilon_x \quad \Delta\epsilon_y \quad \Delta\epsilon_{xy} \}^t$$

$$\underline{C} = \begin{bmatrix} 0 & 1 & 0 & y & 0 & 0 & 0 & 0 \\ 0 & 0 & 0 & 0 & 0 & 0 & 1 & x \\ 0 & 0 & 1 & x & 0 & 1 & 0 & y \end{bmatrix} \qquad (4.22)$$

then the incremental strains within the element vary linearly.

By equating equations (4.4) and (4.21), we have;

$$\underline{B}_e = \underline{C} \cdot \begin{bmatrix} \underline{A}_e^{-1} & \underline{0} \\ \underline{0} & \underline{A}_e^{-1} \end{bmatrix} \qquad (4.23)$$

and;

$$\underline{B}_e = \begin{bmatrix} \frac{\bar{y}-1}{a} & \frac{1-\bar{y}}{a} & \frac{\bar{y}}{a} & -\frac{\bar{y}}{a} & 0 & 0 & 0 & 0 \\ 0 & 0 & 0 & 0 & \frac{\bar{x}-1}{b} & -\frac{\bar{x}}{b} & \frac{\bar{x}}{b} & \frac{1-\bar{x}}{b} \\ \frac{\bar{x}-1}{b} & -\frac{\bar{x}}{b} & \frac{\bar{x}}{b} & \frac{1-\bar{x}}{b} & \frac{1-\bar{y}}{a} & \frac{\bar{y}-1}{a} & \frac{\bar{y}}{a} & -\frac{\bar{y}}{a} \end{bmatrix}$$

where, $\bar{x}=\frac{x}{a}$ and $\bar{y}=\frac{y}{b}$.

By referring to equation (4.4) again, the incremental strains at any point of the element due to incremental nodal displacements are calculated by;

$$\Delta\underset{\sim}{\varepsilon}_e = \underline{B}_e \cdot \Delta\underset{\sim}{\delta}_e$$

which by applying incremental initial strain to the pth layer of the element (e), the incremental stain vector is written as follows;

$$\Delta\underset{\sim}{\varepsilon}_{ep} = \underline{B}_e \cdot \Delta\underset{\sim}{\delta}_e - \Delta\underset{\sim}{\varepsilon}^o_{ep} \qquad (4.24)$$

where,

$$\Delta\underset{\sim}{\varepsilon}^o_{ep} = \left\{ \Delta\epsilon^o_x \quad \Delta\epsilon^o_x \quad \Delta\gamma^o_{xy} \right\}^t_{ep}$$

is the incremental initial strain vector. In the case of the temperature increasing within the structure, the incremental initial strain vector is given by;

$$\Delta\underset{\sim}{\varepsilon}^o_{ep} = \left\{ c.\delta T \quad c.\delta T \quad 0 \right\}^t_{ep}$$

where c is the coefficient of thermal expansion of the material and δT is the incremental temperature of the pth layer of the element.

However, the matrix $\underline{B}_e$ at the centroid of the element with the geometrical properties ($\bar{x}=\frac{1}{2}, \bar{y}=\frac{1}{2}$) reduce to;

$$\underline{B}_{ec} = \frac{1}{2s}\begin{bmatrix} b.\underset{\sim}{\alpha} & 0 \\ 0 & a.\underset{\sim}{\beta} \\ a.\underset{\sim}{\beta} & b.\underset{\sim}{\alpha} \end{bmatrix}$$

where s is the area of the element (e) and,

$$\underset{\sim}{\alpha} = \{ -1 \quad 1 \quad 1 \quad -1 \}$$

$$\underset{\sim}{\beta} = \{ -1 \quad -1 \quad 1 \quad 1 \}$$

Clearly, when the summation of numbers in $\underset{\sim}{\alpha}$ and $\underset{\sim}{\beta}$ are equal to zero, implies that strain does not appear in free body motion.

The incremental stress-displacement relationship of the pth layer of the element (e) is obtained by inserting equation (4.21) into equation (4.5);

$$\Delta \underset{\sim}{\sigma}_{ep} = \underline{D}_{ep} \cdot \underline{C} \begin{bmatrix} \underline{A}_e^{-1} & \underline{0} \\ \underline{0} & \underline{A}_e^{-1} \end{bmatrix} \cdot \Delta \underset{\sim}{\delta}_e \qquad (4.25)$$

and this is the only relationship between incremental stresses of any point within the pth layer of the element and the incremental nodal displacements of the element derived from the above displacement equations.

The elasticity matrix $\underline{D}^*_{ep}$ for concrete material of the pth layer, in the principal directions referring to the equation (3.11) is given by;

$$\underline{D}^*_{ep} = \begin{bmatrix} E_1 & 0 & 0 \\ 0 & E_2 & 0 \\ 0 & 0 & G \end{bmatrix}_{ep}$$

where,

$$E_1 = \frac{(1+\mu\beta_1)\left[1-\left(\frac{\varepsilon_1}{\varepsilon_m}\right)^2\right]\cdot E}{(1-\mu^2)\left[1-\left(2-\frac{1+\mu\beta_1}{1-\mu^2}\cdot\frac{E}{E'}\right)\cdot\frac{\varepsilon_1}{\varepsilon_m}+\left(\frac{\varepsilon_1}{\varepsilon_m}\right)^2\right]^2}$$

$$E_2 = \frac{(1+\mu\beta_2)\left[1-\left(\frac{\varepsilon_2}{\varepsilon_m}\right)^2\right]\cdot E}{(1-\mu^2)\left[1-\left(2-\frac{1+\mu\beta_2}{1-\mu^2}\cdot\frac{E}{E'}\right)\cdot\frac{\varepsilon_2}{\varepsilon_m}+\left(\frac{\varepsilon_2}{\varepsilon_m}\right)^2\right]^2}$$

$$G = \frac{E_1^* \cdot E_2^*}{E_1^* + (1+2\mu)E_2^*}$$

where, μ is the Poisson's ratio, E is the initial modulus of elasticity in uniaxial state of stress, E' is the secant modulus, ε_1 and ε_2 are the strains in the principal co-ordinates, ε_m is the strain value corresponding to the peak value of stress and,

$$\beta_1 = \frac{\varepsilon_2}{\varepsilon_1}, \quad \beta_2 = \frac{\varepsilon_1}{\varepsilon_2}$$

$$E_1^* = \frac{E_1}{F_1}, \quad E_2^* = \frac{E_2}{F_2}$$

where,

$$F_1 = \frac{1+\mu\cdot\beta_1}{1-\mu^2}$$

$$F_2 = \frac{1+\mu\cdot\beta_2}{1-\mu^2}$$

For steel layers the elasticity matrix in principal or global coordinates is given by;

$$\underline{D}^{*}_{ep} = \frac{E_s}{1-\mu^2}\begin{bmatrix} 1 & \mu & 0 \\ \mu & 1 & 0 \\ 0 & 0 & \frac{1}{2}(1-\mu) \end{bmatrix}_{ep}$$

For a layer with a crack in the second principal direction carrying no shear stress along the crack, the elasticity matrix is given by;

$$\underline{D}^{*}_{ep} = \begin{bmatrix} 0 & 0 & 0 \\ 0 & E_2 & 0 \\ 0 & 0 & 0 \end{bmatrix}_{ep}$$

but in fact the two parts of the cracked layer produce a small shear stress along the crack, because of aggregate interlock, and the elasticity matrix must be assumed in the following form;

$$\underline{D}^{*}_{ep} = \begin{bmatrix} 0 & 0 & 0 \\ 0 & E_2 & 0 \\ 0 & 0 & \beta G_c \end{bmatrix}_{ep} \qquad \text{where,} \quad G_c = \frac{E}{2(1+\mu)}$$

where, β is the shear coefficient varies between zero and one, which is assumed to be 0.4 in the present analysis.

When there are two cracks in two perpendicular directions, the elasticity matrix is assumed to be $\underline{0}$, but othewise the shear effect is taken into account.

However, the elasticity matrix in principal co-ordinates is required to be transformed into global co-ordinates as follows;

$$\underline{D}_{ep} = \underline{T}^{t}_{ep} \cdot \underline{D}^{*}_{ep} \cdot \underline{T}_{ep} \qquad (4.26)$$

where, $\underline{T}_{ep}$ is the transformation matrix, which is given by, [Ref. 104].

$$\underline{T}_{ep} = \begin{bmatrix} \cos^2\theta & \sin^2\theta & \frac{1}{2}\sin 2\theta \\ \sin^2\theta & \cos^2\theta & -\frac{1}{2}\sin 2\theta \\ -\sin 2\theta & \sin 2\theta & \cos 2\theta \end{bmatrix}$$

and θ is angle between global and principal directions.

By referring to equations (4.11) and (4.26), the stiffness matrix of pth layer of the element is obtained by;

$$\underline{k}_{ep} = \left|h_{p+1}-h_p\right| \iint_S (\underline{B}_e^t . \underline{T}_{ep}^t . \underline{D}_{ep}^* . \underline{T}_{ep} . \underline{B}_e) . ds \qquad (4.27)$$

where, h_{p+1} and h_p are distances from middle surface of the beam to the surfaces of the pth layer of the element as shown in figure (4.2), i.e, $\left|h_{p+1}-h_p\right|$ is the thickness of the layer.

Finally, the element stiffness matrix of the element (e) is obtained by summation of layers stiffness matrices;

$$\underline{k}_e = \sum_{p=1}^{n} \underline{k}_{ep}$$

and n is the number of layers in the element.

If the transformed elasticity matrix is given by;

$$\underline{D}_{ep} = \begin{bmatrix} d_{11} & d_{12} & d_{13} \\ & d_{22} & d_{23} \\ \text{Sym.} & & d_{33} \end{bmatrix}$$

the stiffness matrix of pth layer of the element becomes as follows;

$$\underline{k}_e = \begin{bmatrix} A & B & C & D & E & F & G & H \\ & I & J & K & L & M & N & O \\ & & A & B & G & H & E & F \\ & & & I & N & O & L & M \\ & & & & P & Q & R & S \\ & \text{Sym.} & & & & T & S & U \\ & & & & & & P & Q \\ & & & & & & & T \end{bmatrix} \qquad (4.28)$$

where,

$$A = \sum_{p=1}^{n} \left\{ s.\Delta h. \left[\tfrac{1}{3}(\bar{b}.d_{11} + \bar{a}.d_{33}) + \tfrac{1}{2}d_{13} \right] \right\}$$

$$B = \sum_{p=1}^{n} \left\{ s.\Delta h. \left(-\tfrac{1}{3}\bar{b}.d_{11} + \tfrac{1}{6}\bar{a}.d_{33} \right) \right\}$$

$$C = -\tfrac{1}{2} \sum_{p=1}^{n} \left\{ s.\Delta h. \left[\tfrac{1}{3}(\bar{b}.d_{11} + \bar{a}.d_{33}) + d_{13} \right] \right\}$$

$$D = \tfrac{1}{3} \sum_{p=1}^{n} \left\{ s.\Delta h. \left(\tfrac{1}{2}\bar{b}.d_{11} - \bar{a}.d_{33} \right) \right\}$$

$$E = \sum_{p=1}^{n} \left\{ s.\Delta h. \left[\tfrac{1}{3}(\bar{b}.d_{13} + \bar{a}.d_{23}) + \tfrac{1}{4}(d_{12} + d_{33}) \right] \right\}$$

$$F = \sum_{p=1}^{n} \left\{ s.\Delta h. \left[-\tfrac{1}{3}\bar{b}.d_{13} + \tfrac{1}{6}\bar{a}.d_{23} + \tfrac{1}{4}(d_{12} - d_{33}) \right] \right\}$$

$$G = -\tfrac{1}{2} \sum_{p=1}^{n} \left\{ s.\Delta h. \left[\tfrac{1}{3}(\bar{b}.d_{13} + \bar{a}.d_{23}) + \tfrac{1}{2}(d_{12} + d_{33}) \right] \right\}$$

$$H = \sum_{p=1}^{n} \left\{ s.\Delta h. \left[\tfrac{1}{6}\bar{b}.d_{13} - \tfrac{1}{3}\bar{a}.d_{23} - \tfrac{1}{4}(d_{12} - d_{33}) \right] \right\}$$

$$I = \sum_{p=1}^{n} \left\{ s.\Delta h. \left[\tfrac{1}{3}(\bar{b}.d_{11}+\bar{a}.d_{33}) - \tfrac{1}{2}d_{13} \right] \right\}$$

$$J = \tfrac{1}{3} \sum_{p=1}^{n} \left\{ s.\Delta h. (\tfrac{1}{2}\bar{b}.d_{11} - \bar{a}.d_{33}) \right\}$$

$$k = \tfrac{1}{2} \sum_{p=1}^{n} s.\Delta h. \left[-\tfrac{1}{3}(\bar{b}.d_{11}+\bar{a}.d_{33}) + d_{13} \right] \}$$

$$L = \sum_{p=1}^{n} \left\{ s.\Delta h. \left[-\tfrac{1}{3}\bar{b}.d_{13} + \tfrac{1}{6}\bar{a}.d_{23} - \tfrac{1}{4}(d_{12}-d_{33}) \right] \right\}$$

$$M = \sum_{p=1}^{n} \left\{ s.\Delta h. \left[\tfrac{1}{3}(\bar{b}.d_{13}+\bar{a}.d_{23}) - \tfrac{1}{4}(d_{12}+d_{33}) \right] \right\}$$

$$N = \tfrac{1}{2} \sum_{p=1}^{n} \left\{ s.\Delta h. \left[\tfrac{1}{3}\bar{b}.d_{13} - \tfrac{1}{3}\bar{a}.d_{23} + \tfrac{1}{2}(d_{12}-d_{33}) \right] \right\}$$

$$O = \tfrac{1}{2} \sum_{p=1}^{n} \left\{ s.\Delta h. \left[-\tfrac{1}{3}(\bar{b}.d_{13}+\bar{a}.d_{23}) + \tfrac{1}{2}(d_{12}+d_{33}) \right] \right\}$$

$$P = \sum_{p=1}^{n} \left\{ s.\Delta h. \left[\tfrac{1}{3}(\bar{a}.d_{22}+\bar{b}.d_{33}) + \tfrac{1}{2}d_{23} \right] \right\}$$

$$Q = \tfrac{1}{3} \sum_{p=1}^{n} \left\{ s.\Delta h. (\tfrac{1}{2}\bar{a}.d_{22} - \bar{b}.d_{33}) \right\}$$

$$R = -\tfrac{1}{2} \sum_{p=1}^{n} \left\{ s.\Delta h. \left[\tfrac{1}{3}(\bar{a}.d_{22}+\bar{b}.d_{33}) + d_{23} \right] \right\}$$

$$S = \tfrac{1}{3} \sum_{p=1}^{n} \left\{ s.\Delta h. (-\bar{a}.d_{22} + \tfrac{1}{2}\bar{b}.d_{33}) \right\}$$

$$T = \sum_{p=1}^{n}\left\{ s.\Omega h.\left[\tfrac{1}{3}(\bar{a}.d_{22}+\bar{b}.d_{33})-\tfrac{1}{2}d_{23}\right]\right\}$$

$$U = \tfrac{1}{2}\sum_{p=1}^{n}\left\{ s.\Omega h.\left[-\tfrac{1}{3}(\bar{a}.d_{22}+\bar{b}.d_{33})+d_{23}\right]\right\}$$

and,

$$\bar{a} = \frac{a}{b}\ ,\quad \bar{b} = \frac{b}{a} \quad \text{and} \quad \Omega h = \left|h_{p+1} - h_p\right|.$$

As we will see in a later section, in analysis of reinforced concrete slabs, the above arrangement of forces and displacements vectors simplify the corresponding formulae and computer programing and also reduce the computational time, while in analysis of reinforced concrete beams, a convenient arrangement of nodal displacements and forces are;

$$\underset{\sim}{\delta}_e = \left\{ u_i \quad v_i \quad u_j \quad v_j \quad u_m \quad v_m \quad u_n \quad v_n \right\}_e^t$$

$$\underset{\sim}{f}_e = \left\{ f_{xi} \quad f_{yi} \quad f_{xj} \quad f_{yj} \quad f_{xm} \quad f_{ym} \quad f_{xn} \quad f_{yn} \right\}_e^t$$

and in this arrangement the relation between the unknown coefficients of displacement functions and incremental nodal displacements become;

$$\Delta\underset{\sim}{\delta}_e = \underline{\underline{A}}'_e .\ \underset{\sim}{a}_8 \qquad (4.29)$$

and there is no symmetry in matrix $\underline{\underline{A}}'_e$.

By referring to figure (4.3), the matrix $\underline{\underline{A}}'_e$ in the global coordinates is written as follows;

$$\underline{A}'_e = \begin{bmatrix} 1 & x_i & y_i & x_i y_i & 0 & 0 & 0 & 0 \\ 0 & 0 & 0 & 0 & 1 & x_i & y_i & x_i y_i \\ 1 & x_j & y_j & x_j y_j & 0 & 0 & 0 & 0 \\ 0 & 0 & 0 & 0 & 1 & x_j & y_j & x_j y_j \\ 1 & x_m & y_m & x_m y_m & 0 & 0 & 0 & 0 \\ 0 & 0 & 0 & 0 & 1 & x_m & y_m & x_m y_m \\ 1 & x_n & y_n & x_n y_n & 0 & 0 & 0 & 0 \\ 0 & 0 & 0 & 0 & 1 & x_n & y_n & x_n y_n \end{bmatrix}$$

and in element coordinates becomes as follows;

$$\underline{A}'_e = \begin{bmatrix} 1 & 0 & 0 & 0 & 0 & 0 & 0 & 0 \\ 0 & 0 & 0 & 0 & 1 & 0 & 0 & 0 \\ 1 & a & 0 & 0 & 0 & 0 & 0 & 0 \\ 0 & 0 & 0 & 0 & 1 & a & 0 & 0 \\ 1 & a & b & s & 0 & 0 & 0 & 0 \\ 0 & 0 & 0 & 0 & 1 & a & b & s \\ 1 & 0 & b & 0 & 0 & 0 & 0 & 0 \\ 0 & 0 & 0 & 0 & 1 & 0 & b & 0 \end{bmatrix}$$

where, s is the area of the element.

Substituting the unknown coefficient vector $\underset{\sim}{a}_8$ from equation (4.29) into equation (4.12), the shape functions become;

$$\underset{\sim}{U} = \begin{bmatrix} \underset{\sim}{\varepsilon} & \underset{\sim}{0} \\ \underset{\sim}{0} & \underset{\sim}{\varepsilon} \end{bmatrix} \cdot \underline{A}'^{-1}_e \cdot \Delta\underset{\sim}{\delta}_e$$

and;

$$\underline{A}_e'^{-1} = \frac{1}{s}\begin{bmatrix} s & 0 & 0 & 0 & 0 & 0 & 0 & 0 \\ -b & 0 & b & 0 & 0 & 0 & 0 & 0 \\ -a & 0 & 0 & 0 & 0 & 0 & a & 0 \\ 1 & 0 & -1 & 0 & 1 & 0 & -1 & 0 \\ 0 & s & 0 & 0 & 0 & 0 & 0 & 0 \\ 0 & -b & 0 & b & 0 & 0 & 0 & 0 \\ 0 & -a & 0 & 0 & 0 & 0 & 0 & a \\ 0 & 1 & 0 & -1 & 0 & 1 & 0 & -1 \end{bmatrix}$$

and the strain matrix $\underline{B}_e'$ in this arrangement becomes;

$$\underline{B}_e' = \underline{C} \cdot \underline{A}_e'^{-1}$$

which is simply obtained as;

$$\underline{B}_e' = \frac{1}{s}\begin{bmatrix} y-b & 0 & b-y & 0 & y & 0 & -y & 0 \\ 0 & x-a & 0 & -x & 0 & x & 0 & a-x \\ x-a & y-b & -x & b-y & x & y & a-x & -y \end{bmatrix}$$

and this strain matrix for the centroid of the element (e) becomes;

$$\underline{B}_e' = \frac{1}{2s}\begin{bmatrix} -b & 0 & b & 0 & b & 0 & -b & 0 \\ 0 & -a & 0 & -a & 0 & a & 0 & a \\ -a & -b & -a & b & a & b & a & -b \end{bmatrix}$$

By referring to the elasticity matrix $\underline{D}_{ep}$ and the stiffness matrix $\underline{k}_{ep}$ of the pth layer of the element, in the previous arrangement of nodal displacements and forces, the stiffness matrix of the element (e) for the present case can be written in the following form;

$$\underline{K}'_e = \sum_{p=1}^{n} \underline{k}'_{ep}$$

gives the element stiffness matrix as follows;

$$\underline{k}'_e = \begin{bmatrix} A & C & E & G & B & D & F & H \\ & A & G & E & J & B & E & F \\ & & P & R & L & N & Q & S \\ & & & P & N & L & S & Q \\ & & & & I & K & M & O \\ & & & & & I & O & M \\ & & & & & & T & U \\ & & & & & & & T \end{bmatrix} \qquad (4.30)$$

where $\underline{k}'_{ep}$ is the stiffness matrix of pth layer of the element.

4.5- Reinforced Concrete Slabs

The analysis of reinforced concrete slabs under external service load and temperature effects is based on the small deflection plate theory basis with the following assumptions;

A- The slab is assumed to be initially flat and its deflection under external loads is produced by displacements of points of reference surface parallel with the slab's surface which can be assumed to be coincident with the middle surface of the slab.

B- The thickness of the slab is less than one tenth of its smallest lateral dimension and remains of constant thickness while deforming.

C- The deflections and slopes of the reference surface are small compared with the thickness of the slab. The deformations are not larger than one tenth of the thickness, and the slopes are small by comparison to unity.

D- The stresses perpendicular to the reference surface, and also the deformations due to transvere shear are neglected and any straight line perpendicular to the middle surface remains straight and perpendicular to the middle surface while deforming.

E- The middle surface strains due to inplane forces (external inplane forces) produced by deflection of the body are negligible compared to the strains produced by bending of the slab.

F- In case of external inplane forces the strains at any point of the body are obtained by superposing the

strains produced by inplane forces and bending of the slab i.e, the Kirchhoff assumption which will be explained in a later section, applies.

4.5.1- A Brief Description Of Plate Formula

Consider a rectangular parallelepiped ABCDA'B'C'D' under perpendicular distributed load F_z cut out of the plate, showing at its middle surface, the positive directions of coordinates and also the internal forces on the surfaces ABCA and A C'B'D are shown in figure (4.4).

From Taylor's series expansion the internal forces on the surfaces D'C'B'A' and B D'A'C of the element are written as follows;

$$M'_x = M_x + \frac{\partial M_x}{\partial x}.dx + \dots$$

$$M'_y = M_y + \frac{\partial M_y}{\partial y}.dy + \dots$$

$$M'_{xy} = M_{xy} + \frac{\partial M_{xy}}{\partial x}.dx + \dots$$

$$M'_{yx} = M_{yx} + \frac{\partial M_{yx}}{\partial y}.dy + \dots$$

$$P'_x = P_x + \frac{\partial P_x}{\partial x}.dx + \dots$$

$$P'_y = P_y + \frac{\partial P_y}{\partial y}.dy + \dots$$

which are shown in figure (4.4) with their positive directions.

Figure (4.5) illustrates the internal forces per unit

length of the middle surface, then;

$$M_x = m_x.dy \ , \quad M_y = m_y.dx$$

$$M_{xy} = m_{xy}.dy \ , \quad M_{yx} = m_{yx}.dx$$

$$P_x = p_x.dy \ , \quad P_y = p_y.dx$$

By neglecting the small quantities of higher order, the above expansions give;

$$M_x' = M_x + \frac{\partial m_x}{\partial x}.ds$$

$$M_y' = M_y + \frac{\partial m_y}{\partial y}.ds$$

$$M_{xy}' = M_{xy} + \frac{\partial m_{xy}}{\partial x}.ds$$

$$M_{yx}' = M_{yx} + \frac{\partial m_{yx}}{\partial y}.ds$$

$$P_x' = P_x + \frac{\partial p_x}{\partial x}.ds$$

$$P_y' = P_y + \frac{\partial p_y}{\partial y}.ds$$

where ds is the area of the middle surface of element.

As there is no inplane forces acting on the body the six equilibrium equations reduce to the following three equations;

$$M_x = 0, \quad M_y = 0, \quad F_z = 0,$$

which give;

$$\frac{\partial m_x}{\partial x} + \frac{\partial m_{yx}}{\partial y} - p_x = 0$$

$$\frac{\partial m_{xy}}{\partial x} + \frac{\partial m_y}{\partial y} - p_y = 0$$

$$\frac{\partial p_x}{\partial x} + \frac{p_y}{\partial y} + F_z = 0$$

and observing that, $m_{xy}=m_{yx}$ [Ref. 19] the above three equations reduce to;

$$\frac{\partial^2 m_x}{\partial x^2} + 2\frac{\partial^2 m_{xy}}{\partial x \partial y} + \frac{\partial^2 m_y}{\partial y^2} + F_z = 0 \qquad (4.31)$$

and the distributed load F_z is generally a function of x and y.

By considering the relationships between strains, stresses and displacements at every point within the element the relationship between external forces and displacements can be obtained as follows;

In an incremental load, any layer of the plate such as pth layer in figure (4.5) can be assumed as an elastic body permits the use of the Hook's law;

$$\underset{\sim}{\sigma} = \underline{D}_p \cdot \underset{\sim}{\varepsilon}$$

where,

$$\underset{\sim}{\varepsilon} = \left\{ \epsilon_x \quad \epsilon_y \quad \gamma_{xy} \right\}^t$$

$$\underset{\sim}{\sigma} = \left\{ \sigma_x \quad \sigma_y \quad \tau_{xy} \right\}^t$$

and $\underline{D}_p$ is the elasticity matrix contains the material properties of pth layer. To obtain the relationships between strain

and deflection at any point of the body a section of the element parallel with the x-axis is assumed where positions befor and after deflection are shown in figure (4.6). From the general assumption (D) of plate theory, the straight lines (AC) and (BD) which are perpendicular to the middle surface of the element, remain straight lines ($A'C'$) and ($B'D'$) and perpendicular to the middle surface of deformed body at points (a') and (b'), respectively and alsofrom the assumption (D) again the displacements of any point of middle surface such as points (a) and (b) are in the z-direction as (a') and (b').

From the assumption (B), any level of the section such as (cd) with the distance (z) from the middle surface remains parallel with the middle surface of the deformed body with distance (z), and hence, (c') and (d') correspond to (c) and (d) in figure (4.6), in which, the inplane displacement of point (c) is $u=c''c'$.

If (θ) is the rotation of straight line ($A'C'$), the rotation of straight line ($B'D'$) using the Taylor's series expansion becomes;

$$\theta' = \theta + \frac{\partial\theta}{\partial x}.dx + \ldots$$

and on the other hand the angle (θ) which is the slope of the middle surface is calculated by;

$$\theta = -\frac{\partial w}{\partial x}$$

and is positive in the anticlockwise direction. To evaluate the elongation of fiber ($c'd'$) the straight line ($b'd''$) is

drawn parallel with $(A'C')$, and by neglecting small terms of higher order we find;

$$d'\overleftarrow{b'}d'' = \theta' - \theta = \frac{\partial\theta}{\partial x}.dx$$

and the elongation of $(c'd')$ is obtained from small triangle $d'b'd''$;

$$d''d' = z.\frac{\partial\theta}{\partial x}.dx$$

and the strain at level (z) becomes as follows;

$$\epsilon_x = \frac{d''d'}{dx} = z.\frac{\partial\theta}{\partial x}$$

or;

$$\epsilon_x = - z.\frac{\partial^2 w}{\partial x^2} = - z.\ \xi_x$$

and similarly;

$$\epsilon_y = - z.\frac{\partial^2 w}{\partial y^2} = - z.\ \xi_y$$

where, ξ_x and ξ_y are curvatures of the middle surface of deformed body in x and y-directions, respectively.

From small triangle $a'c'c''$ the inplane displacement of point (c'') becomes;

$$u = \theta.z$$

or;

$$u = - z.\frac{\partial w}{\partial x}$$

and similarly;

$$v = - z.\frac{\partial w}{\partial y}$$

where u and v are the inplane displacements of point (c).

The shear strain at level (z) is calculated from;

$$\gamma_{xy} = \frac{\partial u}{\partial y} + \frac{\partial v}{\partial x}$$

or;

$$\gamma_{xy} = - z.\frac{\partial^2 w}{\partial x \partial y} - \frac{\partial^2 w}{\partial x \partial y}$$

and by observing that;

$$\frac{\partial^2 w}{\partial x \partial y} = \frac{\partial^2 w}{\partial x \partial y}$$

we find;

$$\gamma_{xy} = - 2z.\frac{\partial^2 w}{\partial x \partial y} = - 2z.\ \xi_{xy}$$

The above strains of any point at level (z) can be shown to be in matrix form as follows;

$$\underset{\sim}{\epsilon}_z = z.\ \underset{\sim}{\xi}$$

where, $\underset{\sim}{\xi}$ is the middle surface curvatures column vector;

$$\underset{\sim}{\xi} = \left\{ - \frac{\partial^2 w}{\partial x^2} \quad - \frac{\partial^2 w}{\partial y^2} \quad - 2\frac{\partial^2 w}{\partial x \partial y} \right\}^t \qquad (4.32)$$

and by substituting the strains $\underset{\sim}{\epsilon}_z$ into equation (4.5) the relationship between middle surface curvatures and stresses of level (z) becomes;

$$\underset{\sim}{\sigma}_z = z.\underline{D}_z \cdot \underset{\sim}{\xi}$$

Finally the stress resultant of pth layer on the

middle surface of the element are calculated by;

$$\underset{\sim}{m}_p = \int_{z_p}^{z_{p+1}} \underset{\sim}{\sigma} . z . dz$$

where z_p and z_{p+1} are distances from middle surface of the element to the top and bottom of the pth layer, respectively, then;

$$\underset{\sim}{m}_p = \underline{D}_p . \underset{\sim}{\xi} . \int_{z_p}^{z_{p+1}} z^2 . dz = \tfrac{1}{3}(z_{p+1}^3 - z_p^3) . \underline{D}_p . \underset{\sim}{\xi}$$

where $\underline{D}_p$ is the elasticity matrix of pth layer.

The stress resultants of the element is calculated by summation of the stress resultants of individual layers;

$$\underset{\sim}{m} = \tfrac{1}{3} \sum_{p=1}^{n} (z_{p+1}^3 - z_p^3) . \underline{D}_p . \underset{\sim}{\xi} \qquad (4.33)$$

which in the special case when the element is isotropic and homogeneous the equation (4.33) reduces to;

$$\underset{\sim}{m} = \frac{h^2}{12} . \underline{D} . \underset{\sim}{\xi}$$

where h is the thickness of the element (or plate) and $\underline{D}$ is the elasticity matrix of the body. Equation (4.33) may be written in the following form

$$\underset{\sim}{m}^t = \tfrac{1}{3} \underset{\sim}{\xi}^t . \sum_{p=1}^{n} (z_{p+1}^3 - z_p^3) . \underline{D}_p$$

where n is the number of layers in the element, however, by

assuming;

$$Z_p = \frac{E_p(z_{p+1}^3 - z_p^3)}{3(1-\mu_p^2)}$$

the bending moments and twisting moment produced by stresses of layers of the element become;

$$m_x = -\sum_{p=1}^{n} Z_p\left(\frac{\partial^2 w}{\partial x^2} + \mu_p \cdot \frac{\partial^2 w}{\partial y^2}\right)$$

$$m_y = -\sum_{p=1}^{n} Z_p\left(\mu_p \cdot \frac{\partial^2 w}{\partial x^2} + \frac{\partial^2 w}{\partial y^2}\right)$$

$$m_{xy} = -\sum_{p=1}^{n} (1-\mu_p) \cdot \frac{\partial^2 w}{\partial x \partial y}$$

where μ_p is the Poisson's ratio of the pth layer.

By substituting the above moments into equation (4.31) the differential equation which is the relationship between external force and lateral displacement becomes as follows;

$$\frac{\partial^4 w}{x^4} + 2\frac{\partial^4 w}{\partial x^2 \partial y^2} + \frac{\partial^4 w}{\partial y^4} - \frac{F_z}{\sum_{p=1}^{n} Z_p} = 0 \qquad (4.34)$$

The rest of the present chapter, includes a numerical method of solution of the differential equation (4.34) by given boundary conditions.

4.5.2- Layered Method Analysis Of Reinforced Concrete Slabs.

The purpose of this section is to obtain analytically the load deflection history for reinforced concrete slabs, under external service load and temperature influence, by introducing a nonlinear finite element technique with rectangular layered elements. The structural material properties permitted for the steel reinforcement are elastic or plastic and the concrete can be elastic, plastic, cracked or fail in compression.

Generally speaking, the analysis of any slab especially under temperature effects where the temperature is distributed over the thickness of the body, is a three dimensional problem. By introducing the stress resultants concept this three dimensional problem is reduced to a two dimensional one.

The basic prerequisite for the analysis of reinforcement concrete slabs is a suitable relationship between stress resultants and strain measurement, especially in incremental form, which reflects the yielding of the reinforcement, biaxial strength, cracking and also compression failure of the concrete as loading progresses or temperature increases. To obtain such a relationship, simplyfing assumptions must be made.

Briefly, for analysis of a slab with the layered method, the slab is replaced by a reference surface, which is analysed as a two dimensional body by dividing it into a

number of two dimensional elements. Since there is only one node at each corner of any element at reference surface of the slab throughout the thickness, the moment about z-direction perpendicular to the slab surface is neglected.

4.5.3- General Assumptions

To investigate the flexural behaviour of a reinforced concrete slab, the structure is divided into a finite number of rectangular elements being interconnected by four corner nodes and is assumed that the moment perpendicular to the slab is negligible, so each node has five degrees of freedom, in which there are three displacements and two rotations.

Each element is divided into a finite number of layers which may have different material properties but these remain constant throughout each layer during each incremental load or temperature. This layering procedure thus allows for changes in material properties at different elements and at different levels throughout the thickness of the slab while retaining the limited number of degrees of freedom associated with the two dimensional approach by enforcing the assumption the normals remain normals.

An advantage of this method is that only a biaxial strength criterion is required for the concrete since each layer is considered to be under a state of plane stress, however only biaxial behaviour of layers is required in order to establish a relationship between stresses and strains.

Clearly, from the above assumptions the shear modes of failure are rendered impossible in the process.

Furthermore, concrete is assumed to have a tension limit and yields in biaxial compression and the reinforcing steel is assumed to be elastic-plastic as explained in chapter three.

In the present method all the elements properties, such as moments, inplane forces, nodal displacements and strains are first assumed on an arbitrary surface parallel to the element surface such as middle surface of element and the strain state of the pth layer produced by external loads is related to the conditions at the reference surface, by utilising the Kirchhoff assumption as;

$$\Delta\underset{\sim}{\epsilon}_p = \Delta\underset{\sim}{\epsilon}_m + h_p \cdot \Delta\underset{\sim}{\xi}_m \qquad (4.35)$$

where, $\Delta\underset{\sim}{\epsilon}_p$ = incremental strain vector of the pth layer,

$\Delta\underset{\sim}{\epsilon}_m$ = incremental strain vector of the reference surface,

$\Delta\underset{\sim}{\xi}_m$ = reference surface curvatures vector, and

h_p = distance of the pth layer from the reference surface of the element.

Finally, the finite element technique is used to analyse the reference surface of the structures with the help of the displacement method.

4.5.4- General Formula

A typical rectangular element in local and global coordinates is shown in figure (4.7), and figure (4.8) illustrates the reference surface which is assumed to be coincident with the middle surface of the element (or slab), with positive directions of nodal displacements and rotations at node (i), and a cross-section of the element is shown in figure (4.9) with its layers properties.

Any layer of the element (e), such as pth layer in figure (4.9), produces a set of inplane incremental internal forces as follows;

$$\Delta \begin{Bmatrix} \underset{\sim}{F}_p \\ 0 \end{Bmatrix}$$

which, by transforming these forces on the reference surface of the element we have;

$$\Delta \begin{Bmatrix} \underset{\sim}{F}_{pr} \\ \underset{\sim}{M}_{pr} \end{Bmatrix} = \begin{Bmatrix} \Delta \underset{\sim}{F}_p \\ \underline{R} . \Delta \underset{\sim}{F}_p \end{Bmatrix}$$

where, $\underline{R}$ is the transformation matrix, $\Delta \underset{\sim}{F}_{pr}$ and $\Delta \underset{\sim}{M}_{pr}$ are the incremental inplane force and moment vectors on the reference surface, respectively and by this transformation, our problem becomes the superposing of two well known problems, i.e, the plane stress and pure bending, for each element.

The inplane degrees of freedom are important for slabs because of the material property variation through the slab thickness as loading progresses and especially as tem-

perature increase a coupling is produced in the constitutive relations between middle surface strains and curvatures and thus between inplane and perpendicular displacements.

The incremental stress-strain relationships at the location of the pth layer are given by;

$$\Delta\underset{\sim}{\sigma}_p = \underline{D}_p \cdot \Delta\underset{\sim}{\epsilon}_p \qquad (4.36)$$

where, $\underline{D}_p$ is the elasticity matrix contains the material properties of the pth layer, which was given in the beams problem, and;

$$\Delta\underset{\sim}{\sigma}_p = \left\{\Delta\sigma_x \quad \Delta\sigma_y \quad \Delta\tau_{xy}\right\}^t_p$$

$$\Delta\underset{\sim}{\epsilon}_p = \left\{\Delta\epsilon_x \quad \Delta\epsilon_y \quad \Delta\gamma_{xy}\right\}^t_p$$

and relating strains at a distance (h) of the pth layer from the reference surface to the middle surface strains and curvatures is;

$$\Delta\underset{\sim}{\epsilon}_h = \Delta\underset{\sim}{\epsilon}_r + h \cdot \Delta\underset{\sim}{\xi}_r \qquad (4.37)$$

where, $\Delta\underset{\sim}{\epsilon}_p$ is the incremental strain vector of level (h), $\Delta\underset{\sim}{\epsilon}_r$ and $\Delta\underset{\sim}{\xi}_r$ are the incremental strain and curvature vectors of the reference surface, respectively.

The incremental stress resultants at the distance (h) are calculated as follows;

$$\Delta\underset{\sim}{F}_h = \int \Delta\underset{\sim}{\sigma}_h \cdot dh \qquad (4.38)$$

$$\Delta \underset{\sim}{M}_h = \int \Delta \sigma_h . h . dh \qquad (4.39)$$

where,

$$\Delta \underset{\sim}{F}_h = \left\{ \Delta F_x \quad \Delta F_y \quad \Delta F_{xy} \right\}_h^t$$

$$\Delta \underset{\sim}{M}_h = \left\{ \Delta m_x \quad \Delta m_y \quad \Delta m_{xy} \right\}_h^t$$

and the integrations (4.38) and (4.39) extend over the total thickness of the pth layer and as the material properties vary discreetly through the thickness of the element, the stress resultants are obtained by summing the results of the above integrations over each individual layers.

By substituting equation (4.37) into equation (4.36), the relationship between incremental stresses of level (h) within the pth layer with respect of incremental strains and curvatures of the reference surface becomes;

$$\Delta \underset{\sim}{\sigma}_p = \underline{D}_p \cdot \Delta \underset{\sim}{\epsilon}_r + \underline{D}_p \cdot \Delta \underset{\sim}{\xi}_r . h \qquad (4.40)$$

and by inserting this incremental stress vector into equation (4.38) and aquation (4.39), the stress resultants of the pth layer are written in the following forms;

$$\Delta \underset{\sim}{F}_p = \int_{h_p}^{h_{p+1}} \underline{D}_p . (\Delta \underset{\sim}{\epsilon}_r + h . \Delta \underset{\sim}{\xi}_r) . dh$$

$$\Delta \underset{\sim}{M}_p = \int_{h_p}^{h_{p+1}} \underline{D}_p . (\Delta \underset{\sim}{\epsilon}_r + h . \Delta \underset{\sim}{\xi}_r) . h . dh$$

where h_{p+1} and h_p are distances from the reference surface to top and bottom of the pth layer, respectively as shown in figure (4.9).

The above integrations are simply evaluated as;

$$\Delta \underset{\sim}{F}_p = \underline{D}_p \cdot \Delta \underset{\sim}{\epsilon}_r (h_{p+1}-h_p) + \tfrac{1}{2}\underline{D}_p \cdot \Delta \underset{\sim}{\xi}_r (h_{p+1}^2-h_p^2)$$

$$\Delta \underset{\sim}{M}_p = \tfrac{1}{2}\underline{D}_p \cdot \Delta \underset{\sim}{\epsilon}_r (h_{p+1}^2-h_p^2) + \tfrac{1}{3}\underline{D}_p \cdot \Delta \underset{\sim}{\xi}_r (h_{p+1}^3-h_p^3)$$

which can be written in a matrix form as follows;

$$\Delta \begin{Bmatrix} F \\ M \end{Bmatrix}_p = \begin{bmatrix} (h_{p+1}-h_p)\underline{D}_p & \tfrac{1}{2}(h_{p+1}^2-h_p^2)\underline{D}_p \\ \tfrac{1}{2}(h_{p+1}^2-h_p^2)\underline{D}_p & \tfrac{1}{3}(h_{p+1}^3-h_p^3)\underline{D}_p \end{bmatrix} \begin{Bmatrix} \Delta\underset{\sim}{\epsilon} \\ \Delta\underset{\sim}{\xi} \end{Bmatrix}_r \qquad (4.41)$$

and hence, all the forces acting on the reference surface are calculated by summing the foregoing results over each layer and the resulting constitutive relations are;

$$\Delta \begin{Bmatrix} \underset{\sim}{F} \\ \underset{\sim}{M} \end{Bmatrix}_e = \sum_{p=1}^{n} \Delta \begin{Bmatrix} \underset{\sim}{F} \\ \underset{\sim}{M} \end{Bmatrix}_p$$

where n is the number of layers in the element (e).

In the present finite element formulations the incremental nodal displacement vector of the reference surface of the element (e), which are numbered in anticlockwise is given by;

$$\Delta \underset{\sim}{\delta}_e = \left\{ \Delta \underset{\sim}{u} \quad \Delta \underset{\sim}{v} \quad \Delta \underset{\sim}{\varphi} \right\}_e^t$$

where,

$$\Delta \underset{\sim}{u}_e = \left\{ \Delta u_i \quad \Delta u_j \quad \Delta u_m \quad \Delta u_n \right\}_e$$

$$\Delta \underset{\sim}{v}_e = \left\{ \Delta v_i \quad \Delta v_j \quad \Delta v_m \quad \Delta v_n \right\}_e$$

are inplane displacement vectors and,

$$\Delta \underset{\sim}{\varphi}_e = \left\{ \Delta w_i \quad \Delta \theta_{xi} \quad \Delta \theta_{yi} \quad \Delta w_j \quad \Delta \theta_{xj} \quad \Delta \theta_{yj} \ \ldots \ \Delta \theta_{yn} \right\}_e$$

and i, j, m and n are nodal numbers of the element (e), and Δw is the incremental displacement in z-direction and $\Delta \theta_x$ and $\Delta \theta_y$ are the incremental retations of corresponding node about y and x-directions respectively.

The corresponding nodal forces are given by;

$$\Delta \underset{\sim}{F}_e = \left\{ \Delta \underset{\sim}{F}_x \quad \Delta \underset{\sim}{F}_y \quad \Delta \underset{\sim}{M} \right\}_e^t$$

where,

$$\Delta \underset{\sim}{F}_{xe} = \left\{ \Delta F_{xi} \quad \Delta F_{xj} \quad \Delta F_{xm} \quad \Delta F_{xn} \right\}_e$$

$$\Delta \underset{\sim}{F}_{ye} = \left\{ \Delta F_{yi} \quad \Delta F_{yj} \quad \Delta F_{ym} \quad \Delta F_{yn} \right\}_e$$

are the inplane forces and,

$$\Delta \underset{\sim}{M}_e = \left\{ \Delta F_{zi} \quad \Delta m_{xi} \quad \Delta m_{yi} \quad \Delta F_{zj} \quad \Delta m_{xj} \quad \Delta m_{yj} \ \ldots \ \Delta m_{yn} \right\}_e$$

which, ΔF_z is the incremental force in z-direction and Δm_x and Δm_y are incremental moments per unit length of reference surface about y and x-directions respectively.

The incremental strains and curvatures of the reference surface of the element are calculated from the equation (4.32);

$$\Delta_{\underset{\sim}{\epsilon}_r} = \begin{Bmatrix} \Delta\epsilon_x \\ \Delta\epsilon_y \\ \Delta\gamma_{xy} \end{Bmatrix}_r = \Delta \begin{Bmatrix} \partial u/\partial x \\ \partial v/\partial y \\ \partial u/\partial y + \partial v/\partial x \end{Bmatrix}_r$$

$$\Delta_{\underset{\sim}{\xi}_r} = \begin{Bmatrix} \Delta\xi_x \\ \Delta\xi_y \\ \Delta\xi_{xy} \end{Bmatrix}_r = -\Delta \begin{Bmatrix} \partial^2 w/\partial x^2 \\ \partial^2 w/\partial y^2 \\ 2.\partial^2 w/\partial x \partial y \end{Bmatrix}_r$$

where u, v and w are displacements of any point of the body.

4.5.5- Displacement Functions

In the displacement formulation of the finite element technique the critical stage is the selection of displacement functions, however, as the present problem as the result of superposing the inplane displacements u, v and perpendicular displacement w, the inplane displacement functions are assumed as in equation (4.15);

$$u = a_1 + a_2 x + a_3 y + a_4 xy$$

$$v = a_5 + a_6 x + a_7 y + a_8 xy$$

The perpendicular displacement function is a fourth-degree polynomial which can be selected to satisfy the partial differential equation (4.34), if $F_z = 0$, is given by 23 unknown coefficients in the following form;

$$w = a_9 + a_{10}x + a_{11}y + a_{12}xy + a_{13}x^2 + a_{14}y^2 + a_{15}x^3$$

$$+ a_{16}x^2y + a_{17}xy^2 + a_{18}y^3 + a_{19}x^3y + a_{20}xy^3 + a_{21}x^2y^2$$

$$+ a_{22}x^4 + a_{23}y^4$$

and simply we have;

$$\frac{\partial^4 w}{\partial x^4} = 24\ a_{22}$$

$$\frac{\partial^4 w}{\partial y^4} = 24\ a_{23}$$

$$\frac{\partial^4 w}{\partial x^2 \partial y^2} = 4\ a_{21}$$

which, by substituting into equation (4.34) and assuming $F_z=0$ we find;

$$a_{21} + 6(a_{22} + a_{23}) = 0 \qquad (4.42)$$

Any of the following five conditions give a fourth-degree polynomial which satisfies the differential equation;

$$a_{21} = a_{22} = a_{23} = 0 \qquad (A)$$

$$a_{21} = 0,\ a_{22} + a_{23} = 0 \qquad (B)$$

$$a_{22} = 0,\ a_{21} + 6\ a_{23} = 0 \qquad (C)$$

$$a_{23} = 0,\ a_{21} + 6\ a_{22} = 0 \qquad (E)$$

$$a_{21} + 6(a_{22} + a_{23}) = 0 \qquad (F)$$

The additional rotations $\partial w/\partial x$ and $\partial w/\partial y$ are also required to define the set of displacement functions in the bending.

Introducing the nodal displacement and rotations into the above functions (w, $\partial w/\partial x$ and $\partial w/\partial y$ a set of twelve simultaneous equations are obtained, in which, the number of unknowns (a_9 to a_{23}) exceeds the number of equations. However a unique solution of these equations is possible only if the condition (A) is considered, and hence, the displacement functions become as follows;

$$u = a_1 + a_2x + a_3y + a_4xy$$

$$v = a_5 + a_6x + a_7y + a_8xy$$

$$w = a_9 + a_{10}x + a_{11}y + a_{12}xy + a_{13}x^2 + a_{14}y^2 + a_{15}x^3 + a_{16}x^2y + a_{17}xy^2 + a_{18}y^3 + a_{19}x^3y + a_{20}xy^3$$

which has been used by many investigators [Ref. 73, 83 and 92].

In addition we have two rotations about two inplane y and x-axes as;

$$\theta_x = \frac{\partial w}{\partial x}$$

$$\theta_y = \frac{\partial w}{\partial y}$$

are the slopes of the perpendicular displacement (w) in the above conditions. However the displacements of a particular point of the reference surface of element (e) can be presented in the following form.

$$\underset{\sim}{U} = \begin{Bmatrix} u \\ v \\ w \\ \theta_x \\ \theta_y \end{Bmatrix} = \begin{Bmatrix} u \\ v \\ w \\ \partial w/\partial x \\ \partial w/\partial y \end{Bmatrix}$$

and this displacements can be expresed in terms of the unknown coefficiens;

$$\underset{\sim}{a}_{20} = \{a_1 \quad a_2 \quad a_3 \cdots a_{20}\}^t$$

as in the equation below;

$$\bar{U} = \begin{bmatrix} \underset{\sim}{g} & \underset{\sim}{0} & \underset{\sim}{0} \\ \underset{\sim}{0} & \underset{\sim}{g} & \underset{\sim}{0} \\ \underset{\sim}{0} & \underset{\sim}{0} & \underset{\sim}{G} \end{bmatrix} \cdot \underset{\sim}{a}_{20} \qquad (4.43)$$

where,

$$\underset{\sim}{g} = \{1 \quad x \quad y \quad xy\}$$

and,

$$\underset{\sim}{G} = \begin{bmatrix} 1 & x & y & xy & x^2 & y^2 & x^3 & x^2y & xy^2 & y^3 & x^3y & xy^3 \\ 0 & 1 & 0 & y & 2x & 0 & 3x^2 & 2xy & y^2 & 0 & 3x^2y & y^3 \\ 0 & 0 & 1 & x & 0 & 2y & 0 & x^2 & 2xy & 3y^2 & x^3 & 3xy^2 \end{bmatrix}$$

Equation (4.43) shows again that the perpendicular displacement and two rotations are independent of the inplane displacements, and hence, the first eight unknowns $\underset{\sim}{a}_8$ are calculated identically as in equation (4.16).

By referring to figure (4.10) and assuming the element nodal properties;

$$(\Delta u_k \quad \Delta v_k \quad \Delta w_k \quad \Delta\theta_{xk} \quad \Delta\theta_{yk} \quad x_k \quad y_k)_{k=i,\ j,\ m,\ n}$$

and using equation (4.43) our simultaneous equations become as follows;

$$\Delta\tilde{\underset{\sim}{\delta}}_e = \begin{bmatrix} \underline{A}_e & \underline{0} & \underline{0} \\ \underline{0} & \underline{A}_e & \underline{0} \\ \underline{0} & \underline{0} & \underline{A}^*_e \end{bmatrix} \cdot \underset{\sim}{a}_{20} \qquad (4.44)$$

where $\Delta\tilde{\underset{\sim}{\delta}}_e$ includes the incremental nodal displacements and rotations of the reference surface of the element (e) in the following order;

$$\Delta\tilde{\underset{\sim}{\delta}}_e = \left\{ \Delta\underset{\sim}{u} \quad \Delta\underset{\sim}{v} \quad \Delta\underset{\sim}{\varphi} \right\}^t_e$$

where,

$$\Delta\underset{\sim}{u}_e = \left\{ \Delta u_i \quad \Delta u_j \quad \Delta u_m \quad \Delta u_n \right\}$$

$$\Delta\underset{\sim}{v}_e = \left\{ \Delta v_i \quad \Delta v_j \quad \Delta v_m \quad \Delta v_n \right\}$$

$$\Delta\underset{\sim}{\varphi}_e = \left\{ \Delta w_i \quad \Delta\theta_{xi} \quad \Delta\theta_{yi} \quad \Delta w_j \quad \Delta\theta_{xj} \quad \Delta\theta_{yj} \ \ldots \ \Delta\theta_{yn} \right\}$$

From equation (4.44), the unknown coefficients become;

becom;

$$\underset{\sim}{a}_{20} = \begin{bmatrix} \underline{A}_e & \underline{0} & \underline{0} \\ \underline{0} & \underline{A}_e & \underline{0} \\ \underline{0} & \underline{0} & \underline{A}^*_e \end{bmatrix}^{-1} \cdot \Delta\tilde{\underset{\sim}{\delta}}_e$$

Matrix $\underline{A}_e$ is identical in analysis of beams which has been given by equation (4.15) in local coordinates and matrix $\underline{A}^*$ in local coordinates is written as follows;

$$
\underline{A}_e^* = \begin{bmatrix}
1 & 0 & 0 & 0 & 0 & 0 & 0 & 0 & 0 & 0 & 0 & 0 \\
0 & 1 & 0 & 0 & 0 & 0 & 0 & 0 & 0 & 0 & 0 & 0 \\
0 & 0 & 1 & 0 & 0 & 0 & 0 & 0 & 0 & 0 & 0 & 0 \\
1 & x_j & 0 & 0 & x_j^2 & 0 & x_j^3 & 0 & 0 & 0 & 0 & 0 \\
0 & 1 & 0 & 0 & 2x_j & 0 & 3x_j^2 & 0 & 0 & 0 & 0 & 0 \\
0 & 0 & 1 & x_j & 0 & 0 & 0 & x_j^2 & 0 & 0 & x_j^3 & 0 \\
1 & x_m & y_m & x_m y_m & x_m^2 & y_m^2 & x_m^3 & x_m^2 y_m & x_m y_m^2 & y_m^2 & x_m^3 y_m & x_m y_m^3 \\
0 & 1 & 0 & y_m & 2x_m & 0 & 3x_m^2 & 2x_m y_m & y_m^2 & 0 & 3x_m^2 y_m & y_m^3 \\
0 & 0 & 1 & x_m & 0 & 2y_m & 0 & x_m^2 & 2x_m y_m & 3y_m^2 & x_m^3 & 3x_m y_m^2 \\
1 & 0 & y_n & 0 & 0 & y_n^2 & 0 & 0 & 0 & y_n^2 & 0 & 0 \\
0 & 1 & 0 & y_n & 0 & 0 & 0 & 0 & y_n^2 & 0 & 0 & y_n^3 \\
0 & 0 & 1 & 0 & 0 & 2y_n & 0 & 0 & 0 & 3y_n^2 & 0 & 0
\end{bmatrix}
$$

The unknown coefficients of the displacement functions however are calculated from;

$$
\underset{\sim}{a}_{20} = \begin{bmatrix}
\underline{A}_e^{-1} & \underline{0} & \underline{0} \\
\underline{0} & \underline{A}^{-1} & \underline{0} \\
\underline{0} & \underline{0} & \underline{A}^{*-1}
\end{bmatrix} \qquad (4.45)
$$

where $\underline{A}^{-1}$ is identical with (4.17), in analysis of beams, and $\underline{A}^{*-1}$ is;

$$\frac{1}{s}\begin{bmatrix}
1 & 0 & 0 & 0 & 0 & 0 & 0 & 0 & 0 & 0 & 0 & 0 \\
0 & 1 & 0 & 0 & 0 & 0 & 0 & 0 & 0 & 0 & 0 & 0 \\
0 & 0 & 1 & 0 & 0 & 0 & 0 & 0 & 0 & 0 & 0 & 0 \\
-1 & -a & -b & 1 & 0 & b & -1 & 0 & 0 & 1 & a & 0 \\
-3\bar{b} & -2b & 0 & 3\bar{b} & -b & 0 & 0 & 0 & 0 & 0 & 0 & 0 \\
-3\bar{a} & 0 & -2a & 0 & 0 & 0 & 0 & 0 & 0 & 3\bar{a} & 0 & -a \\
\frac{2\bar{b}}{a} & \bar{b} & 0 & -\frac{2\bar{b}}{a} & \bar{b} & 0 & 0 & 0 & 0 & 0 & 0 & 0 \\
\frac{3}{a} & 2 & 0 & -\frac{3}{a} & 1 & 0 & \frac{3}{a} & -1 & 0 & -\frac{3}{a} & -2 & 0 \\
\frac{3}{\bar{b}} & 0 & 2 & -\frac{3}{\bar{b}} & 0 & -2 & \frac{3}{\bar{b}} & 0 & -1 & -\frac{3}{\bar{b}} & 0 & 1 \\
\frac{2\bar{a}}{b} & 0 & \bar{a} & 0 & 0 & 0 & 0 & 0 & 0 & -\frac{2\bar{a}}{b} & 0 & \bar{a} \\
-\frac{2\bar{b}}{s} & -\frac{1}{a} & 0 & \frac{2\bar{b}}{s} & -\frac{1}{a} & 0 & -\frac{2\bar{b}}{s} & \frac{1}{a} & 0 & \frac{2\bar{b}}{s} & \frac{1}{a} & 0 \\
-\frac{2\bar{a}}{s} & 0 & -\frac{1}{b} & \frac{2\bar{a}}{s} & 0 & \frac{1}{b} & -\frac{2\bar{a}}{s} & 0 & \frac{1}{b} & \frac{2\bar{a}}{s} & 0 & -\frac{1}{b}
\end{bmatrix}$$

where a and b are the dimensions of the reference surface in x and y-directions respectively, s is the area and; $\bar{b} = \frac{b}{a}$, $\bar{a} = \frac{a}{b}$.

By substituting $\underset{\sim}{a}_{20}$ from equation (4.45) into (4.43) the displacement functions are written in the following form;

$$\underset{\sim}{U} = \begin{bmatrix} \underset{\sim}{g} & \underset{\sim}{0} & \underset{\sim}{0} \\ \underset{\sim}{0} & \underset{\sim}{g} & \underset{\sim}{0} \\ \underline{0} & \underline{0} & \underline{G} \end{bmatrix} \begin{bmatrix} \underline{A}^{-1} & \underline{0} & \underline{0} \\ \underline{0} & \underline{A}^{-1} & \underline{0} \\ \underline{0} & \underline{0} & \underline{A}^{*-1} \end{bmatrix} \cdot \Delta\underset{\sim}{\delta}_e$$

or;

$$\underset{\sim}{\bar{U}} = \begin{bmatrix} \underset{\sim}{\xi} \cdot \underline{\underline{A}}^{-1} & \underset{\sim}{0} & \underset{\sim}{0} \\ \underset{\sim}{0} & \underset{\sim}{\xi} \cdot \underline{\underline{A}}^{-1} & \underset{\sim}{0} \\ \underline{\underline{0}} & \underline{\underline{0}} & \underline{\underline{G}} \cdot \underline{\underline{A}}^{*-1} \end{bmatrix} \cdot \Delta \underset{\sim}{\tilde{\delta}}_e \qquad (4.46)$$

and with the help of equation (4.19) the above displacement functions are written as follows;

$$\underset{\sim}{\bar{U}} = \begin{bmatrix} \underset{\sim}{u} & \underset{\sim}{0} \\ \underset{\sim}{0} & \underline{u}^* \end{bmatrix} \cdot \begin{Bmatrix} \Delta \underset{\sim}{\delta} \\ \Delta \underset{\sim}{\delta}^* \end{Bmatrix}_e \qquad (4.47)$$

where $\underset{\sim}{u} \cdot \Delta \underset{\sim}{\delta}_e$ is the inplane shape function, $\Delta \underset{\sim}{\delta}_e$ is incremental inplane displacement vector, $\Delta \underset{\sim}{\delta}^*_e$ includes the incremental displacements of nodes in z-direction and incremental rotations and;

$$\underline{u}^* = \underline{G} \cdot \underline{A}^{*-1} \qquad (4.48)$$

4.5.6- Strain-Displacement Relationship

The relationship between incremental strains and curvatures at any point of the reference surface with respect to nodal displacements is given by;

$$\Delta \underset{\sim}{\tilde{\epsilon}}_{er} = \underline{\underline{\bar{B}}}_e \cdot \Delta \underset{\sim}{\tilde{\delta}}_e \qquad (4.49)$$

where $\underline{\underline{\bar{B}}}_e$ is the strain matrix. The strain vector $\underset{\sim}{\tilde{\epsilon}}_{er}$ of the reference surface of element (e) is defined as;

$$\underset{\sim}{\tilde{\epsilon}}_{er} = \left\{ \epsilon_x \quad \epsilon_y \quad \gamma_{xy} \quad \xi_x \quad \xi_y \quad \xi_{xy} \right\}^t_{er}$$

which, referring to equation (4.32) we have;

$$\tilde{\xi}_{er} = \left\{ \frac{\partial u}{\partial x} \quad \frac{\partial v}{\partial y} \quad \frac{\partial u}{\partial y}+\frac{\partial v}{\partial x} \quad -\frac{\partial^2 w}{\partial x^2} \quad -\frac{\partial^2 w}{\partial y^2} \quad -2\frac{\partial^2 w}{\partial x \partial y} \right\}^t_{er}$$

or;

$$\Delta\tilde{\xi}_{er} = \begin{bmatrix} \partial/\partial x & 0 & 0 & 0 & 0 \\ 0 & \partial/\partial y & 0 & 0 & 0 \\ \partial/\partial y & \partial/\partial x & 0 & 0 & 0 \\ 0 & 0 & 0 & -\partial/\partial x & 0 \\ 0 & 0 & 0 & 0 & -\partial/\partial y \\ 0 & 0 & 0 & -\partial/\partial y & -\partial/\partial x \end{bmatrix} (\bar{U})$$

and by substituting the shape function $\bar{U}$ from equation (4.47) the incremental strains and curvatures of reference surface become as follows;

$$\Delta\tilde{\xi}_{er} = \begin{bmatrix} \partial/\partial x & 0 & 0 & 0 & 0 \\ 0 & \partial/\partial y & 0 & 0 & 0 \\ \partial/\partial y & \partial/\partial x & 0 & 0 & 0 \\ 0 & 0 & 0 & -\partial/\partial x & 0 \\ 0 & 0 & 0 & 0 & -\partial/\partial y \\ 0 & 0 & 0 & -\partial/\partial y & -\partial/\partial x \end{bmatrix} \left(\begin{bmatrix} \underset{\sim}{u} & \underset{\sim}{0} \\ \underset{\sim}{0} & \underset{\sim}{u}^* \end{bmatrix} \right) \cdot \left\{ \begin{matrix} \Delta\underset{\sim}{\delta} \\ \Delta\underset{\sim}{\delta}^* \end{matrix} \right\}_e \qquad (4.50)$$

and with the help of equation (4.47) we find;

$$\Delta\tilde{\xi}_{er} = \underline{\bar{C}} \cdot \begin{bmatrix} \underline{A}_e^{-1} & \underline{0} & \underline{0} \\ \underline{0} & \underline{A}^{-1} & \underline{0} \\ \underline{0} & \underline{0} & \underline{A}^{*-1} \end{bmatrix} \cdot \left\{ \begin{matrix} \Delta\underset{\sim}{\delta} \\ \Delta\underset{\sim}{\delta}^* \end{matrix} \right\}_e \qquad (4.51)$$

and;

$$\underline{\bar{C}} = \begin{bmatrix} \underline{C} & \underline{0} \\ \underline{0} & \underline{C}^* \end{bmatrix}$$

where, $\underline{C}$ is identical with 3*8 matrix in analysis of beams and;

$$\underline{C}^{*}=\begin{bmatrix} 0 & 0 & 0 & 0 & -2 & 0 & -6x & -2y & 0 & 0 & -6xy & 0 \\ 0 & 0 & 0 & 0 & 0 & -2 & 0 & 0 & -2x & -6y & 0 & -6xy \\ 0 & 0 & 0 & -2 & 0 & 0 & 0 & -4x & -4y & 0 & -6x^{2} & -6y^{2} \end{bmatrix}$$

By equating equation (4.51) with equation (4.49) the strain matrix of the reference surface becomes;

$$\underline{B}_{e} = \underline{C}.\begin{bmatrix} \underline{A}_{e}^{-1} & \underline{0} & \underline{0} \\ \underline{0} & \underline{A}_{e}^{-1} & \underline{0} \\ \underline{0} & \underline{0} & \underline{A}_{e}^{*-1} \end{bmatrix}$$

or;

$$\underline{B}_{e} = \begin{bmatrix} \underline{B}_{e} & \underline{0} \\ \underline{0} & \underline{B}_{e}^{*} \end{bmatrix} \qquad (4.52)$$

and matrix $\underline{B}_{e}$ is identical with strain matrix of beam elements as in (4.26), and the additional strain matrix $\underline{B}_{e}^{*}$ is;

$$\underline{B}_{e}^{*} = \underline{C}^{*} \cdot \underline{A}_{e}^{*-1}$$

which is simply calculated;

$$\underline{B}_{e}^{*}=\begin{bmatrix} A & B & O & -A & C & O & D & E & O & -D & F & O \\ G & O & H & I & O & J & -I & O & K & -G & O & L \\ M & N & P & -M & Q & -P & M & -Q & R & -M & -N & -R \end{bmatrix}$$

where;

$$A = \frac{6}{a^{2}}(1-2\bar{x})(1-\bar{y})$$

$$B = \frac{2}{a}(2-3\bar{x})(1-\bar{y})$$

$$C = \frac{2}{a}(1-3\bar{x})(1-\bar{y})$$

$$D = -\frac{6}{a^2}(1-2\bar{x})\bar{y}$$

$$E = \frac{2}{a}(1-3\bar{x})\bar{y}$$

$$F = \frac{2}{a}(2-3\bar{x})\bar{y}$$

$$G = \frac{6}{b^2}(1-\bar{x})(1-2\bar{y})$$

$$H = \frac{2}{b}(1-\bar{x})(2-3\bar{y})$$

$$I = \frac{6}{b^2}\bar{x}(1-2\bar{y})$$

$$J = \frac{2}{b}\bar{x}(2-3\bar{y})$$

$$K = \frac{2}{b}\bar{x}(1-3\bar{y})$$

$$L = \frac{2}{b}(1-\bar{x})(1-3\bar{y})$$

$$M = \frac{2}{ab}\ 1-6(\bar{x}+\bar{y})+6(\bar{x}^2+\bar{y}^2)$$

$$N = \frac{2}{b}(1-\bar{x})(1-3\bar{x})$$

$$P = \frac{2}{a}(1-\bar{y})(1-3\bar{y})$$

$$Q = -\frac{2}{b}\bar{x}(2-3\bar{x})$$

$$R = \frac{2}{a}\bar{y}(2-3\bar{y})$$

and; $\bar{x} = \frac{x}{a}$, $\bar{y} = \frac{y}{b}$.

The above additional strain matrix for the centroid

of the reference surface is written as follows; where s is the area of the reference surface,

$$\underline{B}^{*}_{ec} = \begin{bmatrix} 0 & b & 0 & 0 & -b & 0 & 0 & -b & 0 & 0 & b & 0 \\ 0 & 0 & a & 0 & 0 & a & 0 & 0 & -a & 0 & 0 & -a \\ -4 & -\frac{1}{2}a & -\frac{1}{2}b & 4 & -\frac{1}{2}a & \frac{1}{2}b & -4 & \frac{1}{2}a & \frac{1}{2}b & 4 & \frac{1}{2}a & -\frac{1}{2}b \end{bmatrix}$$

4.5.7- Stress-Strain Relationship

The relationship between incremental stresses and strains at a level (h) from the reference surface of element (e) is given in usual form as;

$$\Delta\underset{\sim}{\sigma}_h = \underline{D}_h \cdot \Delta\underset{\sim}{\epsilon}_h \qquad (4.53)$$

where $\underline{D}_h$ is the elasticity matrix includes the material properties of the level (h) and;

$$\Delta\underset{\sim}{\sigma}_h = \left\{ \Delta\sigma_x \quad \Delta\sigma_y \quad \Delta\tau_{xy} \right\}^t_h$$

$$\Delta\underset{\sim}{\epsilon}_h = \left\{ \Delta\epsilon_x \quad \Delta\epsilon_y \quad \Delta\gamma_{xy} \right\}^t_h$$

and from equation (4.37) the strains at the level (h) related to the reference surface strains and curvatures may be written in the following matrix form;

$$\Delta\underset{\sim}{\epsilon}_h = \left[\underline{I} \quad \underline{I}.h \right] . \Delta\underset{\sim}{\epsilon}_{er} \qquad (4.54)$$

where $\underline{I}$ is 3×3 identity matrix and (h) is the distance of level (h) from the reference surface of the element.

Substituting equation (4.54) into equation (4.53), gives the relationships between reference surface strains and stresses of level (h);

$$\Delta\underset{\sim}{\sigma}_h = \underline{\underline{D}}_h \cdot \left[\underline{\underline{I}} \quad \underline{\underline{I}}.h\right] \cdot \Delta\underset{\sim}{\epsilon}_{er} \tag{4.55}$$

4.5.8- Stress-Displacement Relationship

The relationship between incremental displacements (nodal displacements of reference surface) and incremental stresses of level (h) is obtained by substituting $\Delta\tilde{\underset{\sim}{\epsilon}}_{er}$ from equation (4.49) into equation (4.55) which gives;

$$\Delta\underset{\sim}{\sigma}_h = \underline{\underline{D}}_h \cdot \left[\underline{\underline{I}} \quad \underline{\underline{I}}.h\right] \cdot \underline{\underline{\tilde{B}}}_e \cdot \Delta\tilde{\underset{\sim}{\delta}}_e$$

and by inserting $\underline{\underline{\tilde{B}}}_e$ from equation (4.52) we find;

$$\Delta\underset{\sim}{\sigma}_h = \underline{\underline{D}}_h \cdot \left[\underline{\underline{I}} \quad \underline{\underline{I}}.h\right] \cdot \begin{bmatrix} \underline{\underline{B}}_e & \underline{\underline{0}} \\ \underline{\underline{0}} & \underline{\underline{B}}^*_e \end{bmatrix} \cdot \Delta\underset{\sim}{\delta}_e \tag{4.56}$$

4.5.9- Stiffness Matrix

By the help of virtual work, the stiffness matrix of the pth layer of the element is calculated as follows;

$$\Delta\tilde{\underset{\sim}{\delta}}^t_e \cdot \Delta\underset{\sim}{f}_{ep} = \int_v \Delta\tilde{\underset{\sim}{\epsilon}}^t_h \cdot \Delta\underset{\sim}{\sigma}_h \cdot dv \tag{4.57}$$

where v is the volume of the pth layer, $\Delta\underset{\sim}{f}_{ep}$ is the incremental force vector on the reference surface transformed

from the pth layer, $\Delta \tilde{\tilde{\varepsilon}}_h$ is the incremental virtual strain vector of level (h) and $\Delta \tilde{\tilde{\delta}}_e$ includes the incremental virtual displacements of reference surface.

By substituting equation (4.54) into equation (4.57) we have;

$$\Delta \tilde{\tilde{\delta}}_e^t \cdot \Delta \tilde{f}_{ep} = \int_s \int_{h_p}^{h_{p+1}} \Delta \tilde{\tilde{\varepsilon}}_{er}^t \cdot \begin{bmatrix} \underline{\underline{I}} & \underline{\underline{I}}.h \end{bmatrix}^t \cdot \Delta \tilde{\sigma}_h \cdot dh \cdot ds \qquad (4.58)$$

where s is the area of the reference surface, h_p and h_{p+1} are the distances from reference surface to the bottom and top of the pth layer.

Finally, $\Delta \tilde{\tilde{\varepsilon}}_{er}$ and $\Delta \tilde{\sigma}_h$ are substituted from equation (4.49) and equation (4.56) into equation (4.58);

$$\Delta \tilde{\tilde{\delta}}_e^t \cdot \Delta \tilde{f}_{ep} = \int_s \int_{h_p}^{h_{p+1}} \Delta \tilde{\tilde{\delta}}_e^t \cdot \begin{bmatrix} \underline{\underline{B}}_e & \underline{\underline{0}} \\ \underline{\underline{0}} & \underline{\underline{B}}_e^* \end{bmatrix}^t \cdot \begin{bmatrix} \underline{\underline{I}} \\ \underline{\underline{I}}.h \end{bmatrix} \underline{\underline{D}}_h \cdot \begin{bmatrix} \underline{\underline{I}} & \underline{\underline{I}}.h \end{bmatrix} \begin{bmatrix} \underline{\underline{B}} & \underline{\underline{0}} \\ \underline{\underline{0}} & \underline{\underline{B}}^* \end{bmatrix} \Delta \tilde{\delta}_e dV$$

which gives the stiffness matrix of the pth layer as follows;

$$\underline{\underline{k}}_{ep} = \int_s \int_{h_p}^{h_{p+1}} \begin{bmatrix} \underline{\underline{B}}_e & \underline{\underline{0}} \\ \underline{\underline{0}} & \underline{\underline{B}}_e^* \end{bmatrix}^t \cdot \begin{bmatrix} \underline{\underline{I}} \\ \underline{\underline{I}}.h \end{bmatrix} \underline{\underline{D}}_h \cdot \begin{bmatrix} \underline{\underline{I}} & \underline{\underline{I}}.h \end{bmatrix} \cdot \begin{bmatrix} \underline{\underline{B}}_e & \underline{\underline{0}} \\ \underline{\underline{0}} & \underline{\underline{B}}_e^* \end{bmatrix} .ds.dh$$

or;

$$\underline{\underline{k}}_e = \int_s \int_{h_p}^{h_{p+1}} \begin{bmatrix} \underline{\underline{B}}^t \cdot \underline{\underline{D}}_h \cdot \underline{\underline{B}} & h \cdot \underline{\underline{B}}^t \cdot \underline{\underline{D}}_h \cdot \underline{\underline{B}}^* \\ h \cdot \underline{\underline{B}}^{*t} \cdot \underline{\underline{D}}_h \cdot \underline{\underline{B}} & h^2 \cdot \underline{\underline{B}}^{*t} \cdot \underline{\underline{D}}_h \cdot \underline{\underline{B}}^* \end{bmatrix} .ds.dh \qquad (4.59)$$

and this stiffness matrix may be written in the following form;

$$\bar{\underline{k}}_{ep} = \begin{bmatrix} \underline{k}_e & \underline{k}_e^* \\ \underline{k}_e^{*t} & \underline{k}_e^{**} \end{bmatrix}_p$$

where $\underline{k}_e$ is identical with the stiffness matrix of beam element as in equation (4.28), and the additional stiffness matrix $\underline{k}_{ep}^*$ and $\underline{k}_{ep}^{**}$ are obtained thus;

$$\underline{k}_{ep}^* = \tfrac{1}{2}(h_{p+1}^2 - h_p^2) \cdot \int_s \underline{B}_e^t \cdot \underline{D}_h \cdot \underline{B}_e^* \cdot ds \qquad (4.60)$$

$$\underline{k}_{ep}^{**} = \tfrac{1}{3}(h_{p+1}^3 - h_p^3) \cdot \int_s \underline{B}_e^{*t} \cdot \underline{D}_h \cdot \underline{B}_e^* \cdot ds \qquad (4.61)$$

However, the stiffness matrix of the element (e) is calculated from the summation of the layers stiffnes matrices,

$$\bar{\underline{k}}_e = \sum_{p=1}^{n} \bar{\underline{k}}_{ep} = \sum_{p=1}^{n} \begin{bmatrix} \underline{k}_{ep} & \underline{k}_{ep}^* \\ \underline{k}_{ep}^{*t} & \underline{k}_{ep}^{**} \end{bmatrix}$$

and clearly, in a symmetrical element, when the material properties have symmetry with respect to the middle surface of the element and the reference surface is assumed to be coincident with the middle surface, the matrix $\bar{\underline{k}}_e$ becomes as in below;

$$\bar{\underline{k}}_e = \begin{bmatrix} \sum_{p=1}^{n} \underline{k}_{ep} & \underline{0} \\ \underline{0} & \sum_{p=1}^{n} \underline{k}_{ep}^{**} \end{bmatrix}$$

To calculate the additional stiffness matrices in equations (4.60) and (4.61), a few integrals must be evaluated, which are given in appendix I, however these additional stiffness matrices are given by;

$$\underline{k}_e^* = \begin{bmatrix} A & B & C & D & E & F & G & H & I & O & J & K \\ L & M & N & P & Q & R & S & -I & T & U & V & W \\ X & E & -V & D^* & E^* & F^* & -Z & B^* & K & G^* & H & I \\ Y & Q & C^* & H^* & I^* & O^* & -A^* & -F & W & J^* & -I & T \\ -G & H & I & -O & J & K & -A & B & C & -D & E & F \\ -S & -I & T & -U & V & W & -L & M & N & -P & Q & R \\ Z & B^* & K & -G & H & I & -X & E & -V & -D^* & E^* & F^* \\ A^* & -F & W & -J^* & -I & T & -Y & Q & C^* & K^* & I^* & Q^* \end{bmatrix}$$

where,

$$A = \tfrac{1}{2} \sum_{p=1}^{n} \left\{ \tfrac{1}{b} \Omega h_p^2 (-\tfrac{1}{2} d_{12} + \tfrac{1}{2} \bar{b} . d_{13} + d_{33}) \right\}$$

$$B = -\tfrac{1}{2} \sum_{p=1}^{n} \left\{ \Omega h_p^2 (\tfrac{1}{3} \bar{b} . d_{11} + \tfrac{1}{2} d_{13} + \tfrac{1}{6} \bar{a} . d_{33}) \right\}$$

$$C = -\tfrac{1}{2} \sum_{p=1}^{n} \left\{ \Omega h_p^2 (\tfrac{1}{2} d_{12} + \tfrac{1}{6} \bar{b} . d_{13} + \tfrac{1}{3} \bar{a} . d_{23}) \right\}$$

$$D = -\tfrac{1}{2} \sum_{p=1}^{n} \left\{ \tfrac{1}{b} \Omega h_p^2 (\tfrac{1}{2} d_{12} + \tfrac{1}{2} b . d_{13} + d_{33}) \right\}$$

$$E = \tfrac{1}{2} \sum_{p=1}^{n} \left\{ \Omega h_p^2 (\tfrac{1}{3} \bar{b} . d_{11} + \tfrac{1}{6} \bar{a} . d_{33}) \right\}$$

$$F = -\tfrac{1}{2} \sum_{p=1}^{n} \left\{ \Omega h_p^2 (\tfrac{1}{2} d_{12} - \tfrac{1}{6} \bar{b} . d_{13} + \tfrac{1}{6} \bar{a} . d_{23}) \right\}$$

$$G = \tfrac{1}{2} \sum_{p=1}^{n} \left\{ \tfrac{1}{b} \Omega h_p^2 (\tfrac{1}{2} d_{12} + \tfrac{3}{2} \bar{b} . d_{13} + d_{33}) \right\}$$

$$H = \frac{1}{12} \sum_{p=1}^{n} \left\{ \Omega h_p^2 (\bar{b}.d_{11} - \bar{a}.d_{33}) \right\}$$

$$I = -\frac{1}{12} \sum_{p=1}^{n} \left\{ \Omega h_p^2 (\bar{b}.d_{13} - \bar{a}.d_{23}) \right\}$$

$$J = -\tfrac{1}{4} \sum_{p=1}^{n} \left\{ \Omega h_p^2 (\tfrac{1}{3}\bar{b}.d_{11} + d_{13} - \tfrac{1}{3}\bar{a}.d_{33}) \right\}$$

$$K = \frac{1}{6} \sum_{p=1}^{n} \left\{ \Omega h_p^2 (\tfrac{1}{2}\bar{b}.d_{13} + \bar{a}.d_{23}) \right\}$$

$$L = -\tfrac{1}{2} \sum_{p=1}^{n} \left\{ \frac{1}{a}. \Omega h_p^2 (\tfrac{1}{2}d_{12} - \tfrac{1}{2}\bar{a}.d_{23} - d_{33}) \right\}$$

$$M = -\tfrac{1}{2} \sum_{p=1}^{n} \left\{ \Omega h_p^2 (\tfrac{1}{2}d_{12} + \tfrac{1}{6}\bar{a}.d_{23} + \tfrac{1}{3}\bar{b}.d_{13}) \right\}$$

$$N = -\tfrac{1}{2} \sum_{p=1}^{n} \left\{ \Omega h_p^2 (\tfrac{1}{3}\bar{a}.d_{22} + \tfrac{1}{2}d_{23} + \tfrac{1}{6}\bar{b}.d_{33}) \right\}$$

$$O = \tfrac{1}{2} \sum_{p=1}^{n} \left\{ \frac{1}{b}. \Omega h_p^2 (\tfrac{1}{2}d_{12} - \tfrac{3}{2}\bar{b}.d_{13} - d_{33}) \right\}$$

$$P = \tfrac{1}{2} \sum_{p=1}^{n} \left\{ \frac{1}{a}. \Omega h_p^2 (\tfrac{1}{2}d_{12} - \tfrac{3}{2}\bar{a}.d_{23} - d_{33}) \right\}$$

$$Q = \frac{1}{6} \sum_{p=1}^{n} \left\{ \Omega h_p^2 (\tfrac{1}{2}\bar{a}.d_{23} + \bar{b}.d_{13}) \right\}$$

$$R = -\tfrac{1}{4} \sum_{p=1}^{n} \left\{ \Omega h_p^2 (\tfrac{1}{3}\bar{a}.d_{22} + \tfrac{1}{2}d_{23} - \tfrac{1}{3}\bar{b}.d_{33}) \right\}$$

$$S = \tfrac{1}{2} \sum_{p=1}^{n} \left\{ \frac{1}{a}. \Omega h_p^2 (\tfrac{1}{2}d_{12} + \tfrac{3}{2}\bar{a}.d_{23} + d_{33}) \right\}$$

$$T = \frac{1}{12} \sum_{p=1}^{n} \left\{ \Omega h_p^2 (\bar{a}.d_{22} - \bar{b}.d_{33}) \right\}$$

$$U = -\tfrac{1}{2} \sum_{p=1}^{n} \left\{ \frac{1}{a}. \Omega h_p^2 (\tfrac{1}{2}d_{12} + \tfrac{1}{2}\bar{a}.d_{23} + d_{33}) \right\}$$

$$V = -\tfrac{1}{4}\sum_{p=1}^{n}\left\{\Omega h_p^2\left(d_{22} - \tfrac{1}{3}\bar{a}.d_{23} + \tfrac{1}{3}\bar{b}.d_{13}\right)\right\}$$

$$W = \frac{1}{6}\sum_{p=1}^{n}\left\{\Omega h_p^2\left(\bar{a}.d_{22} + \tfrac{1}{2}\bar{b}.d_{33}\right)\right\}$$

$$X = \tfrac{1}{2}\sum_{p=1}^{n}\left\{\frac{1}{b}.\,\Omega h_p^2\left(\tfrac{1}{2}d_{12} - \tfrac{1}{2}\bar{b}.d_{13} + d_{33}\right)\right\}$$

$$Y = \tfrac{1}{2}\sum_{p=1}^{n}\left\{\frac{1}{a}.\,\Omega h_p^2\left(\tfrac{1}{2}d_{12} + \tfrac{3}{2}\bar{a}.d_{23} - d_{33}\right)\right\}$$

$$Z = \tfrac{1}{2}\sum_{p=1}^{n}\left\{\frac{1}{b}.\,\Omega h_p^2\left(\tfrac{1}{2}d_{12} + \tfrac{3}{2}\bar{b}.d_{13} - d_{33}\right)\right\}$$

$$A^* = \tfrac{1}{2}\sum_{p=1}^{n}\left\{\frac{1}{a}.\Omega h_p^2\left(\tfrac{1}{2}d_{12} - \tfrac{1}{2}\bar{a}.d_{23} + d_{33}\right)\right\}$$

$$B^* = -\tfrac{1}{4}\sum_{p=1}^{n}\left\{\Omega h_p^2\left(\tfrac{1}{3}\bar{b}.d_{11} - \tfrac{1}{2}d_{13} - \tfrac{1}{3}\bar{a}.d_{33}\right)\right\}$$

$$C^* = -\tfrac{1}{4}\sum_{p=1}^{n}\left\{\Omega h_p^2\left(\tfrac{1}{3}\bar{a}.d_{22} - d_{23} - \tfrac{1}{3}\bar{b}.d_{33}\right)\right\}$$

$$D^* = \tfrac{1}{2}\sum_{p=1}^{n}\left\{\frac{1}{b}.\,\Omega h_p^2\left(\tfrac{1}{2}d_{12} + \tfrac{1}{2}\bar{b}.d_{12} - d_{33}\right)\right\}$$

$$E^* = -\tfrac{1}{2}\sum_{p=1}^{n}\left\{h_p^2\left(\tfrac{1}{3}\bar{b}.d_{11} - \tfrac{1}{2}d_{13} + \tfrac{1}{6}\bar{a}.d_{33}\right)\right\}$$

$$F^* = \tfrac{1}{2}\sum_{p=1}^{n}\left\{\Omega h_p^2\left(\tfrac{1}{2}d_{12} - \tfrac{1}{6}\bar{b}.d_{13} - \tfrac{1}{3}\bar{a}.d_{23}\right)\right\}$$

$$G^* = -\tfrac{1}{2}\sum_{p=1}^{n}\left\{\frac{1}{b}.\,\Omega h_p^2\left(\tfrac{1}{2}d_{12} - \tfrac{3}{2}\bar{b}.d_{13} + \tfrac{1}{6}d_{33}\right)\right\}$$

$$H^* = -\tfrac{1}{2}\sum_{p=1}^{n}\left\{\frac{1}{a}.\,\Omega h_p^2\left(\tfrac{1}{2}d_{12} + \tfrac{1}{2}\bar{a}.d_{23} - d_{33}\right)\right\}$$

$$I^* = \tfrac{1}{2}\sum_{p=1}^{n}\left\{\Omega h_p^2\left(\tfrac{1}{2}d_{12} - \tfrac{1}{6}\bar{a}.d_{23} - \tfrac{1}{3}\bar{b}.d_{13}\right)\right\}$$

$$J^* = \tfrac{1}{2} \sum_{p=1}^{n} \left\{ \frac{1}{\bar{a}} \cdot \Omega h_p^2 \left(\tfrac{1}{2} d_{12} - \tfrac{3}{2} \bar{a} \cdot d_{23} + d_{33} \right) \right\}$$

$$K^* = \tfrac{1}{2} \sum_{p=1}^{n} \left\{ \frac{1}{\bar{a}} \cdot \Omega h_p^2 \left(\tfrac{1}{2} d_{12} - d_{33} \right) \right\}$$

$$Q^* = -\tfrac{1}{2} \sum_{p=1}^{n} \left\{ \Omega h_p^2 \left(\tfrac{1}{3} \bar{a} \cdot d_{22} - \tfrac{1}{2} d_{23} + \tfrac{1}{6} \bar{b} \cdot d_{33} \right) \right\}$$

where a and b are dimensions of the reference surface in x and y-directions, respectively and d_{11}, d_{12}, d_{13}, d_{22}, d_{23} and d_{33} are the members of elasticity matrix in global coordinates and $\bar{a} = a/b$, $\bar{b} = b/a$, $\Omega h_p^2 = h_{p+1}^2 - h_p^2$.

Also we have;

$$\underline{k}_{ep}^{**} = \begin{bmatrix}
\bar{A} & \bar{B} & \bar{C} & \bar{D} & \bar{E} & \bar{F} & \bar{G} & \bar{H} & \bar{I} & \bar{J} & \bar{K} & \bar{L} \\
 & \bar{M} & \bar{N} & -\bar{E} & \bar{O} & \bar{P} & -\bar{H} & \bar{Q} & -\bar{P} & \bar{R} & \bar{S} & \bar{P} \\
 & & \bar{T} & \bar{U} & \bar{P} & \bar{V} & -\bar{I} & -\bar{P} & \bar{W} & -\bar{L} & \bar{P} & \bar{X} \\
 & & & \bar{A} & -\bar{B} & \bar{C} & \bar{J} & -\bar{R} & \bar{I} & \bar{G} & \bar{Y} & \bar{Z} \\
 & & & & \bar{A}^* & \bar{B}^* & -\bar{K} & \bar{S} & \bar{P} & -\bar{Y} & \bar{C}^* & -\bar{P} \\
 & & & & & \bar{D}^* & -\bar{L} & \bar{P} & \bar{X} & -\bar{Z} & -\bar{P} & \bar{E}^* \\
 & & & & & & \bar{A} & -\bar{B} & -\bar{C} & \bar{D} & -\bar{E} & -\bar{F} \\
 & & & & & & & \bar{M} & \bar{N} & \bar{E} & \bar{O} & \bar{P} \\
 & & & & & & & & \bar{T} & -\bar{U} & \bar{P} & \bar{V} \\
 & & & & & & & & & \bar{A} & \bar{B} & -\bar{C} \\
 & & & & & & & & & & \bar{A}^* & \bar{B}^* \\
 & & & & & & & & & & & \bar{D}^*
\end{bmatrix}$$

Sym.

where;

$$A = \frac{1}{3s} \sum_{p=1}^{n} \left\{ \Omega h_p^3 (4\bar{b}^2 . d_{11} + 2d_{12} + 4\bar{a}^2 . d_{22} + 5.6 d_{33}) \right\}$$

$$B = \frac{1}{3s} \sum_{p=1}^{n} \left\{ \Omega h_p^3 (2\bar{b} . b . d_{11} + a . d_{12} + 0.4a . d_{33}) \right\}$$

$$C = \frac{1}{3s} \sum_{p=1}^{n} \left\{ \Omega h_p^3 (b . d_{12} + 2\bar{a} . a . d_{22} + 0.4b . d_{33}) \right\}$$

$$D = - \frac{1}{3s} \sum_{p=1}^{n} \left\{ \Omega h_p^3 (4\bar{b}^2 . d_{11} + 2d_{12} - 2\bar{a}^2 . d_{22} + 5.6 d_{33}) \right\}$$

$$E = \frac{1}{3a} \sum_{p=1}^{n} \left\{ \Omega h_p^3 (2\bar{b} . d_{11} + 0.4\bar{a} . d_{33}) \right\}$$

$$F = - \frac{1}{3b} \sum_{p=1}^{n} \left\{ \Omega h_p^3 (\bar{b} . d_{12} - \bar{a} . d_{22} + 2d_{23} + 0.4\bar{b} . d_{33}) \right\}$$

$$G = - \frac{1}{3s} \sum_{p=1}^{n} \left\{ \Omega h_p^3 (2\bar{b}^2 . d_{11} - 2d_{12} + 2\bar{a}^2 . d_{22} - 5.6 d_{33}) \right\}$$

$$H = \frac{1}{3a} \sum_{p=1}^{n} \left\{ \Omega h_p^3 (\bar{b} . d_{11} + 2d_{13} - 0.4\bar{a} . d_{33}) \right\}$$

$$I = \frac{1}{3b} \sum_{p=1}^{n} \left\{ \Omega h_p^3 (\bar{a} . d_{22} + 2d_{23} - 0.4\bar{b} . d_{33}) \right\}$$

$$J = \frac{1}{3s} \sum_{p=1}^{n} \left\{ \Omega h_p^3 (2\bar{b}^2 . d_{11} - 2d_{12} - 4\bar{a}^2 d_{22} - 5.6 d_{33}) \right\}$$

$$K = \frac{1}{3a} \sum_{p=1}^{n} \left\{ \Omega h_p^3 (\bar{b} . d_{11} - \bar{a} . d_{12} - 2d_{13} - 0.4\bar{a} . d_{33}) \right\}$$

$$L = \frac{2}{3b} \sum_{p=1}^{n} \left\{ \Omega h_p^3 (\bar{a} . d_{22} + 0.2\bar{b} . d_{33}) \right\}$$

$$M = \frac{1}{9} \sum_{p=1}^{n} \left\{ \Omega h_p^3 (4\bar{b} . d_{11} + 3d_{13} + 1.6\bar{a} . d_{33}) \right\}$$

$$N = \frac{1}{18} \sum_{p=1}^{n} \left\{ \Omega h_p^3 (6d_{12} + \bar{b}.d_{13} + \bar{a}.d_{23}) \right\}$$

$$\bar{O} = \frac{1}{9} \sum_{p=1}^{n} \left\{ \Omega h_p^3 (2\bar{b}.d_{11} - 0.4\bar{a}.d_{33}) \right\}$$

$$P = -\frac{1}{18} \sum_{p=1}^{n} \left\{ \Omega h_p^3 (\bar{b}.d_{13} + \bar{a}.d_{23}) \right\}$$

$$\bar{Q} = \frac{1}{9} \sum_{p=1}^{n} \left\{ \Omega h_p^3 (\bar{b}.d_{11} + 3d_{13} + 0.4\bar{a}.d_{33}) \right\}$$

$$R = \frac{1}{3\bar{a}} \sum_{p=1}^{n} \left\{ \Omega h_p^3 (\bar{b}.d_{11} - \bar{a}.d_{12} + 2d_{13} - 0.4\bar{a}.d_{33}) \right\}$$

$$S = \frac{1}{9} \sum_{p=1}^{n} \left\{ \Omega h_p^3 (2\bar{b}.d_{11} - 1.6\bar{a}.d_{33}) \right\}$$

$$\bar{T} = \frac{1}{9} \sum_{p=1}^{n} \left\{ \Omega h_p^3 (4\bar{a}.d_{22} + 3d_{23} + 1.6\bar{b}.d_{33}) \right\}$$

$$\bar{U} = -\frac{1}{3\bar{b}} \sum_{p=1}^{n} \left\{ \Omega h_p^3 (\bar{b}.d_{12} - \bar{a}.d_{22} - 2d_{23} + 0.4\bar{b}.d_{33}) \right\}$$

$$\bar{V} = \frac{1}{9} \sum_{p=1}^{n} \left\{ \Omega h_p^3 (2\bar{a}.d_{22} - 1.6\bar{b}.d_{33}) \right\}$$

$$\bar{W} = \frac{1}{9} \sum_{p=1}^{n} \left\{ \Omega h_p^3 (\bar{a}.d_{22} + 3d_{23} + 0.4\bar{b}.d_{33}) \right\}$$

$$X = \frac{1}{9} \sum_{p=1}^{n} \left\{ \Omega h_p^3 (2\bar{a}.d_{22} - 0.4\bar{b}.d_{33}) \right\}$$

$$Y = -\frac{1}{3\bar{a}} \sum_{p=1}^{n} \left\{ \Omega h_p^3 (\bar{b}.d_{11} - 2d_{13} - 0.4\bar{a}.d_{33}) \right\}$$

$$Z = \frac{1}{3\bar{b}} \sum_{p=1}^{n} \left\{ \Omega h_p^3 (\bar{a}.d_{22} - 2d_{23} - 0.4\bar{b}.d_{33}) \right\}$$

$$A^* = \frac{1}{9} \sum_{p=1}^{n} \left\{ \Omega h_p^3 (4\bar{b}.d_{11} - 3d_{13} - 0.4\bar{b}.d_{33}) \right\}$$

$$B^* = -\frac{1}{18} \sum_{p=1}^{n} \left\{ \Omega h_p^3 (6d_{12} - \bar{b}.d_{13} - \bar{a}.d_{23}) \right\}$$

$$\bar{C}^* = \frac{1}{9} \sum_{p=1}^{n} \left\{ \Omega h_p^3 (\bar{b}.d_{11} - 3d_{13} + 0.4\bar{a}.d_{33}) \right\}$$

$$D^* = \frac{1}{9} \sum_{p=1}^{n} \left\{ \Omega h_p^3 (4\bar{a}.d_{22} - 3d_{23} + 1.6\bar{b}.d_{33}) \right\}$$

$$E^* = \frac{1}{9} \sum_{p=1}^{n} \left\{ \Omega h_p^3 (\bar{a}.d_{22} - 3d_{23} + 0.4\bar{b}.d_{33}) \right\}$$

where s is the area of the reference surface and; $\bar{a} = a/b$, $\bar{b} = b/a$ and $\Omega h_p^3 = h_{p+1}^3 - h_p^3$.

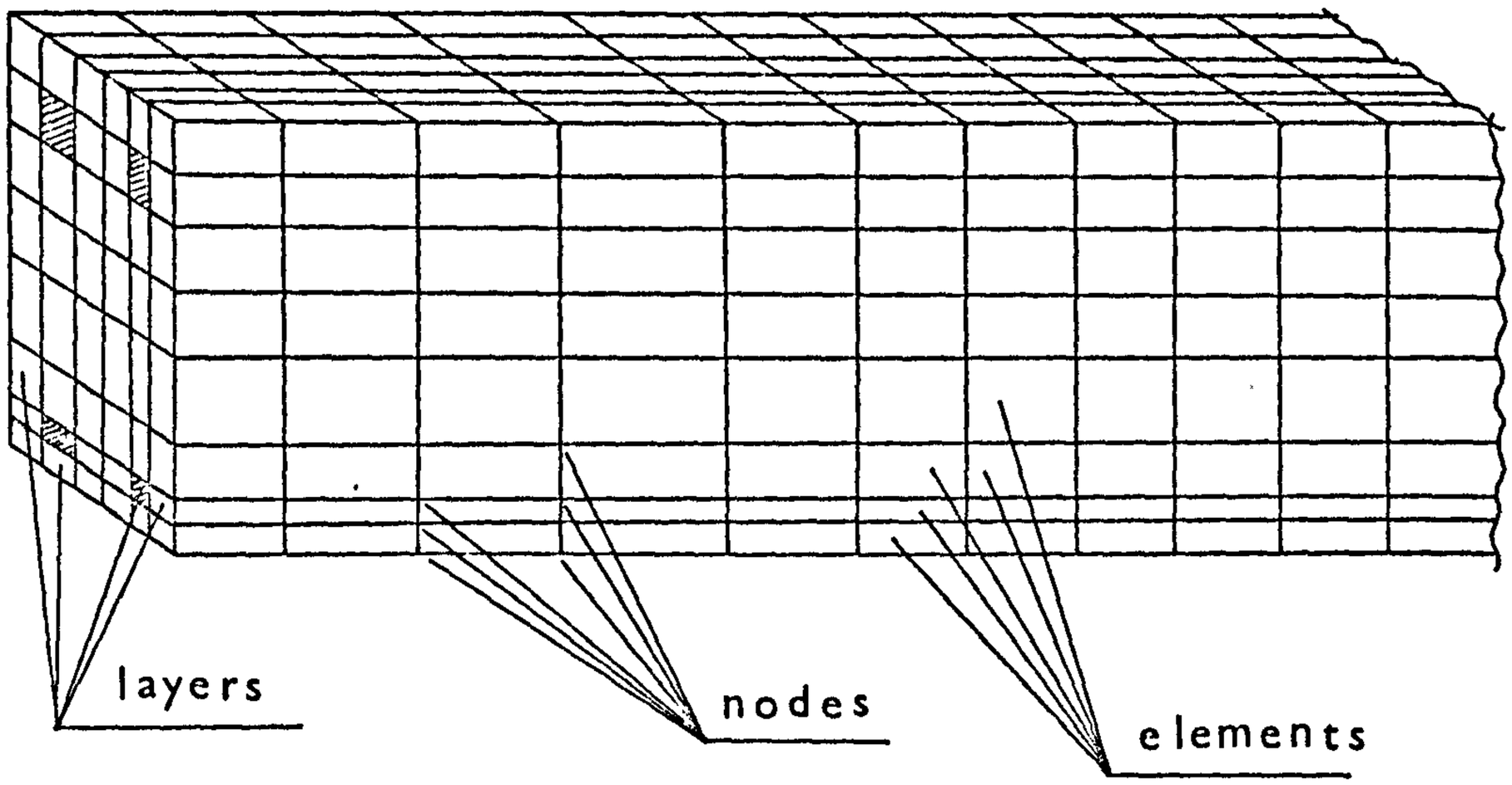

Fig.4.1_ A typical division of a rectagular beam into a finite number of elements and layers.

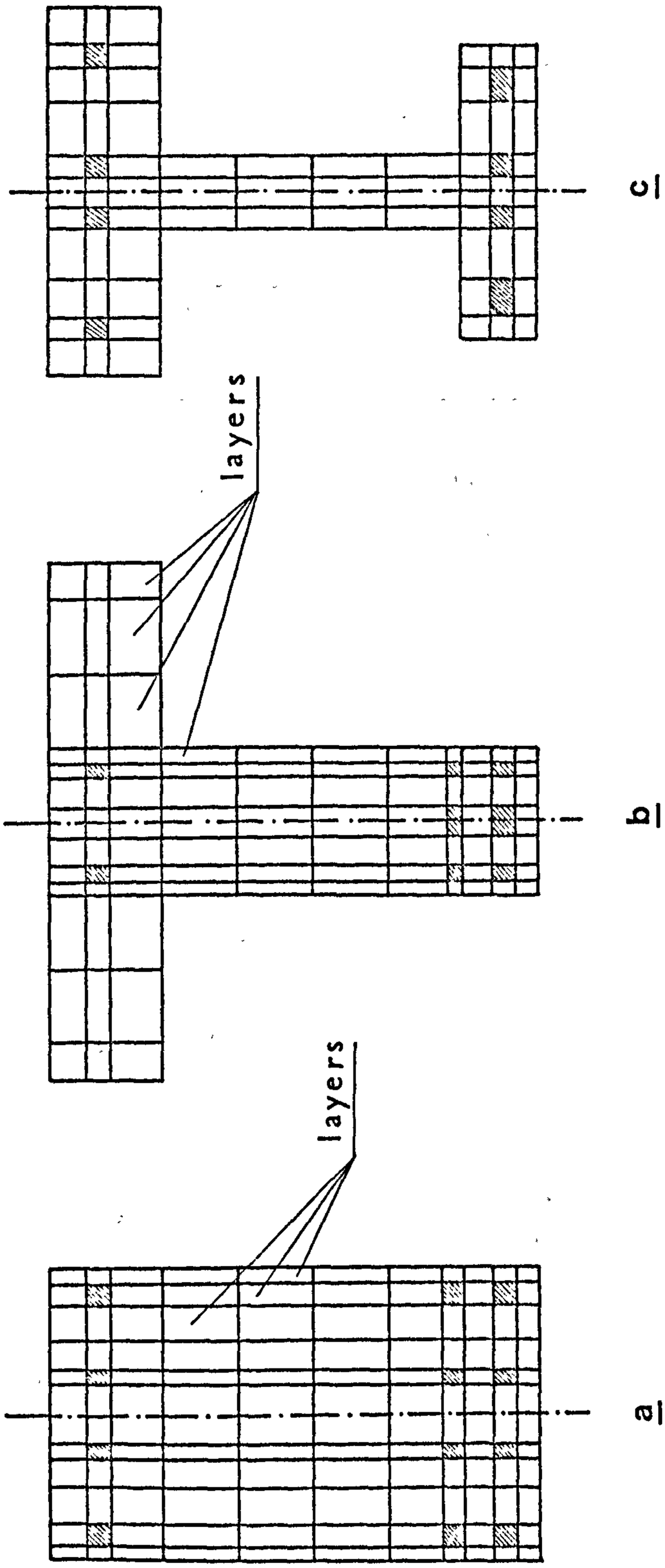

Fig.4.2_Cross sections of rectangular, Tee and I beams in layered finite element method of analysis.

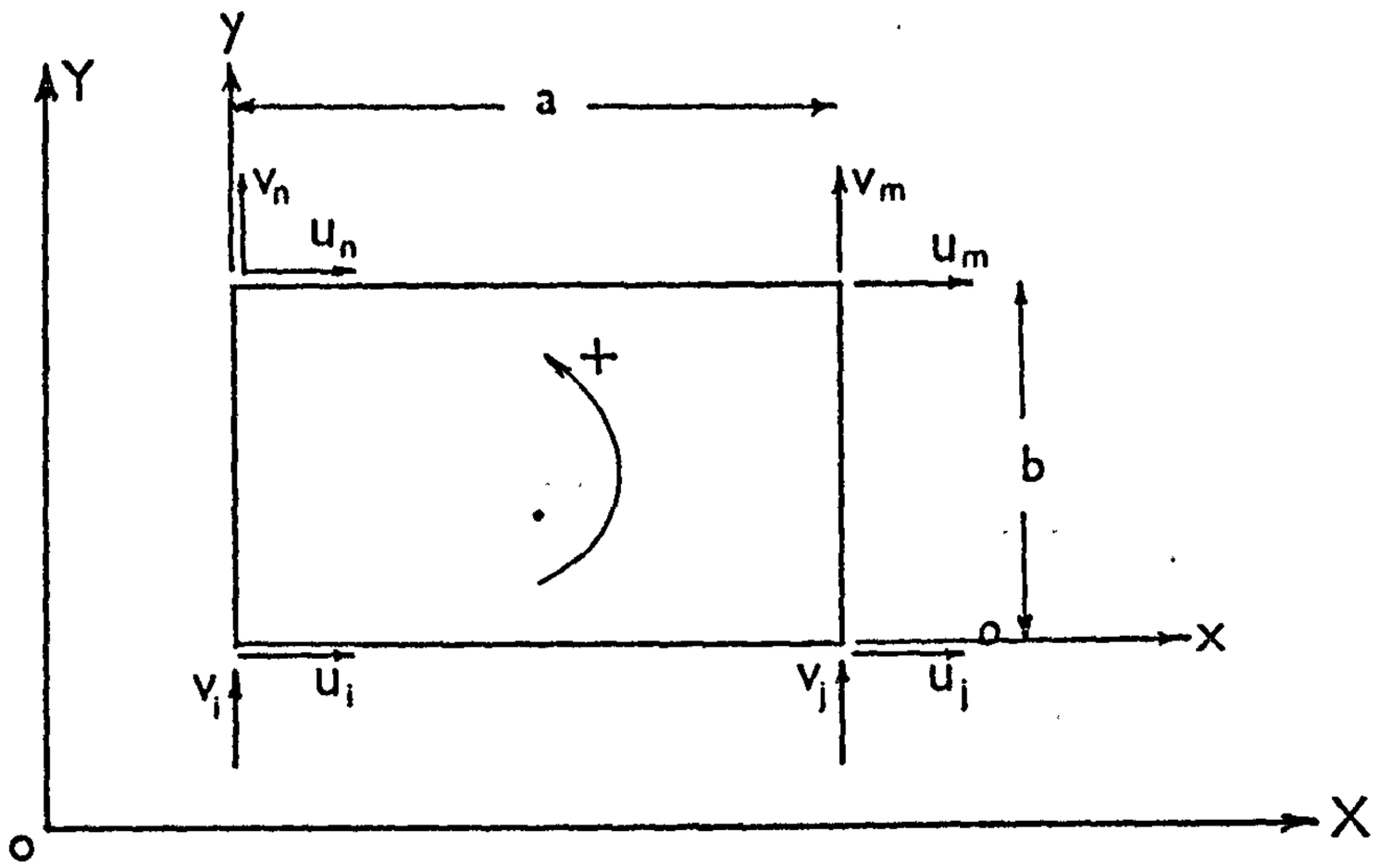

Fig.4.3_ A typical rectangular element in local and global coordinates in finite element method

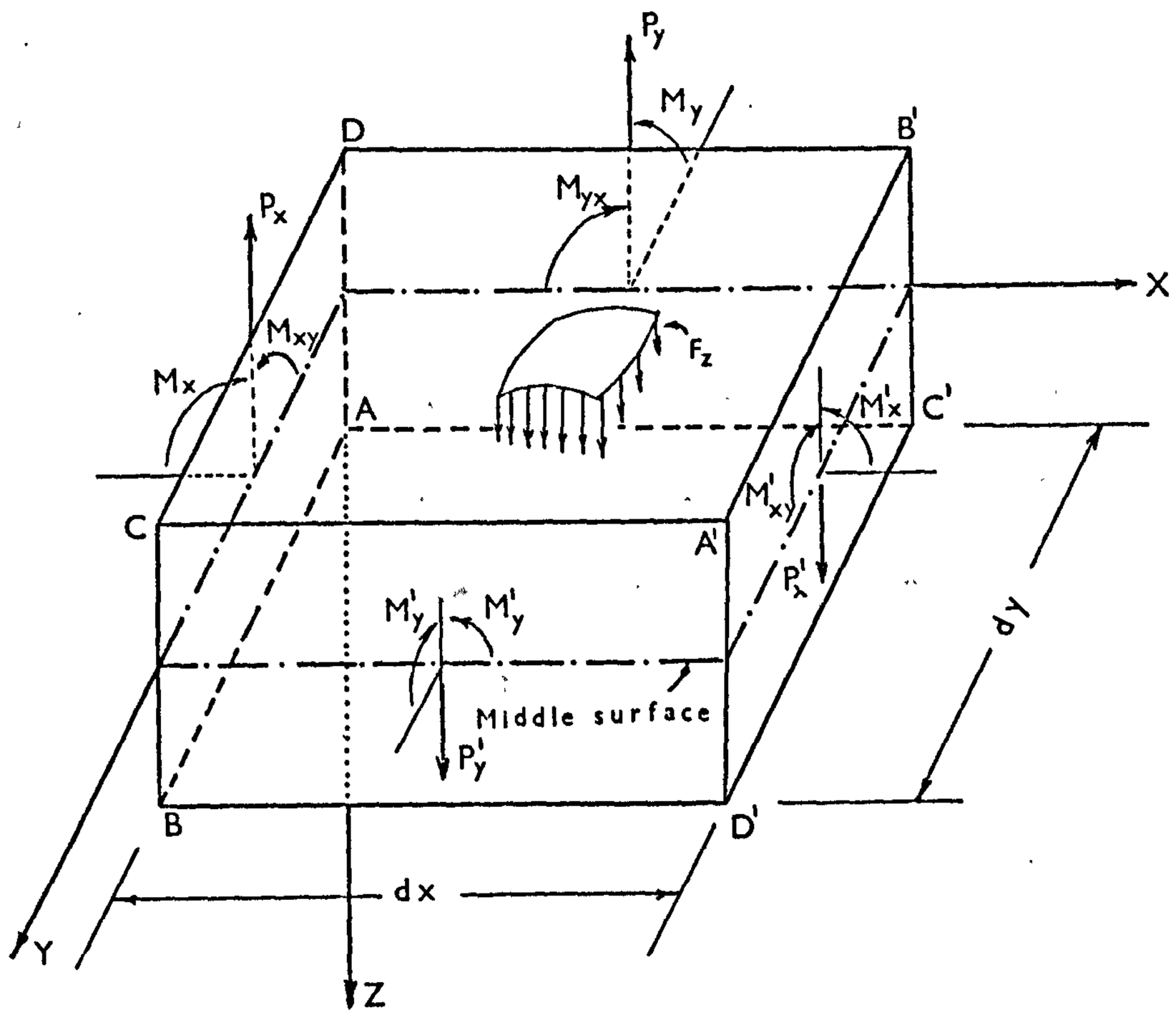

Fig.4.4_ A typical element cut of the plate with positive directions of the internal forces at its middle surface.

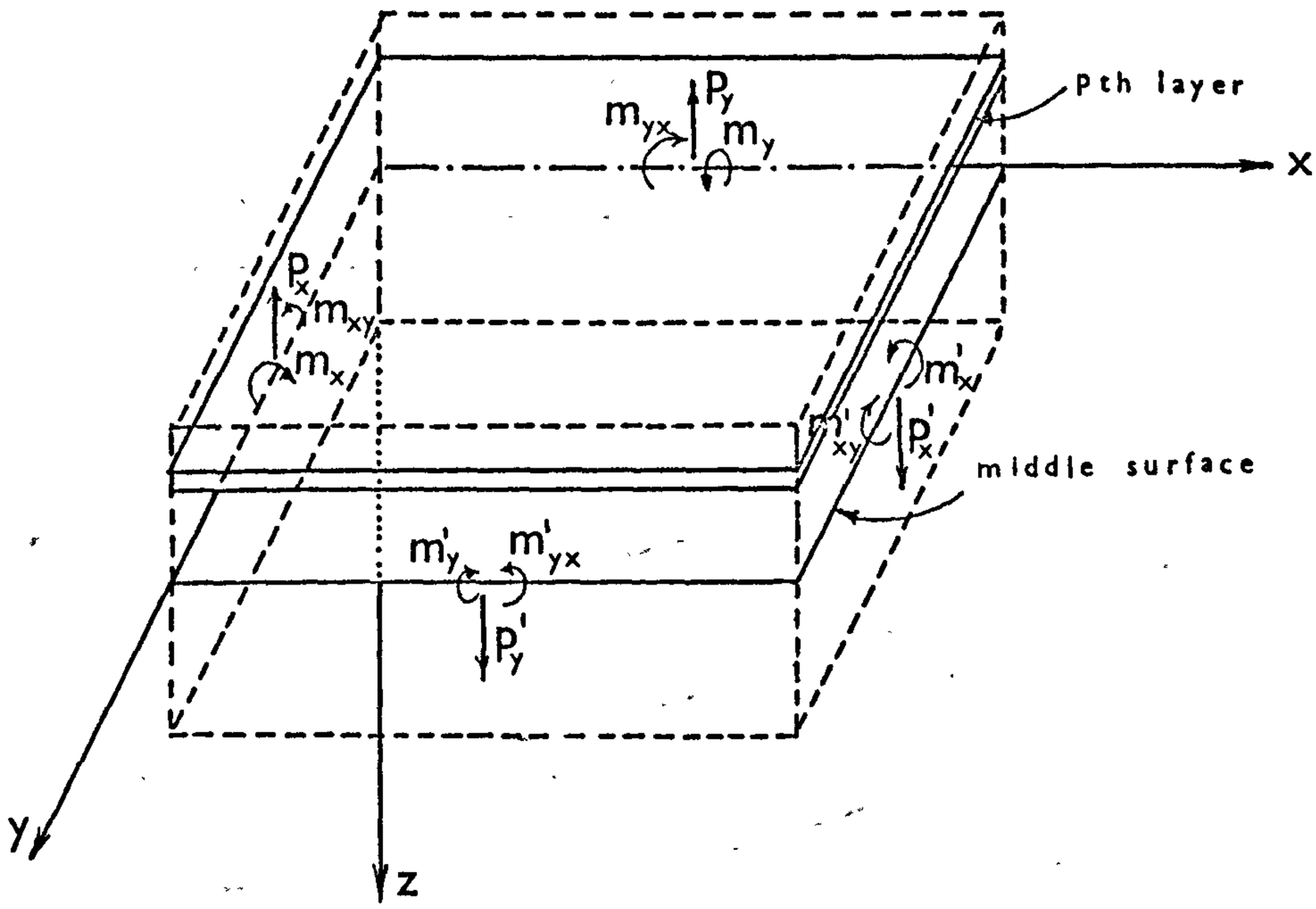

Fig.4.5 A typical rectangular element of plate with internal forces per unit length of the middle surface due to internal forces of the pth layer.

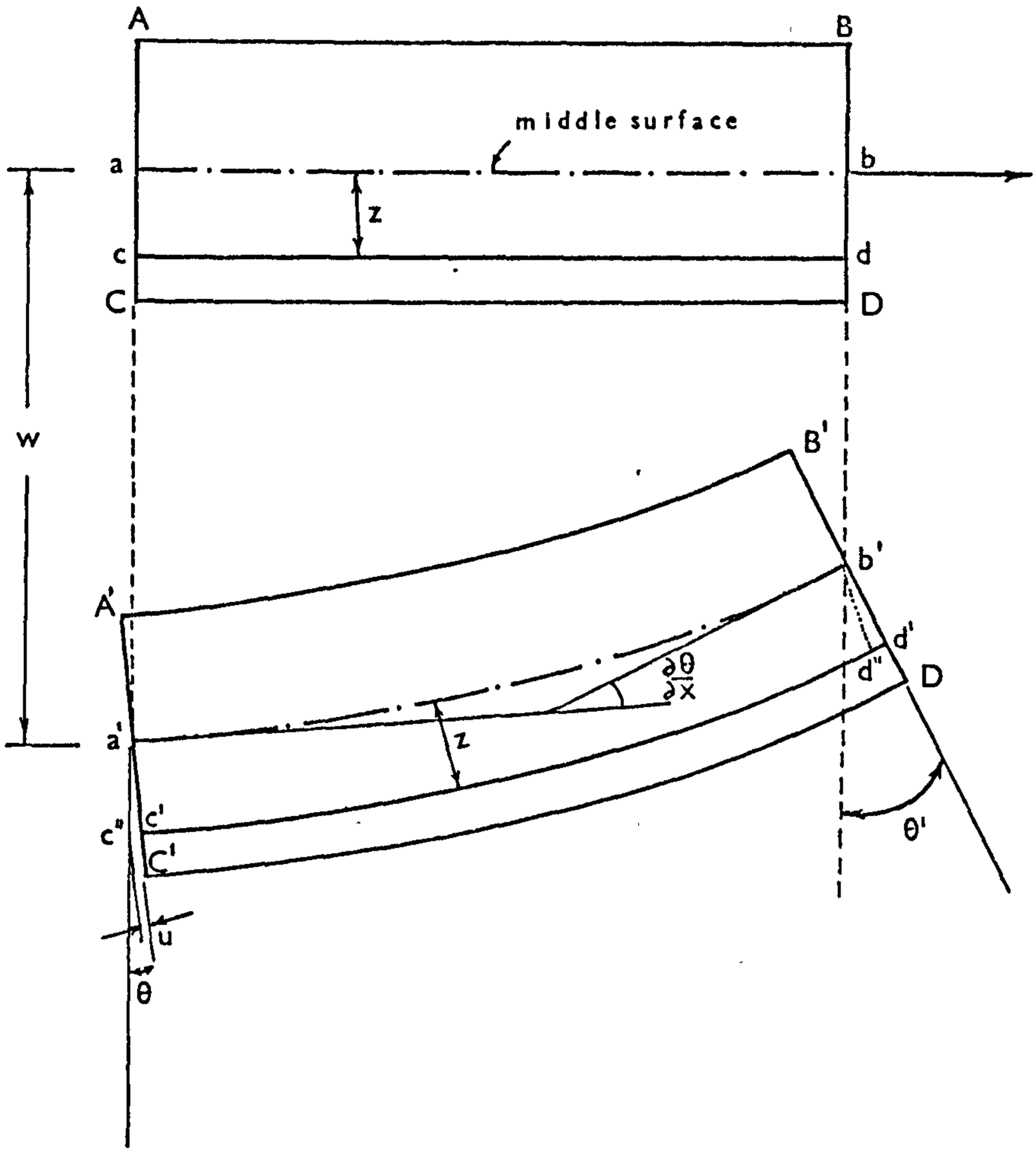

Fig.4.6_Cross section of an element of plate parallel with λ_axis befor and after deflection.

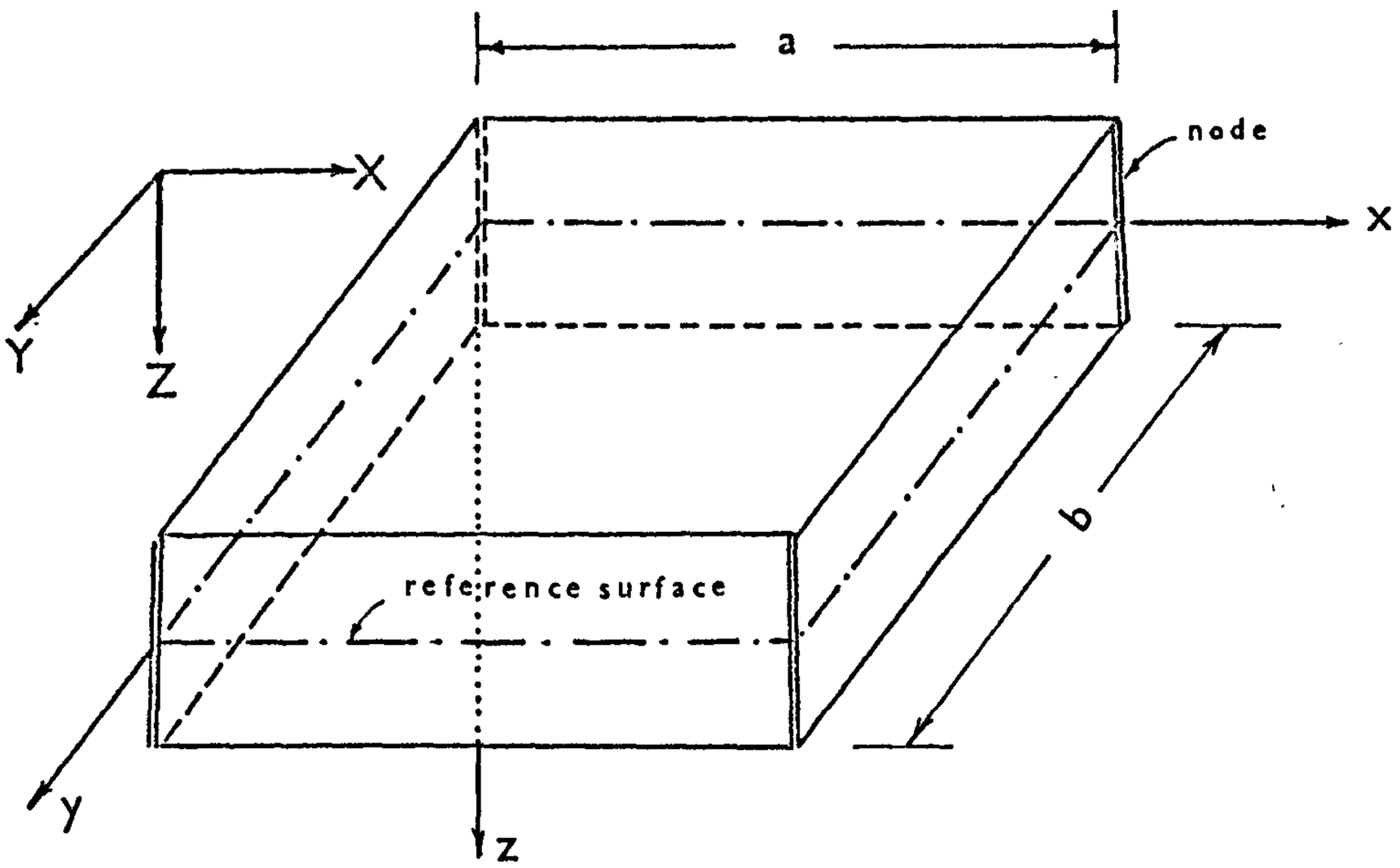

Fig.4.7_A typical rectangular element of slab.

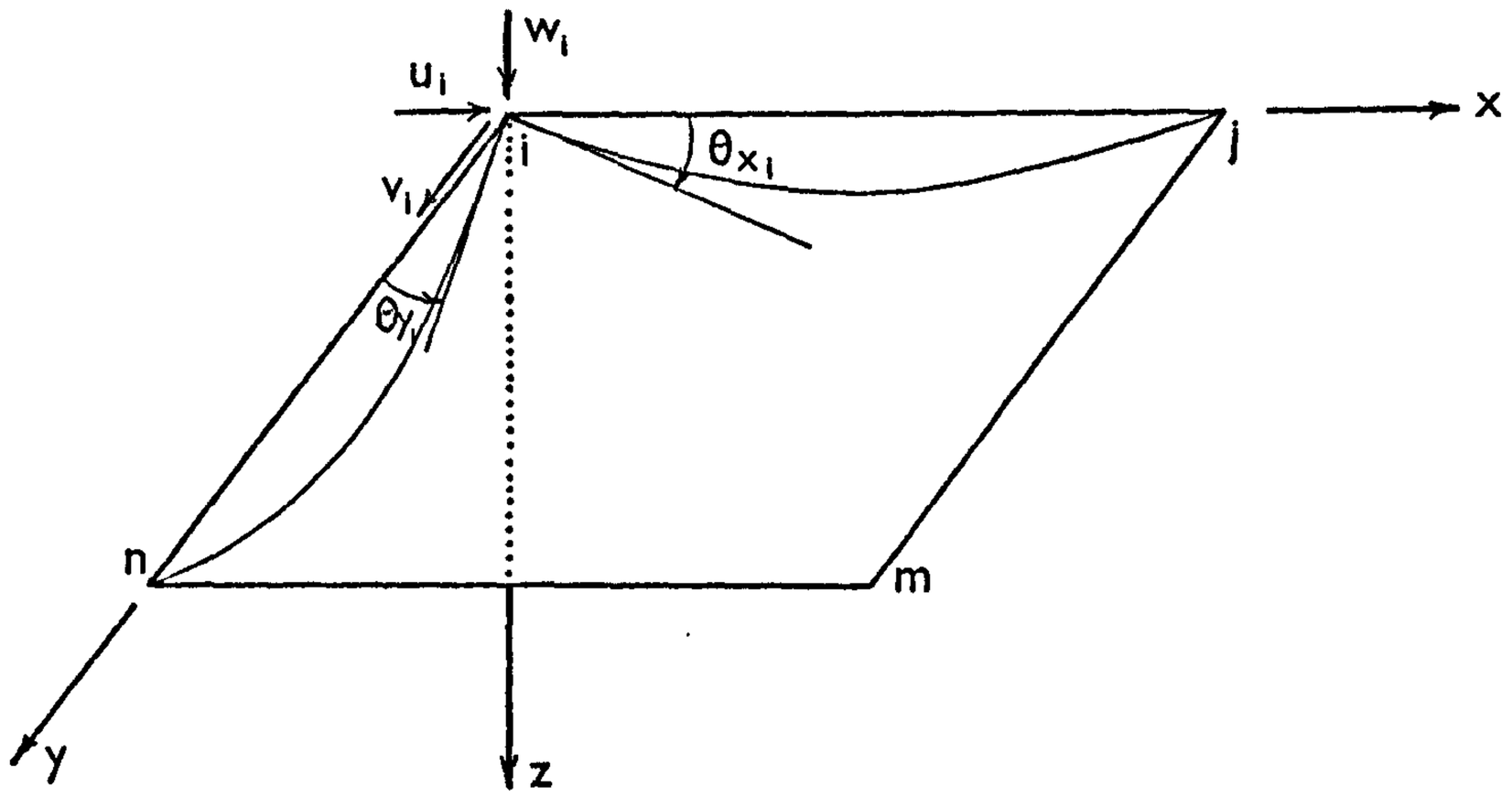

Fig.4.8_Reference surface of a typical elemet of slab with positive directions of rotations and displacements at node j.

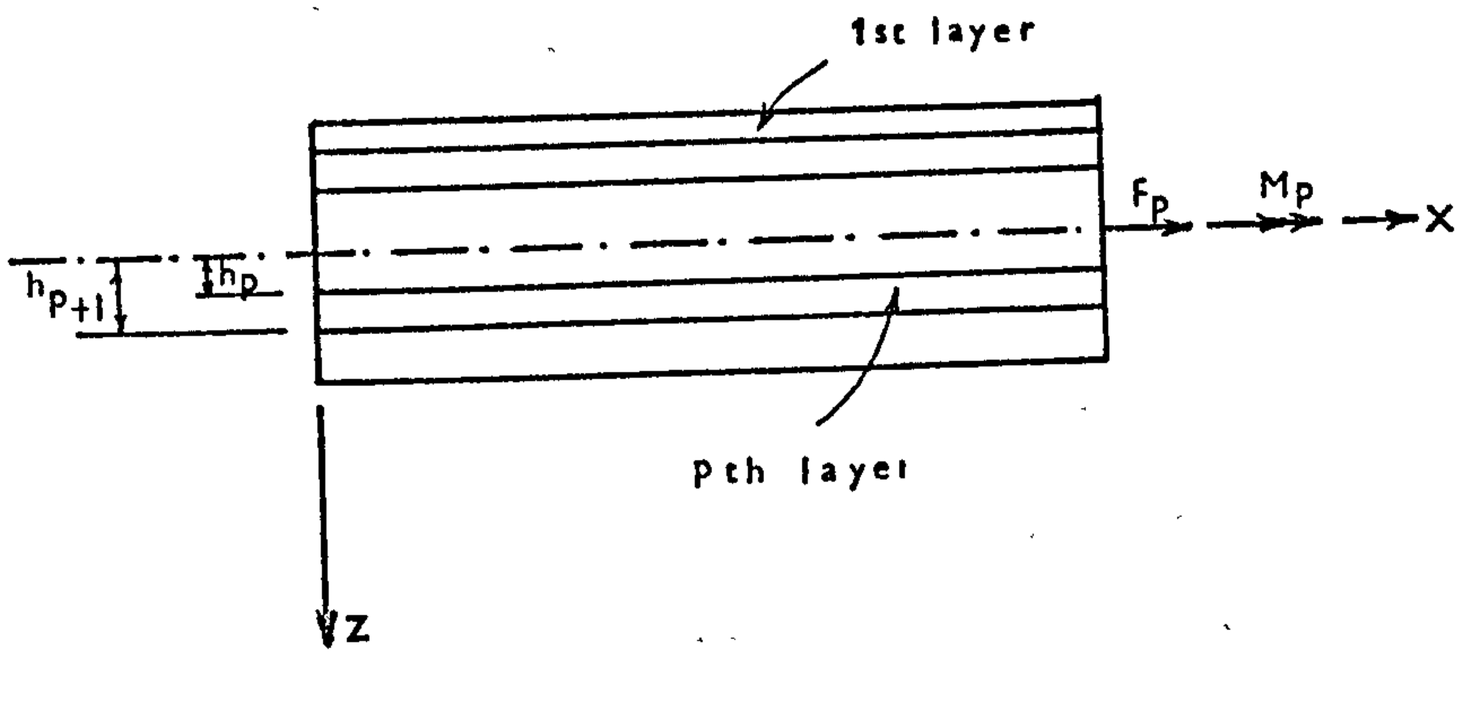

Fig.4.9_Cross section of an element of slab.

CHAPTER FIVE

V- Conduction Of Heat

5.1- Introduction

In this chapter the modes of heat transfer are introduced very briefly along with the basic quantitive relationships for determining the rates of heat transfer, and in the next chapter some of the analytical solutions of heat conduction equation are given to find the distribution of temperature within the structural elements such as beams, slabs and columns and some of these results are compared with some numerical solutions.

In fact any heat equations are non-linear and unhomogeneous, but by simplifying the geometrical characteristics and material properties, the heat equation become linear and homogeneous differential equations in which, each term contains either the dependent variable or one of its derivatives. By this simplifying the heat equation of the conduction becomes a Laplace's or Poisson's differential equation for steady or non-steady state temperature, respectively.

5.2- Heat Transfer

Strictly speaking, heat transfer is a phenomenon occuring only at boundaries of system and its laws find application in many fields of science, and the civil and constructional engineers need considerable knowledge of the

subject.

Generally, heat is transferred by radiation, convention and conduction and they occur seperately or simultaneously. Seperate equations may be written to describe each mechanism, and when two or three mechanisms occur simultaneously it is sometimes possible to add the seperate effects, but sometimes it is necessary to assume the equation of participating mechanisms together.

A- Radiation Heat Transfer

Radiation occurs most freely in vacuum which is characteristically different from the convection and conduction, also it is freely transmitted in air and, in general, is partially reflected and partially absorbed by solids.

A very significant difference between radiation and other types is, no medium is required for propagation of radiant energy, and the radiant exchange between surfaces is, in fact, a maximum when the space between surfaces is evacuated.

Transmission of radiation, which occurs in solids as well as in fluids, is an interesting phenomenon because it can occur through a cold non-absorbing medium between two other bodies. Radiant heat exchange between two bodies depends on the differences between their temperature raised to approximately the fourth power, and the emission of radiant energy given by Stefan and Boltzmann is;

$$H_b = S.K.T^4$$

where H_b is the radiant energy from a black body, S is area,

T is the absolute temperature and K is the Stefan Boltzmann constant.

Radiation is then important in gases and liquids, but in solids the radiation is usually negligible.

B- Convection Heat Transfer

The second basic mode of heat transfer is convection which, is the gross motion of the fluid itself, such that fresh fluid is continually available heating or cooling. The heat transfer by convection, involves energy exchange between a bulk fluid and a surface or interface.

Heat may be transferred by natural convection such that occurs between a solid and a fluid when there is a temperature difference between solid and fluid. The simple expression of Newton's law of cooling or the Newton rate equation of convection was given in 1701 by;

$$H = K.S.(T_2 - T_1)$$

where H is the rate of convection heat transfer, S is the area perpendicular to the direction of heat flow, K is the convection hear transfer coefficient, T_2 is the surface temperature of solid and T_1 is the fluid temperature, then $T_2 - T_1$ is the temperature driving force, and this temperature deriving force determines whether heat transfer is to or from a given surface.

The Newton rate equation is seldom written in a vector form because of its direction and magnitude.

Finally, convection is important in gases and liquids,

but in solids it is absent.

C- Conduction Heat Transfer

Conduction is a kind of heat transfer in solid materials and occurs between two parts of a body by two different temperatures and also occurs within liquids and gases.

Generally speaking, conduction of heat in solids is a transfer of internal energy and this energy is energy of the molecules and atoms.

The conduction of heat is primarily a molecular phenomenon requiring a temperature gradient as a driving force and a quantitive expression relating a temperature gradient, the nature of the conducting medium. The rate of heat transfer by conduction was given in 1822 by Fourier.

Throughout of the present chapter we shall assume conduction of heat only in solid materials without any heat generation within the body itself.

5.3- Temperature Equation

Generally, the temperature at a point (p) within a body heated on the boundaries depends on time, position of the point and material properties at this point and also throughout of the body. Mathematically, the dependence of temperature on the position of the point p($\vec{r}$), time interval (δt) and material properties (h) should be expressed as a unique function of these variables, i.e.,

$$T = T\left[p(\vec{r}), \delta t, h \right]$$

This function of temperature usually is a continuous function of time by any boundary and initial conditions and also is a continuous function of position of point (p) within an isotropic homogeneous material. The locus of points with the same temperature at a certain time is called the isothermal surface, and this isothermal surface with constant temperature (T_o) is given by;

$$T\left[p(\vec{r}), \delta t, h \right] = T_o$$

In steady state temperature, the temperature does not vary with time and the temperature of any point within the body depends on the position of this point and boundary temperature. Mathematically, it is possible to assume that the steady state temperature is a result of special case of non-steady temperature when the time tends to infinity;

$$T_s = \text{Limit } T_n \Big|_{t \longrightarrow \infty}$$

As we shall see later, for isotropic homogeneous materials, when there is no heat generation within the body itself, the temperature value within the body under steady state case is also independent of material properties, then,

$$T_{si} = T\left[p(\vec{r}) \right]$$

In steady state temperature the rate of heat flow by conduction within a solid in u-direction is proportional to the temperature gradient in this direction and the area of

flow perpendicular to u-direction;

$$\vec{H}_u = K_u \cdot S_u \cdot \vec{\nabla}_u T$$

where $\vec{H}_u$ is the rate of flow of heat in u-direction, S_u is the area of the material proposed perpendicular to the direction of heat flow, K_u is called the thermal conductivity of material in u-direction is one of the material properties, and;

$$\nabla_u T = \frac{\partial T}{\partial u}$$

By definition that, the positive heat flow is in the direction of negative temperature gradient, the Fourier's equation of rate of heat transfer of conduction is written as follows;

$$\vec{H}_u = - K_u \cdot S_u \cdot \vec{\nabla}_u T$$

and this equation may be written in the following form;

$$\vec{h}_u = - K_u \cdot \vec{\nabla}_u T \qquad (5.1)$$

where, $\vec{h}_u = \vec{H}_u / S$ is the rate of the heat flow per unit area per unit time in u-direction is called the flux of heat across any surface of element around any point within the body, and because of its direction and magnitude, $\vec{h}_u$ behaves as a vector.

The divergence of flux $\vec{h}_u$ is given by;

$$\varepsilon_u = \frac{\partial \vec{h}_u}{\partial \vec{u}} \qquad (5.2)$$

and this gradient is not a vector.

5.4- Heat equation

In this section we find the differential equation of conduction of heat in cartesian coordinates up to three dimensional body, by assuming the time variable, and in the next chapter we give the temperature equations within the body in two seperate conditions as follows;

1- Steady state temperature with constant temperature on the boundaries of the body.

2- Non-steady state temperature with constant temperature on the boundaries which may be used for variable surface temperature by assuming a step function of time-temperature on the boundaries.

Consider an infinitesimal small rectangular paralelepiped element of lengths dx, dy and dz around point (p) as shown in figure (5.1).

The gradient of flux at point (p) within this element in the x-direction is (g_x), and the rate of heat flowing into the element in this direction is;

$$-g_x(dy.dz).dx = -g_x.dv$$

where dv is the volume of the element. Similarly ($-g_y.dv$) and ($-g_z.dv$) are the rate of heat flowing into the element in y and z-directions, respectively, then the rate of flow of heat flowing into the element is;

$$-(g_x + g_y + g_z).dv \qquad (A)$$

On the other hand the rate of heat is being stored within the element is;

$$\rho.c.\frac{\partial T}{\partial t}.dv \qquad (B)$$

where (ρ) is the density of material and (c) is the specific heat of the element. By equating (A) and (B) and assuming there is no heat generation within the element, the heat conduction equation becomes as follows;

$$g_x + g_y + g_z + \rho.c.\frac{\partial T}{\partial t} = 0 \qquad (C)$$

By using equation (5.2), equation (C) may be written in the following form;

$$\frac{\partial h_x}{\partial x} + \frac{\partial h_y}{\partial y} + \frac{\partial h_z}{\partial z} + \rho.c.\frac{\partial T}{\partial t} = 0 \qquad (D)$$

or;

$$\nabla h + \rho.c.\frac{\partial T}{\partial t} = 0$$

By substituting equation (5.1) into equation (D) the heat conduction equation becomes as follows

$$\frac{\partial}{\partial x}(K_x.\frac{\partial T}{\partial x}) + \frac{\partial}{\partial y}(K_y.\frac{\partial T}{\partial y}) + \frac{\partial}{\partial z}(K_z.\frac{\partial T}{\partial z}) = \rho.c.\frac{\partial T}{\partial t} \qquad (E)$$

or;

$$\sum_{i=1}^{3}\left\{ \frac{\partial}{\partial u_i}(K_{u_i}.\frac{\partial T}{\partial u_i})\right\} = \rho.c.\frac{\partial T}{\partial t}$$

Experiments show that, every property of material such as thermal conductivity, density and specific heat varies with variation of temperature as discussed in chapter three. For isotropic homogeneous material the thermal conductivity at every point in any direction is the same and varies with temperature only, then in isotropic homo-

geneous materials;

$$K_x = K_y = K_z = K$$

and the heat equation of conduction reduces to;

$$\frac{\partial^2 T}{\partial x^2} + \frac{\partial^2 T}{\partial y^2} + \frac{\partial^2 T}{\partial z^2} = \frac{1}{h} \cdot \frac{\partial T}{\partial t}$$

or;

$$\nabla^2 T = \frac{1}{h} \cdot \frac{\partial T}{\partial t} \qquad (5.3)$$

where, $h = \frac{K}{\rho c}$ is called the diffusivity of substance, and ∇^2 is the well known Laplace's notation of second order.

In steady state temperature when temperature value is independent of time, the differential equation of flow of heat becomes;

$$\nabla^2 T = 0 \qquad (5.4)$$

Equation (5.4) shows that, in steady state temperature case for an isotropic homogeneous material, when there is no heat generation within the body, the temperature at any point of the body is also independent of material properties.

5.5- Boundary And Initial Conditions

Generally, in homogeneous materials the temperature is given by a continuous and unique function of x, y, z and time, but it may be discontinuous on the boundary of the body. The initial condition gives the temperature value within the body and also on the boundary when the time tends to a given value, say zero for starting point.

The boundary condition is the surface temperature and it may be constant or a function of x, y, z and time and also it may be a step function as we will see in the next chapter. Fire condition is an example when the boundary temperature varies with time.

Now we consider the following boundary and initial conditions when the surface temperature is independent of time;

$$T = g(x, y, z) \qquad \text{on the boundary}$$

$$T = f(x, y, z) \qquad \text{initially, when time tends to zero}$$

In fact, equation (5.3) is a linear partial differential equation, in which, if T_s and T_n^* be two ordinary solutions of this linear equation, $T_s + T_n^*$ will be another solution of equation (5.3), then by assuming $T = T_s + T_n^*$ the equation (5.3) becomes as follows;

$$(h.\nabla^2 T_s - \frac{\partial T_s}{\partial t}) + (h.\nabla^2 T_n^* - \frac{\partial T_n^*}{\partial t}) = 0$$

and the following differential equations satisfy this equation;

$$\nabla^2 T_s - \frac{1}{h}.\frac{\partial T_s}{\partial t} = 0$$

$$\nabla^2 T_n^* - \frac{1}{h}.\frac{\partial T_n^*}{\partial t} = 0$$

and by assuming T_s is independent of time we have;

$$\nabla^2 T_s = 0 \qquad \text{(a)}$$

$$\nabla^2 T_n^* = \frac{1}{h}.\frac{\partial T_n^*}{\partial t} \qquad \text{(b)}$$

Equation (a) is the differential equation of flow of heat within the body in steady state temperature, whose boundary temperature is given by;

$$T = g(x, y, z)$$

and equation (b) is the differential equation of conduction of heat throughout the body, whose boundary and initial conditions are given by;

$$T = 0 \qquad \text{boundary temperature}$$

$$T = f(x, y, z) - T_s \quad \text{initial condition.}$$

then, in general case, it follows that, when the surface temperature is independent of time we can assume conduction of heat within the body in steady state temperature by given temperature on the boundary and non-steady state temperature by zero temperature on the boundary and also the initial condition, superposition of these two results gives the temperature equation within the body.

In other case when the surface temperature varies with time we assume that this surface temperature is constant and independent of time in any time intervals.

5.6- A Particular Solution

It is well known that, the general solutin of equation (5.4) in three dimensional body is;

$$T = f_1(x + i_1 y + i_2 z) + f_2(x + j_1 y + j_2 z)$$

where, f_1 and f_2 are differentiable functions and i_1, i_2, j_1

and j_2 are real or complex constants satisfy the following quadric equations;

$$1 + i_1^2 + i_2^2 = 0$$

$$1 + j_1^2 + j_2^2 = 0$$

In two dimensional, for instance, we have;

$$i_2 = j_2 = 0, \quad i_1 = (-1)^{\frac{1}{2}} \text{ and } \quad j_1 = \bar{I},$$

and the general solution is given by;

$$T = f_1(x + iy) + f_2(x + \bar{I}y)$$

However, these general solutions are not useful in the present study, specially for geometrical conditions of the body heated from the boundaries, and generally, it is not possible to find the general solution of heat equation satisfying all the conditions, but with the help of some particular solutions we will able to introduce some temperature equations for some special and practical boundary and geometrical conditions.

These equations will be used for studies to find the distribution of temperature within some structural members, such as beams and slabs and also some results will be then compared with a numerical solution in the next chapter.

To find a particular solution of equation (5.3), consider the following function;

$$T = X(x).Y(y).Z(z).\theta(t) \qquad (A)$$

that, each term on the right hand side of this function varies with one variable only, and by substituting this function into equation (5.3), we find;

$$\frac{1}{X}.\frac{d^2X}{dx^2} + \frac{1}{Y}.\frac{d^2Y}{dy^2} + \frac{1}{Z}.\frac{d^2Z}{dz^2} = \frac{1}{\theta h}.\frac{d\theta}{dt} \qquad (B)$$

Each term of this expression is a function of own variable only, and hence, each must be equal to a constant, then equation (B) seperates into fourordinary and linear differential equations;

$$\frac{d^2X}{dx^2} - A^2.X = 0$$

$$\frac{d^2Y}{dy^2} - B^2.Y = 0$$

$$\frac{d^2Z}{dz^2} - C^2.Z = 0$$

$$\frac{d\theta}{dt} - h.\lambda.\theta = 0$$

where A, B and C are arbitrary constants, real or complex, and;

$$\lambda = A^2 + B^2 + C^2 \qquad (5.5)$$

and for a steady state temperature (λ) is equal to zero.

The general solutions of the above equations are given by;

$$X = a_1.Exp(Ax) + a_2.Exp(-Ax)$$

$$Y = b_1.\mathrm{Exp}(By) + b_2.\mathrm{Exp}(-By)$$

$$Z = c_1.\mathrm{Exp}(Cz) + c_2.\mathrm{Exp}(-Cz)$$

$$\Theta = \mathrm{Exp}(\lambda ht)$$

respectively, where a_i, b_i and c_i which(i=1,2) are the integrals arbitrary constants that may be real or complex, and the integral constant of the last equation has been assumed to be equal with unity.

By substituting the above solutions into equation (A) we find a particular solution of heat conduction equation (5.3) or (5.4) and by this particular solution we will find the temperature equations within one, two and three dimensional body under steady and non-steady state temperature in chapter six.

5.7- A Numerical Solution

The classical formulations and solutions of heat conduction equation will be presented in chapter six, while the present section includes a numerical method to calculate the distribution of temperature within the body with the help of computer programs.

In the numerical method of solution the body is divided into a finite number of small elements which have the same dimensions throughout the body and the accuracy of the results depends on these dimensions and number of the elements.

strictly speaking, it is assumed that the temperature

within each element varies linearly, and this is infact all linear functions satisfy the heat equation.

Before going on the details of numerical method of solution it is necessary to remember the Taylor's series expansion of a function around a point in a given range.

Assume that, the following function of (n) variables;

$$V = f(u_1, u_2, u_3, \ldots, u_n)$$

continuous in range;

$$a_i \leq u_i \leq b_i \qquad i=1,2,3, \ldots, n$$

possesses all differential coefficients up to the pth order at all points in the foregoing range.

If two points;

$$O(u_1^o, u_2^o, u_3^o, \ldots, u_n^o)$$

$$A(u_1^o + \varepsilon_1 \cdot \delta u_1, u_2^o + \varepsilon_2 \cdot \delta u_2, u_3^o + \varepsilon_3 \cdot \delta u_3, \ldots, u_n^o + \varepsilon_n \cdot \delta u_n)$$

are assumed to be in the forementioned range, the Taylor's series expansion around point (O) is written as follows;

$$V_A = \sum_{p=0}^{p} \frac{1}{p!} \left[\sum_{n=1}^{n} (\varepsilon_i \cdot \delta u_i)\left(\frac{\partial V}{\partial u_i}\right) \right]_{(p^*)} + R_p$$

where, (p^*) gives the order of partial differentiations of function (V) with respect to its variables and also powers of $(\varepsilon_i \delta u_i)$ as in Binom expansion, R_p is the remainder of Taylor's expansion which includes $(\varepsilon_i \delta u_i)$ with higher power than (p), and $\varepsilon_i = +1$ or -1 or zero.

The first term of Taylor's series expansion when p = 0, is;

$$\frac{1}{0!}\,(\varepsilon_i \delta u_i)^0 \cdot \left(\frac{\partial V}{\partial u_i}\right)_{(0^*)} = V_0$$

then the Taylor's series is written as follows;

$$V_A = V_0 + \sum_{p=1}^{p} \frac{1}{p!}\left[\sum_{n=1}^{n} (\varepsilon_i \delta u_i)\left(\frac{\partial V}{\partial u_i}\right)\right]_{(p^*)} + R_p \qquad (5.6)$$

For a three dimensional function (n=3) the following relationship can be derived from equation (5.6);

$$V_{A_1}+V_{A_2}+V_{A_3}+V_{A_4}=4V_0+2\left(\delta u_1^2 \frac{^2V}{u_1^2} + \delta u_2^2 \frac{^2V}{u_2^2}\right) + R_3 \qquad (5.7)$$

where R is the remainder of the expansion and is neligible, and;

$$V_0 = f(u_1^o,\ u_2^o)$$

$$V_{A_1} = f(u_1^o + \delta u_1,\ u_2^o + \delta u_2)$$

$$V_{A_2} = f(u_1^o + \delta u_1,\ u_2^o - \delta u_2)$$

$$V_{A_3} = f(u_1^o - \delta u_1,\ u_2^o + \delta u_2)$$

$$V_{A_4} = f(u_1^o - \delta u_1,\ u_2^o - \delta u_2)$$

Equation (5.7) is the general formula to solve the second order Laplace and Poisson's differential equations by numerical method.

By inserting $\delta u_1=0, (\varepsilon_1=0)$ and again $\delta u_2=0, (\varepsilon_2=0)$ in

equation (5.7) we find;

$$\frac{\partial^2 V}{\partial u_1^2}=\frac{1}{\partial u_1^2}\ f(u_1^o+\delta u_1,\ u_2^o)+f(u_1^o-\delta u_1,u_2^o)-2f(u_1^o,\ u_2^o)$$

$$\frac{\partial^2 V}{\partial u_2^2}=\frac{1}{\partial u_2^2}\ f(u_1^o,\ u_2^o+\delta u_2)+f(u_1^o,\ u_2^o-\delta u_2)-2f(u_1^o,u_2^o) \qquad (5.8)$$

and these are the basic finite difference formula of the two dimensional problem.

Similarly, for a three variable function we find;

$$\frac{\partial^2 V}{\partial u_1^2}=\frac{1}{\delta u_1^2}\ f(u_1^o+\ u_1,u_2^o,u_3^o)+f(u_1^o-\ u_1,u_2^o,u_2^o)-2f(u_1^o,u_2^o,u_3^o)$$

$$\frac{\partial^2 V}{\partial u_2^2}=\frac{1}{\delta u_2^2}\ f(u_1^o,u_2^o+\ u_2,u_3^o)+f(u_1^o,u_2^o-\ u_2,u_3^o)-2f(u_1^o,u_2^o,u_3^o) \qquad (5.9)$$

$$\frac{\partial^2 V}{\partial u_2^2}=\frac{1}{\delta u_2^2}\ f(u_1^o,u_2^o,u_3^o+\ u_3)+f(u_1^o,u_2^o,u_3^o-\ u_3)-2f(u_1^o,u_2^o,u_3^o)$$

which are used to solve the three dimensional problems of the subject.

For a two dimensional body under steady state temperature, equation (5.8) gives;

$$\frac{1}{\delta^2 x}\ T(x_o+\delta x,y_o)+T(x_o-\delta x,y_o)-2T(x_o,y_o)\ +$$

$$\frac{1}{\delta^2 x}\ T(x_o,y_o+\delta y)+T(x_o,y_o-\delta y)-2T(x_o,y_o)\ =\ 0$$

and by referring to figure (5.2) this equation is written in the following form;

$$\frac{1}{\delta^2 x}(T_{+A}+T_{-A})+\frac{1}{\delta^2 y}(T_{+B}+T_{-B})-2T_o(\frac{1}{\delta^2 x}+\frac{1}{\delta^2 y})\ =\ 0 \qquad (5.10)$$

Equation (5.10) is a linear relationship between temperatures of five nodes of the body and by writting this equation for all nodes of the body we have a simultaneous equation, which gives the distribution of temperature within the two dimensional body heated from boundaries.

In a special case when x = y this relationship reduces to the following form;

$$T_{+A}+T_{-A}+T_{+B}+T_{-B}-4T_{o} = 0$$

It should be realized that, if the rectangular body is divided (n) by (m), there will be (n-2)(m-2) linear equations and these equations are independent of each other include (n-2)(m-2) unknowns if the temperature values on the all sides of the body are being given. In other case, when the temperature on one side of the body is unknown (as in semi-infinite depth body), the simultaneous equation involves (n-2) or (m-2) more unknowns and unsulable and this method is not useful any more.

The simultaneous equations of temperature may be written as follows;

$$\underline{H} \cdot \underset{\sim}{T} = \underset{\sim}{P} \qquad (a)$$

where $\underline{H}$ is a square matrix called the coefficient matrix, $\underset{\sim}{T}$ is a column vector includes the main unknowns (the nodal temperature), and finally $\underset{\sim}{P}$ is a known column vector.

Because of the independency of all foregoing linear equations, $\underline{H}$ is a non-singular matrix, then;

$$\underset{\sim}{T} = \underline{\underline{H}}^{-1} \cdot \underset{\sim}{P} \qquad \text{(b)}$$

There are some special methods to solve the above simultaneous equation by computer.

One of the numerical method to solve equation (a) is the Gauss elimination method. In this method, the coefficient matrix is reduced to upper triangular form by successive elimination of the variables (unknowns), for instance the first unknown is eliminated from the last (n-1) equations by suitable operations with the first equation. The second variable is then eliminated from the last (n-2) equations by suitable operations with the second equation, in its modified form with the coefficient of the first unknown zero. The process is continued until the last equation is reached when the coefficient matrix has been reduced to upper triangular form.

The right hand side of equation (a) are successively modified as the process continues and the unknowns finally evaluated by a back-substitution.

This method of solving all linear simultaneous equations gives satisfactory results, but leads to more complicated programming with banded matrices.

Another method to solve the linear simultaneous equations (a) is the Gauss-Seidel iteration technique. In this earliest approximation method, each equation is used to obtain a new value of the unknown associated with it in terms of the current values of the other unknown, the cycle being repeated until a sufficiently accurate answer has been

obtained.

The main flow chart of a computer program to obtain the distribution of temperature within two dimensional body under steady state temperature, by using the Gauss-Seidel iteration method is given in appendix II and also some of the temperature values within a two dimensional body as comparing with the classical solution are given in appendix II.

For a three dimensional body under steady state temperature equation (5.9) gives;

$$\frac{1}{\delta^2 x}(T_{+A}+T_{-A})+\frac{1}{\delta^2 y}(T_{+B}+T_{-B})+\frac{1}{\delta^2 z}(T_{+C}+T_{-C})-2T_o(\frac{1}{\delta^2 x}+\frac{1}{\delta^2 y}+\frac{1}{\delta^2 z}) = 0$$

and seven nodes T_{+A}, T_{-A}, T_{+B}, T_{-B}, T_{+C}, T_{-C} and T_o are shown in figure (5.4).

In a special meshing when $\delta x = \delta y = \delta z$, the linear equation reduces to;

$$T_{+A}+T_{-A}+T_{+B}+T_{-B}+T_{+C}+T_{-C}-6T_o = 0$$

If the rectangular parallelepiped body is divided n by m by p, there will be (n-2)(m-2)(p-2) linear relationships between unknowns, if the temperature values on the all surfaces of the body are known, while in other case the above simultaneous equations are unsulable.

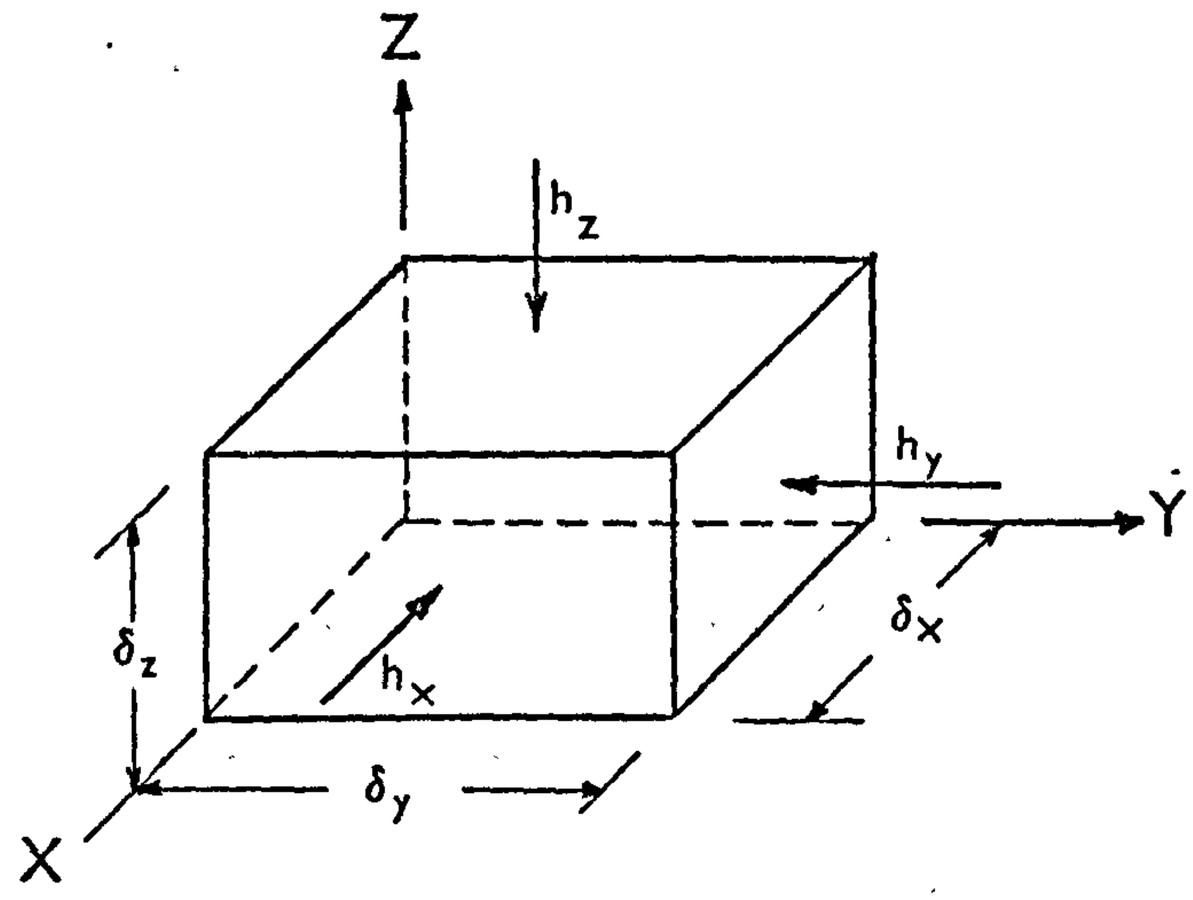

Fig.5.1- An infinitesimal small element of a heated body.

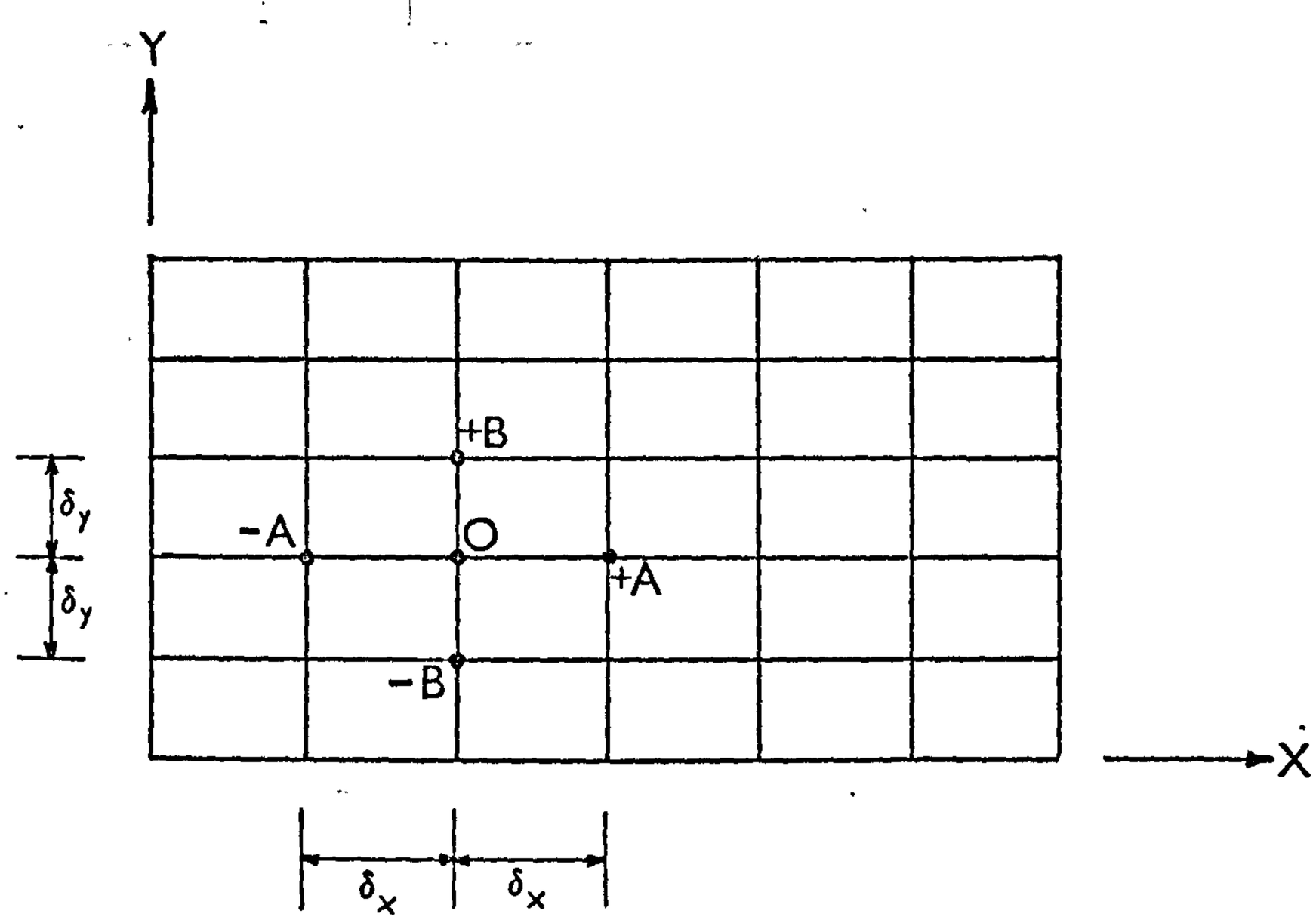

Fig.5.2- A typical division of a two dimensional body for numerical solution of heat equation.

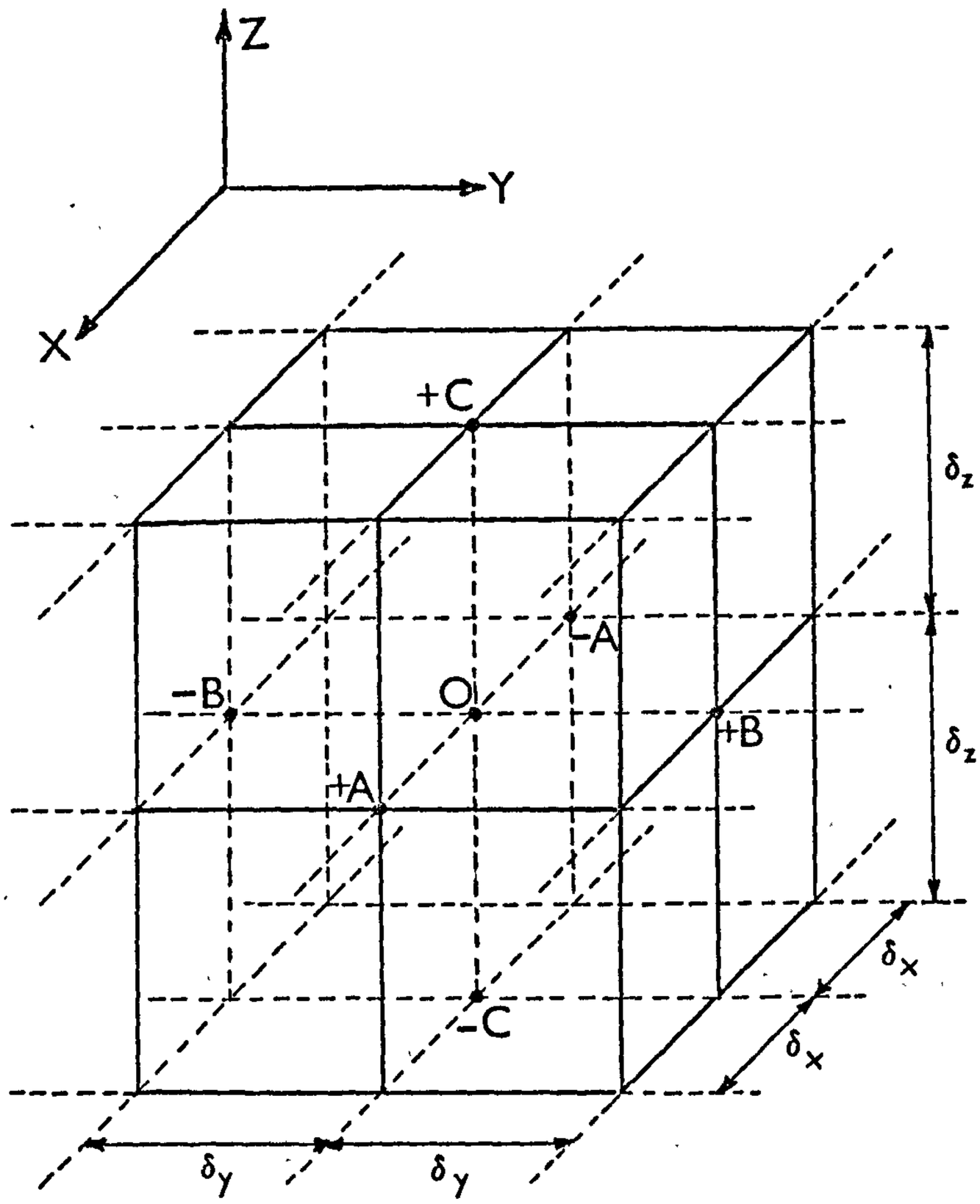

Fig.5.3- A typical division of a three dimensional body for numerical solution of the heat equation.

CHAPTER SIX

VI- Analytical Solution Of Heat Equation

6.1- Introduction

The analytical solution of heat problems frequently leads to a series of differential equations, whose solution is very tedious if not impossible. In some special cases, with adoption of certain assumptions, the governing equations of heat problem become simpler and solution is analytically possible.

However, in practice, the complex geometrics, boundary conditions and different properties of the body itself and also structure do not justify the use of these simplifications. On the other hand the analytical and classical solution of heat equation, especially for isotropic homogeneous materials and also for semi-infinite depth body, will be more suitable and convenient for calculating the distribution of temperature within a body and also reducing the computational time. In analysis of a reinforced concrete element such as beam or slab it is possible to assume that steel and concrete are different but isotropic homogeneous materials.

In the present chapter we start with steady state temperature to find the temperature equation within a solid body up to three dimensional and introduce some practical boundary temperature to find the first term of non-steady state temperature equation.

When temperature under a steady state is independent of time the equation (4.5) becomes;

$$A^2 + B^2 + C^2 = 0 \qquad (6.1)$$

6.2- One Dimensional Body

In one dimensional body the temperature varies in one direction only, say x-direction, and the temperature function within the body under steady state temperature becomes linear;

$$\frac{d^2T}{dx^2} = 0$$

or;

$$T = ax + b$$

where, a and b are integral arbitrary constants, which are calculated from the following boundary conditions;

$$T = T_o \qquad \text{when } x = 0$$

$$T = T_1 \qquad \text{when } x = 1$$

and the temperature equation becomes;

$$T_s = T_o + \frac{x}{1}(T_1 - T_o) \qquad (6.2)$$

6.3- Two Dimensional Body

This section is included to determine the temperature equation within;

1- Finite depth body.

2- Semi-infinite depth body.

of a rectangular element, length (L) and height (d), under

steady state temperature by constant temperature at every point of body surface.

The particular solution of heat conduction equation, for this special case is given by;

$$T=\left[a_1 Exp(\Lambda x)+a_2 Exp(-\Lambda x)\right]\left[b_1 Exp(By)+b_2 Exp(-By)\right] \qquad (6.3)$$

where,

$$A^2 + B^2 = 0$$

6.3.1- Finite Depth Body

In a case of finite depth body consider the following boundary conditions as in figure (6.1);

1)- $T = 0$ when $x = 0$ and $x = L$,

2)- $T = 0$ when $y = d$,

3)- $T = f(x)$ when $y = 0$.

From the first boundary condition and using equation (6.3), a_1+a_2 becomes zero and;

$$A = \frac{k\pi}{L}i$$

where, k is a positive integer and $i = (-1)^{\frac{1}{2}}$, then;

$$B = \frac{k\pi}{L}$$

and the temperature equation becomes as follows;

$$T = \left[b_1' Exp(By)+b_2' Exp(-By)\right].\sin\frac{k\pi}{L}x \qquad (6.4)$$

where,

$$b_1' = -2b_1 i \text{ and } b_2' = -2b_2 i.$$

The second boundary condition gives;

$$b_1' = - b_1 \text{Exp}(2\frac{k\pi}{L}d)$$

and;

$$T_k = \eta_k . \sinh\left[\frac{k\pi}{L}(d-y)\right] . \sin\frac{k\pi}{L}x$$

where, η_k is an arbitrary constant for each step of integer k. Finally from the last boundary condition we have the following transcendental equation;

$$f(x) = \eta_k . \sinh\frac{k\pi}{L}d . \sin\frac{k\pi}{L}x$$

By using the Fourier's sine series we find;

$$\eta_k = \frac{2}{L} . \frac{I_k}{\sinh\frac{k\pi}{L}d}$$

where,

$$I_k = \int_0^L f(x) . \sin\frac{k\pi}{L}x . dx \qquad (6.5)$$

thus, the temperature equation for a finite depth body under steady state temperature, heated from one side becomes;

$$T_s = \frac{2}{L} \sum_{k=1}^{\infty} I_k . \frac{\sin\frac{k\pi}{L}x}{\sinh\frac{k\pi}{L}d} . \sinh\frac{k\pi}{L}(d-y) \qquad (6.6)$$

Now it must be proved that this infinite series is a convergent series. By the ratio and comparison test method the ratio of the modulus of each term to the modulus of

preceding term is;

$$\frac{T_{k+1}}{T_k}=\left[\frac{I_{k+1}}{I_k}\cdot\frac{\sin\frac{k+1}{L}\pi x}{\sin\frac{k\pi}{L}x}\right]\cdot\frac{\sin\frac{k\pi}{L}d}{\sin\frac{k+1}{L}\pi d}\cdot\frac{\sinh\frac{k+1}{L}\pi(d-y)}{\sinh\frac{k\pi}{L}(d-y)}$$

The value of the first term on the right hand side of this ratio, when k is bigger than any big whole number, is unit and when k tends to infinity the ratio becomes;

$$\text{Limit}\ \left.\frac{T_{k+1}}{T_k}\right|_{k\rightarrow\infty} = \text{Exp}\left(-\frac{\pi}{L}y\right) \qquad (6.7)$$

since this value is positive and less than a unit, the series converges with any given value of y and L.

6.3.2- Semi-infinite Depth Body

For a semi-infinite depth body consider the following boundary conditions;

1)- $T = 0$ when $x=0$ and $x=L$,

2)- $T = 0$ when $y=\infty$,

3)- $T = f(x)$ when $y=0$.

Equation (6.4) satisfies the first boundary condition and also satisfies the second boundary condition when b'_1 is zero, and finally from the third boundary condition we have;

$$f(x) = b'_1.\sin\frac{k\pi}{L}x$$

and by using Fourier's sine series we find;

$$T_s = \frac{2}{L}\sum_{k=1}^{\infty}\left\{I_k.\text{Exp}\left(-\frac{k\pi}{L}y\right).\sin\frac{k\pi}{L}x\right\} \qquad (6.8)$$

where, I_k has been given in equation (6.5).

Equation (6.7) is independent of height of the body then the ratio and comparison test method proves that the series (6.8) also converges and in fact when (d), in equation (6.6) tends to infinity we could find the equation (6.8) directly, and hence, equation (6.8) is a convergent series.

It should be realized that, the numerical solutions of equations (6.6) and (6.8) are possible but the computing time is high. In a later section these solutions will be re-examind so as to reduce the computational time considerably.

6.3.3- Practical Forms Of surface Temperature

In this section we introduce two different basic and practical types of surface temperature f(x), that may be used in analysis of reinforced concrete beams and slabs.

6.3.4- Type One

Consider the case of local heating at a boundary with following properties at y = 0, as shown in figure (6.2);

$$f(x) = T_1 \qquad \text{when} \quad 0 \le x \le a$$

$$f(x) = T_1 + \Delta_{21} \cdot \frac{x-a}{b-a} \qquad \text{when} \quad a \le x \le b$$

$$f(x) = T_3 + \Delta_{23} \cdot \frac{x-c}{b-c} \qquad \text{when} \quad b \le x \le c$$

$$f(x) = T_3 \qquad \text{when} \quad c \le x \le L$$

The value of I_k is calculated from equation(6.5);

$$I_k=\frac{2}{k}(T_1-T_2\cos k\pi)+\frac{2L}{k^2\pi^2}\left(\Delta_{12}\frac{s_a-s_b}{a-b}+\Delta_{32}\frac{s_b-s_c}{b-c}\right) \qquad (6.9)$$

where,

$$s_q = \sin\frac{k\pi}{L}q$$

In the present type of surface temperature f(x), we consider four special forms of boundary temperature as in below;

A- First Form

For the first case of the surface temperature f(x) assume the following properties as shown in figure (6.3-a);

$a=b=0$, $T_1=T_2=L$, $T_3=0$ and $c=L$.

From equation (6.9) we find;

$$I_k = \frac{2}{k\pi}\cdot T_1$$

and by substituting in equation (6.6) and equation (6.8) the temperature equations for finite and semi-finite depth bodies under steady state temperature become;

$$T_s = \frac{2T_1}{\pi}\sum_{k=1}^{\infty}\left\{\frac{\sinh\frac{k\pi}{L}(d-y)}{k.\sinh\frac{k\pi}{L}d}.\sin\frac{k\pi}{L}x\right\} \qquad (6.10)$$

$$T_s = \frac{2T_1}{\pi}\sum_{k=1}^{\infty}\left\{\frac{\sin\frac{k\pi}{L}x}{k.\mathrm{Exp}\frac{k\pi}{L}y}\right\} \qquad (6.11)$$

respectively. To economise the computational time, equation (6.11) can be reduced to a single term as follows;

By introducing the complex variable;

$$Z = \mathrm{Exp}\left[\frac{\pi}{L}(ix - y)\right] \qquad (6.12)$$

equation (6.11) can be written in the following form;

$$T_s = \frac{T_1}{\pi} i(\bar{U} - U)$$

where U and $\bar{U}$ are conjugate and;

$$U = \sum_{k=1}^{\infty} \frac{1}{k} . Z^k$$

and to calculate $\bar{U}$ we have;

$$dU = \left(\sum_{k=0}^{\infty} Z^k \right) . dZ$$

or,

$$dU = \frac{1}{1-Z} . dZ$$

then;

$$U = -\mathrm{Ln}\left[c(1-Z)\right]$$

where c is integral constant, which is calculated by initial value U=0 when Z=0, i.e. c=0 and;

$$U = -\mathrm{Ln}(1-Z)$$

and the conjugate of U is written in the same equation;

$$\bar{U} = -\mathrm{Ln}(1-\bar{Z})$$

then, the temperature equation reduces to a single term as

follows;

$$T_s = \frac{T_1}{\pi}.Ln(\frac{1-Z}{1-\bar{Z}})^i$$

and by a simple mathematical operation we find;

$$T_s = \frac{2T_1}{\pi}.\theta$$

where,

$$\tan\theta = \frac{\sin\frac{\pi}{L}x}{Exp(\frac{\pi}{L}y)-\cos\frac{\pi}{L}x}$$

thus;

$$T_s = \frac{2T_1}{\pi}.\tan^{-1}\left[\frac{\sin\frac{\pi}{L}x}{Exp(\frac{\pi}{L}y)-\cos\frac{\pi}{L}x}\right] \qquad (6.13)$$

The isothermal lines (or surfaces) are given by;

$$y = \frac{\pi}{L}.Ln(\cot an\frac{\pi.T_s}{2.T_1}.\sin\frac{\pi}{L}x + \cos\frac{\pi}{L}x)$$

and it is clear that, all isothermal lines intersect points (x=0,y=0) and (x=L,y=0).

B- Second Form

For the second form of boundary temperature, consider the conditions as shown in figure (6.3-b).

In the present case we have;

$T_1=0$, $T_2=T_3=T_r$, a=0 and b=c=L,

then by substituting (L-x) instead of x and also T_r instead of T_1 in equation (6.13) we find the temperature equation for semi-infinite depth body;

$$T_s = \frac{2T_r}{\pi}.\tan^{-1}\left[\frac{\sin\frac{\pi}{L}x}{\mathrm{Exp}(\frac{\pi}{L}y) + \cos\frac{\pi}{L}x}\right] \qquad (6.14)$$

and the isothermal lines (or surfaces) are given by;

$$y = \frac{L}{\pi}.\mathrm{Ln}(\mathrm{cotan}\frac{T_s}{2T_r}.\sin\frac{\pi}{L}x - \cos\frac{\pi}{L}x)$$

In the present form of boundary temperature the value of I_k is;

$$I_k = \frac{(-1)^{k-1}}{k}.\frac{2T_r}{\pi}$$

and the temperature equation for a finite depth body is then written as follows;

$$T_s = \frac{2T_r}{\pi}\sum_{k=1}^{\infty}\frac{\sinh\frac{k\pi}{L}(d-y)}{\sin\frac{k\pi}{L}d}.\sin\frac{k\pi}{L}x \qquad (6.15)$$

C- Third Form

The general linear surface temperature as shown in figure (6.4) can be derived from superposition of two above forms. By adding equation (6.13) to equation (6.14), the equation for a semi-infinite depth body becomes as follows;

$$T_s=\frac{2T_1}{\pi}.\tan^{-1}\left[\frac{\sin\frac{\pi}{L}x}{\mathrm{Exp}(\frac{\pi}{L}y)-\cos\frac{\pi}{L}x}+\frac{2T_r}{\pi}\right].\tan^{-1}\left[\frac{\sin\frac{\pi}{L}x}{\mathrm{Exp}(\frac{\pi}{L}y)+\cos\frac{\pi}{L}x}\right] \qquad (6.16)$$

and to check, that the new solutions are valid, we can superpose the two triangular distribution of temperature on the boundary and compare with a known solution. By taking,

$$T_l = T_r = T_o$$

and adding two terms in equation (4.16) we have;

$$T_s = \frac{2T_o}{\pi}\left\{\tan^{-1}\left[\frac{\sin\frac{\pi}{L}x}{\mathrm{Exp}(\frac{\pi}{L}y)-\cos\frac{\pi}{L}x}\right] + \tan^{-1}\left[\frac{\sin\frac{\pi}{L}x}{\mathrm{Exp}(\frac{\pi}{L}y)+\cos\frac{\pi}{L}x}\right]\right\}$$

or;

$$\tan(\frac{\pi T_s}{2T_o}) = \tan\left\{\tan^{-1}\left[\frac{\sin\frac{\pi}{L}x}{\mathrm{Exp}(\frac{\pi}{L}y)-\cos\frac{\pi}{L}x}\right] + \tan^{-1}\left[\frac{\sin\frac{\pi}{L}x}{\mathrm{Exp}(\frac{\pi}{L}y)+\cos\frac{\pi}{L}x}\right]\right\}$$

then;

$$\tan(\frac{\pi T_s}{2T_o}) = \frac{\sin\frac{\pi}{L}x}{\sinh(\frac{\pi}{L}y)}$$

and finally;

$$T_s = \frac{2T_o}{\pi}.\tan^{-1}\left[\frac{\sin\frac{\pi}{L}x}{\sinh(\frac{\pi}{L}y)}\right] \qquad (6.17)$$

which is identical to Carslaw and Jaeger solution [Ref. 100] for flow of heat conduction in a rectangular body with a uniform temperature on the boundary.

Also by adding equations (6.10) and (6.15) the temperature equation for a finite depth body under steady state linear and uniform surface temperature become;

$$T_s = \frac{2}{\pi}\sum_{k=1}^{\infty}\left\{\left[T_1-(-1)^k.T_r\right].\frac{\sinh\left[\frac{k\pi}{L}(d-y)\right]}{\sinh(\frac{k\pi}{L})d}.\sin\frac{k\pi}{L}x\right\} \qquad (6.18)$$

$$T_s = \frac{2T_o}{\pi}\sum_{k=1}^{\infty}\left\{\frac{\sinh\left[\frac{2k-1}{L}\pi(d-y)\right]}{(2k-1)\sinh\left[\frac{2k-1}{L}\pi d\right]}.\sin\frac{2k-1}{L}\pi x\right\} \qquad (6.19)$$

respectively, and from equation (6.17) the isothermal lines

or surfaces are given by;

$$y = \frac{L}{\pi}.\sinh^{-1}\left[\left(\cotan\frac{T_s}{2T_o}.\sin\frac{\pi}{L}x\right)\right]$$

which may be written in a logarithm form.

D- Fourth Form

Consider a linear and symmetrical surface temperature as shown in figure (6.5). For this porpose, by substituting;

$$T_1=T_3=0,\ T_2=T_m,\ a=0,\ b=\tfrac{1}{2}L \text{ and } c=L,$$

into equation (6.9) we find;

$$I_k = (-1)^k.\frac{8T_m}{(2k+1)^2\pi^2} \qquad k=0,\ 1,\ 2,\ 3,\ \ldots$$

and for a semi-infinite depth body the temperature equation is written as follows;

$$T_s = \frac{8T_m}{\pi^2}\sum_{k=0}^{\infty}\left\{\frac{(-1)^k}{(2k+1)^2}.\frac{\sin\frac{2k+1}{L}\pi x}{\mathrm{Exp}\frac{2k+1}{L}\pi y}\right\} \qquad (6.20)$$

To reduce the summation in equation (6.20) to a single term we can differentiate T_s with respect to x (or y) and operate as follows;

$$dT_s = \frac{4T_m}{\pi L}(\bar{U} + U).dx$$

where U and $\bar{U}$ are conjugate and;

$$U = \sum_{k=0}^{\infty}\frac{(-1)^k}{2k+1}.z^{2k+1}$$

which, Z has been given in equation (6.12), then;

$$dU = \sum_{k=0}^{\infty}\left\{(-1)^k.Z^{2k}\ .dZ\right\}$$

or;

$$dU = (1+Z^2)^{-1}.dZ$$

and,

$$U = \tan^{-1}Z + c$$

where c is the integral arbitrary constant which, by applying the initial value U=0 when Z=0, becomes zero, and;

$$U = \tan^{-1}Z$$

and similarly;

$$\bar{U} = \tan^{-1}\bar{Z}$$

then;

$$dT_s = \frac{4T_m}{L}(\tan^{-1}Z + \tan^{-1}\bar{Z}).dx$$

and by a simple mathematical operation we get;

$$dT_s = \frac{4T_m}{L}.\tan^{-1}\left\{\frac{\cos\frac{\pi}{L}x}{\sinh\frac{\pi}{L}y}\right\}$$

then;

$$T_s = \frac{4T_m}{L}\int_0^x \tan^{-1}\left\{\frac{\cos\frac{\pi}{L}x}{\sinh\frac{\pi}{L}y}\right\}dx \qquad (6.21)$$

and this equation may be written in the following form;

$$T_s = -\frac{4T_m}{L}\int_0^y \tan^{-1}\frac{\sin\frac{\pi}{L}x}{\cosh\frac{\pi}{L}y}.dy \qquad (6.22)$$

then;

$$T_s=\frac{2T_m}{L}\left[\int_0^x \tan^{-1}\frac{\cos\frac{\pi}{L}x}{\sinh\frac{\pi}{L}y}dx+\int_y^0 \tan^{-1}\frac{\sin\frac{\pi}{L}x}{\cosh\frac{\pi}{L}y}dy\right] \qquad (6.23)$$

These integrations have no known mathematical solution but can be evaluated numerically more economically than can equation (6.20). The next section will describe a way of solving these boundary conditions by means of a stepped boundary temperature as in figure (6.6).

The temperature equation for the present boundary condition in the case of finite depth body is given by;

$$T_s=\frac{8T_m}{\pi^2}\sum_{k=0}^{\infty}\left\{\frac{(-1)^k}{(2k+1)^2}.\frac{\sinh\frac{2k+1}{L}\pi(d-y)}{\sinh\frac{2k+1}{L}\pi d}.\sin\frac{2k+1}{L}\pi x\right\} \qquad (6.24)$$

6.3.5- Type Two

For the second type of surface temperature f(x), consider a boundary condition with the following properties at y=0 as shown in figure (6.7);

$f(x) = T_1$ when $0 \le x \le a$,

$f(x) = T_2$ when $a \le x \le b$,

$f(x) = T_3$ when $b \le x \le L$.

By using equation (6.5), I_k becomes;

$$I_k = \frac{2}{k\pi}(T_1-T_3\cos k\pi+\Delta_{21}\cos\frac{k\pi}{L}a+\Delta_{32}\cos\frac{k\pi}{L}b) \qquad (6.25)$$

In the present type we assume some special forms of the boundary temperature for finite and semi-infinite depth body as follows;

6.3.5.1- General Form

Consider a general case of a symmetric and uniform surface temperature along y=0 equal to T_o at x=a to x=L-a as shown in figure (6.8). From equation (6.25) we find;

$$I_k = \frac{2}{(2k+1)} \cdot \cos\frac{2k+1}{L}\pi a$$

and the temperature equation for a finite and semi-infinite depth body become as follows;

$$T_s = \frac{2T_o}{\pi} \sum_{k=0}^{\infty} \left\{ \frac{\cos\frac{2k+1}{L}\pi a}{2k+1} \cdot \frac{\sin\frac{2k+1}{L}\pi(d-y)}{\sinh\frac{2k+1}{L}\pi d} \cdot \sin\frac{2k+1}{L}\pi x \right\} \qquad (6.26)$$

$$T_s = \frac{2T_o}{\pi} \sum_{k=0}^{\infty} \left\{ \frac{\cos\frac{2k+1}{L}\pi a}{2k+1} \cdot \frac{\sin\frac{2k+1}{L}\pi x}{\mathrm{Exp}\frac{2k+1}{L}\pi y} \right\} \qquad (6.27)$$

respectively.

It is too difficult to find the summation in equation (6.27) to reduce in a single form except when $\frac{L}{a}$ is a whole number, but by solving the following problems we will be able to introduce a solution of the summation of equation (6.27).

A- First Form

For the first form we assume that $\frac{L}{a}$=6, then;

$$I_k = \frac{2T_o}{(2k+1)\pi} \cdot \cos\frac{2k+1}{6}\pi$$

and the temperature equation for a semi-infinite depth body is written in the following form;

$$T = T_1 - T_5 - T_7 + T_{11}$$

where;

$$T_n = \frac{2T_o}{\pi}(3)^{\frac{1}{2}} \cdot \sum_{k=0}^{\infty}\left\{ \frac{1}{12k+n} \cdot \frac{\sin\frac{12k+n}{L}\pi\, x}{Exp(\frac{12k+n}{L}\pi y)} \right\}$$

and with the help of the complex variable (6.12), the above temperature equation becomes;

$$T = \frac{(3)^{\frac{1}{2}}}{\pi i}(U - \bar{U}) \qquad (6.28)$$

where, U and $\bar{U}$ are conjugate and;

$$U = U_1 - U_5 - U_7 + U_{11}$$

in which;

$$U_n = \sum_{k=0}^{\infty} \frac{Z^{12k+n}}{12k+n}$$

and to calculate U we have;

$$dU = dU_1 - dU_5 - dU_7 + dU_{11}$$

and by some simple mathematical operations we find;

$$dU = \left[(1-Z^4)(1-Z^6) \cdot \sum_{k=0}^{\infty} Z^{12k}\right] .dZ$$

where;

$$\sum_{k=0}^{\infty} z^{12k} = \frac{1}{1-z^{12}}$$

then,

$$U = \int \frac{1-z^2}{1-z^2+z^4} \cdot dz$$

or;

$$U = \frac{(3)^{\frac{1}{2}}}{6} \cdot \mathrm{Ln}\left[e^{c} \cdot \frac{z^2 + (3)^{\frac{1}{2}}z + 1}{z^2 - (3)^{\frac{1}{2}}z + 1}\right]$$

where, c is integral arbitrary constant which is calculated by initial value u=0 when Z=0, and becomes zero; thus,

$$U = \frac{(3)^{\frac{1}{2}}}{6} \cdot \mathrm{Ln}\left[\frac{z^2 + (3)^{\frac{1}{2}}z + 1}{z^2 - (3)^{\frac{1}{2}}z + 1}\right]$$

$$\bar{U} = \frac{(3)^{\frac{1}{2}}}{6} \cdot \mathrm{Ln}\left[\frac{z^2 + (3)^{\frac{1}{2}}z + 1}{z^2 + (3)^{\frac{1}{2}}z + 1}\right]$$

and finally by substituting U and $\bar{U}$ in equation (6.28) the temperature equation becomes as follwes;

$$T_s = \frac{T_o}{\pi}(\theta_1 - \theta_2)$$

where,

$$\tan\theta_n = \frac{\mathrm{Exp}(-\frac{\pi}{L}y) \cdot \sin\frac{2\pi}{L}x - (-1)^n \cdot (3)^{\frac{1}{2}} \cdot \sin\frac{\pi}{L}x}{\mathrm{Exp}(-\frac{\pi}{L}y)\cos\frac{2\pi}{L}x - (-1)^n \cdot (3)^{\frac{1}{2}} \cdot \cos\frac{\pi}{L}x + \mathrm{Exp}(\frac{\pi}{L}y)}$$

thus,

$$T_s = \frac{T_o}{\pi} \cdot \tan^{-1}\left[2(3)^{\frac{1}{2}} \frac{\sin\frac{\pi}{L}x \cdot \sinh\frac{\pi}{L}y}{\cos\frac{2\pi}{L}y + \cos^2\frac{\pi}{L}x - 1\frac{1}{2}}\right] \qquad (6.29)$$

and the isothermal lines can be easily found.

B- Second Form

For the second form of boundary condition assume that $\frac{L}{a}$ is equal 4, then;

$$I_k = \frac{2T_o}{(2k+1)\pi} \cdot \cos\frac{2k+1}{4}\pi \ ,$$

and the temperature equation may be written in the following form;

$$T_s = T_1 - T_3 - T_5 + T_7$$

where,

$$T_s = \frac{2T_o}{\pi}(2)^{\frac{1}{2}} \sum_{k=0}^{\infty}\left\{ \frac{1}{12k+n} \cdot \frac{\sin\frac{12k+n}{L}\pi x}{\mathrm{Exp}\frac{12k+n}{L}\pi y} \right\}$$

then,

$$T_s = \frac{(2)^{\frac{1}{2}}}{\pi i}(U - \bar{U})$$

where;

$$U = U_1 - U_3 - U_5 + U_7$$

and;

$$U_n = \sum_{k=0}^{\infty} \frac{Z^{12k+n}}{12k+n}$$

To obtain the value of U we have;

$$dU = dU_1 - dU_3 - dU_5 + dU_7$$

or;

$$dU = (1 + Z^2)(1 - Z^2)^2 \cdot \sum_{k=0}^{\infty} Z^{12k} \cdot dZ$$

and by substituting,

$$\sum_{k=0}^{\infty} z^{12k} = \frac{1}{1-z^{12}}$$

we find;

$$U = \int \frac{(1 + z^2)(1 - z^2)^2}{1 - z^{12}} \cdot dz$$

and this integration is evaluated by partial fraction method which gives the value of U and the temperature equation is written as follows;

$$T_s = \frac{T_o}{\pi}(\theta_1 - \theta_2)$$

where,

$$\tan \theta_n = \frac{\mathrm{Exp}(-\frac{\pi}{L}y)\sin\frac{2\pi}{L}x-(-1)^n.(2)^{\frac{1}{2}}.\sin\frac{\pi}{L}x}{\mathrm{Exp}(-\frac{\pi}{L}y)\cos\frac{\pi}{L}x-(-1)^n.(2)^{\frac{1}{2}}\cos\frac{\pi}{L}x+\mathrm{Exp}(\frac{\pi}{L}y)}$$

thus,

$$T_s = \frac{T_o}{\pi}.\tan^{-1}\left[2(2)^{\frac{1}{2}}.\frac{\sin\frac{\pi}{L}x.\sinh\frac{\pi}{L}y}{\cosh\frac{2\pi}{L}y + \cos\frac{2\pi}{L}x-1}\right] \qquad (6.30)$$

and the isothermal lines can be easily written.

C- Third Form

When $\frac{L}{a}$ is equal to 3 we have;

$$I_k = \frac{2T_o}{\pi}(\cos\frac{k\pi}{3} - \cos\frac{2k\pi}{3})$$

By following the way that explained in the last two special forms the temperature equation in the present form of boundary condition becomes as follows;

$$T_s = \frac{T_o}{\pi}.\tan^{-1}\left[2\frac{\sin\frac{\pi}{L}x.\sinh\frac{\pi}{L}y}{\cos\frac{2\pi}{L}x+\cosh\frac{2\pi}{L}y-\frac{1}{2}}\right] \qquad (6.31)$$

By analogy to the previous particular forms (the three solutions above), we can write the general solution of the equation (6.27) as follows;

$$T_s = \frac{T_o}{\pi}.\tan^{-1}\left[\frac{4\cos\frac{\pi}{L}a.\sin\frac{\pi}{L}x.\sinh\frac{\pi}{L}y}{\cosh\frac{2\pi}{L}y+\cos\frac{2\pi}{L}x-2\cos^2\frac{\pi}{L}a}\right] \qquad (6.32)$$

or;

$$T_s = \frac{T_o}{\pi}.\tan^{-1}\left[\frac{2\cos\frac{\pi}{L}a.\sin\frac{\pi}{L}x.\sinh\frac{\pi}{L}y}{\cosh^2\frac{\pi}{L}y-\sin^2\frac{\pi}{L}x-\cos^2\frac{\pi}{L}a}\right] \qquad (6.33)$$

As a ckeck, by substituting $a=\frac{L}{6}$, $a=\frac{L}{4}$ and $a=\frac{L}{3}$ into equation (6.33), it reduces to equations (6.29), (6.30) and (6.31) respectively. In a particular case when a=0, the equation (6.33) reduces to equation (6.17), since;

$$2\tan^{-1}\left[\frac{\sin\frac{\pi}{L}x}{\sinh\frac{\pi}{L}y}\right] = \tan^{-1}\left[\frac{4\sin\frac{\pi}{L}x.\sinh\frac{\pi}{L}y}{\cosh\frac{2\pi}{L}y+\cos\frac{2\pi}{L}-2}\right]$$

In the present problem the boundary temperature function f(x), is discontinuous along y=0 at x=a and x=L-a, then it must be checked that the general solution (6.33) satisfies this discontinuous boundary condition.

By substituting y=0 into equation (6.33) the surface temperature along y=0 becomes;

$$f(x) = \frac{T_o}{\pi}.\tan^{-1}\left[\frac{2\cos\frac{\pi}{L}a.\sin\frac{\pi}{L}x}{1-\left(\sin^2\frac{\pi}{L}x+\cos^2\frac{\pi}{L}a\right)}.\sinh(0)\right]$$

and, if x varies within range $0 \leq x \leq a$ or $L-a \leq x \leq L$ the value of;

$$\sin^2 \frac{\pi}{L}x + \cos^2 \frac{\pi}{L}a$$

is less than one and the surface temperature becomes;

$$f(x) = \frac{T_o}{\pi}.\tan^{-1}(\varepsilon)$$

where ε is a positive infinitesimal, then by x tending to a or to L-a within the above range, ε tends to zero but still positive, hence;

$$f(x) = \frac{T_o}{\pi}.\tan^{-1}(+0) = 0$$

and when x varies within the range $a \leq x \leq L-a$ the value of,

$$\sin^2 \frac{\pi}{L}x + \cos^2 \frac{\pi}{L}a$$

is bigger than one and the surface temperature becomes;

$$f(x) = \frac{T_o}{\pi}.\tan^{-1}(-\varepsilon)$$

where ε is again a positive infinitesimal and when x tends to a or L-x within the range $L-a \leq x \leq a$, ε tends to zero but still positive, then;

$$f(x) = \frac{T_o}{\pi}.\tan^{-1}(-0) = \frac{T_o}{\pi}. = T_o$$

thus, the equation (6.33) satisfies the discontinuous boundary conditions.

With equation (6.33) we are able now to simulate any symmetrical temperature distribution at the boundary by

changing the value of a and T_o and adding the solutions. This results is a considerable saving of computer time in both steady and non-steady state temperature; figure (6.9).

6.3.6- Sine Equation Surface Temperature

In a special and more practical case of boundary temperature we consider a symmetrical temperature along y=0 with maximum temperature T_o at the middle of the surface by following equation;

$$f(x) = T_o.\sin\frac{\pi}{L}x$$

For a finite depth body and above boundary condition, equation (6.4) gives;

$$T_o.\sin\frac{\pi}{L}x = (b_1' + b_2').\sin\frac{k\pi}{L}x \qquad (A)$$

and,

$$b_1'.Exp(\frac{k\pi}{L}d) + b_2'.Exp(-\frac{k\pi}{L}d) = 0 \qquad (B)$$

Equation (A) is valid when k=1, then;

$$b_1' + b_2' = T_o$$

$$b_1'.Exp(\frac{2\pi}{L}) + b_2' = 0$$

then, b_1' and b_2' are evaluated from these simultaneous equations, and by substituting the results into equation (6.4) we find;

$$T_s = T_o \frac{\sinh\frac{\pi}{L}(d-y)}{\sinh\frac{\pi}{L}d}.\sin\frac{\pi}{L}x \qquad (6.34)$$

by d tending to an infinite value, in equation (6.34), the temperature equation for a semi-infinite depth body becomes;

$$T_s = T_o \frac{\sin\frac{\pi}{L}x}{\mathrm{Exp}\frac{\pi}{L}y} \qquad (6.35)$$

6.3.7- Reducing The Computer Time

The numerical solution for equation (6.6) to calculate the distribution of temperaure within a finite depth body is very time consuming. However the previous solutions for a semi-infinite depth body can be employed to reduce the computational time for finite depth body as explained in below;

Equation (6.6) requires many more terms for an accurate solution than does equation (6.8), specially in case of the previous particular forms.

A considerable saving of computer time can be made by adopting equation (6.8) to serve the boundary condition of equation (6.6), using an iterative technique.

The boundary temperature f_1 at y=d is calculated from the boundary condition f_o at y=0.

A boundary temperature $(-f_1)$ at y=d is superimposed and a new temperature $(-f_2)$ at y=0 derived. The reverse of this temperature i.e., $(+f_2)$ is added to initial condition and f_3 at y=d again calculated.

The newly calculated boundary temperature is always very much smaller than the previous value and the series converges very rapidly to the solution when the temperature at y=d is zero and the initial boundary condition agrees with

the initial temperature at y=0.

The condition expressed in equation (4.8) applies when a rectangular body such as slab or beam is heated on one side only whereas equation (6.6) applies to the case of column or beam heated on more than one side.

6.4- Three Dimensional Body

In this section we consider a rectangular parallelepiped body length L, height d and thickness b heated on one side, in two seperate finite and semi-infinite depth geometrical conditions. The particular solution of heat equation for three dimensional body under steady state case is given by;

$$T_s=[a_1 Exp(\Lambda x)+a_2 Exp(-\Lambda x)][b_1 Exp(By)+b_2 Exp(-By)]\cdot$$

$$[c_1 Exp(Cz)+c_2 Exp(-Cz)]$$

where;

$$A^2 + B^2 + C^2 = 0 \qquad (6.36)$$

6.4.1- Semi-infinite Depth Body

For a semi-infinite depth body consider the following boundary conditions;

1)- $T = 0$ when $x = 0$ and $x = L$,

2)- $T = 0$ when $y = 0$ and $y = d$,

3)- $T = 0$ when $z = \infty$,

4)- $T = f(x,y)$ when $z = 0$.

From the first boundary condition and using the particular solution, a_1+a_2 becomes zero and,

$$A = \frac{k\pi}{L}i$$

and similarly from the second boundary condition, b_1+b_2 becomes zero and,

$$B = \frac{N\pi}{d}i$$

where k and N are positive integers and $i=(-1)^{\frac{1}{2}}$, and by substituting A and B into equation (6.36) we find;

$$C^2 = \frac{k^2\pi^2}{L^2} + \frac{N^2\pi^2}{d^2} \qquad (6.37)$$

and the general term of temperature equation is written as follows;

$$T_{k,N} = [c_1' Exp(Cz) + C_2' Exp(-Cz)] \sin\frac{k\pi}{L}x . \sin\frac{N\pi}{d}y \qquad (6.38)$$

and this equation satisfies the third boundary condition if $C \leq 0$ and $c_1'=0$ (or $C \geq 0$ and $c_2'=0$) and by applying the last boundary condition we have;

$$f(x,y) = c_2' . \sin\frac{k\pi}{L}x . \sin\frac{N\pi}{d}y \qquad (6.39)$$

By using the double Fourier's series we find;

$$c_2' = \frac{4}{Ld} . I_{k,N}$$

where,

$$I_{k,N} = \int_0^d \sin\frac{N\pi}{d}y . dy \int_0^L f(x,y) . \sin\frac{k\pi}{L}x . dx \qquad (6.40)$$

and the temperature equation for a three dimensional semi-infinite depth body under steady state temperature becomes;

$$T_s = \frac{4}{Ld} \sum_{k=1}^{\infty} I_{k,N} \frac{\sin\frac{k\pi}{L}x . \sin\frac{N\pi}{d}y}{Exp\left\{\left[\left(\frac{k\pi}{L}\right)^2+\left(\frac{N\pi}{d}\right)^2\right]^{\frac{1}{2}} . z\right\}} \qquad (6.41)$$

6.4.2- Finite Depth Body

For a finite depth rectangular parallelepiped body, consider the following boundary temperatures;

1)- $T = 0$ when $x = 0$ and $x = L$,

2)- $T = 0$ when $y = 0$ and $y = d$,

3)- $T = 0$ when $z = b$,

4)- $T = f(x,y)$ when $z = 0$.

Equation (6.38) satisfies the first and second boundary conditions and from the third boundary condition we have;

$$c_2' = - c_1' . Exp(2Cb)$$

where C has been given in equation (6.37), then the general term of temperature equation becomes;

$$T_{k,N} = \eta_{k.N} . \sinh(b-z)C . \sin\frac{N\pi}{d}y . \sin\frac{k\pi}{L}x$$

where, $\eta_{k,N}$ is an arbitrary constant. From the last boundary condition we have;

$$\eta_{k,N} . \sinh(Cb) . \sin\frac{N\pi}{d}y . \sin\frac{k\pi}{L}x = T_{k,N}$$

and by using the Fourier's double sine series we find;

$$\eta_{k,N} = \frac{4}{Ld} \cdot \frac{I_{k,N}}{\sinh(Cb)}$$

and $I_{k,N}$ has been given in equation (6.40). Finally the temperature equation for a finite depth body under steady state temperature becomes as follows;

$$T_s = \frac{4}{Ld} \sum_{\substack{k=1 \\ N=1}}^{\infty} \left\{ I_{k,N} \frac{\sinh(b-z)C}{\sinh(Cb)} \sin\frac{k\pi}{L}x \cdot \sin\frac{N\pi}{d}y \right\} \qquad (6.42)$$

For the present problem we consider some special and practical forms of boundary temperature to calculate the distribution of temperature within a three dimensional body under steady state case.

A- First Form

For the first form of boundary temperature assume a uniform temperature T_o along the surfaces z = 0.

The value of $I_{k,N}$ is calculated from equation (6.40), then;

$$I_{k,N} = \frac{4LdT_o}{(2k+1)(2N+1)\pi^2}$$

and by substituting into equation (6.41) and (6.42) the temperature equations for semi-infinite and finite depth body become;

$$T_s = \frac{16T_o}{\pi^2} \sum_{\substack{k=0 \\ N=0}}^{\infty} \left\{ \frac{\sin\frac{2k+1}{L}\pi x \cdot \sin\frac{2N+1}{d}\pi y}{(2k+1)(2N+1) \cdot \mathrm{Exp}(Cb)} \right\} \qquad (6.43)$$

$$T_s = \frac{16T_o}{\pi^2} \sum_{\substack{k=0 \\ N=0}}^{\infty} \left\{ \frac{\sinh(b-z)C \cdot \sin\frac{2k+1}{L}\pi x \cdot \sin\frac{2N+1}{d}\pi y}{(2k+1)(2N+1) \cdot \sinh(Cb)} \right\} \qquad (6.44)$$

respectively, where;

$$C = \pi\left[\left(\frac{2k+1}{L}\right)^2 + \left(\frac{2N+1}{d}\right)^2\right]^{\frac{1}{2}}$$

B- Second Form

In a more practical form of boundary temperature, consider a special temperature equation along surface z=0 by the following equation;

$$f(x,y) = T_o.\sin\frac{\pi}{L}x.\sin\frac{\pi}{d}y$$

where T_o is the maximum value of temperature at the centroid of the heated surface.

For a finite depth body, and using equation (6.38) we have;

$$T_o\sin\frac{\pi}{L}x.\sin\frac{\pi}{d}y = (c_1' + c_2')\sin\frac{k\pi}{L}x.\sin\frac{N\pi}{d}y$$

and this expression gives;

$$k = N = 1$$

then;

$$c_1' + c_2' = T_o$$

and by applying the boundary temperature T=0 at z=b we find;

$$c_1'.Exp(Cb) + c_2'.Exp(-Cb) = 0,$$

i.e

$$c_1' = -\frac{T_o Exp(-Cb)}{2\sinh(Cb)} \quad \text{and} \quad c_2' = \frac{T_o Exp(Cb)}{2\sinh(Cb)}$$

and finally the temperature equation for a finite depth body becomes as follows;

$$T_s = T_o \frac{\sinh(b-z)C}{\sinh(Cb)} .\sin\frac{\pi}{L}x.\sin\frac{\pi}{d}y \qquad (6.45)$$

where;

$$C = \pi(\frac{1}{L^2} + \frac{1}{d^2})^{\frac{1}{2}}$$

In equation (6.45), as b tends to an infinity the temperature equation for a semi-infinite depth body becomes;

$$T_s = T_o \frac{\sin\frac{\pi}{L}x.\sin\frac{\pi}{d}y}{Exp(Cz)} \qquad (6.46)$$

6.4.3- Reducing The Computer Time

To reduce the computer time as in two dimensional problem we consider some special type of surface temperature to reduce the summation of the double series to a single form. For this porpose we introduce a special coefficient (γ) as follows;

$$C.\gamma = \frac{N\pi}{d} + \frac{k\pi}{L}$$

where C has been given in a general form as in equation (4.37), then;

$$\gamma = (1 + 2kN.\frac{Ld}{C})^{\frac{1}{2}}$$

The value of (γ) varies from (γ_1) when n = k = 1 to (γ_∞) when n = k = ∞, then

$$\gamma_1 = 1 \leq \gamma \leq \gamma_\infty = (1 + \frac{2Ld}{d^2+L^2})^{\frac{1}{2}}$$

In case of a beam or slab heated along the largest side where the minimum value of L is longer than (6d), the maximum value of (γ) becomes 1.14, then;

$$1 \leq \gamma \leq 1.14$$

However, for any structural element a suitable value of this coefficient is given by;

$$\gamma = 0.5 + \left(0.25 + \frac{0.5Ld}{d^2+L^2}\right)^{\frac{1}{2}}$$

By substituting the value of (γ), equation (6.41) reduces to the following form;

$$T_s=\frac{4}{Ld}\sum_{\substack{k=1\\N=1}}^{\infty} I_{k,N}\,\frac{\sin\frac{N\pi}{d}y.\sin\frac{k\pi}{L}x}{Exp(\frac{N\pi}{d}z).Exp(\frac{k\pi}{L}z)} \qquad (6.47)$$

in case of;

$$f(x,y) = f_1(x).f_2(y)$$

equation (6.47) can be written in the following form;

$$T_s=\frac{2}{L}\left(\sum_{k=1}^{\infty} I_k.\frac{\sin\frac{k\pi}{L}x}{Exp\frac{k\pi}{L}z}\right).\frac{2}{d}\left(\sum_{N=1}^{\infty} I_N.\frac{\sin\frac{N\pi}{d}y}{Exp\frac{N\pi}{d}z}\right) \qquad (6.48)$$

By comparing equation (6.48) with equation (6.8) we conclude that, the approximate value of temperature within a three dimensional semi-infinite depth body heated on one side, is equal to the two dimensional case multiplied by a factor of two values of temperature, which is calculated by assuming the temperature flow in two perpendicular directions.

Now by this condition and with the help of temperature

equations for two dimensional body we are able to write the temperature equation in three dimensional body in one single term only.

For example, the temperature equation within a three dimensional body heated on one side by uniform temperature T_o is calculated from equation (6.48), by assuming;

$$f_1(x) = T_o \ , \ f_2(y) = 1,$$

along z=0, then, by using equation (6.17) we have;

$$T_s = \frac{4T_o}{2}\tan^{-1}\left[\frac{\sin\frac{\pi}{L}x}{\sinh\frac{\pi}{L}z_1}\right].\tan^{-1}\left[\frac{\sin\frac{\pi}{d}y}{\sinh\frac{\pi}{d}z_1}\right]$$

where,

$$z_1 = \frac{z}{\gamma}$$

For a second example consider a linear temperature distribution along surface z=0, by following function;

$$f(x,y) = \frac{T_1}{L}(L - x)$$

In this case we assume two following equations in two perpendicular x and y-directions along surface z=0,

$$f_1(x) = \frac{T_1}{L}(L - x)$$

$$f_2 = 1$$

and with the help of equation (6.48) and using equation (6.13) the temperature equation within the three dimensional semi-infinite depth body under steady state case is written as follows;

$$T_s = \frac{4T_1}{2}\tan^{-1}\left[\frac{\sin\frac{\pi}{L}x}{\mathrm{Exp}(\frac{\pi}{L}z_1)-\cos\frac{\pi}{L}x}\right].\tan^{-1}\left[\frac{\sin\frac{\pi}{d}y}{\mathrm{Exp}(\frac{\pi}{d}z_1)-\cos\frac{\pi}{d}y}\right]$$

6.5- Non-steady State Temperature

In this section we find the temperature equation within one, two and three dimensional body, in which, the temperature is independent of time on the boundary but it varies with time within the body and generally we have;

$$\lambda = A^2 + B^2 + C^2$$

6.5.1- One Dimensional Body

In one dimensional body when the temperature varies in one direction only, say x-direction, the differential equation of conduction of heat is written;

$$\frac{\partial^2 T}{\partial x^2} = \frac{1}{h}\cdot\frac{\partial T}{\partial t}$$

and the particular solution of this equation is given by;

$$T_n = [a_1\mathrm{Exp}(Ax) + a_2\mathrm{Exp}(-Ax)]\cdot\mathrm{Exp}(A^2ht) \qquad (6.49)$$

Now we consider the following boundary and initial conditions;

$T = T_o$ at $x = 0$ and $t = 0$ at $x = L$ on the boundary and $T = g(x)$ throughout of the body when time value tends to zero for initial condition.

By referring to section (5.5) our problem seperates

into two following problems;

A- Steady state temperature by given boundary conditions. This problem has been solved in a previous section, and the temperature equation can be found by inserting $T_1=0$ in equation (6.2), then;

$$T_s = T_o(1 - \frac{x}{L}) \qquad (6.50)$$

B- Non-steady state temperature with zero temperature on the boundary and with given initial conditions. For this second problem the boundary and initial conditions are as follows;

$T_n^* = 0$ at $x = 0$ and $x = L$ on the boundary.

$T_n^* = g(x) - T_s$ initially when time tends to zero.

By applying the boundary condition in particular solution (6.49) we find;

$$a_1 + a_2 = 0, \quad A = \frac{k\pi}{L}i$$

then;

$$Tn_k^* = \eta_k . Exp(-\frac{k^2\pi^2}{L^2}) . \sin\frac{k\pi}{L}x$$

where k is a positive integer and η_k is an arbitrary constant for each step of k.

From initial condition we have;

$$g(x) - T_s = \eta_k . \sin\frac{k\pi}{L}x$$

and the arbitrary constant η_k is calculated by;

$$\int_0^L \left[g(x) - T_o(1 - \frac{x}{L})\right] . \sin\frac{k\pi}{L}x . dx = \eta_k \int_0^L \sin^2 \frac{k\pi}{L}x . dx$$

Practically, the initial temperature $g(x)$ is usually constant equal β, then, by a simple mathematical operation the value of η_k becomes;

$$\eta_k = \frac{2}{k\pi}(\beta - T_o - T_o \cos k\pi)$$

and the temperature equation of second term of (T_n) becomes as follows;

$$T_n^* = \frac{2}{\pi} \sum_{k=1}^{\infty} \frac{1}{k} \cdot \frac{-T_o - T_o \cos k\pi}{\mathrm{Exp}(\frac{k^2\pi^2}{L^2}ht)} \cdot \sin\frac{k\pi}{L}x$$

and finally the temperature equation within a one dimensional body in non-steady state case by constant initial temperature is written as follows;

$$T_n = T_s + T_n^*$$

then;

$$T_n = T_o(1-\frac{x}{L}) + \frac{2}{\pi} \sum_{k=1}^{\infty} \frac{1}{k} \cdot \frac{\beta - T_o - T_o \cos k\pi}{\mathrm{Exp}(\frac{k^2\pi^2}{L^2}ht)} \cdot \sin\frac{k\pi}{L}x$$

In a most practical case when the initial temperature is zero our temperature equation is written in the following form;

$$T_n = T_o(1-\frac{x}{L}) - \frac{4T_o}{\pi} \sum_{k=0}^{\infty} \frac{\sin\frac{2k+1}{L}\pi x}{(2k+1).\mathrm{Exp}(\frac{2k+1}{L})^2.\pi^2.ht}$$

6.5.2- Two Dimensional Body

For a two dimensional rectangular body under non-steady state temperature let us assume the following boundary

and initial conditions;

1)- $T = 0$ at $x = 0$ and $x = L$

2)- $T = 0$ at $y = d$,

3)- $T = f(x)$ at $y = 0$,

4)- $T = g(x,y)$ when $t = 0$.

By referring to section (5.6), the particular solution of heat equation is given by;

$$T_n = [a_1 Exp(Ax) + a_2 Exp(-Ax)][b_1 Exp(By) + b_2 Exp(-By)] Exp(\lambda ht)$$

where,

$$\lambda = A^2 + B^2$$

By referring again to the result of section (5.5) we first assume a steady state temperature case by given temperature on the boundary. This steady state case has been solved in section (6.3) and the temperature equation in the general form has been given by;

$$T_s = \frac{2}{L} \sum_{k=1}^{\infty} \left\{ I_k \cdot \frac{\sinh \frac{k\pi}{L}(d-y)}{\sin \frac{k\pi}{L} d} \cdot \sin \frac{k\pi}{L} x \right\}$$

where,

$$I_k = \int_0^L f(x) \cdot \sin \frac{k\pi}{L} x \cdot dx$$

To obtain the second equation (T_n^*) we assume zero temperature on the boundaries and the following initial condition;

$$T_n^* = g(x,y) - T_s \quad \text{when } t = 0,$$

then, we have the boundary and initial conditions as below;

$$T_n^* = 0 \qquad \text{when } x = 0 \text{ and } x = L,$$

$$T_n^* = 0 \qquad \text{when } y = 0 \text{ and } y = d,$$

$$T_n^* = g(x,y) - T_s \qquad \text{when } t = 0.$$

By using the particular solution and assuming the boundary conditions we find;

$$a_1+a_2=0,\ b_1+b_2=0,\ A=\frac{k\pi}{L}i \text{ and } B=\frac{N\pi}{L}i,$$

where k and N are positive integer and $i=(-1)^{\frac{1}{2}}$, then;

$$\lambda = -\left(\frac{k^2\pi^2}{L^2} + \frac{N^2\pi^2}{d^2}\right)$$

and the second term of temperature equation becomes as follows,

$$T_n^* = \eta_{k,N}\,\mathrm{Exp}(\,ht).\sin\frac{k\pi}{L}x.\sin\frac{N\pi}{d}y$$

From the initial condition when time value tends to zero we find;

$$\eta_{k,N}.\sin\frac{k\pi}{L}x.\sin\frac{N\pi}{d}y = g(x,y) - T_s \qquad (6.51)$$

and to calculate the arbitrary constant $\eta_{k.N}$ we have,

$$\eta_{k.N}\int_0^L X^2dx\int_0^d Y^2dy=\int_0^d Ydy\int_0^L gXdx-\frac{2I_k}{\sin\frac{k\pi}{L}d}\int_0^d \sin\frac{k\pi}{L}(d-y)dy.$$

$$\int_0^L X^2.dx$$

where,

$$X = \sin\frac{k\pi}{L}x \quad , \quad Y = \sin\frac{N\pi}{d}y$$

and by some mathematical operation, the arbitrary constant $\eta_{k,N}$ becomes as follows;

$$\eta_{k,N} = \frac{4J}{Ld} + \frac{4N\pi I_k}{d^2.L.\lambda} \cos N\pi$$

where,

$$J = \int_0^d Y dy \int_0^L g(x,y).X.dx$$

and the second term of temperature equation of non-steady state case becomes;

$$T_n^* = \sum_{\substack{k=1 \\ N=1}}^{\infty} \eta_{k,N}.\mathrm{Exp}(\lambda ht).\sin\frac{k\pi}{L}x.\sin\frac{N\pi}{d}y$$

and the temperature equation is given by;

$$T_n = T_s + T_n^*$$

In a special case when the initial temperature f(x,y) is constant (β), the value of J becomes;

$$J = \frac{4\beta.d.L}{kN\pi^2}.\sin^2\frac{N\pi}{2}.\sin^2\frac{k\pi}{2}$$

and finally, when the initial temperature is assumed to be zero the value of J becomes zero.

For a particular case of boundary temperature consider a sine temperature equation on the surface of the body. The temporature equation for this special case for steady state

temperature has been found in section (6.3.6) and is given by;

$$T_s = T_o \cdot \frac{\sinh(d-y)\frac{\pi}{L}}{\sinh\frac{\pi}{L}d} \cdot \sin\frac{\pi}{L}x$$

where k = N = 1. By continuing the above method and assuming the initial temperature g(x,y) at t = 0, equation (6.51) reduces to;

$$\eta_{k,N} \cdot \sin\frac{k\pi}{L}x \cdot \sin\frac{N\pi}{d}y = g(x,y) - T_o \cdot \frac{\sinh\frac{\pi}{L}(d-y)}{\sinh\frac{\pi}{L}d} \sin\frac{\pi}{L}x$$

and when the initial temperature is zero we have;

$$\eta_{k,N} \cdot \sin\frac{k\pi}{L}x \cdot \sin\frac{N\pi}{d}y = - T_o \cdot \frac{\sinh\frac{\pi}{L}(d-y)}{\sinh\frac{\pi}{L}d} \cdot \sin\frac{\pi}{L}x$$

then, k = 1 and;

$$\eta_{1,N} \cdot \sin\frac{N\pi}{d}y = - T_o \cdot \frac{\sinh\frac{\pi}{L}(d-y)}{\sinh\frac{\pi}{L}d}$$

To calculate $\eta_{1,N}$ we multiply the both sides of above expression with,

$$\sin\frac{N\pi}{d}y \cdot dy$$

and integrate within range, $0 \leq y \leq d$, we find;

$$\eta_{1,N} = \frac{2T_o\pi N}{d^2\lambda}$$

where,

$$\lambda = - \left(\frac{N^2\pi^2}{d^2} + \frac{\pi^2}{L^2}\right)$$

and the second term of temperature equation becomes;

$$T_n^* = \frac{2\pi T_o}{d^2} \cdot \sin\frac{\pi}{L}x \cdot \sum_{N=1}^{\infty}\left\{ \frac{N}{\lambda} \cdot \frac{\sin\frac{N\pi}{d}y}{Exp(-\lambda ht)}\right\}$$

and the temperature equation is written as follows;

$$T_n = T_s + T_n^*$$

6.5.3- Treatment Of Boundary Condition

The semi-infinite depth body when heated on one side is more practical case of the present subject, and clearly, by d tending to infinity in previous solutions the second term of temperature equation (T_n^*) becomes zero, and the solutions are useless. To overcome this difficulty we insert a large value of d in the above solutions. Furthermore, as we explained in a previous section we can find the temperature equation within a body under non-steady state temperature when heated on two or more sides, and the equation is obtained by changing the length of the body and assuming a new boundary temperature.

6.5.4- Three Dimensional Body

The present section is included to obtain temperature equation within a rectangular parallelepiped length L, height d and thickness b heated on one side under non-steady state temperature by following boundary and initial conditions;

1)- $T = 0$ at $x = 0$ and $x = L$,

2)- $T = 0$ at $y = 0$ and $y = d$,

3)- $T = 0$ at $z = b$

4)- $T = f(x,y)$ at $z = 0$,

5)- $T = g(x,y,z)$ when $t = 0$.

By referring to section (6.4.2) the first term of temperature equation is obtained for steady state case by given boundary conditions and this equation has been given by equation (6.42). To calculate the second term of tem_ perature equation (T_n^*) we consider a zero temperature on the boundaries and following initial condition;

$$T_n^* = g(x,y,z) - T_s$$

Equation (6.38) satisfies the boundary zero temperature at x=0, x=L, y=0 and y=d, and by applying a zero temperature at z=0 and z=b we find;

$$c_1' + c_2' = 0, \quad c_1' . \mathrm{Exp}(2Cb) + c_2' = 0,$$

then;

$$C = \frac{M\pi}{b} i$$

where M is a positive integer. The second term of temperature equation is written as;

$$T_n^* = \eta_{k,N,M} . \sin\frac{k\pi}{L}x . \sin\frac{N\pi}{d}y . \sin\frac{M\pi}{b}z . \mathrm{Exp}(\lambda ht)$$

where,

$$\lambda = A^2 + B^2 + C^2 = -\left(\frac{k^2\pi^2}{L^2} + \frac{N^2\pi^2}{d^2} + \frac{M^2\pi^2}{b^2}\right)$$

To calculate the arbitrary costant $\eta_{k,N,M}$ we apply the initial condition and multiply the both sides of the expression with,

$$\sin\frac{k\pi}{L}x.\sin\frac{N\pi}{d}y.\sin\frac{M\pi}{b}z.dx.dy.dz$$

and integrate over the volume of the body we have;

$$\eta_{k,N,M}.\int_0^L X^2.dx\int_0^d Y^2.dy\int_0^b Z^2.dz = \int_v g.X.Y.Z.dv -$$

$$\frac{4I_{k,N}}{Ldsinh(Cb)}.\int_0^b Z.\sinh(b-z)C.dz\int_0^L X^2.dx\int_0^d Y^2.dy$$

where,

$$X = \sin\frac{k\pi}{L}x,\ Y = \sin\frac{N\pi}{d}y,\ Z = \sin\frac{M\pi}{b}z,$$

and v is the volume of the body. By some simple mathematical operations we find,

$$\eta_{k,N,M} = \frac{8J}{v} + I_{k,N}.\frac{dN\pi cosN}{bV\lambda}$$

where,

$$J = \int_v g(x,y,z).X.Y.Z.dv$$

and the second term of temperature equation is written as follows;

$$T_n^* = \sum_{\substack{k=1\\N=1\\M=1}}^{\infty}\left\{\eta_{k,N,M}.\frac{\sin\frac{k\pi}{L}x.\sin\frac{N\pi}{d}y.\sin\frac{M\pi}{b}z}{Exp(-\lambda ht)}\right\}$$

and finally temperature equation within a three dimensional body under non-steady state temperature becomes;

$$T_n = T_s + T_n^* \qquad (6.52)$$

In a special case when the initial temperature is constant (β) we have;

$$J = \frac{\beta . v}{8kNM\pi^3} . \sin^2 \frac{k\pi}{2} . \sin^2 \frac{N\pi}{2} . \sin \frac{M\pi}{2}$$

and the arbitrary constant reduces to;

$$\eta_{k,N,M} = \frac{\beta}{kNM\pi^3} . \sin^2 \frac{k\pi}{2} . \sin^2 \frac{N\pi}{2} . \sin^2 \frac{M\pi}{2} + I_{k,n} \frac{N\pi \cos N\pi}{b^2 L \lambda}$$

and by assuming initial zero temperature this arbitrary constant becomes;

$$\eta_{k,N,M} = I_{k,N} . \frac{N\pi \cos N\pi}{b^2 L \lambda}$$

In case of sine temperature equation on the boundary and assuming initial zero temperature and with the help of equation (6.45) we find; k = N = 1, and;

$$\eta_{1,1,M} . \sin \frac{M\pi}{b} z = - \frac{T_o}{\sinh(Cb)} . \sinh(b-z)C$$

and the arbitrary constant $\eta_{1,1,M}$ is calculated as follows;

$$\eta_{1,1,M} \int_0^b \sin^2 \frac{M\pi}{b} z . dz = - \frac{T_o}{\sinh(Cb)} . \int_0^b \sinh(b-z)C . \sin \frac{k\pi}{b} z . dz$$

or;

$$\eta_{1,1,M} = \frac{2T_o M\pi \cos M\pi}{b^2 \lambda}$$

where,

$$C = \pi . \left(\frac{1}{L^2} + \frac{1}{d^2} \right)$$

$$\lambda = - (C^2 + \frac{M^2\pi^2}{b^2})$$

In analysis of reinforced concrete beams and slabs under temperature effect, the temperature on the body due to fire, increases with time and is not constant, but in the previous solutions the boundary temperatures have been assumed to be independent of time. To overcome to this differences we assume the temperature on the surface of beam or slab is constant within any time intervals by assuming a stepped time temperature relationship and the diffusivity of material at any required point within the body is calculated with an iterative technique at each time interval or temperature increment to obtain an accurate distribution of temperature within the members.

6.6- A Comparison With Numerical Solution

To compare the above solutions with the numerical method of solution which explained in chapter five a distribution of temperature within a two dimensional body is calculated with the help of the classical solution of heat equation and the results are compared with the numerical calculations.

For a two dimensional homogeneous body under steady state temperature a rectangular body, length 65 cm and height 25 cm, is divided into 117 rectangular elements length 5 cm and height 5 cm . For boundary temperature a uniform constant temperature 100 ^{o}C is applied along the largest side of the body, then the distribution of temperature for classical

solution is calculated from equation (6.19).

Section (2) of appendix II includes the temperature values at the centroids of the elements for one half of the body, which have been evaluated by classical solution and numerical method.

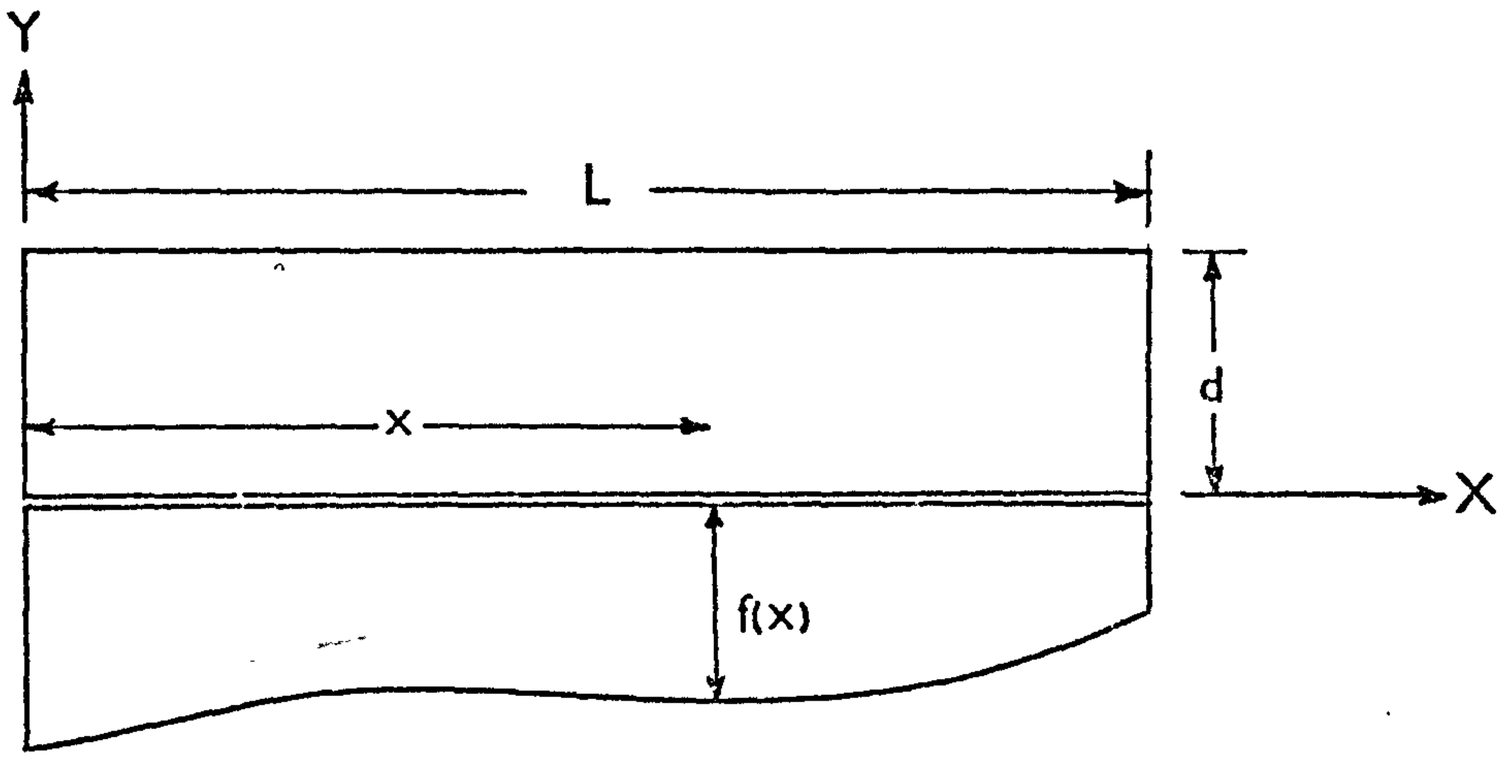

Fig. 6.1- A typical two dimensional body with boundary temperature.

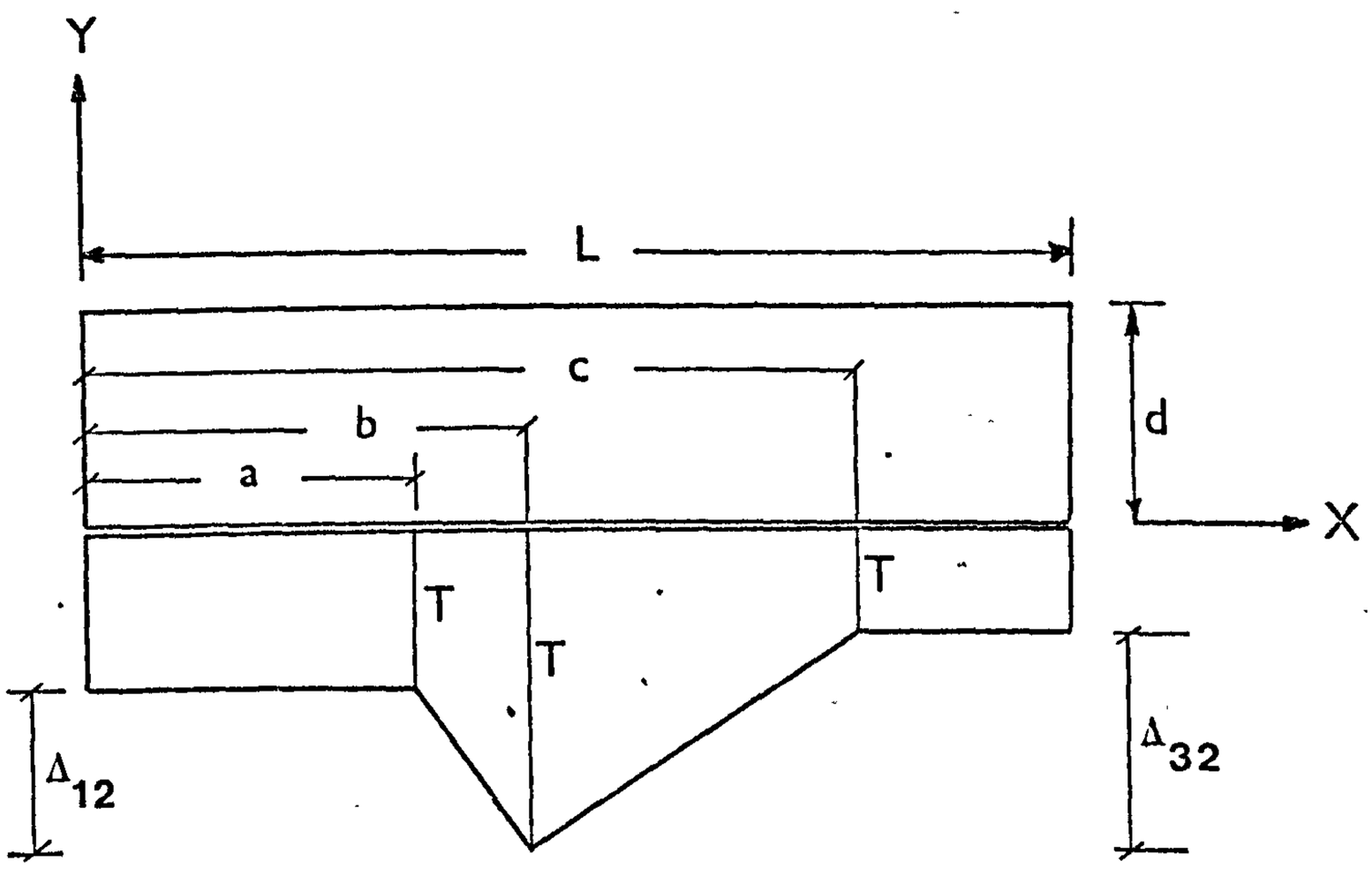

Fig. 6.2- Combination of uniform and linear boundary temperatures.

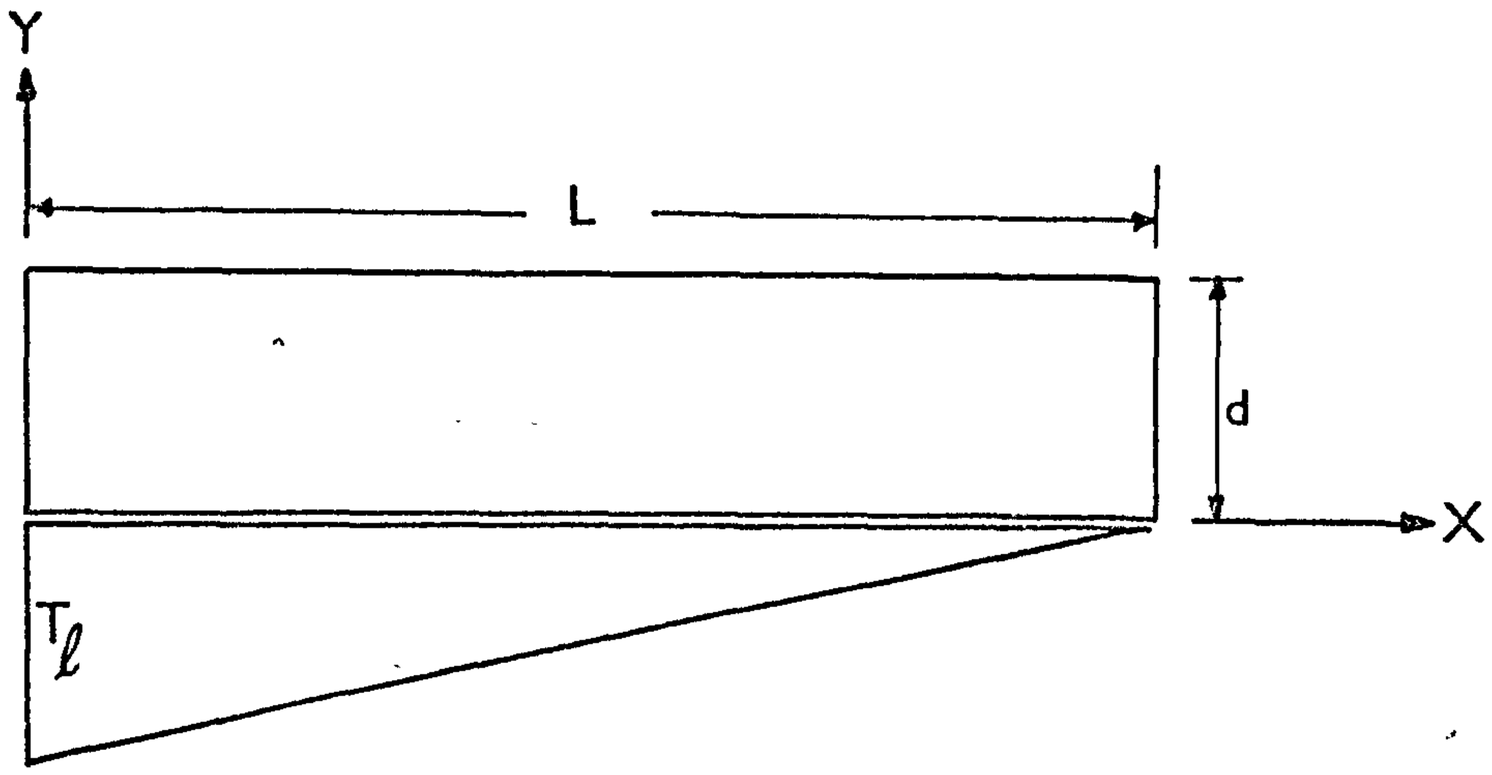

a

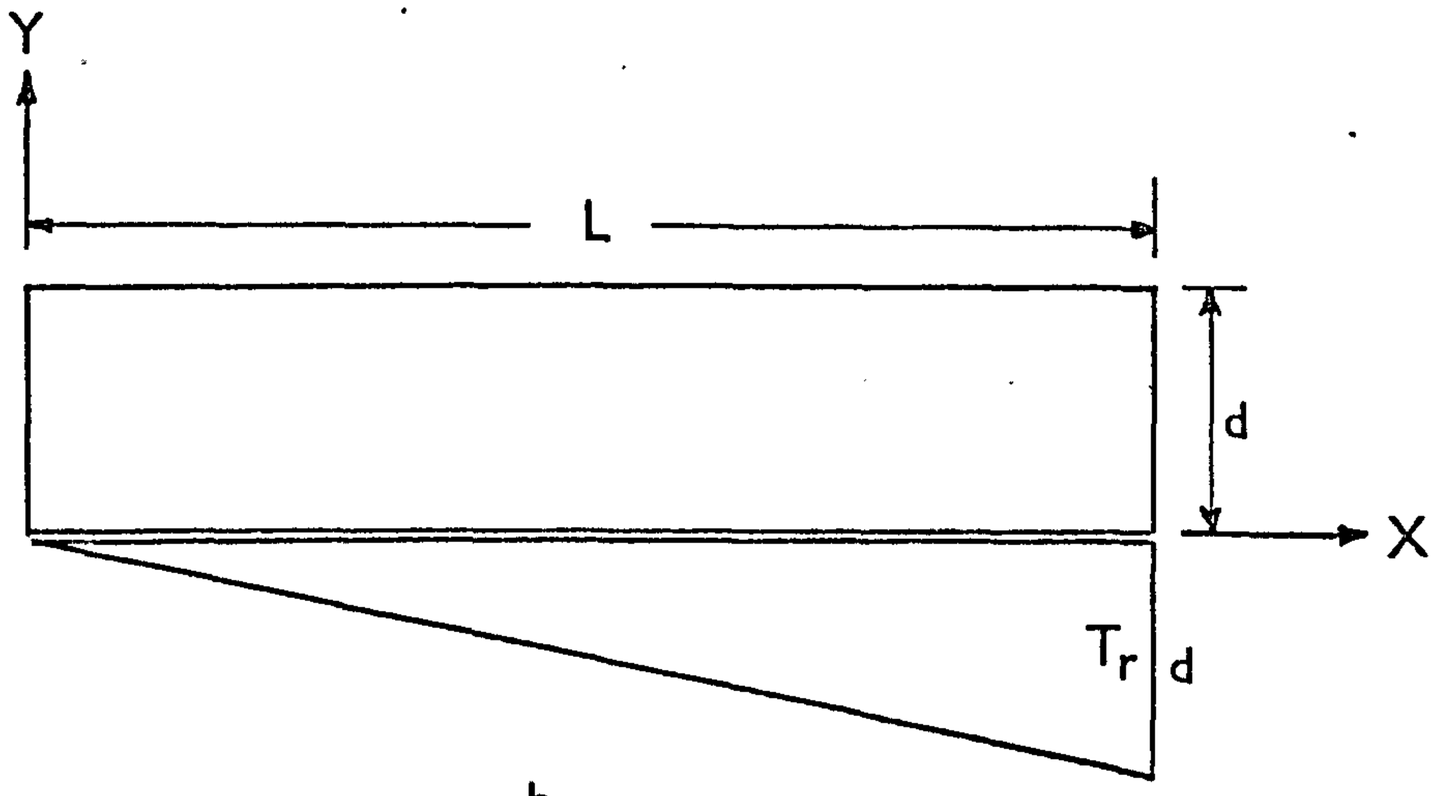

b

Fig. 6.3- Linear boundary temperature for a two dimensional body.

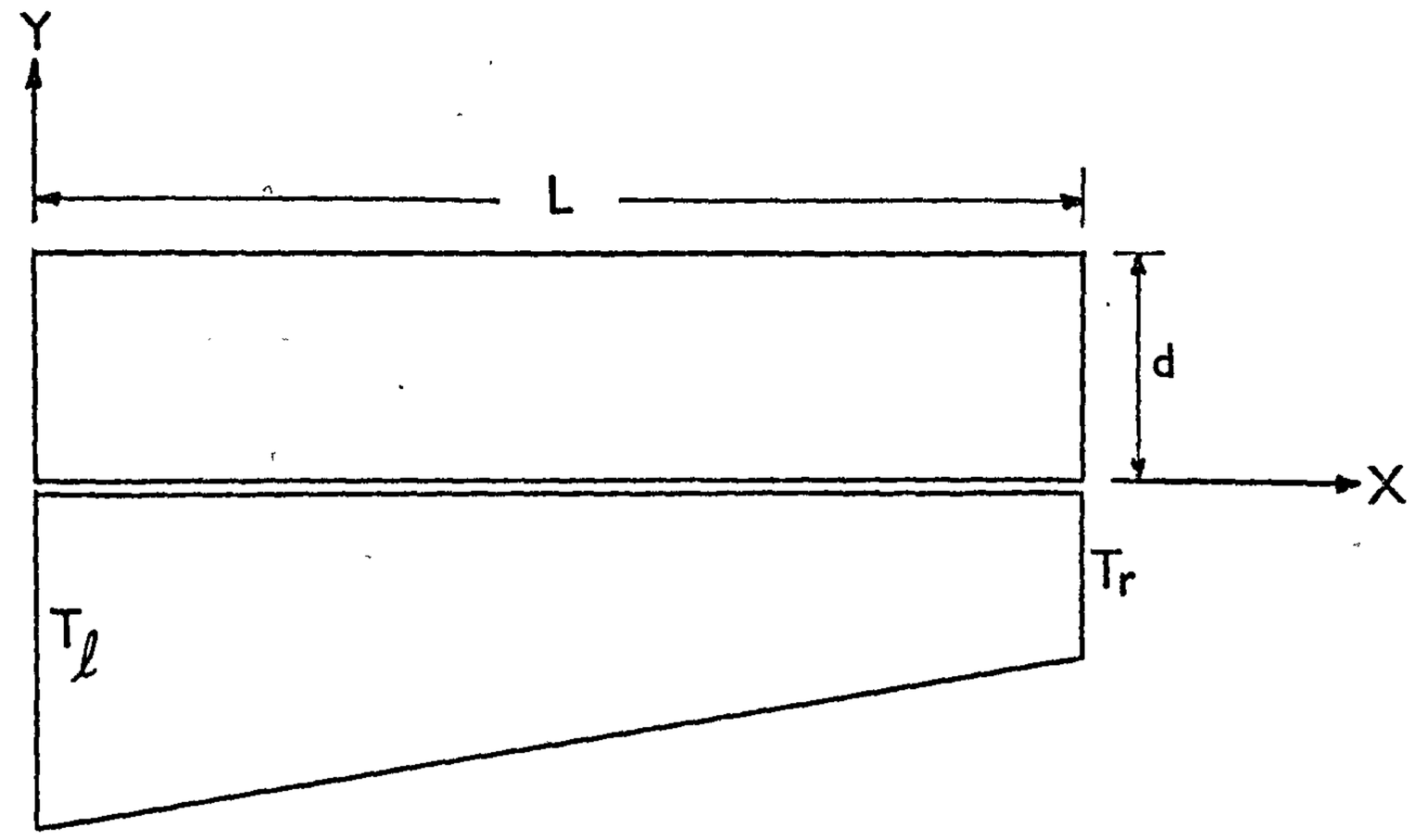

Fig. 6.4- Combination of a linear and a uniform temperature on the boundary.

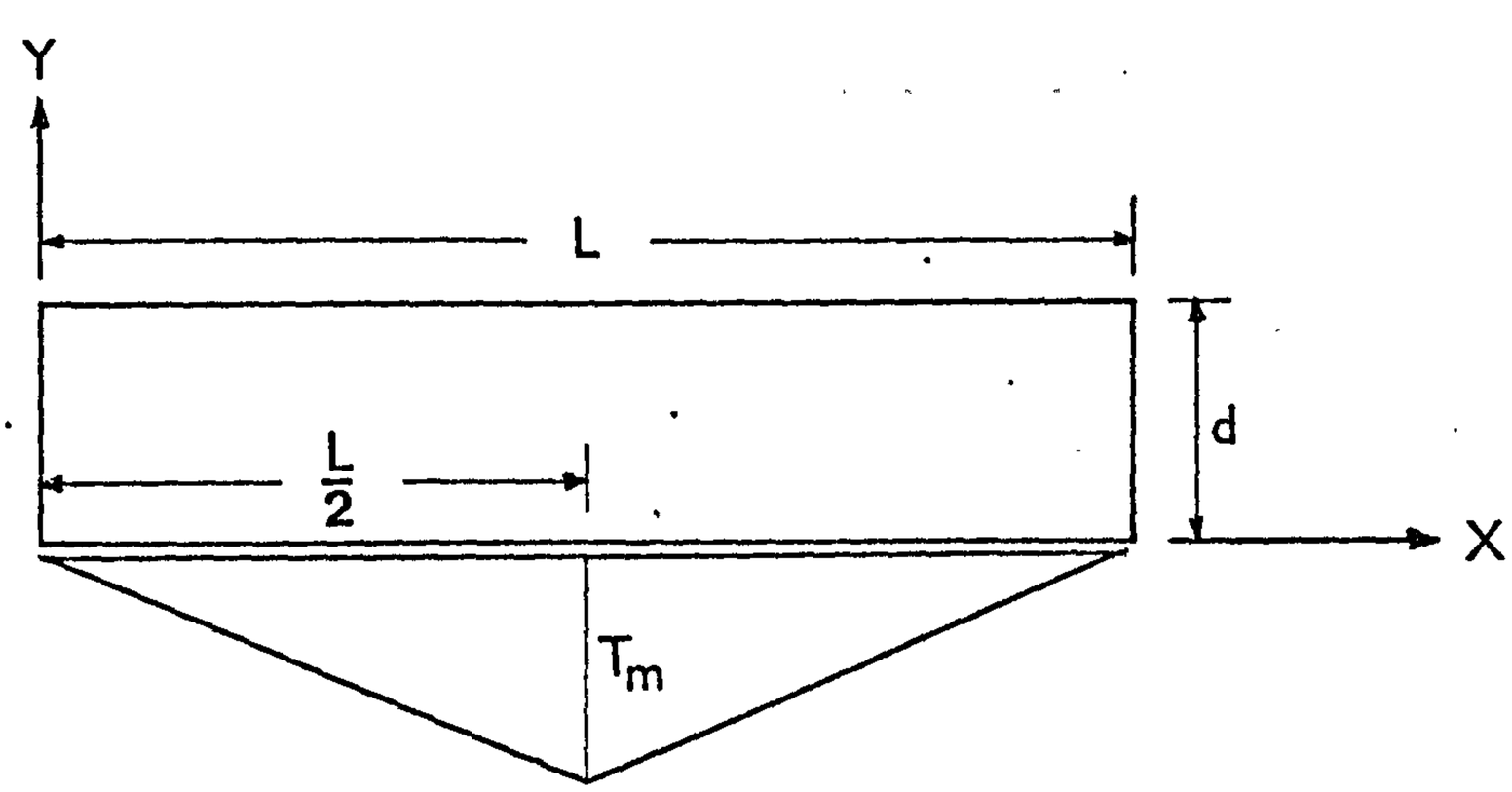

Fig. 6.5- A symmetrical and linear surface temperature on the boundary.

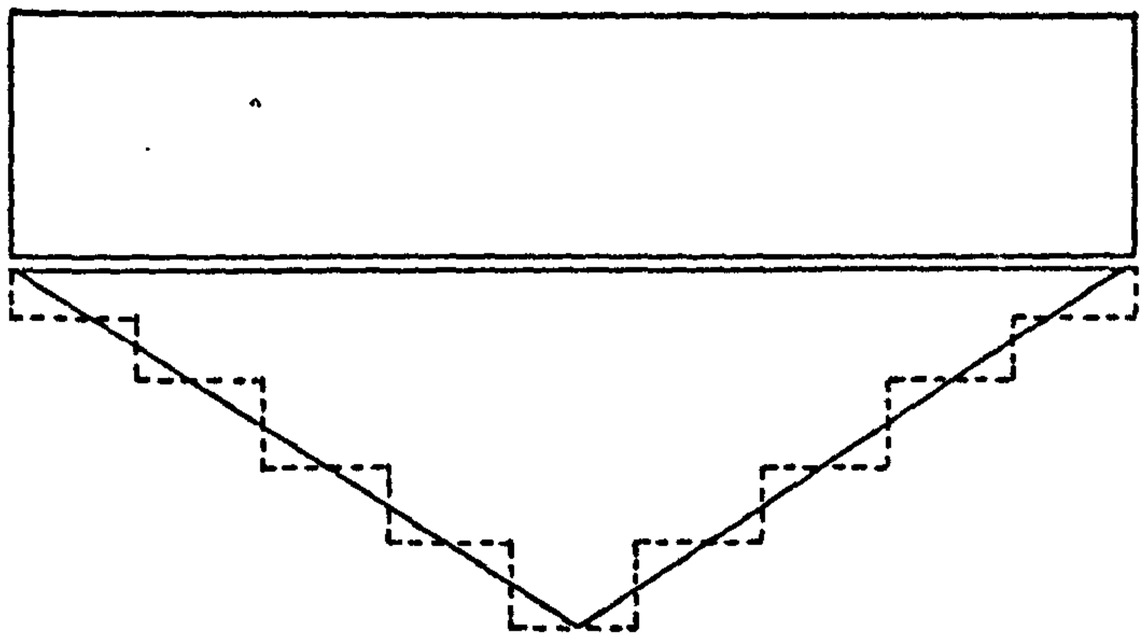

Fig. 6.6- Stepped boundary temperature for a linear boundary condition of two dimensional body

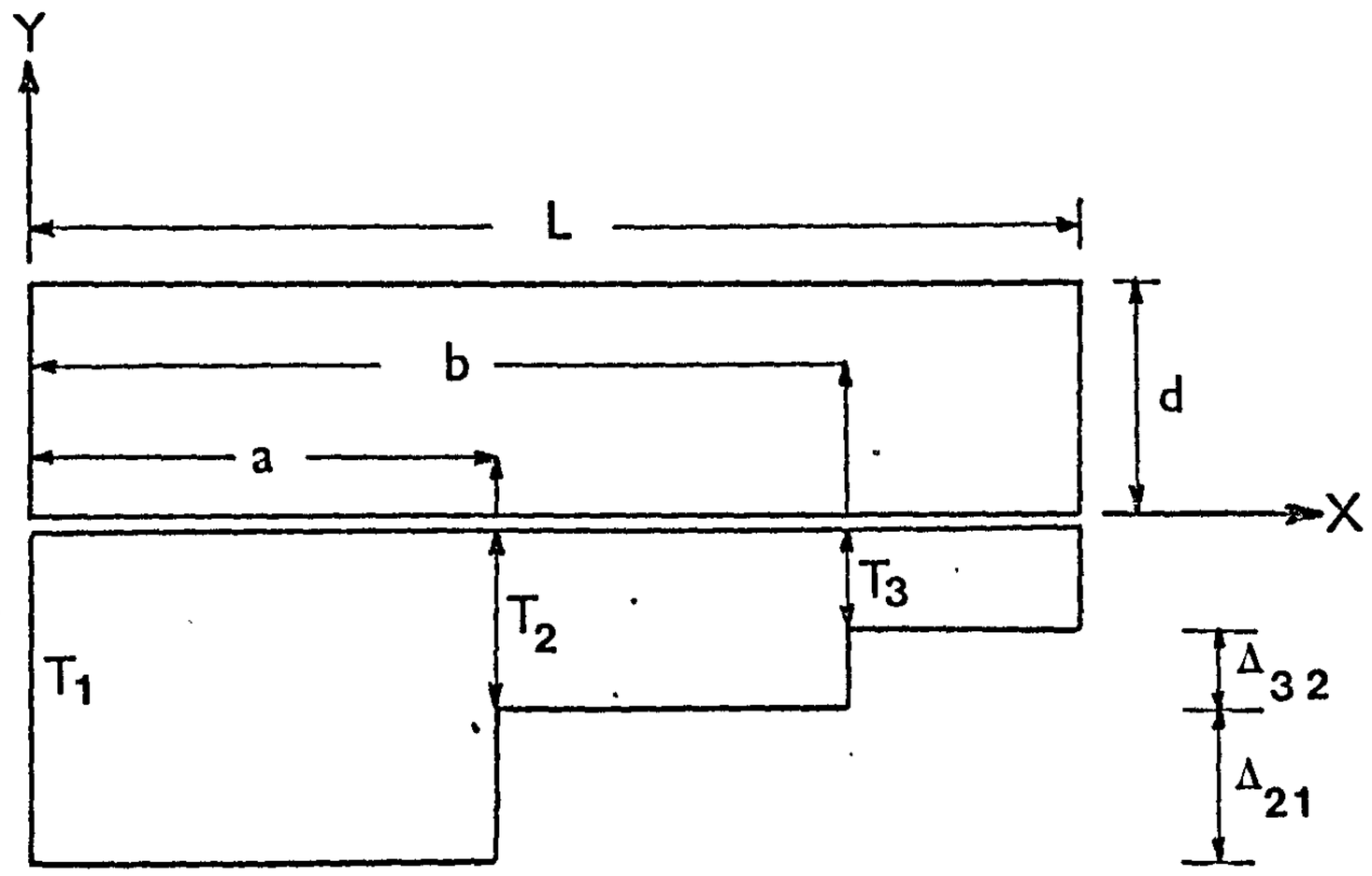

Fig. 6.7- Combination of linear temperature distributions on one side of a two dimensional body.

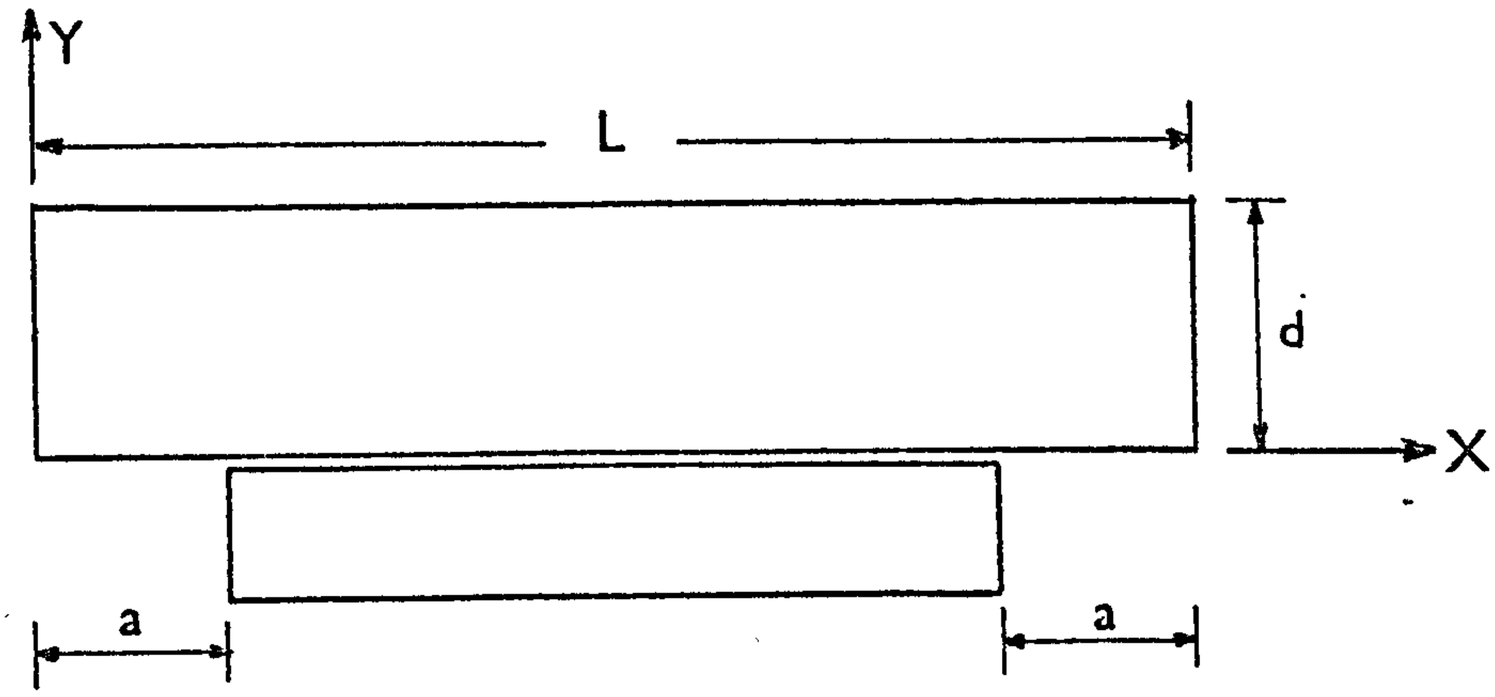

Fig.6.8- A general uniform temperature distribution on the boundary of a two dimensional body.

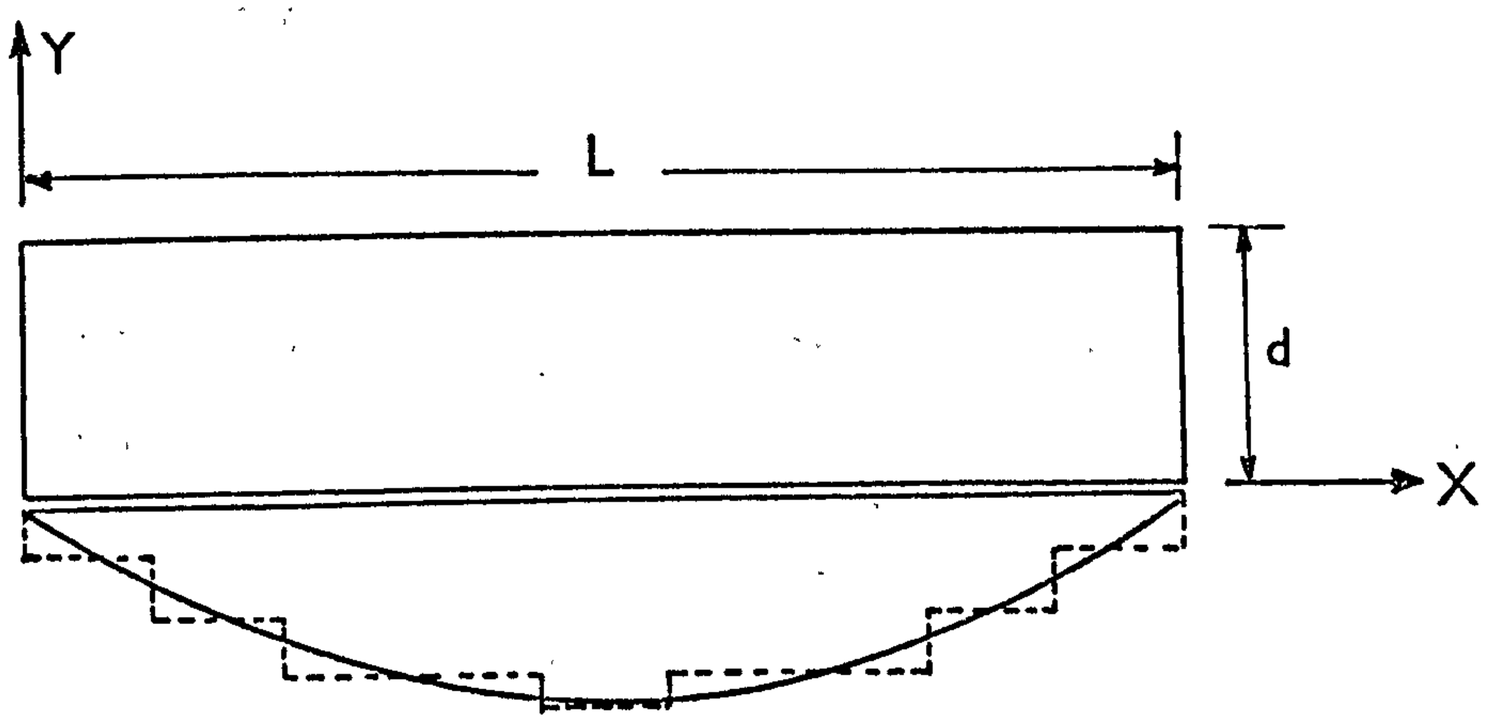

Fig.6.9- Stepped boundary temperature for a symmetrical distribution of temperature.

CHAPTER SEVEN

VII- Analysis Of Beams

7.1- Object And Scope

In general , reinforced concrete members under high temperature can be very complex. This is attributed to the influence of many physical, mechanical and geometrical factors of the particular structure which can be assumed to be constant under a given load at constant room temperature but vary significantly and become interdependent under high temperature.

The purpose of this chapter is to obtain analytically the behaviour of reinforced concrete beams under service load and high temperature. Two simply supported Tee beams were considered for which the corresponding experimental data is available [Ref. 93]. The beams were loaded incrementally up to the service load, followed by an increase in temperature similar to the condition applied to the experimental beams in [Ref. 93]. The results of the analysis were then compared with those available from the test result.

One of the members were analysed under the same temperature condition without the external load. A comparison of the two analytical model was finally carried out.

With the computer program developed it is possible to analyse any cross sectional symmetric reinforced concrete beams including rectangular beams, box beams, I and T beams with any boundary restraints and surface temperatures with distrubutions as described in chapter six.

7.2- Experimental Investigation

Twenty four rectangular beams provided with a cast slab at the top to form T-beams were investigated by Malhotra [Ref. 93] under service load and high temperature. The top slab was provided primarily to simulate the exposure of the beam to the heating conditions as would be experienced in practice when forming part of a floor construction. This arrangement also facilitated the application of load on the upper surface of the beams. The beams were made at the Building Fire Research Station under controlled laboratory conditions with a design cube strength 5000 lb/in^2 (35 $N./mm^2$) at 28 days. During the manufacture of the beams thermocouples were attached at selected points to the reinforcements and embedded in the concrete section in specimens to obtain a record of temperature gradients.

Two reinforced concrete beams of 7.6 m., length, number 18 and 19 [Ref. 93], which were chosen for comparison were provided with tensile reinforcement consisting of six bars of 22 mm (7/8 in.) diameter arranged in two layers of three each, and with two compressive reinforcements in one layer, as shown in figure (7.1) and (7.2). An arrangement of double links of 11 mm diameter mild steel bars was used and these were spaced at 305 mm centers. The downstand of beam measured 380 mm deep by 280 mm wide with the slab at the top being 810 mm wide by 152 mm thick and reinforced with 11 mm diameter hooked bars at 150 mm centers. The position of the bars was such that for beam No. 18 the concrete cover to the outermost bars was 38 mm from the soffit as well as

the sides whilst in the case of beam No. 19 it was 25 mm.

Before subjecting to the fire tests, the beams were stored under cover in the laboratory for a period of up to three years so that the concrete would ottain stable moisture conditions.

During the tests, the ends of the beams were positioned over specially strengthened recesses in the end walls and were supported over steel bearing plates. The positioning of the beams was such that the top slab projected about 150 mm above the top of the furnace.

A design load of 18.4 tons was opplied to the beams No. 18 and 19 tons was applied to the beam No. 19 at four points at 1/8 and 3/8 from the nominal span from each support as shown in figure (7.1-a). The beams were loaded prior to the heating and the test load was kept constant for the whole duration of heating in conformity with the requirements of the British Standard for fire resistance tests.

7.3- Analytical Models Of The Beams

The two analytical models for beams number 18 and 19 which were investigated by Malhotra [Ref. 93] are in figures (7.3) and (7.6). It will be noted that the first model covers the geometrical conditions of the beam No. 18 and the second model with more elements and layers and therefore consumes more computer time and storage covers the conditions of the beam No. 19. As the second model contains more elements a more accurate representation results. Since symmetrical

conditions exist for both beams, only one half of each beam was divided into rectangular elements, each element being then divided into a number of layers.

As the first beam pertaining to beam No. 18 was divided into 248 rectangular elements with 32 nodes in x-direction (horizontal direction) and 9 nodes in the vertical direction (y-direction) as shown in figure (7.3), with the largest elements appearing towards the centroid and the smallest elements near the free boundary of the beam and at the level of the reinforcements. Each element was divided into ten horizontal layers throughout the thickness, half of which are shown in figure (7.4), where each layer includes either concrete or steel. The total number of layers was 2160. This model was provided with tensile reinforcement consisting of three bars at one level, each having a rectangular area 22×34.5 mm^2 giving a total tensile reinforcement cross-section area of 2280 mm^2 as compared to 2277 mm^2 in the experimental model. The centroid of the tensile reinforcement coincide with the experimental position. Figure (7.4-a) illustrates the positions of the compressive and tensile reinforcement with corresponding layers in figure (7.4-b) for both the cross-section of elements at any vertical section.

Two links each 22×10 mm^2 in cross-section giving a total cross-section area of 440 mm^2 were positioned, instead of the double links of 11 mm diameter, giving an area 380 mm^2 for the experiment. Finally, in order to reduce the computer time and storage the hooked bars of the slab at the top of

the beam were ignored.

In this simply supported beam (No. 18), the node No. 10, as in figure (7.3), was assumed to move in the x-direction and fixedin a vertical position. As the beam was under fully symmetrical conditions, the nodes 280 to 288 at the middle of the beam were assumed to be free in the vertical direction and fixed in the horizontal position. The element and nodal numbering of elements 1 to 48 and 216 to 248 for analytical model of beam No. 18 are shown in figure (7.5).

The second analytical model patterned to analyse the beam No. 19 was divided into 372 elements with 32 nodes in the x-direction (horizontal direction) and 13 nodes in the y-direction (vertical direction) as shown in figure (7.6), in which the smallest elements are positioned at the free surfaces of the beam. In this model the beam was divided into 3968 layers by dividing each element of the beam into 10 and the slab at the top into 12 layers throughout the thickness. Half the cross-section of the beam is shown in figure (7.7). The element and nodal numbering of elements 1 to 72 and 325 to 372 are shown in figure (7.8). This analytical model was provided with six tensile reinforcement each of 19×20 mm^2 cross-sectional area arranged at two levels of three each, which give the total tensile reinforcement area of 2280 mm^2 as compared to 2277 mm^2 in experimental model. Also two compressive reinforcing bars were arranged at a level within the slab as shown. The tensile reinforcement was positioned so that the concrete cover to the outermost was 25 mm from the soffit as well as the sides, as in

experimental model. Figure (7.7-a) illustrates the position of the tensile and compressive reinforcing bars with the corresponding layers and cross-section of elements throughout half a thickness section. Four links each of 10×10 mm^2 cross-section area giving a total area of 400 mm^2 were positioned, instead of double links provided in the test of 11 mm diameter, giving an area of 380 mm^2. A single reinforcing bar 10×10 mm^2 in area was assumed for the slab at the top of the beam.

For the simply supported condition, node 14 was assumed to move in the horizontal direction and fixed in the vertical position. Also all nodes at the middle of the beam (nodes 404 to 416), figure (7.8), were assumed to be fixed in the horizontal direction and free in the vertical position.

7.4- Heat And Loading Condition

Half of the 18.4 tons load was applied at two points on half of the beam by six equal incremental values (1.53 tons each) at 1/8 and 3/8 of the span from the left support as in the experiment (see figure (7.3)).

The first load (91 cm. from the support), was divided into two equal loads and applied at nodes No. 117 and 126, and the second load also divided into two equal values and applied at nodal points 225 and234.

Half of 19 tons load was applied to the analytical model of beam No. 19 at nodes No. 144 and 288 by six equal increments of 1.58 tons, as shown in figure (7.6).

A uniform temperature distribution was assumed on three sides of each beam and the temperature value within each layer was calculated from the classical solution of the heat equation, by using equation (6.52) for each side of the beams. The temperature on the surfaces of the beams were applied incrementally and calculated from the British Standard Fire, Time-Temperature relationship [Ref. 105], is shown in figure (7.9).

As the time-temperature curve increases more rapidly initially, the time intervals were shorted for the first three temperature increments which were applied at 1.5, 5 and 15 minutes. The rest of the temperature increments were kept equal to 15 minutes as in figure (7.10).

7.5- Behaviour Of Beams Under Service Load

A- Beam No. 18

Cracks appeared in layers of elements No. 201, 217 and 233 at the central section of the beam within the concrete cover below the links after the first load increment of 3.06 tons. The orientation of the cracks were in a vertical direction. These cracks propagated under the second and third increments within the concrete layers and new cracks appeared at all concrete layers of the elements No. 209, 210, 225, 241, 242 and 243. The maximum tensile stress apeared within the tensile reinforcement at the middle of the beam underhalf the service load(at the end of the third load increment)

within the steel layer of the element No. 242, which were surrounded by cracked concrete layers of elements No. 241 and 243. The distribution of tensile stress within the tensile bar at the end of the third load increment when the beam was under half the service load was approximately uniform at the middle of the beam between two point loads as shown in figure (7.11). This longitudinal distribution of tensile stress was approximately linear stationed at the support at one end increasing linearly to 35 N./ mm^2 at L = 1.07 m. The rate of stressing increased at L = 1.07 m, and a stress of 85 N./ mm^2 and the rate of increased reduced therefore as shown in figure (7.12).

The original cracks propagated under the 4th, 5th and 6th load increments through part of the height of the beam and series of new cracks initiated are propagated seperately as in figure (7.12).

As in the case of the beam under half the service load, the maximum tensile stress of the tensile reinforcement appeared at the middle of the beam between two loads, under the full service load. The distributions of tensile stress between support and the load point No. 1 and also between the load points No. 1 and No. 2 was approximately linear with different slope also this distribution was uniform in between as given in figure (7.11).

Finally, a maximum deflection of 13.3 mm was attained at the middle of the beam under the whole service load.

B- Beam No. 19

The behaviour of the beam No. 19 under the service load (19 tons) was approximately similar to the beam No. 18 with rapid propagation of cracks. The cracks started to propagate from the elements No. 367, 349, 325 and 301, and new cracks appeared at each incremental load. The deflection of the beam was slightly larger than that for beam No. 18. The maximum deflection at the middle of this beam at service load was 17.4 mm. The crack pattern through the height of the beam No. 19 under service load is shown in figure (7.16). The longitudinal distribution of tensile stress within the reinforcement was uniform at the middle of the beam and linear between the support and the load point No. 1 and varied between two point loads at a different gradient, similar to the behaviour of the beam No. 18.

7.6- Behaviour Of members subjected To fire and Comparison With The Experimental Results

The first incremental surface temperature 200°C corresponding to a time interval of 1.5 minutes which was applied to the both beams had a slight effect on the deflections of the members. The beams expanded slightly and the horizontal movements of the points at the supports (node No. 10 for beam No. 18 and node No. 14 for the beam No. 19) were about 45% of that was under service load. No new cracks appeared within beam No. 18 and none of the previous cracks propagated within the members at this temperature increment.

The second incremental surface temperature 440 °C was applied from time-temperature relationship, figure (7.10), which corresponded to a time interval of 5 minutes. For beam No. 18 three cracks which had occured under service load started to branch diagonally towards the load within elements No. 244, 212 and 196. As the members were heated from three sides, the maximum temperature within each element occured at the outer layers of the elements and hence the cracks first appeared within the concrete cover. Since the concrete cover is small compared with the other concrete layers, the concrete layers of the elements surrounding the reinforcement (layer No. 4 in the case of beam No. 18 and layer No. 5 in the case of beam No. 19, as in figures 7.4 and 7.7) are considered in this explanation. However the analytical model of beam No. 19 showed more response under temperature loading. Two elements of this beam No. 331 and 307 (layers No. 5) cracked under the first temperature increment and propagated to elements No. 332 and 308 in the second incremental temperature. Also three new crack branches started under the second temperature increment which apeared within elements No. 288 and 264. The maximum deflections of beams No. 18 and No. 19 under the second temperature increment were 23.4 mm and 27.7 mm, respectively. All the crack branches propagated through the height of the both the members under the third temperature increment and a series of new crack branches appeared. The surface temperature in this increment corresponding to 15 minutes time interval was 660 °C. The crack pattern of the beam No. 18 at the end of the third incremental temperature is shown in figure (7.13).

The tensile stresses within the reinforcement of the both members were reduced by about 15% at every steel layers except at the middle of the beams which reduced to less than 10%. The distribution of tensile stresses within the reinforcing bars of beams No. 18 and No. 19 are shown in figures (7.11) and (7.20), respectively. As illustrated in these two figures the distributions of tensile stresses are still linear between support and the load No. 1, and also between the two point loads with different slopes. The distribution is still uniform at the middle of the beam No. 19 but for the beam No. 18 a peak was reached at the middle of the member within element No. 241 (steel layer No. 3, figure 7.4-a). These simple uniform and linear distributions of the tensile stress become less uniform after half an hour heating, as shown in figures (7.11) and (7.20). The tensile stresses of both beams, under temperature loading, generally increased between supports and the loads No. 1 and reach peak values in the vicinity of these loads, then reduced at the rest of the bars. The tensile stresses within the reinforcement of both members remain approximately constant between the middle of the beams and middle of the loads No. 1 and No. 2, (see figure 7.20). For both members the first crack within the slabs at the top of the rectangular beams appeared at 1½ hour heating, which are shown with dotted lines in figures (7.14) and (7.18).

Double cracks appeared within both beams after two hour heating as shown in figures (7.15) and (7.18), in which three layers of the beam No. 18 and five layers of the beam No. 19 have developed double cracks. These double cracks

appeared in the vicinity of the loads in both members.

Finally, beam No. 18 collapsed after 2¼ hour heating when the crack branches at the middle of the beam propagated throughout the height of the member and all the tensile reinforcing bars at this point reached their yeild stress.

Beam No. 19, collapsed after 2¾ hour heating for the same reason as above. The crack pattern within this member at 2½ hour heating is shown in figure (7.19).

The horizontal movements at the supports of the beams were approximately linear during the heating up to about 1½ hour heating and after raching a peak value at about 2 hour heating for beam No. 18 and about 2¼ hour heating for beam No. 19 they reduced slightly. Figure (7.21) illustrates the horizontal movement of the node No. 14 (at the support) of beam No. 19 due to expansion of the body and is shown by a dotted line.

As the members expanded horizontally, they also expanded slightly in a vertical direction. The expansion of the middle section of beam No. 19 at different time intervals is shown in figure (7.22).

A comparison with the available experimental results [Ref. 93] indicates the followin;

1- The distribution of temperature within the analytical models was the same for both members, and was slightly different for the experimental time-temperature relationship within the reinforcement at the same particular points. The mean values of temperature of eight steel layers within the elements No. 219, 221, 267, 269, 315, 317, 363 and 365 were

calculated at each incremental temperature and plotted and is shown in figure (7.23) to compare with the experimental mean values of the reinforcement temperatures. As this figure illustrates, the maximum gap between the analytical values and experimental results occured after half an hour heating particularly for the mean reinforcement temperature of beam No. 18. This may be because of the evaporation of moisture of the beam which has not been taken into account in the analysis. For this reason the calculated value of temperature is considerably more than the experimental result within one hour heating. The calculated mean values of temperature after one hour heating are less than (about 10 to 12%) the experimental results. The main reason for this discrepency is that the temperature which could flow within the reinforcement itself along the beams was not considered in the classical solution, because of mathematical difficulties. The discrepency between calculated mean value of the reinforcement temperature and experimental results could be reduced by taking the temperature of more steel layers, especially at the bottom level of tensile reinforcement of beam No. 19.

2- The time-deflection curves of the analytical and experimental results of the beam No. 18 are shown in figure (7.24). The maximum gap between analytical and experimental deflection results (up to $2\frac{1}{4}$ hour heating) was not more than 12% and the analytical model of the member No. 18 deflected more rapidly at the begining of the heating up to one hour. This may be because of a more rapid increase in temperature

within the body, than the experimental result, figure (7.23). The main reason that the analytical model has deflected less than experimental result after 1½ hour heating is that the concrete elements and layers of this model were considerably larger and stiffer and not able to distribute the internal forces throughout the members.

The reason that the analytical model of beam No. 18 collapsed about half an hour earlier is that this model included a large number of concrete layers and the cracked layers released considerable forces due to crack to the surrounding elements making the member much weaker and the surrounding steel layers therefore carried large tensile stresses which made the steel reinforcement, especially at the middle of the beam, to reach yeilding.

The cracks at this location propagated more quickly reaching the whole height of the member after two hour heating as shown in figure (7.15).

The analytical model of beam No. 19 collapsed after 2¾ hour heating before reaching the next temperature increment (three hour heating). The time-deflection curve for the central section of this member was closer to the experimental result as shown in figure (7.25). The maximum deflection difference between experimental and analytical results appeared after 2½ hour heating at a higher temperature, but the maximum deflection gap between experimental and analytical models was not more than 10 to 12% as shown in figure (7.25).

7.7- Behaviour Of Unloaded Beam Subjected To Fire

To study the behaviour of an unloaded beam under high temperature, the previous incremental temperature was applied on the beam No. 18 without applying any external load. The beam collapsed after $2\frac{3}{4}$ hour heating befor reaching the next incremental temperature, as compared to $2\frac{1}{2}$ hour heating in the previous analysis. It deflected downward, as in the previous loading and heating. The time-deflection relationships for the two cases are shown in figure (7.26).

Generally, the beam started to crack after 5 minutes heating when the surface temperature reached 440 ^{o}C, and the first series of cracks appeared within the concrete cover, within all layers of elements from No. 121 to the middle of the beam.

The first layers (Fig. 7.4) of the elements No. 170, 186, 202, 218 and 234 were cracked after five minutes heating. The first layer of the slab at the top of the rectangular beam cracked at 10 points in the vicinity of the beam's links which are shown with dotted lines in figure (7.27). As the cracks were propagated at the bottom of the member, some internal cracks (within layers No. 4 in figure 7.4) apeared at the top of the beam as shown in figure (7.28). These cracks propagated rapidly during the next temperature increments up to half an hour heating, especially the cracks at the top of the beam which propagated downwards within the beam and concrete cover, as shown in figure (7.29). These temperature increments did not effect the internal cracks at the bottom of the beam as at the top where internal cracks

propagated downwards as in figure (7.30). Four cover layers were cracked in two directions during half an hour heating.

As the cracks at the top propagated within the concrete cover and within the beam some layers were crushed after one hour heating. These collapses appeared at the bottom of the member in the vicinity of tensile reinforcement as shown in figures (7.31) and (7.32).

More layers were crushed and cracked (especially in the vicinity of the support) during the second hour heating as in figure (7.34). The positions of collapses and cracks at $2\frac{3}{4}$ hour heating, a few minutes befor ultimate conditions, are shown in figures (7.35) and (7.36). As the figure (7.36) illustrates, collapses occured within the beam at the bottom and at the top of the member at the middle, in two neighbouring section and the beam became too flexible causing the collapse. By comparing two figures (7.35) and (7.36), it is concluded that the outer layers of the slab at the top was still in tension as the internal layers failed in compression. The distributions of stress in x-direction throughout the height of the beam at the middle of the member at different time intervals are shown in figure (7.37). As these figures illustrate, the top and bottom of the beam are in compression while the center of the beam is in tension during heating.

The tensile stress within the tensile reinforcement of the member increased with increase in temperature and the first yield appeared at the middle of the beam at about one hour heating. The distribution of these tensile stresses at nine time intervals are shown in figure (7.38).

7.8- Behaviour Of Unreinforced And Unloaded Concrete Beam Subjected To Fire.

To study the behaviour of an unreinforced and unloaded concrete beam, the mathematical model of the beam No. 18 was used omitting the steel layers and replacing them with the concrete. The previous surface temperature was applied on this model with shorter time intervals to obtain more accurate results, especially for deflection of the body and at ultimate condition.

The beam collapsed a few minutes after 80 minutes heating before reaching the next incremental temperature corresponding to 85 minute interval. The surface temperature increments were applied at eight time intervals 1.5, 5, 10, 15, 30, 45, 60 and 80 minutes. During the first ten minutes heating the middle of the beam deflected downwards and about 100 cm of the body of the beam from the support deflected upwards as shown in figure (7.43). The structure started to crack after ten minutes heating when the surface temperature was 580 ^{o}C, three cracks appearing at the internal layers (layers No. 4 and 5 in figure 7.4) of elements No. 153, 185 and 233. Although the stress value varied throughout the thickness of the beam (throughout the layers of every element), the maximum tensile stress appeared within the internal layers and the maximum compressive stress appeared at the outer layers at the bottom of the beam during the first five minutes heating. During the second five minutes heating, while the tensile stress at the internal layers (layers No. 4 and 5) of the beam was still maximum, the compressive stress within the outer layers at the

bottom of the body decreased considerably and the maximum tensile stress appeared at the internal elements and layers of the body at the middle section of the beam as shown in figures(7.41) and (7.44).

The beam started to deflect upwards after ten minutes heating. All outer layers of the elements from element No. 161 to the middle of the beam cracked and double cracks appeared at outer layers of elements No. 185, 186, 193, 194, 201, 202, 209, 210, 217, 218, 225, 226, 227, 233, 234, 241, 242 and 243 after 15 minutes heating. For numbering of the beam see figure (7.3). Also cracks appeared at the internal layers of the elements at the middle of the beam. In the meantime compressive stresses apeared at the outer layers of the elements at the top of the beam which was in tension during the first ten minutes heating. Also the internal layers at the top part of the middle section of the beam became tension, which was in compression in the previous ten minutes heating. Two internal layers between the above tension and compression elements and layers cracked during the next two incremental temperatures corresponding to 30 and 45 minutes intervals as shown in figure (7.41). The continued to deflect upwards at 30 and 45 minutes heating but the maximum deflection appeared at point No. 244 (see figure 7.5), about 50 cm from the middle of the structure as shown in figure (7.40). The cracks which appeared within the internal layers of elements No. 244, 235 and 228 closed during the 45 minute of heating and the stresses became compressive during the next incremental temperatures as shown in figure (7.41). The beam started to deflect downwards again

after 45 minutes heating as shown in figure (7.40) and finally collapsed at about 80 minutes heating when the maximum deflection at the middle of the beam was about 100 mm.

The distributions of stress throughout the height of the beam within the internal layers (layers No. 5 in figure 7.4) at the middle and at the section A-A, 47 cm from the middle section of the beam are shown in figures (7.41) and (7.42), respectively. Also the distributions of stress throughout the height of the body within the outer layers (layers No. 2) at the middle of the beam at six time intervals are shown in figure (7.44).

The deflections of the beam at four time intervals are shown in figure (7.43).

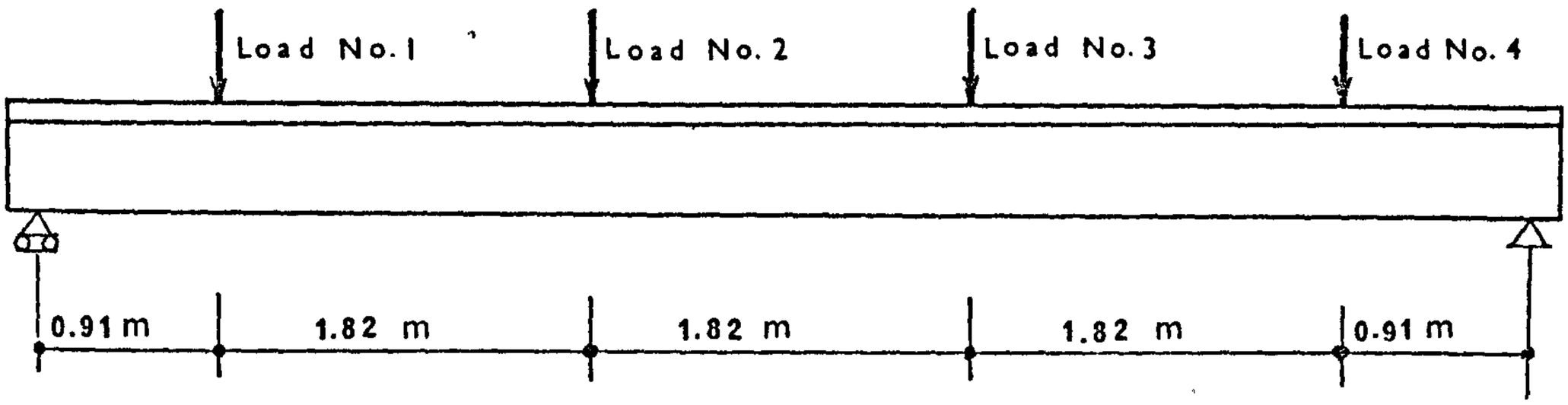

a

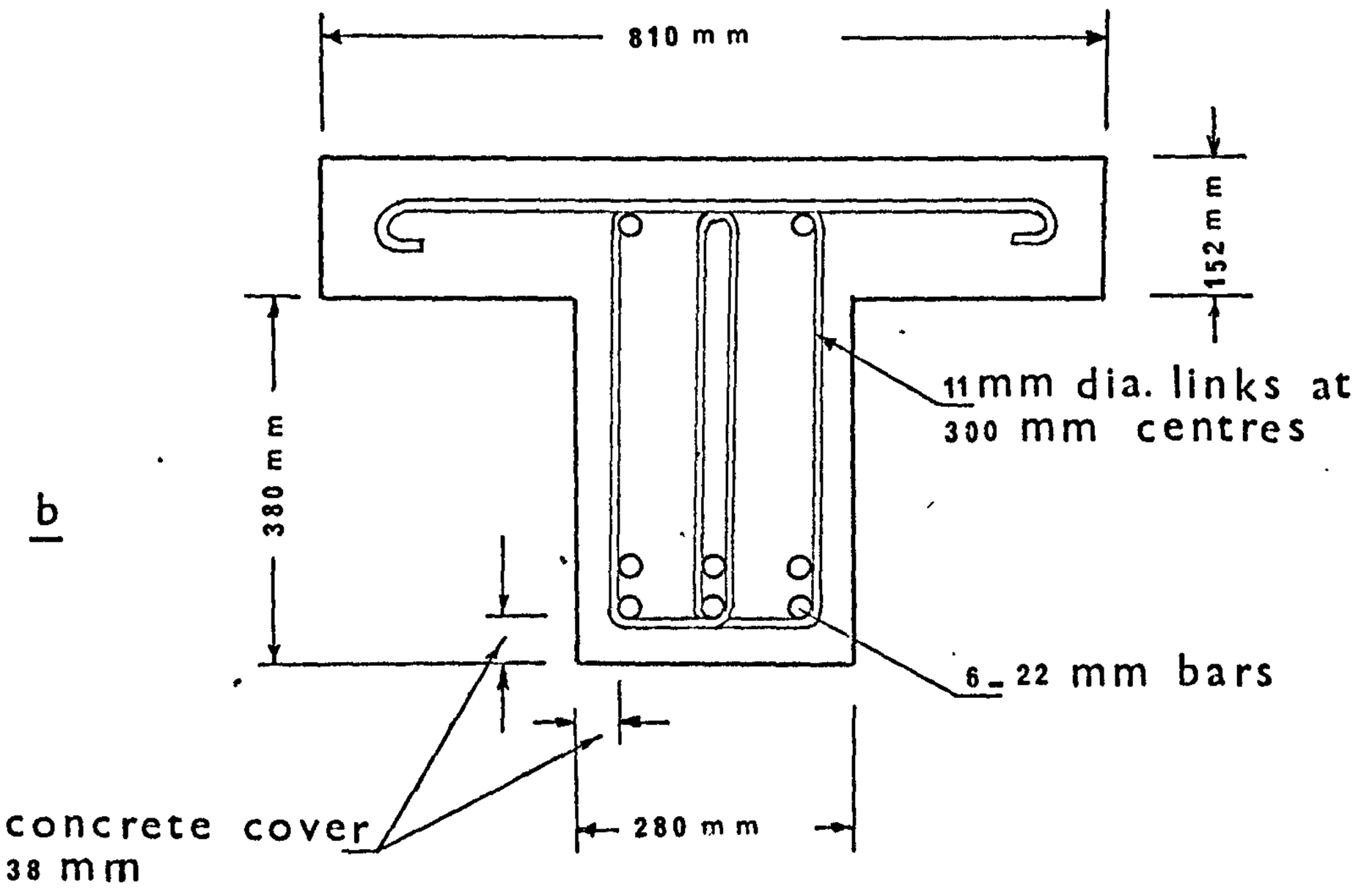

b

Fig.7.1 - Load condition of beam Nos. 18 and 19; Ref. 93, and cross-section of beam No. 18.

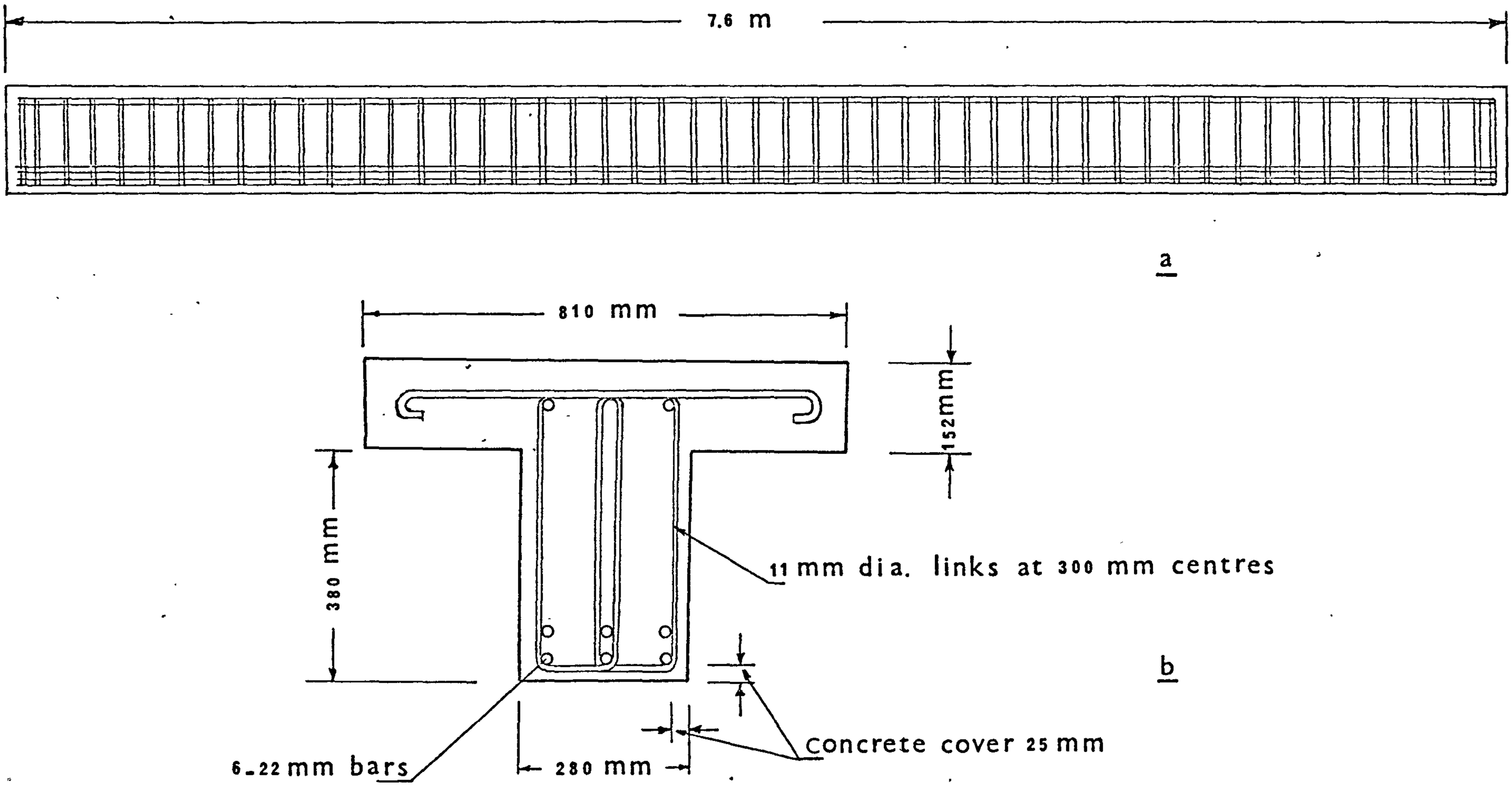

Fig. 7.2-Links Position of beam Nos. 18 and 19; Ref. 93, and cross-section of beam No. 19.

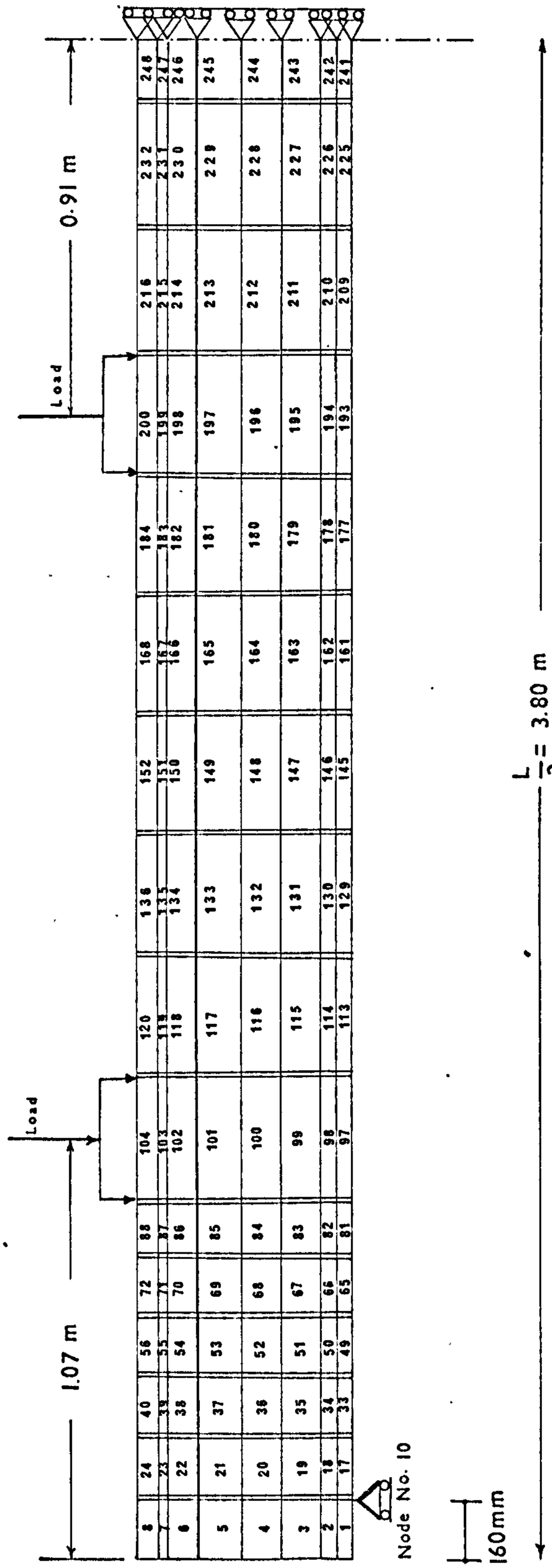

Fig.7.3- Analytical model of beam No. 18: Ref. 93, with 248 elements and 1080 layers.

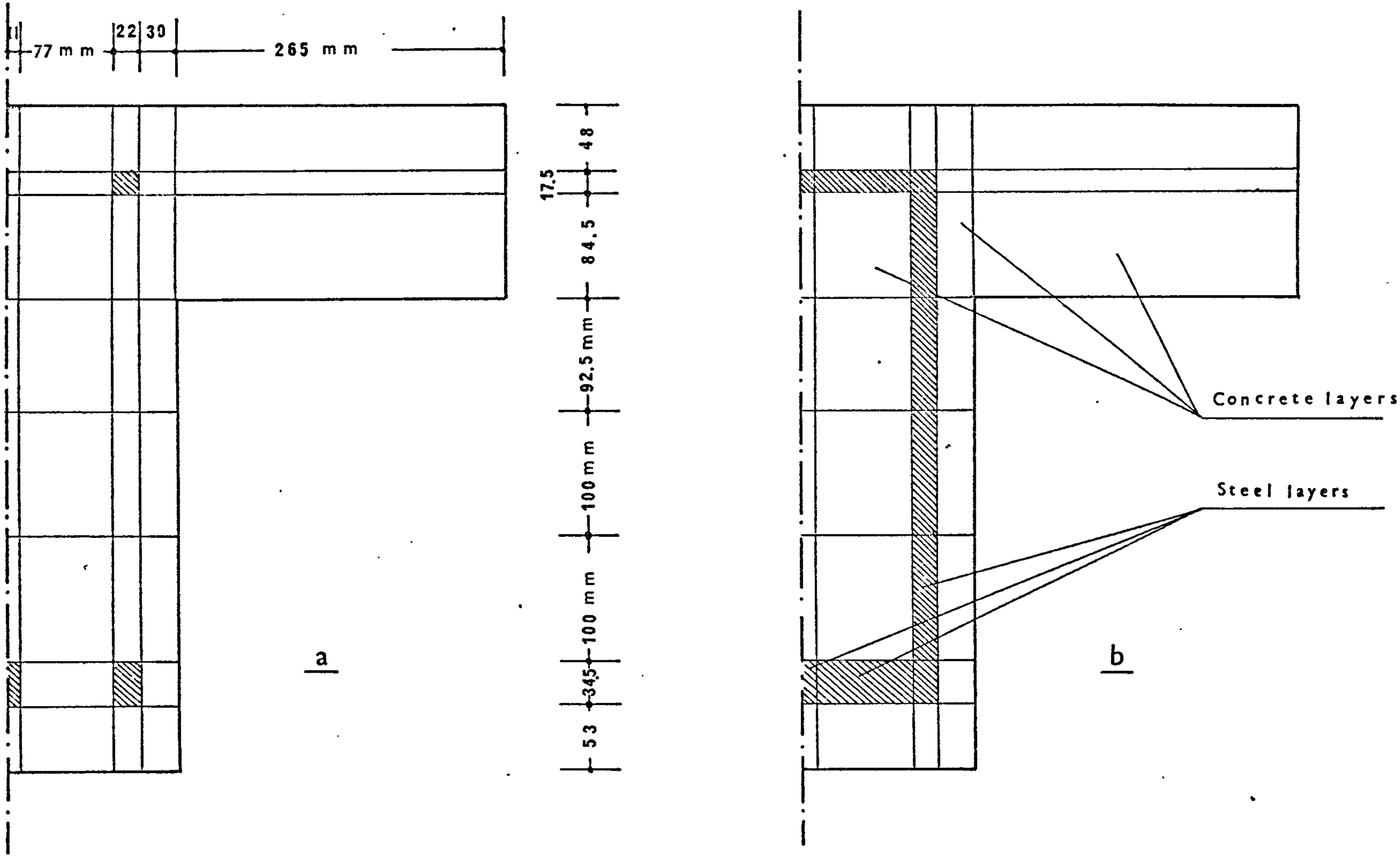

Fig.7.4 – A cross-section of analytical model for beam No. 18; Ref. 93, with layers positions.

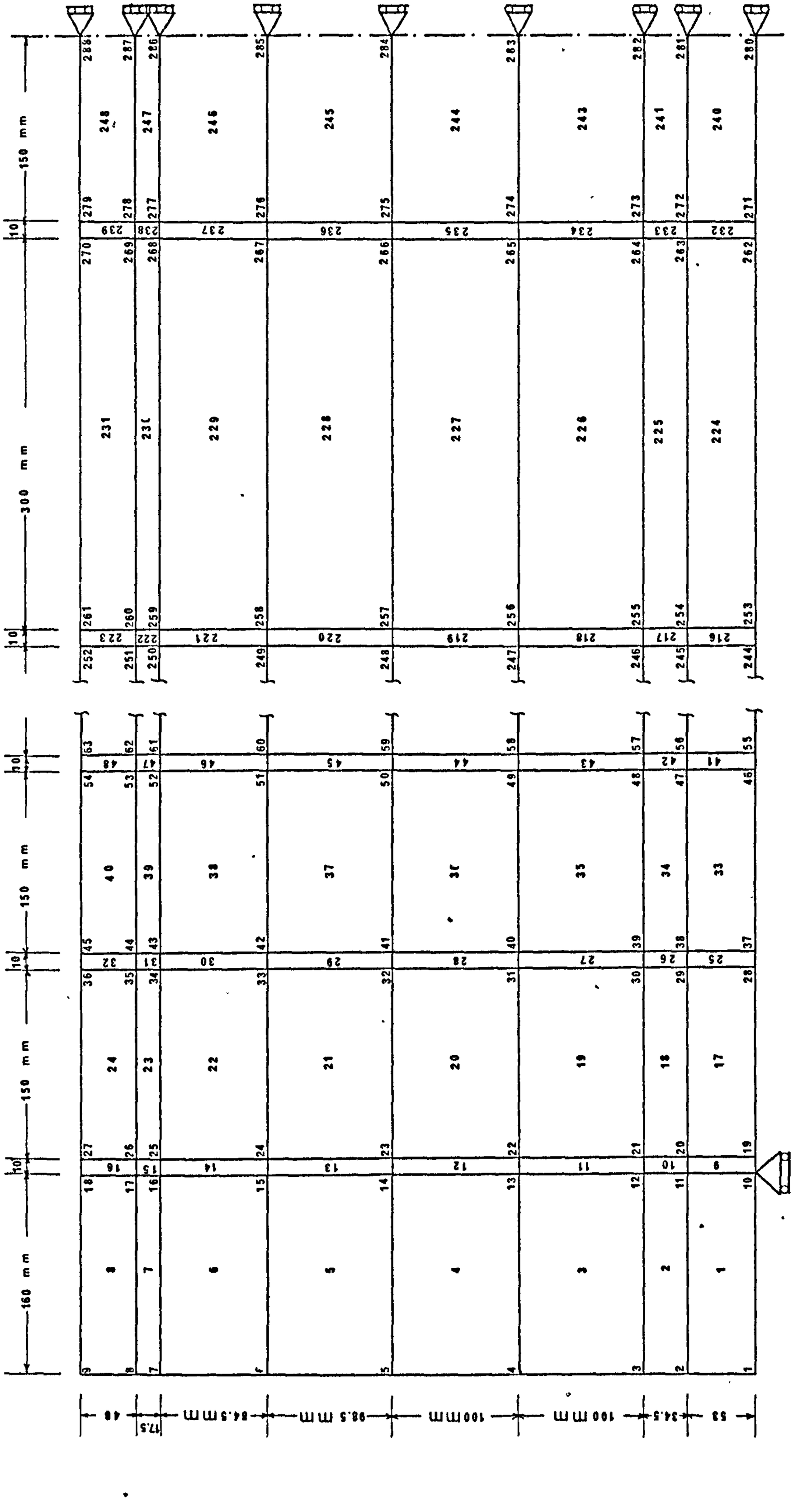

Fig. 7.5– The element and nodal numbering of elements 1 to 48 and 216 to 248 for analytical model No. 18: Ref. 93.

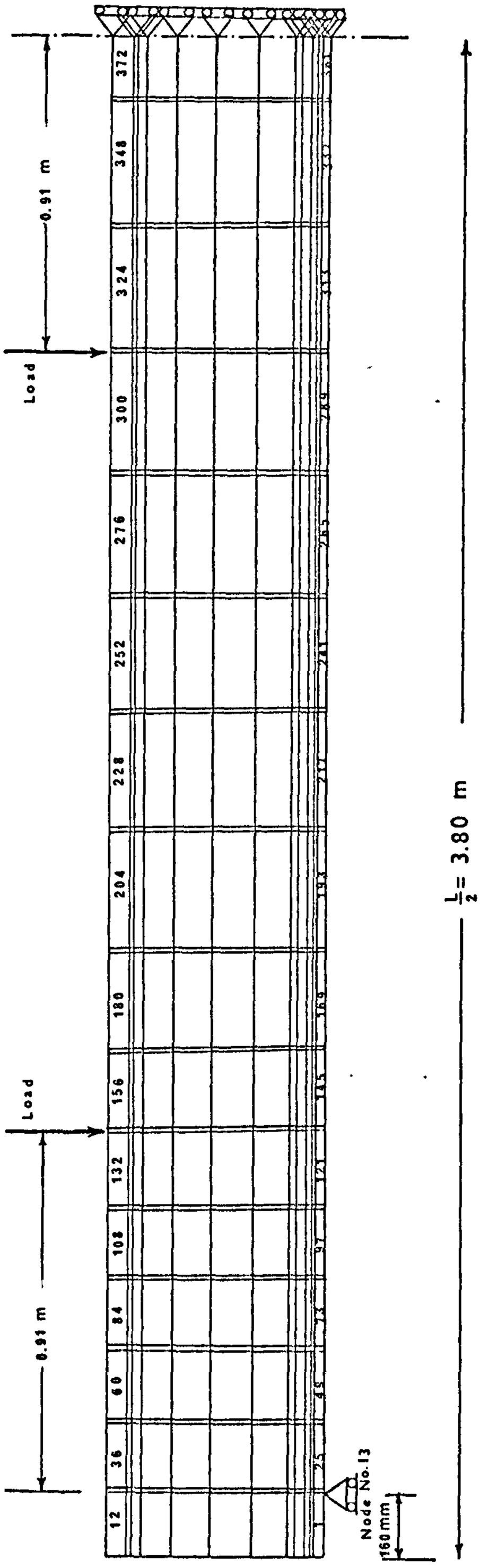

Fig.7.6- Analytical model of beam No. 19 with 372 elements and 3968 layers.

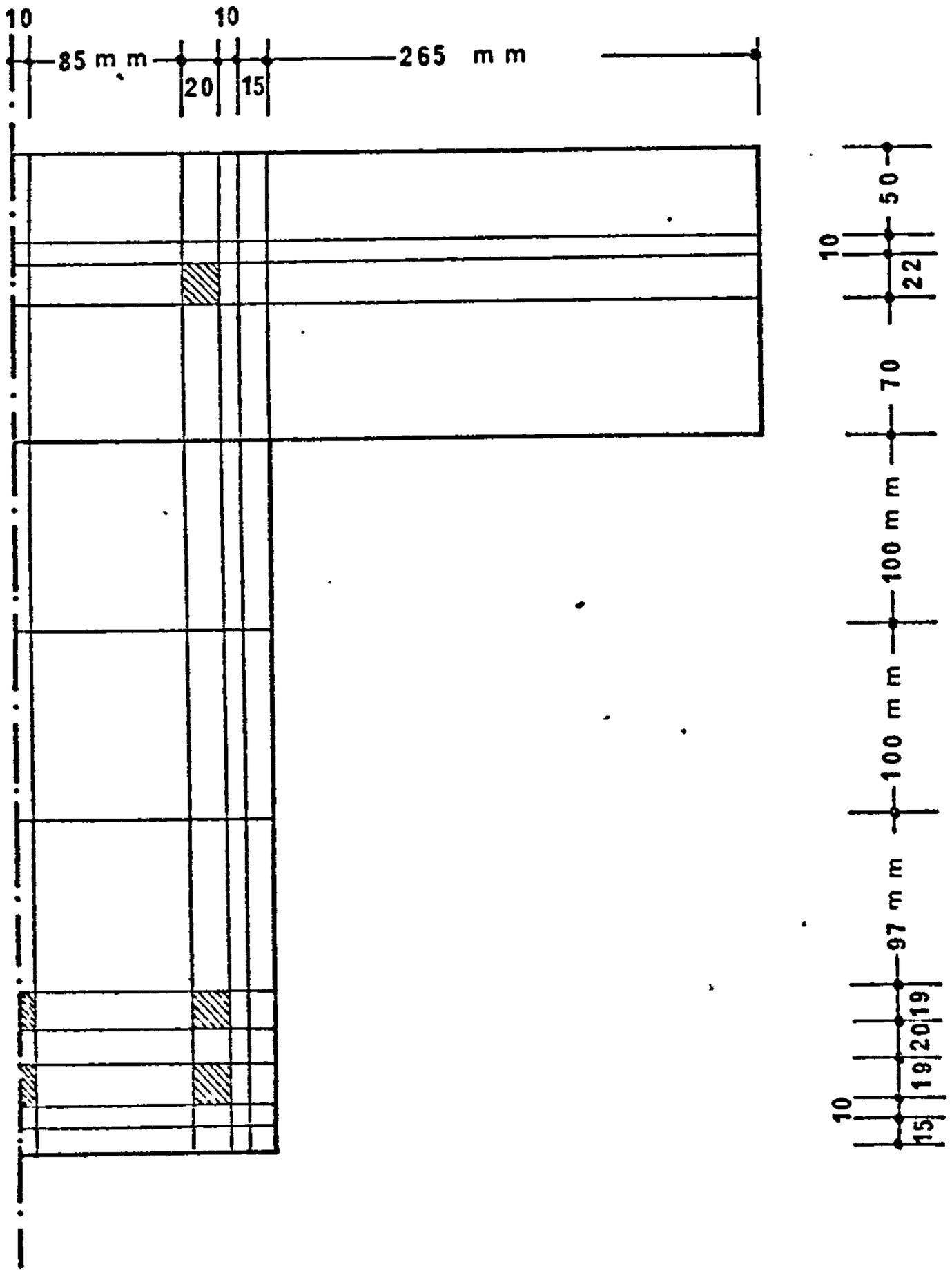

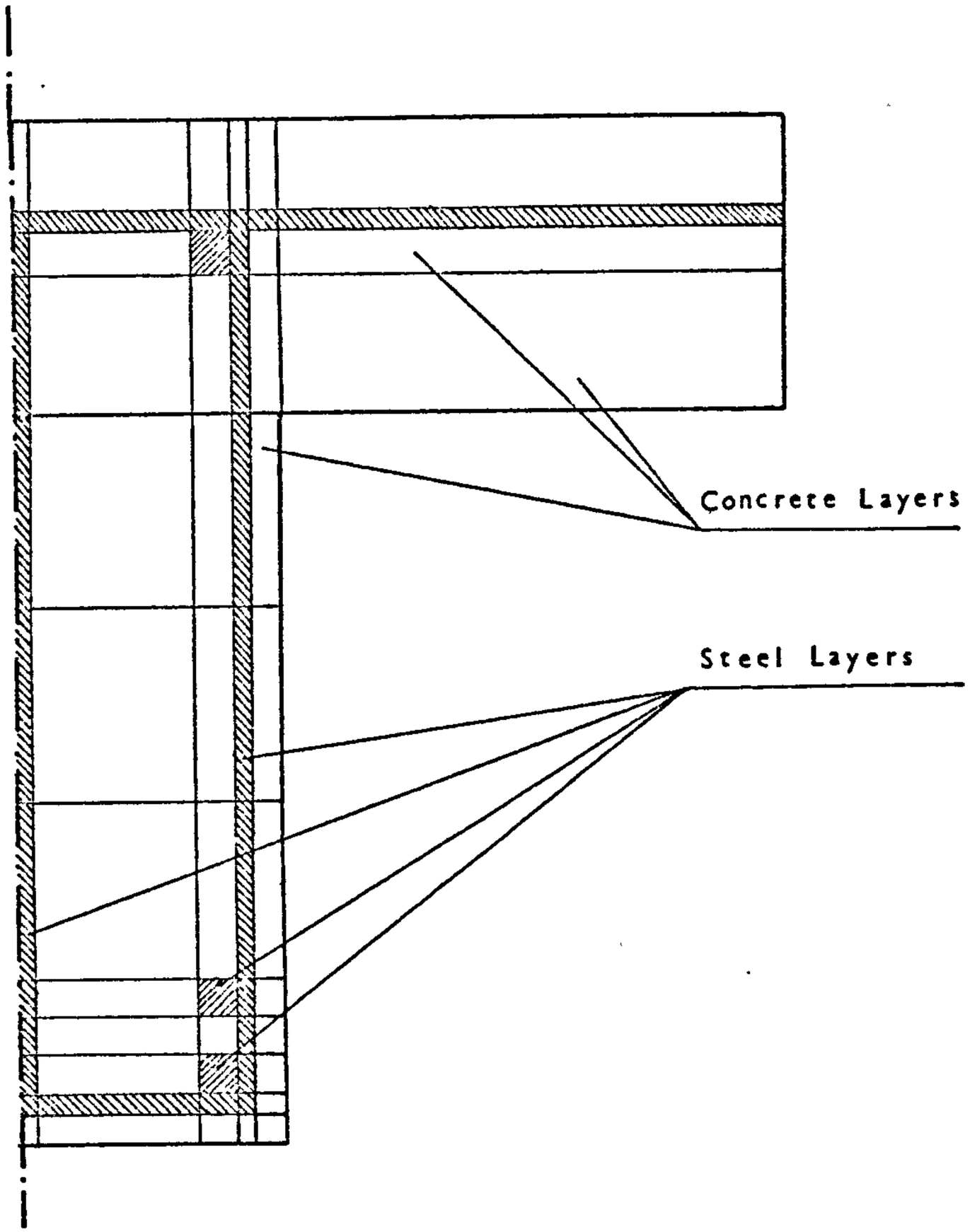

Fig. 7.7_ A cross_section of analytical model for beam No. 19 with layers Positions.

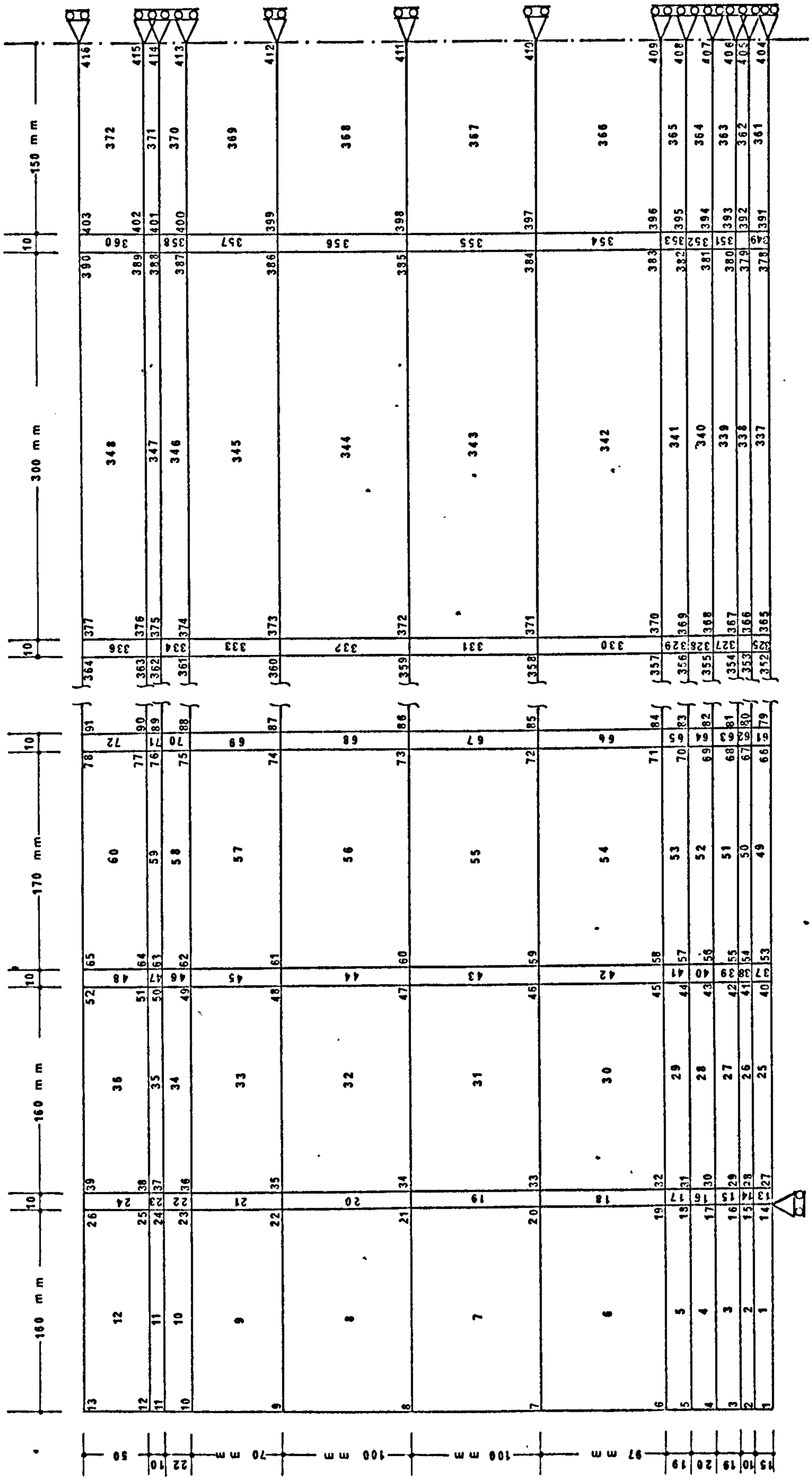

Fig. 7.8– Element and nodal numbring of elements 1 to 72 and 325 to 372 for analytical model of beam No. 19.

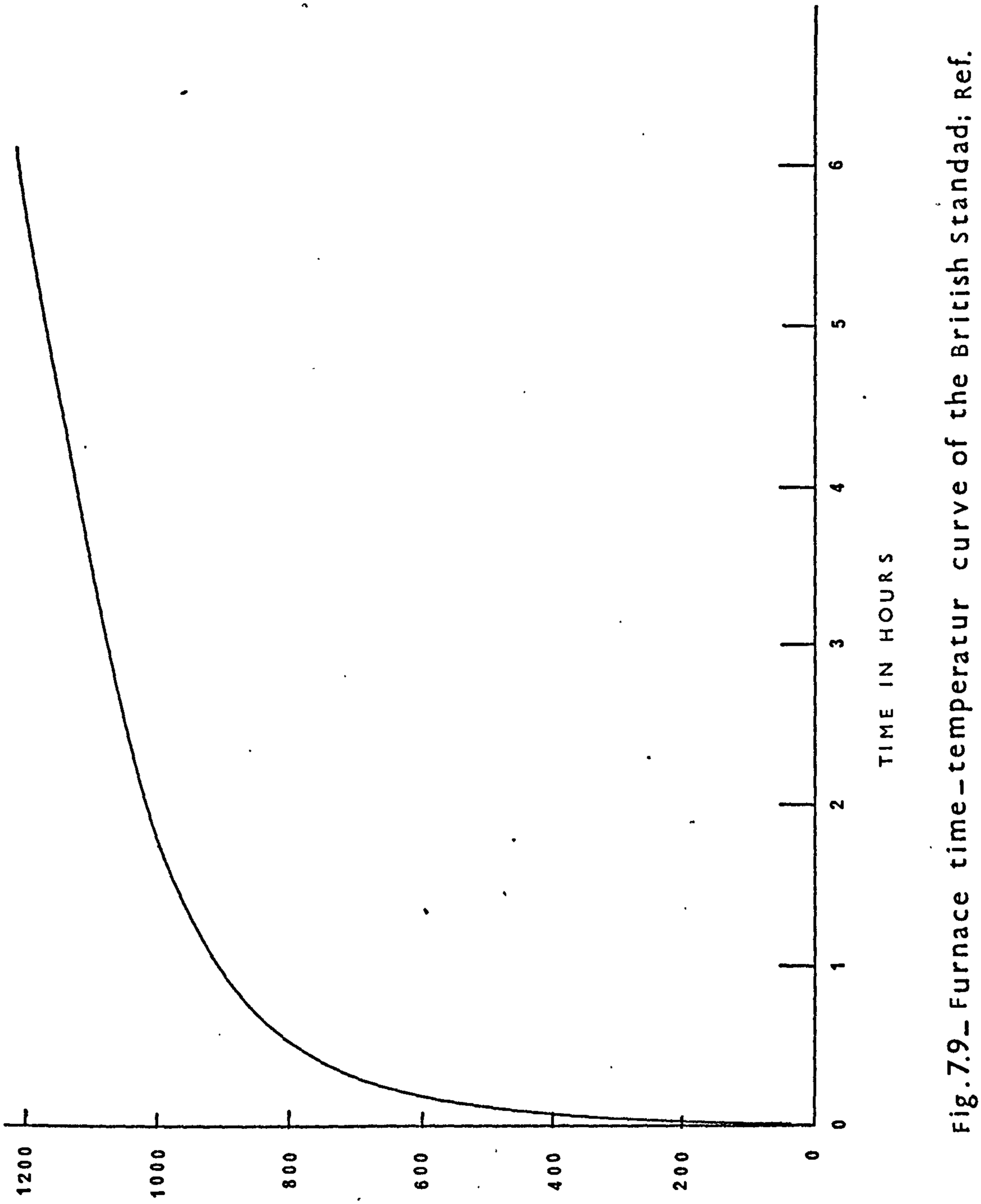
TEMPERATURE IN °C
1200
1000
800
600
400
200
0
0
1
2
3
4
5
6
TIME IN HOURS
Fig.7.9_ Furnace time-temperatur curve of the British Standad; Ref.

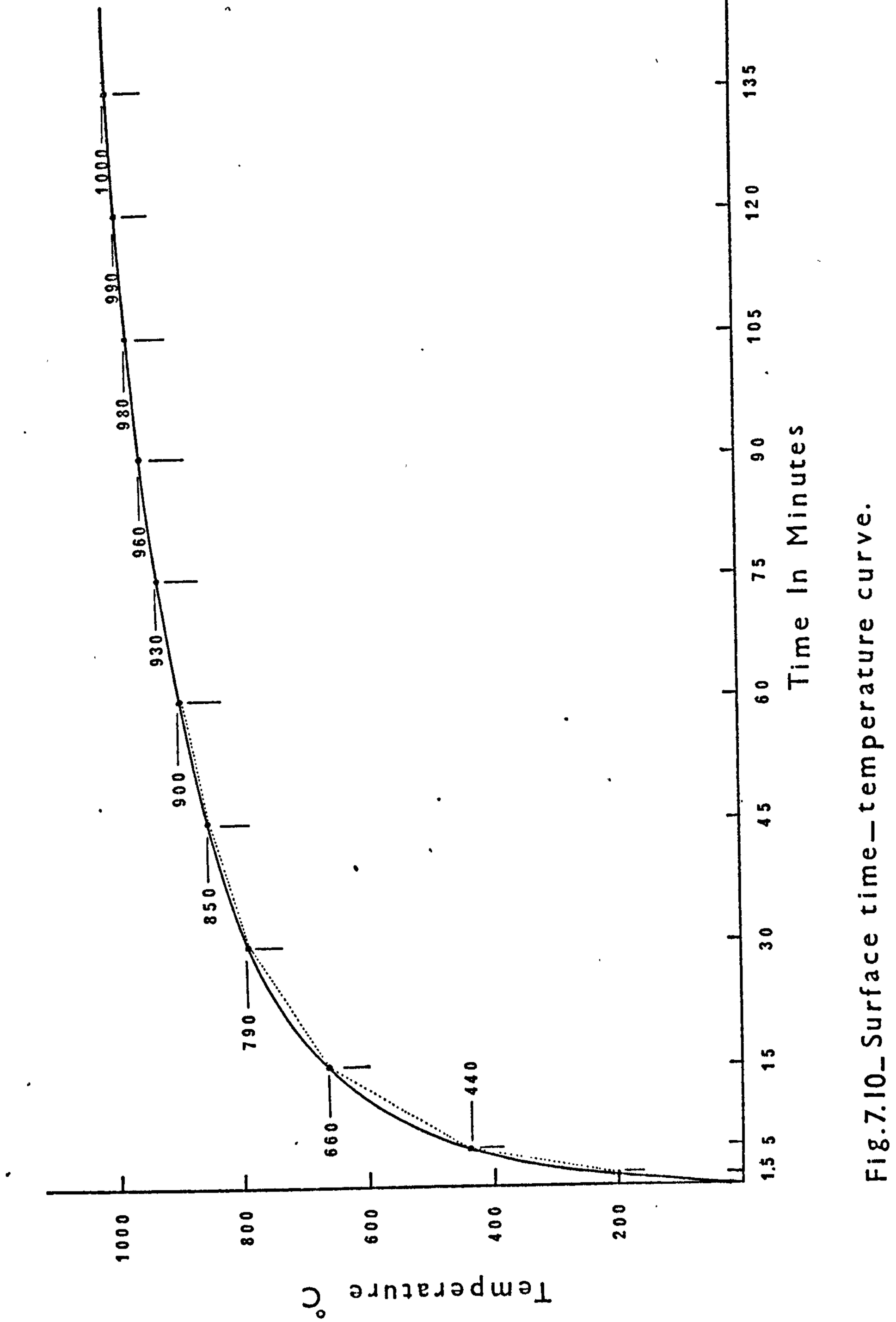

Fig.7.10_ Surface time—temperature curve.

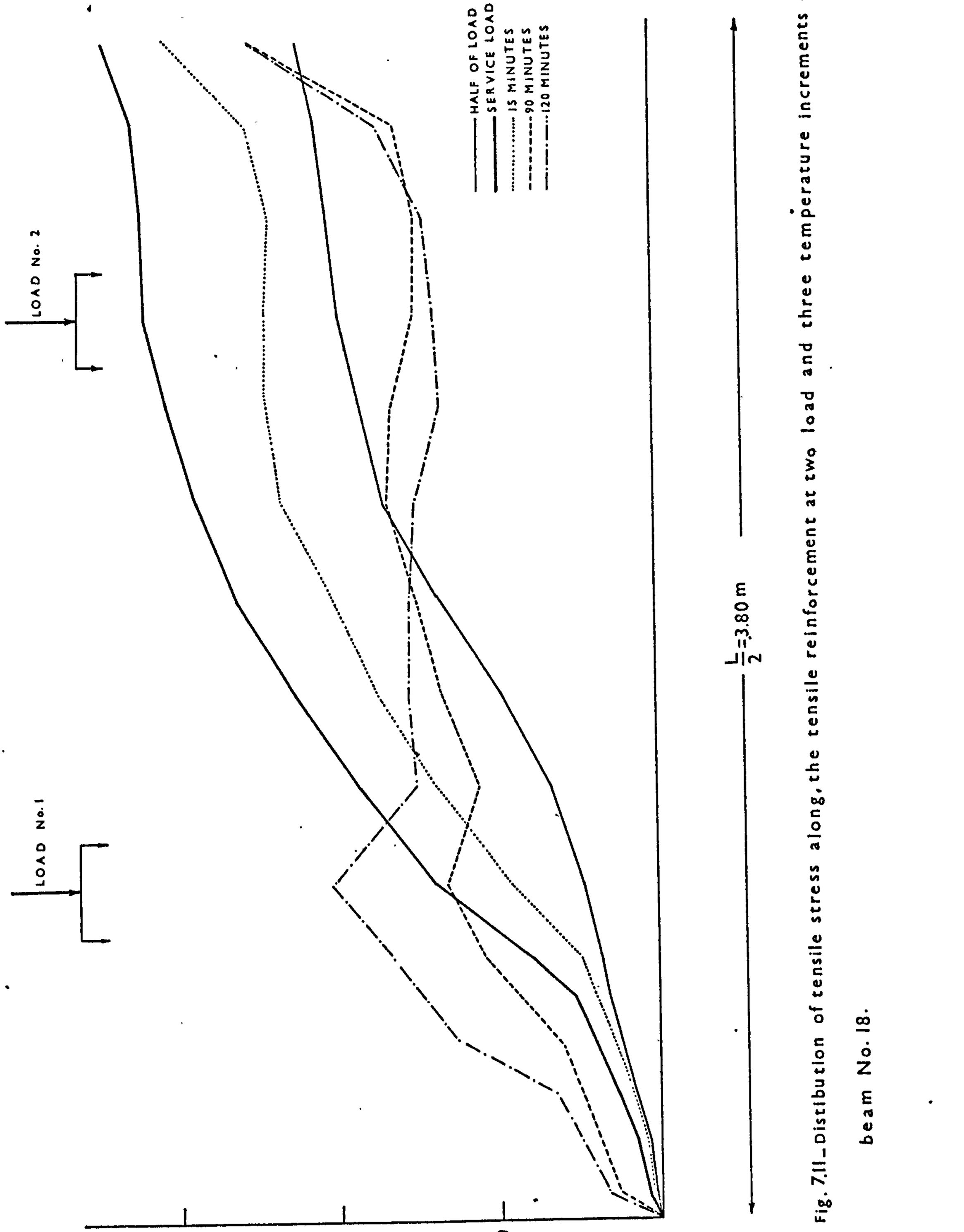

Fig. 7.11–Distribution of tensile stress along, the tensile reinforcement at two load and three temperature increments of beam No. 18.

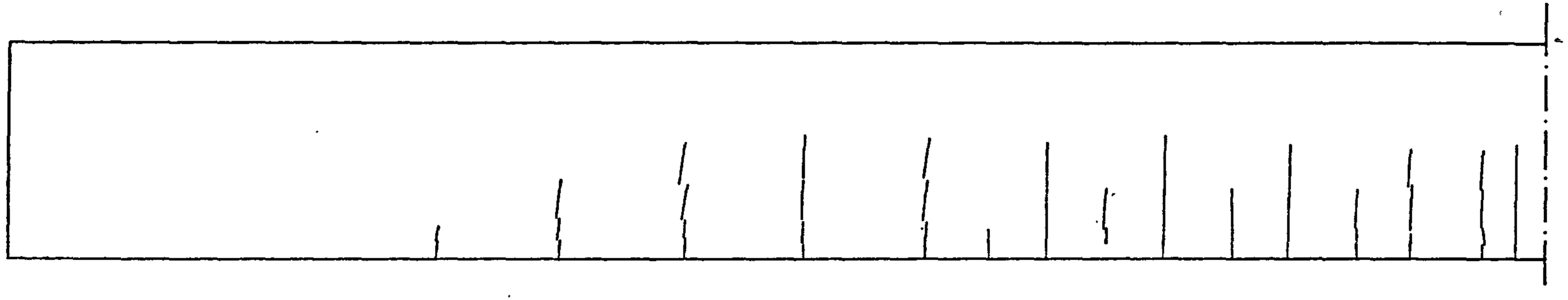

Fig.7.12_The propagation of cracks through the height of the beam No.18 under the service load.

Fig.7.13_The propagation of cracks through the height of the beam No.18 under the service load and up to 15 minutes heating.

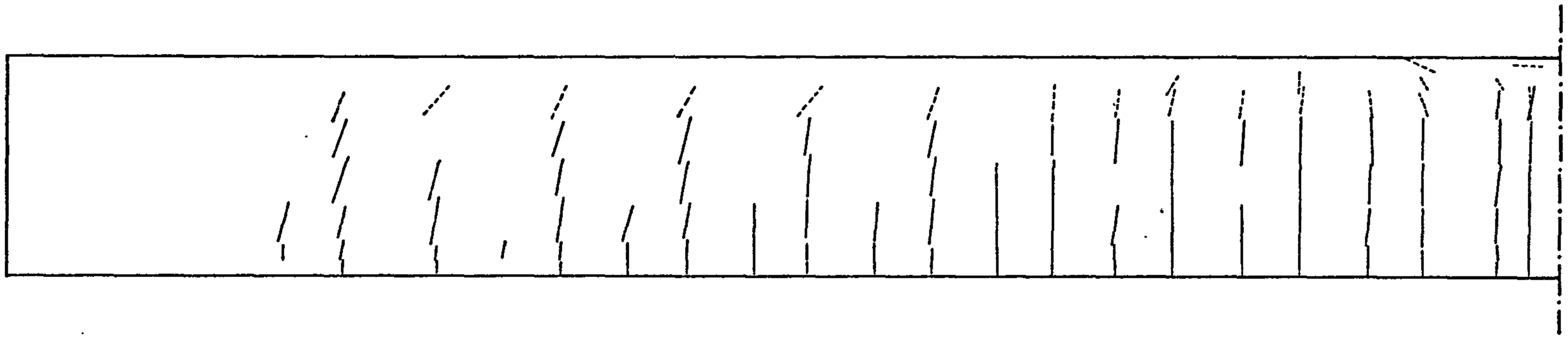

Fig. 7.14 – The propagation of cracks through the height of the beam No. 18 under service load and up to 90 minutes heating.

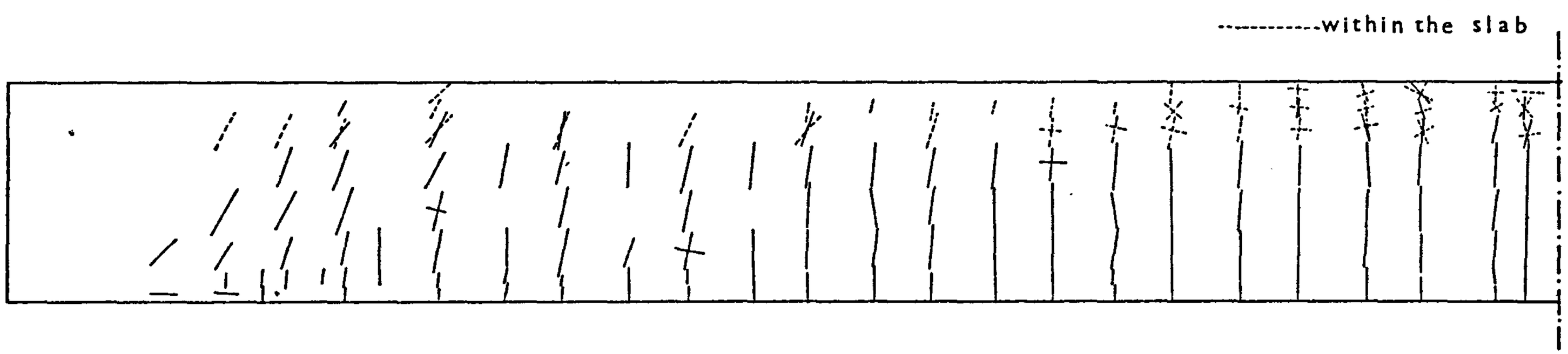

Fig. 7.15 – The propagation of cracks through the height of the beam No. 18 under service load and up to 120 minutes heating.

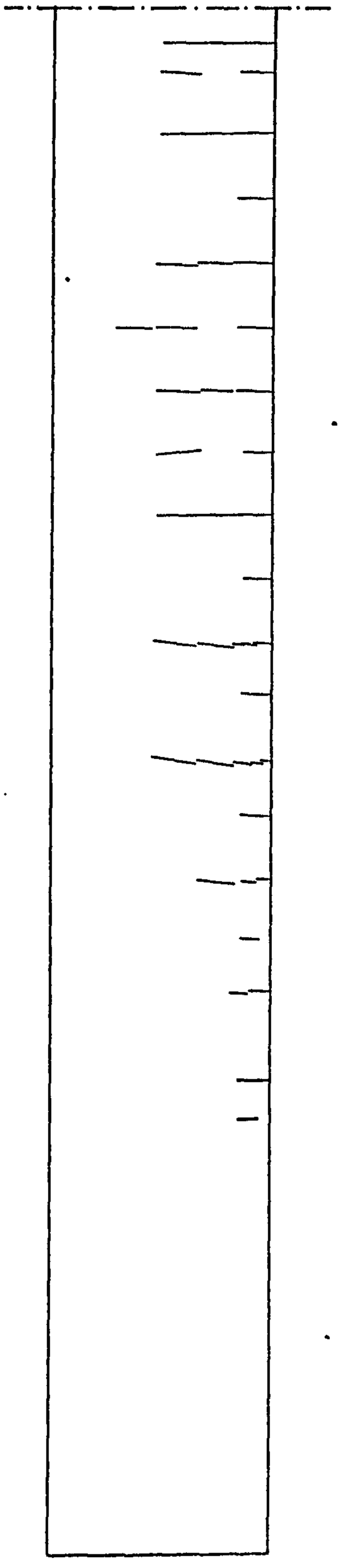

Fig.7.16– The propagation of cracks through the height of the beam No. 19 under service load.

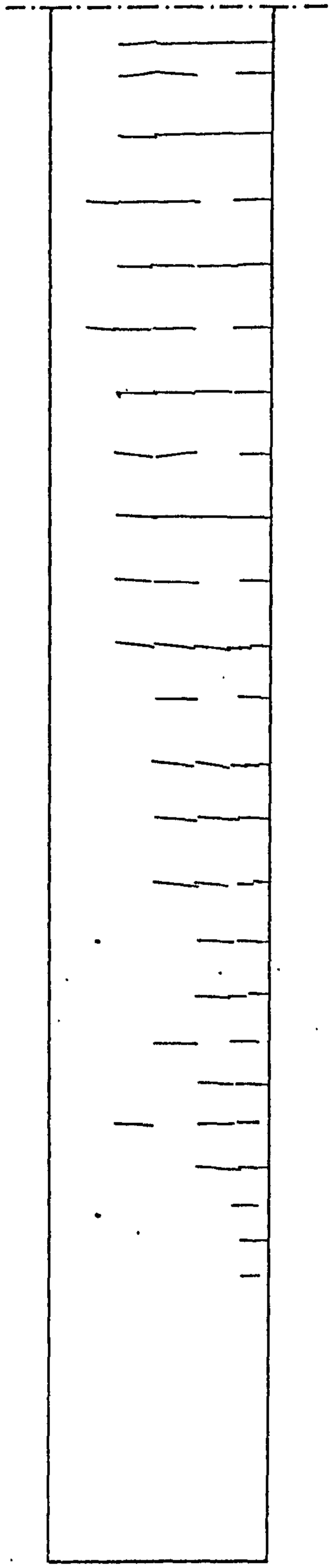

Fig.7.17–The propagation of cracks through the height of the beam No. 19 under service load and up to one hour heating.

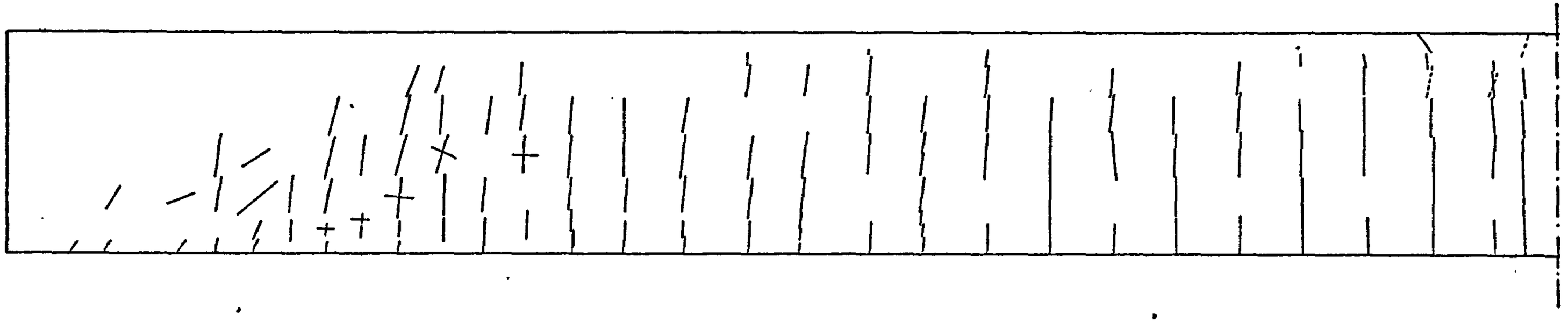

Fig. 7.18–The propagation of cracks through the height of the beam No.19 under the service load and up to two hour heating.

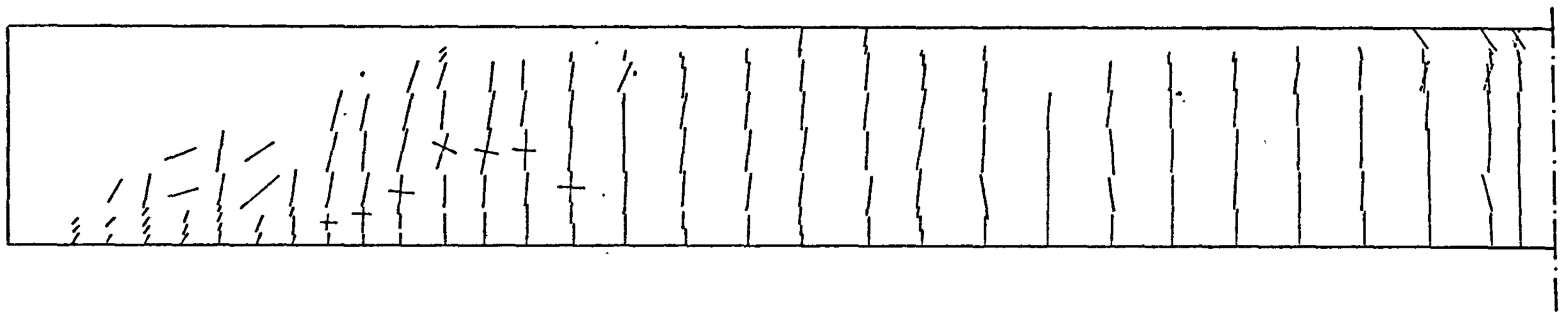

Fig.7.19–The propagation of cracks through the height of the beam No.19 under the service load and up to $2\frac{1}{2}$ heating.

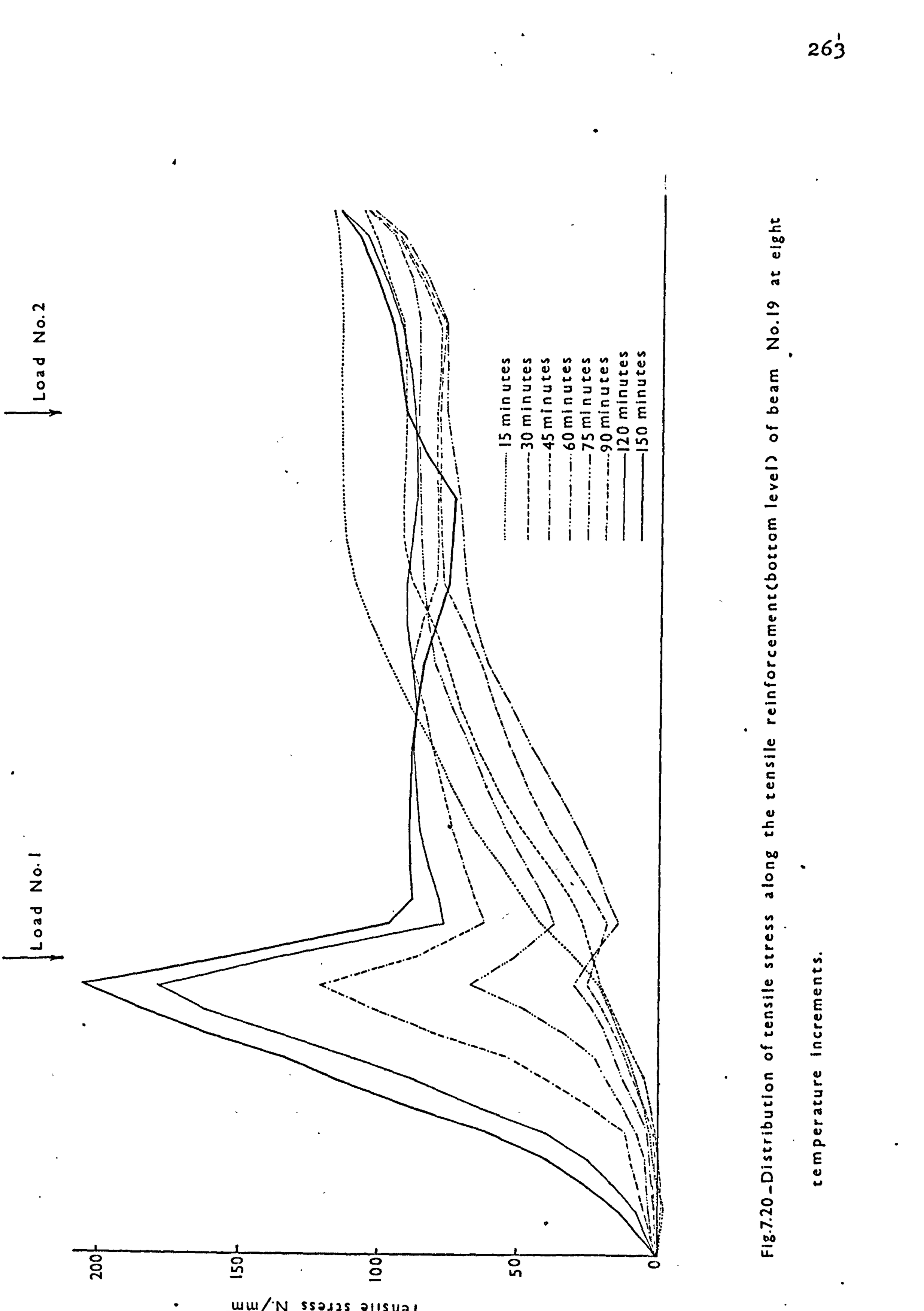

Fig.7.20–Distribution of tensile stress along the tensile reinforcement(bottom level) of beam No.19 at eight temperature increments.

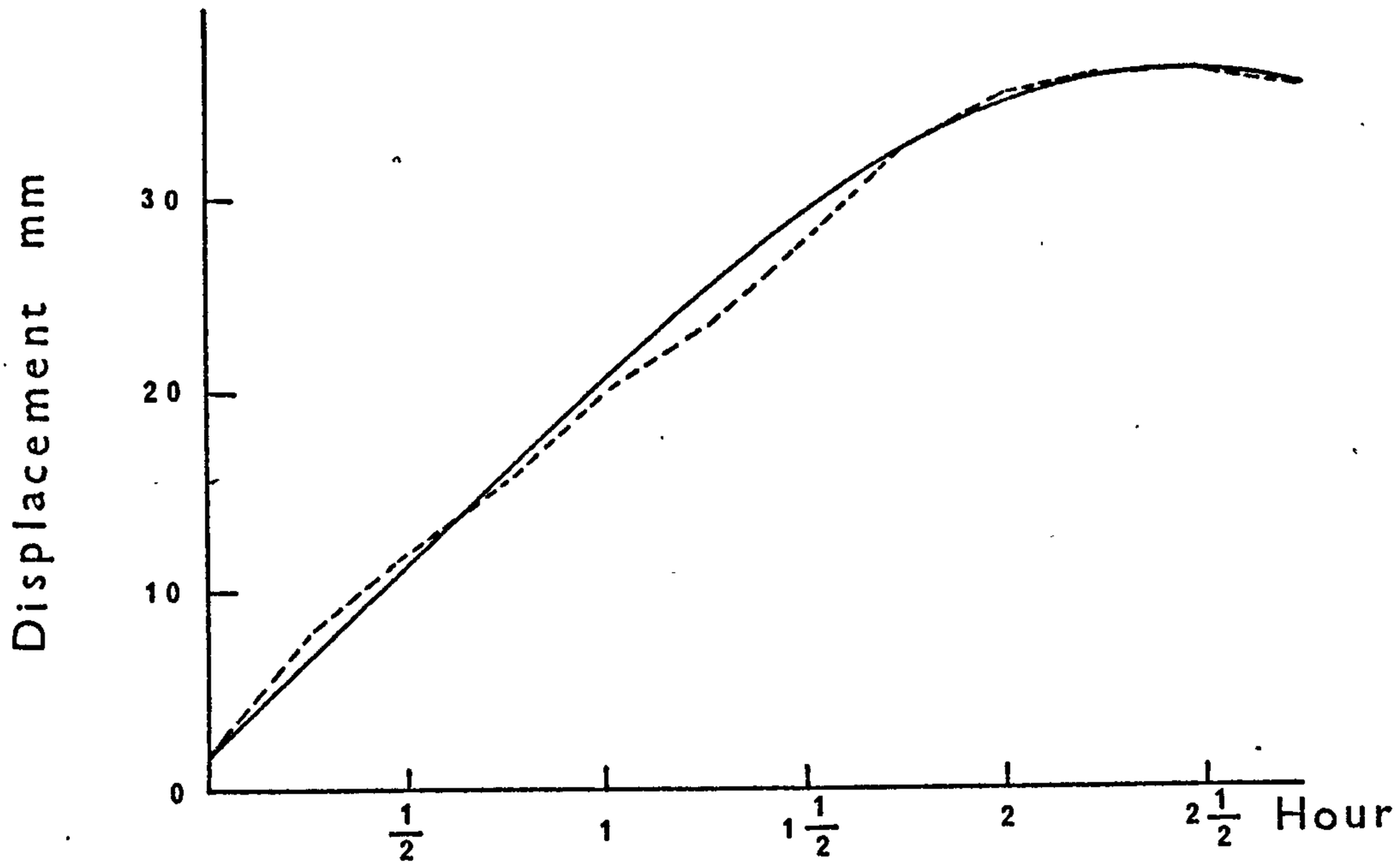

Fig. 7.21_Time—Displacement of the node at the support of the beam No. 19

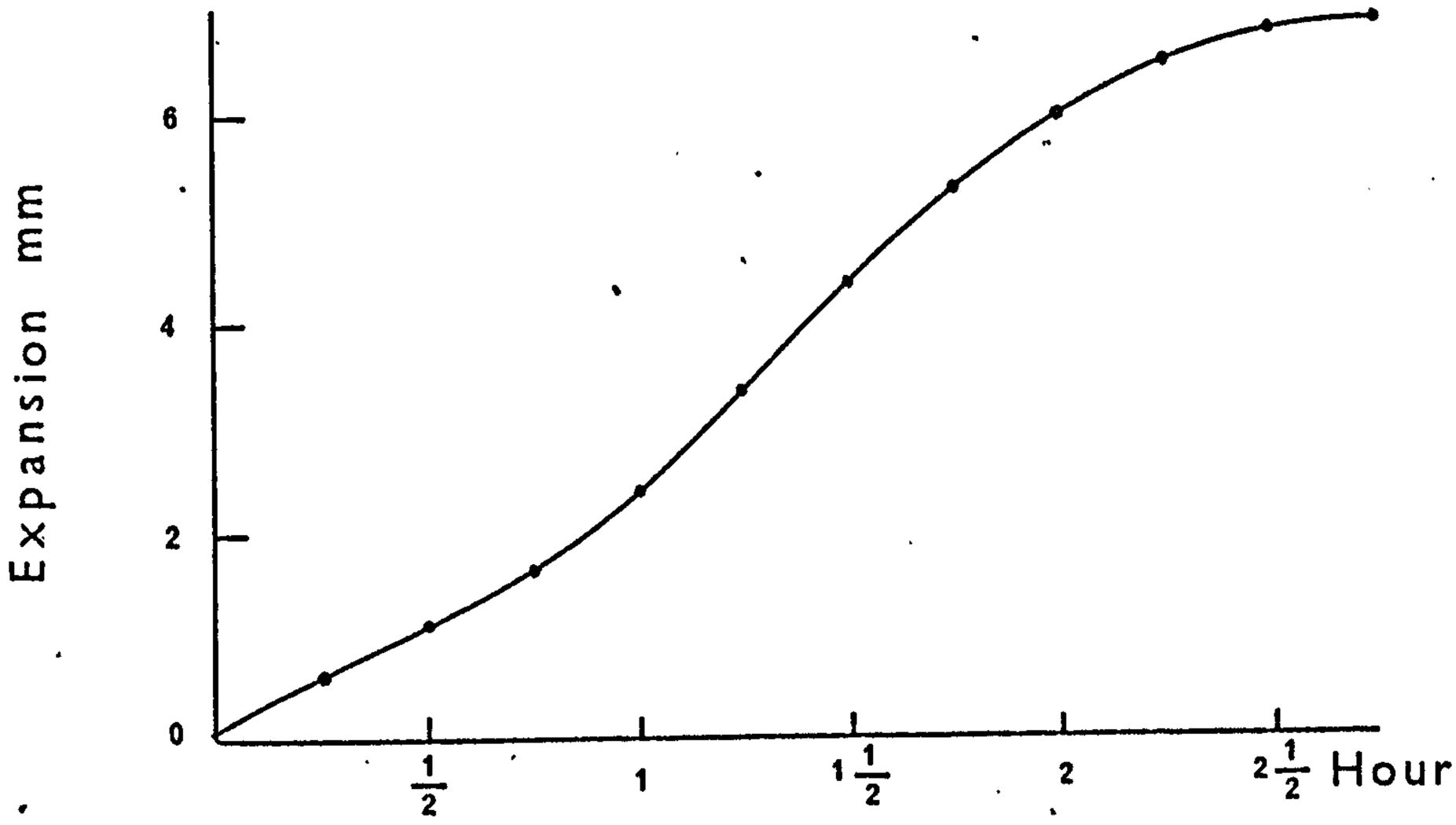

Fig. 7.22_Expansion of the middle section of the beam No. 19 in vertical direction.

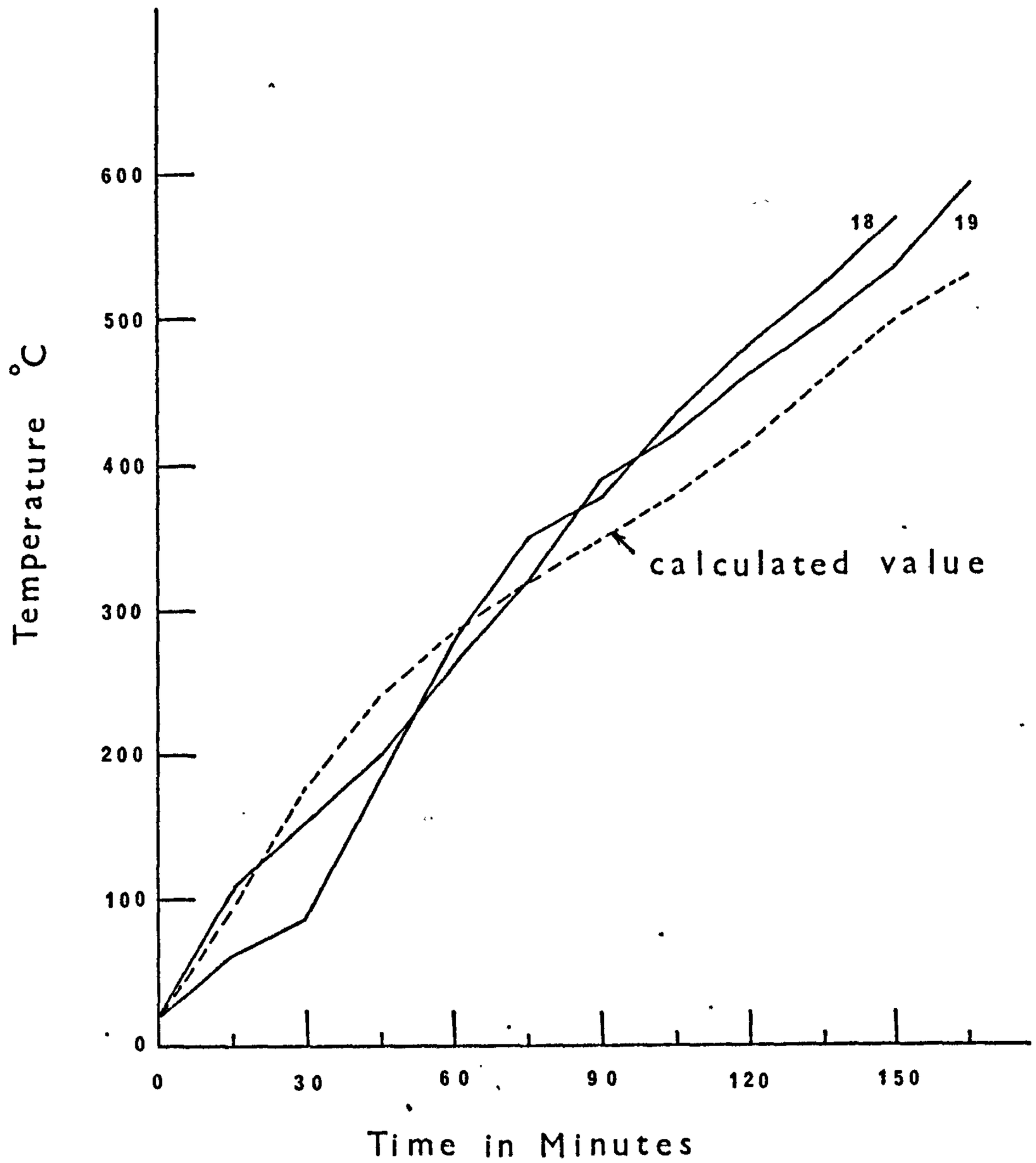

Fig. 7.23 — The experimental and analytical mean reinforcement temperature of the members.

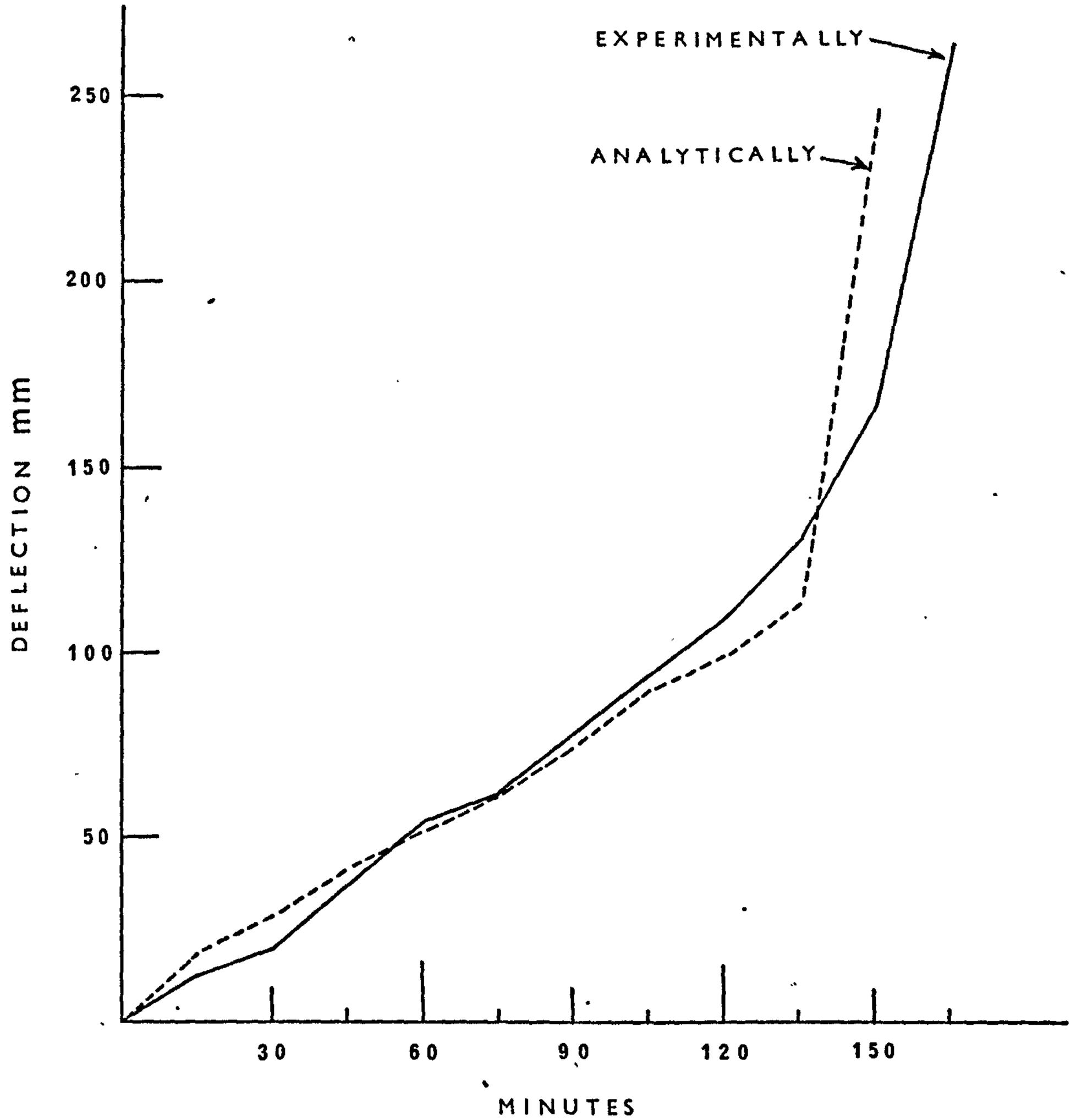

Fig. 7.24_Central deflection of beam No. 18; Ref. 93

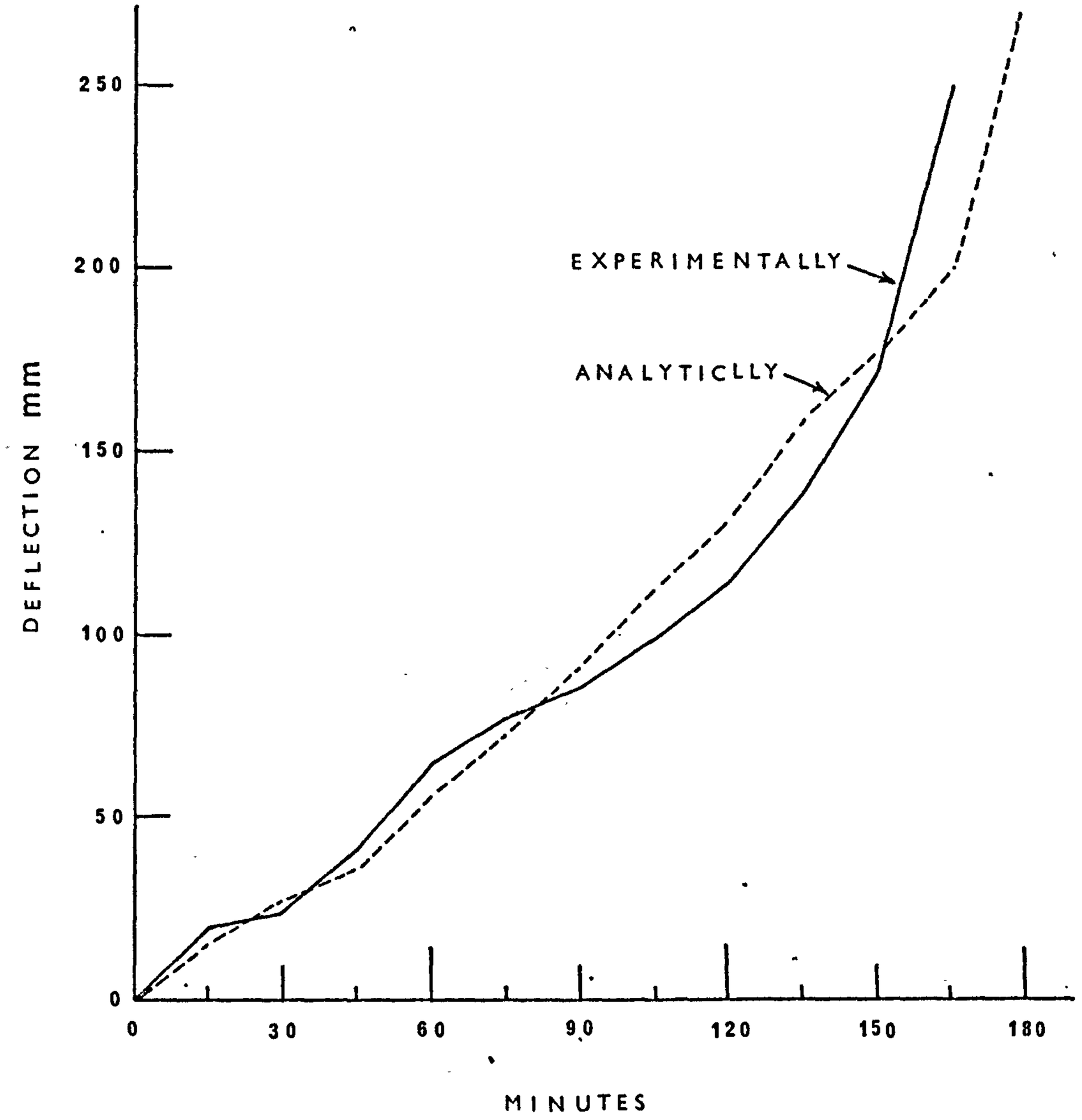

Fig. 7.25_Central deflection of beam No. 19; Ref. 93.

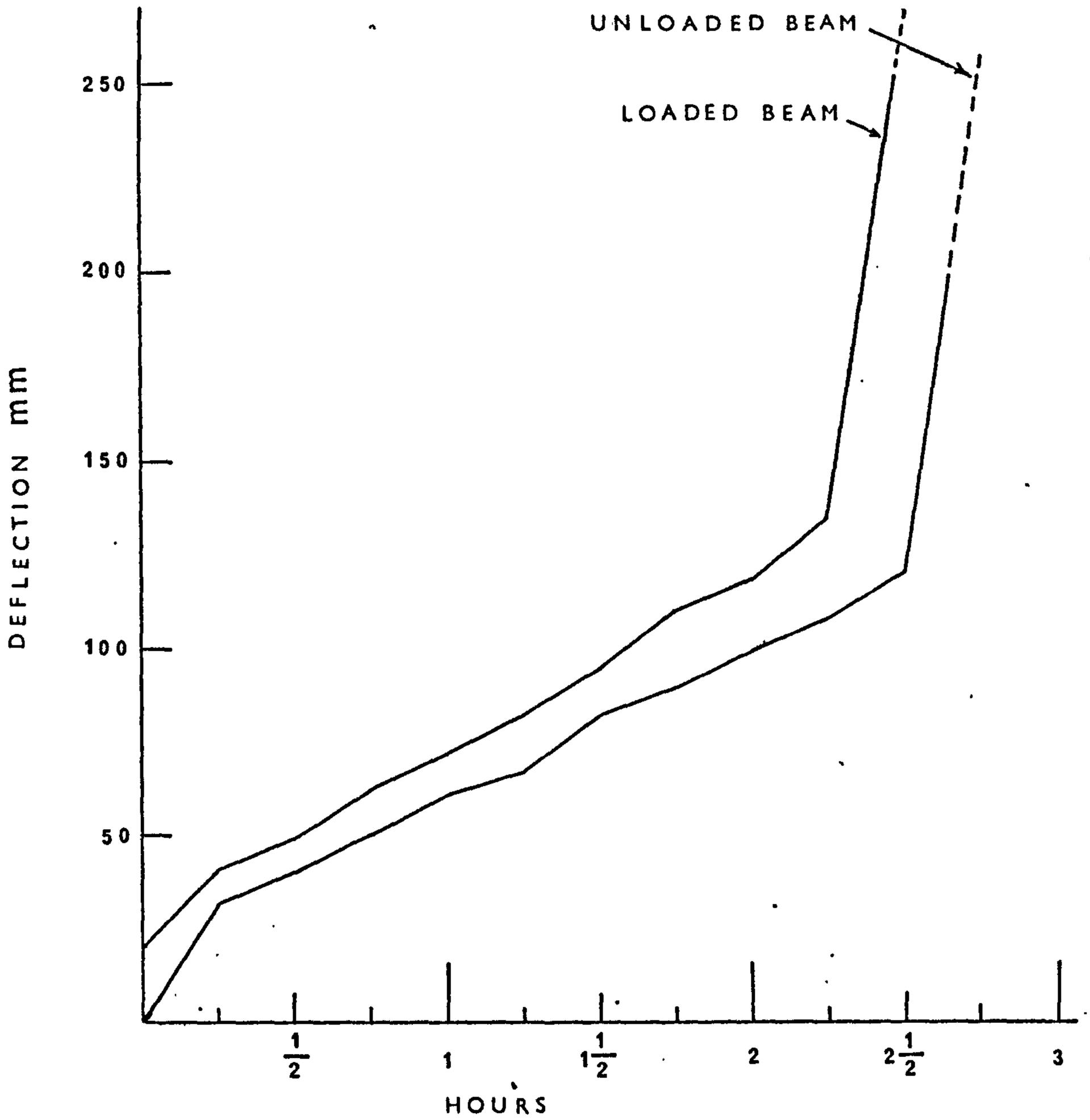

Fig.7.26_Central deflections of loaded and unloaded beam; No. 18.

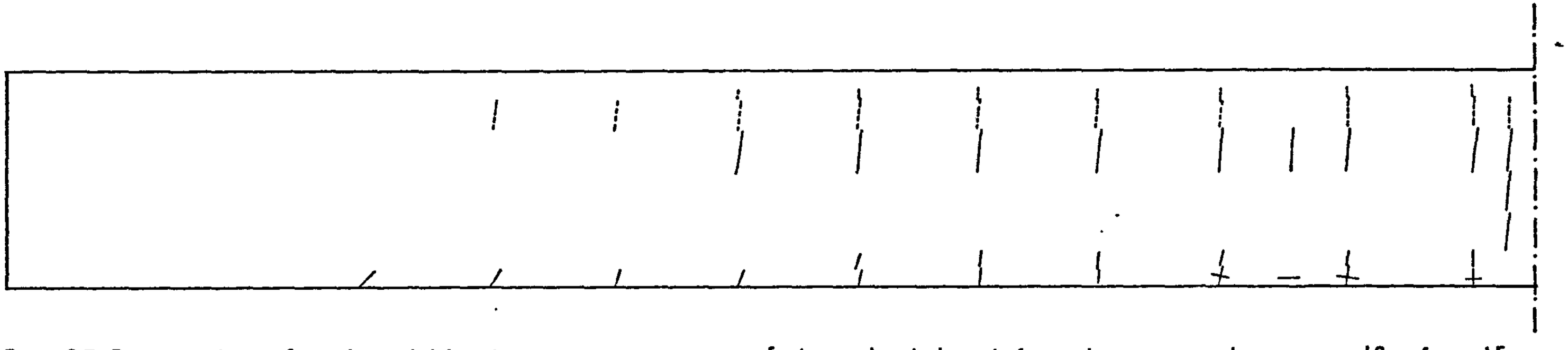

Fig. 7.27- Propagation of cracks within the concrete cover of the unloaded reinforced concrete beam; No. 18 after 15 minutes heating

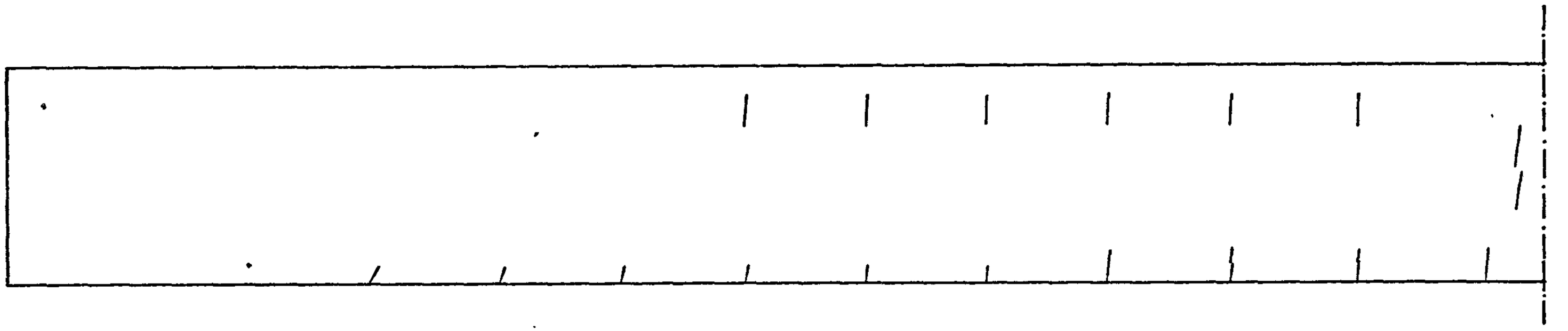

Fig. 7.28 - Propagation of cracks within the body (layers No. 4) of the unloaded reinforced concrete beam No. 18 under 15 minute heating.

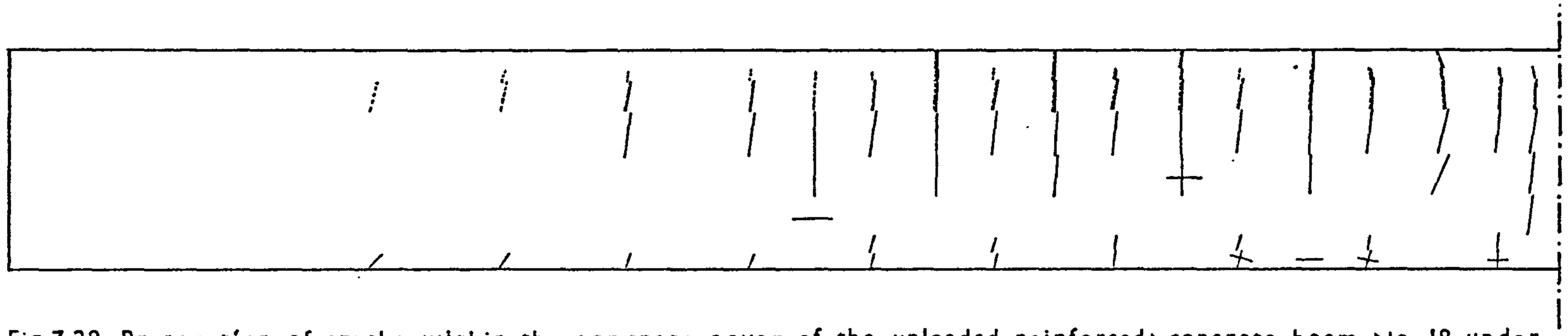

Fig.7.29_Propagation of cracks within the concrete cover of the unloaded reinforced concrete beam No. 18 under half an hour heating.

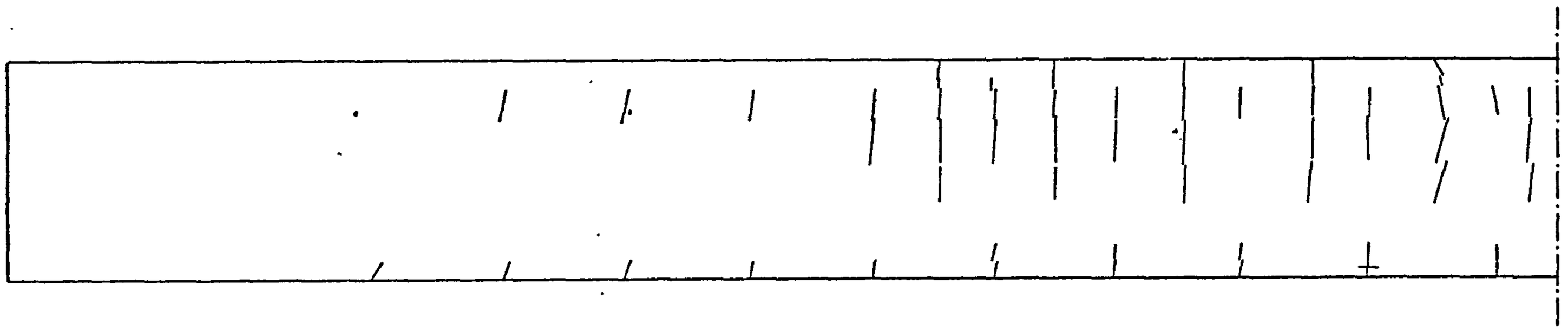

Fig.7.30_Propagation of cracks within the body (layers No. 4) of the unloaded reinforced concrete beam No. 18 under half an hour heating.

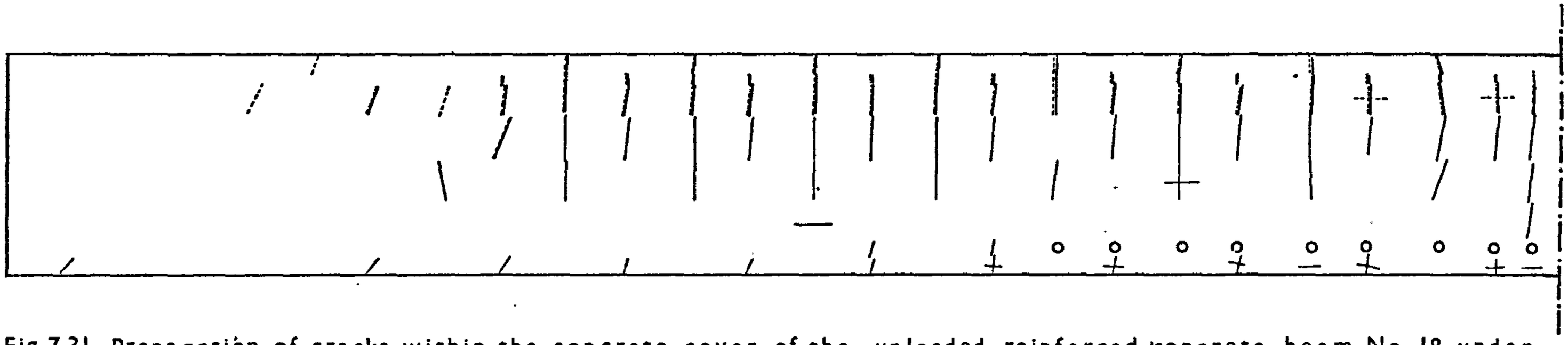

Fig.7.31_Propagation of cracks within the concrete cover of the unloaded reinforced concrete beam No. 18 under one hour heating.

o_crushed layers

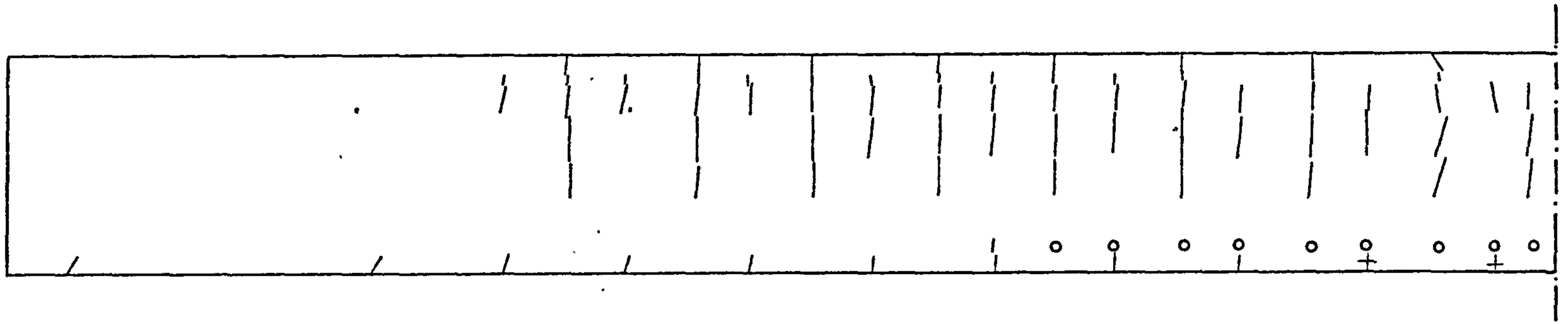

Fig.7.32_Propation of cracks within the body (layers No.4) of the unloaded reinforced concrete beam No. 18 under one hour heating.

o_crushed layers

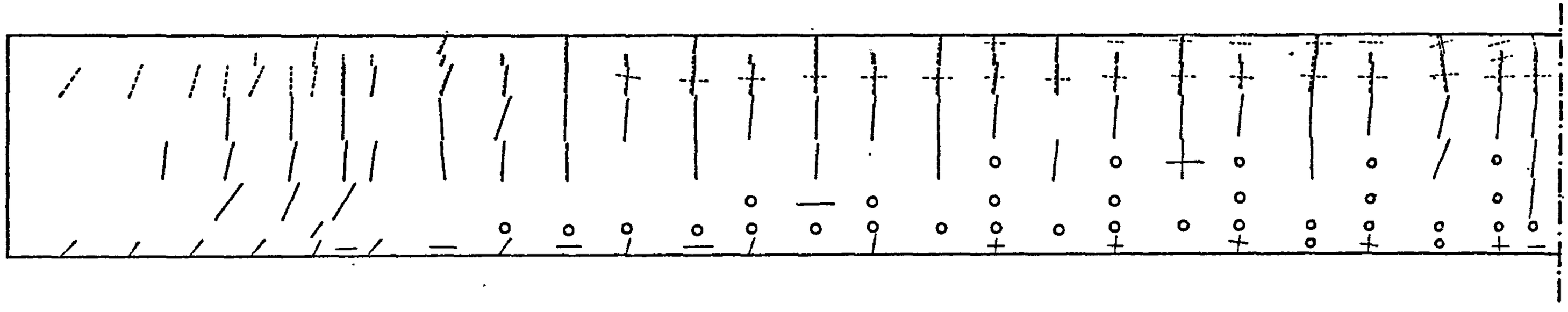

Fig.7.33_Propagation of cracks within the concrete cover of the unloaded reinforced concrete beam No. 18 under two hour heating.

o_crushed layers

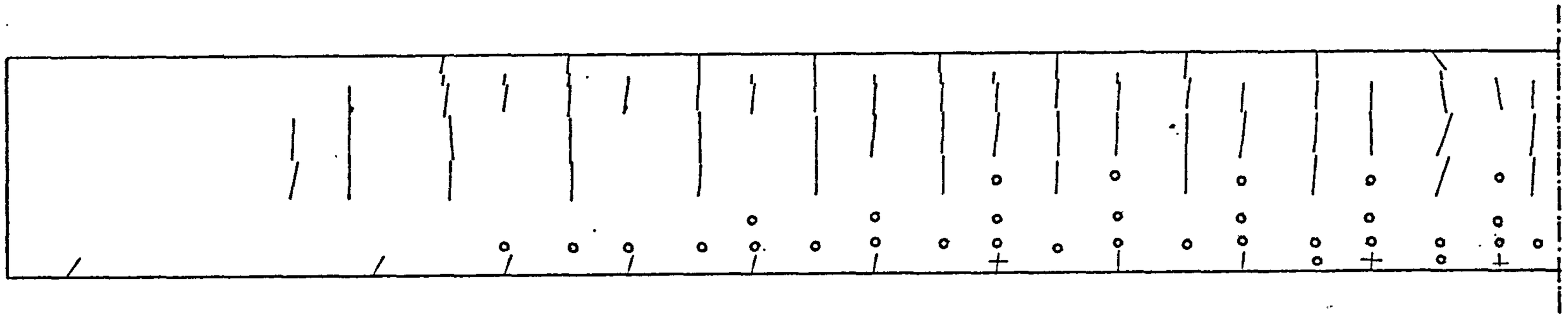

Fig.7.34_Propagation of cracks within the body (layers No.4) of the unloaded reinforced concrete beam No.18 under two hour heating.

o_crushed layers

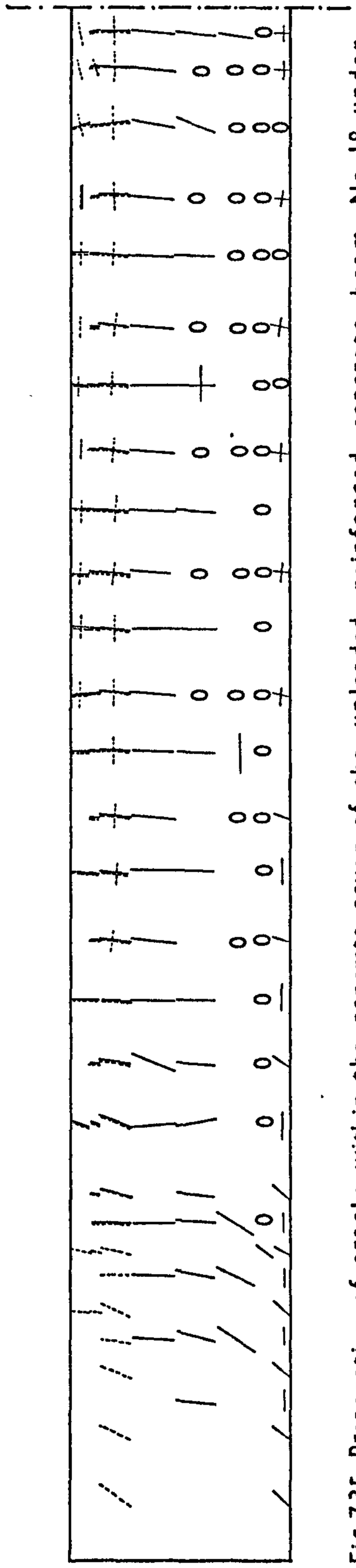

Fig.7.35_Propagation of cracks within the concrete cover of the unloaded reinforced concrete beam No.18 under $2\frac{3}{4}$ hour heating.

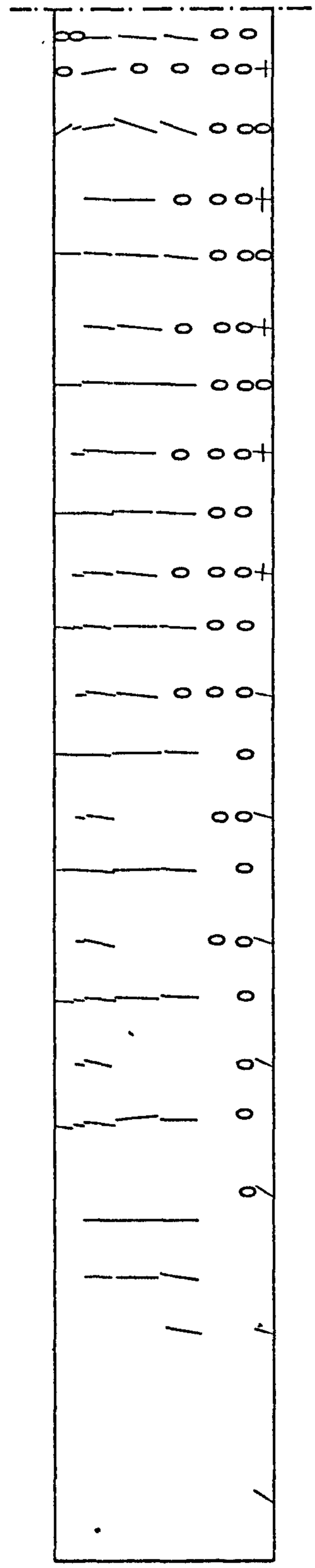

Fig.7.36_Propagation of cracks within the body (layers No.4) of the unloaded reinforced concrete beam No.18 under $2\frac{3}{4}$ hour heating.

0_collapsed

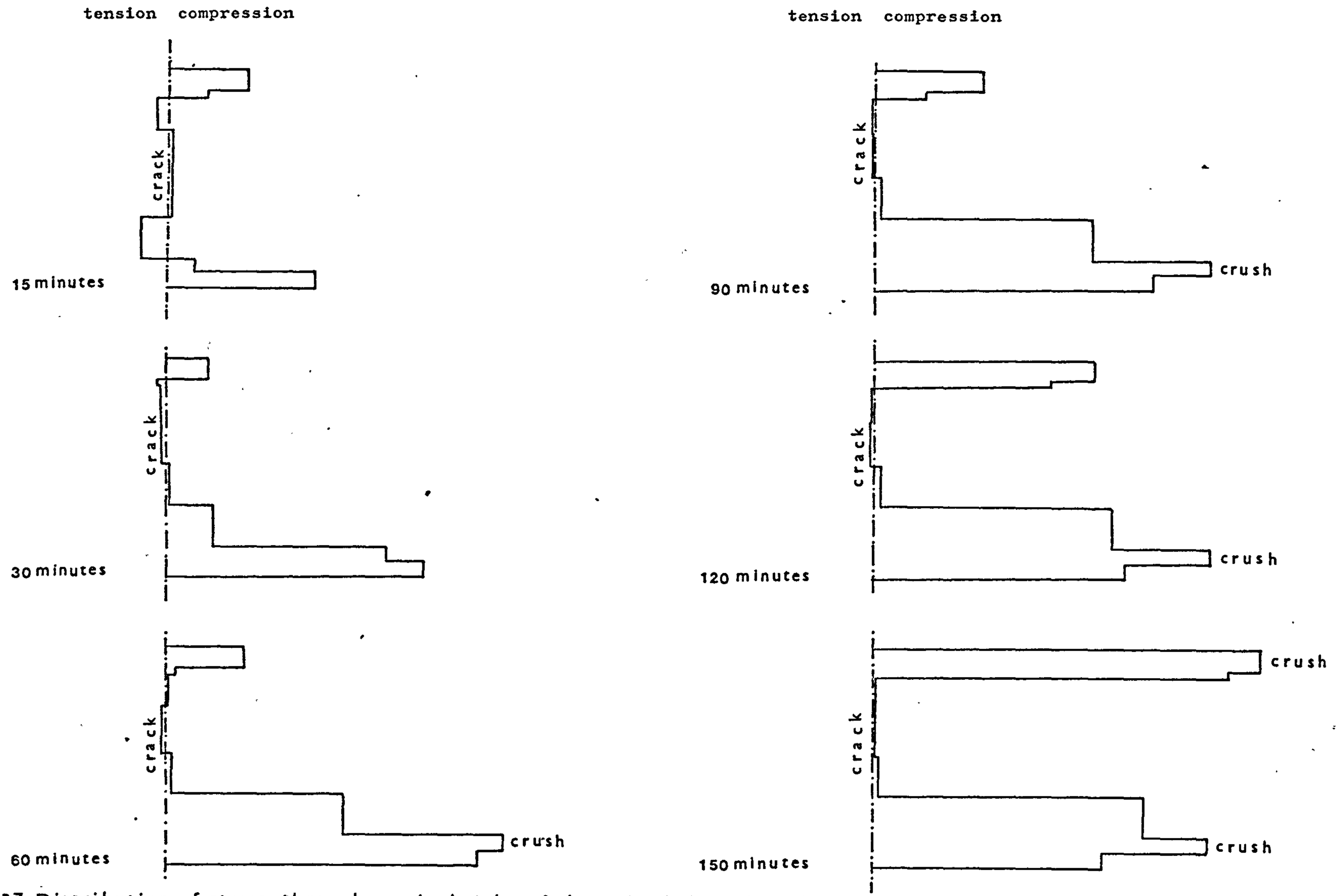

Fig. 7.37–Distribution of stress throughout the height of the unloaded reinforced concrete beam No. 18 at the middle of the body during the heating.

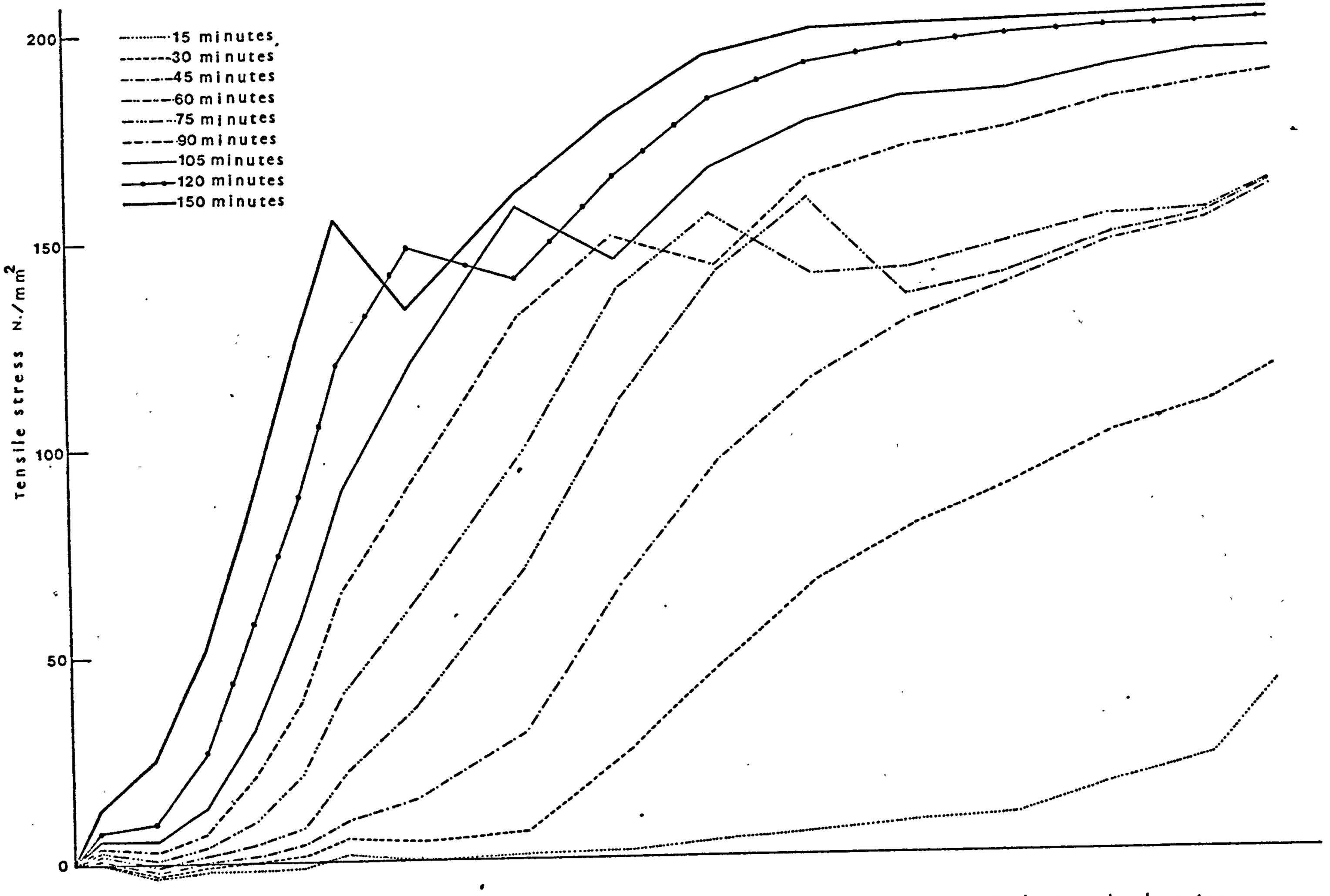

Fig.7.38_Distribution of tensile stress within reinforcement of unloaded beam No. 18 during the heating.

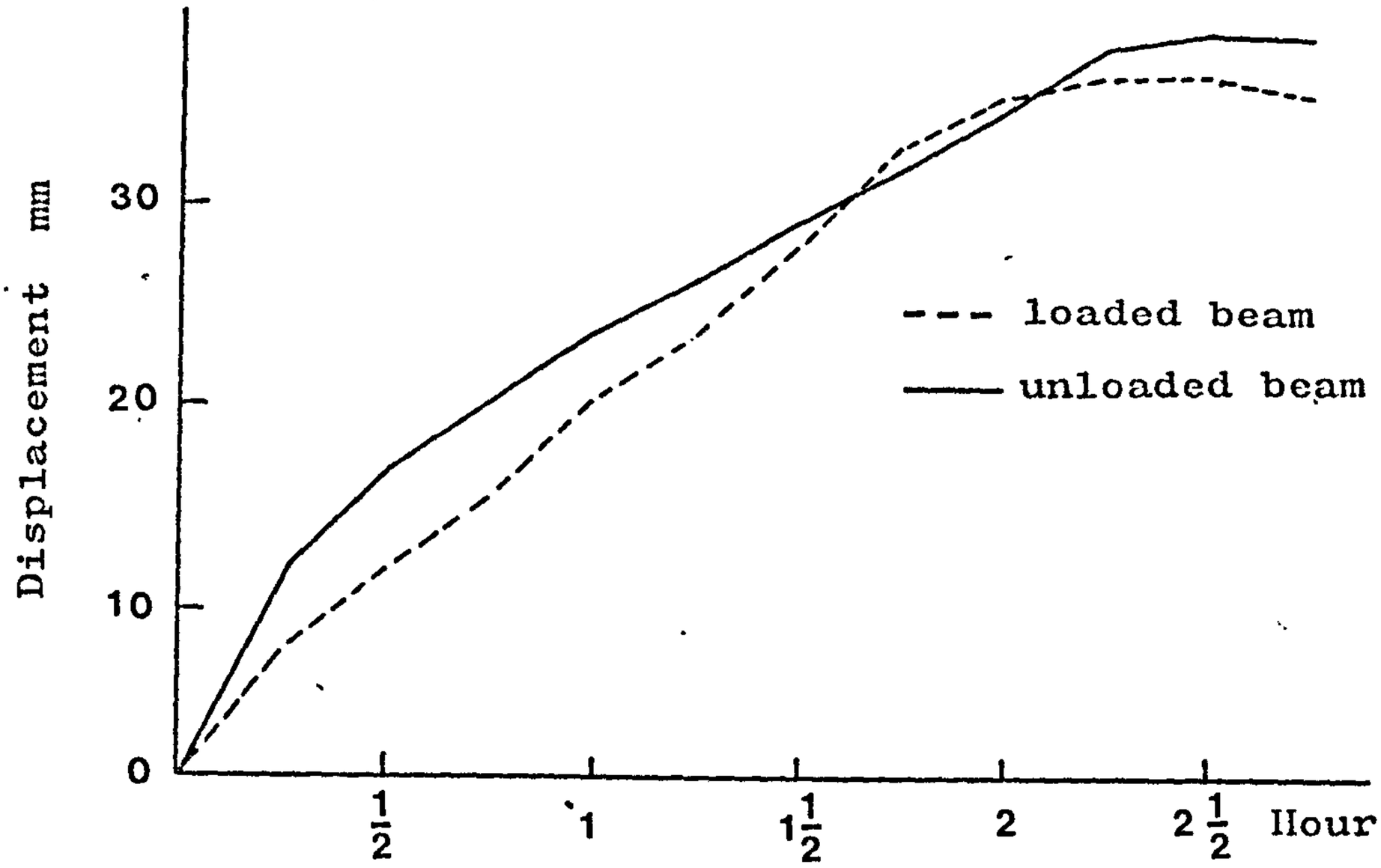

Fig. 7.39- Horizontal movement of the point at the support of unloaded beam, comparing with loaded beam.

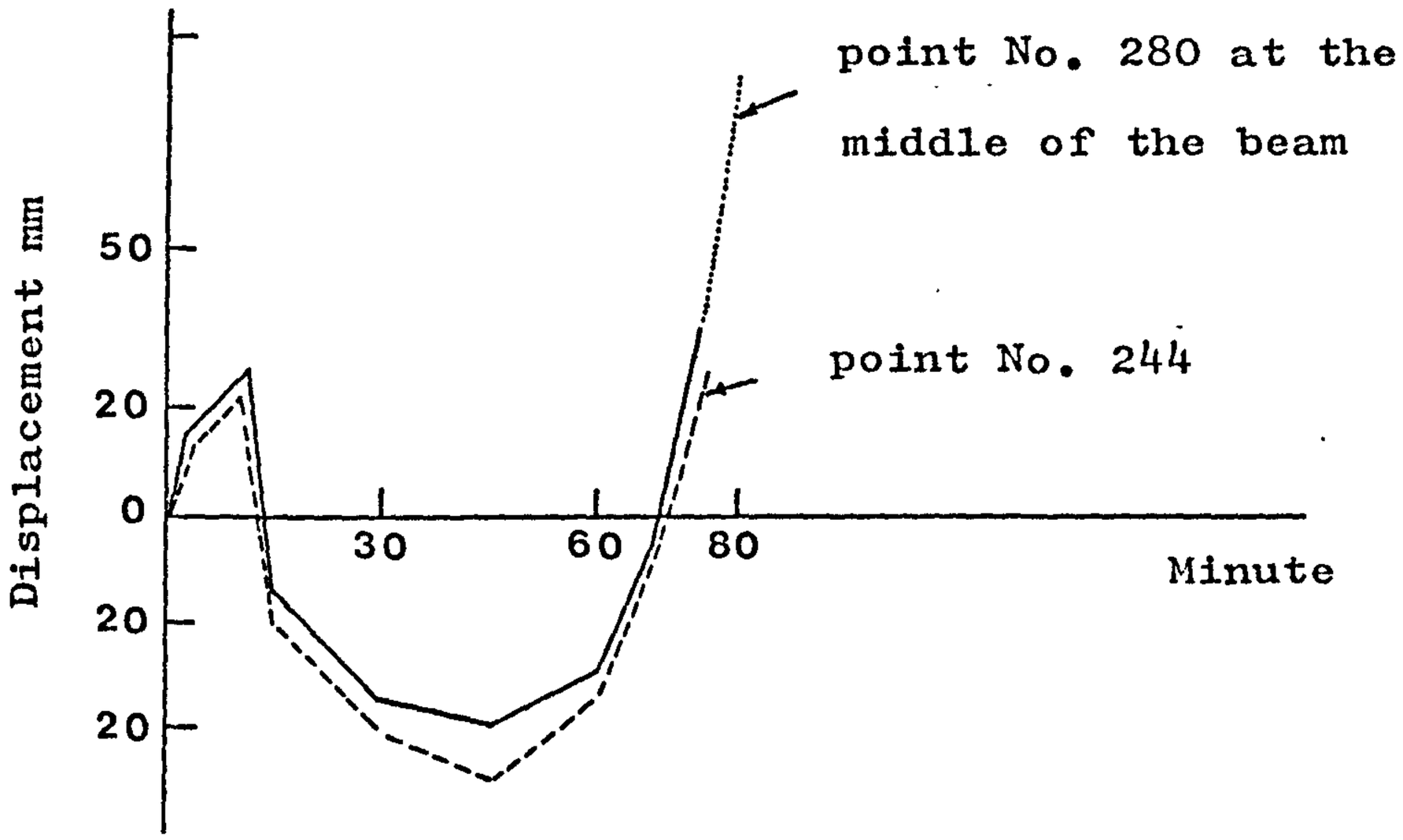

Fig. 7.40- Time-deflection relationships of points No. 280 and 244 of the unreinforced and unloaded beam subjected to fire.

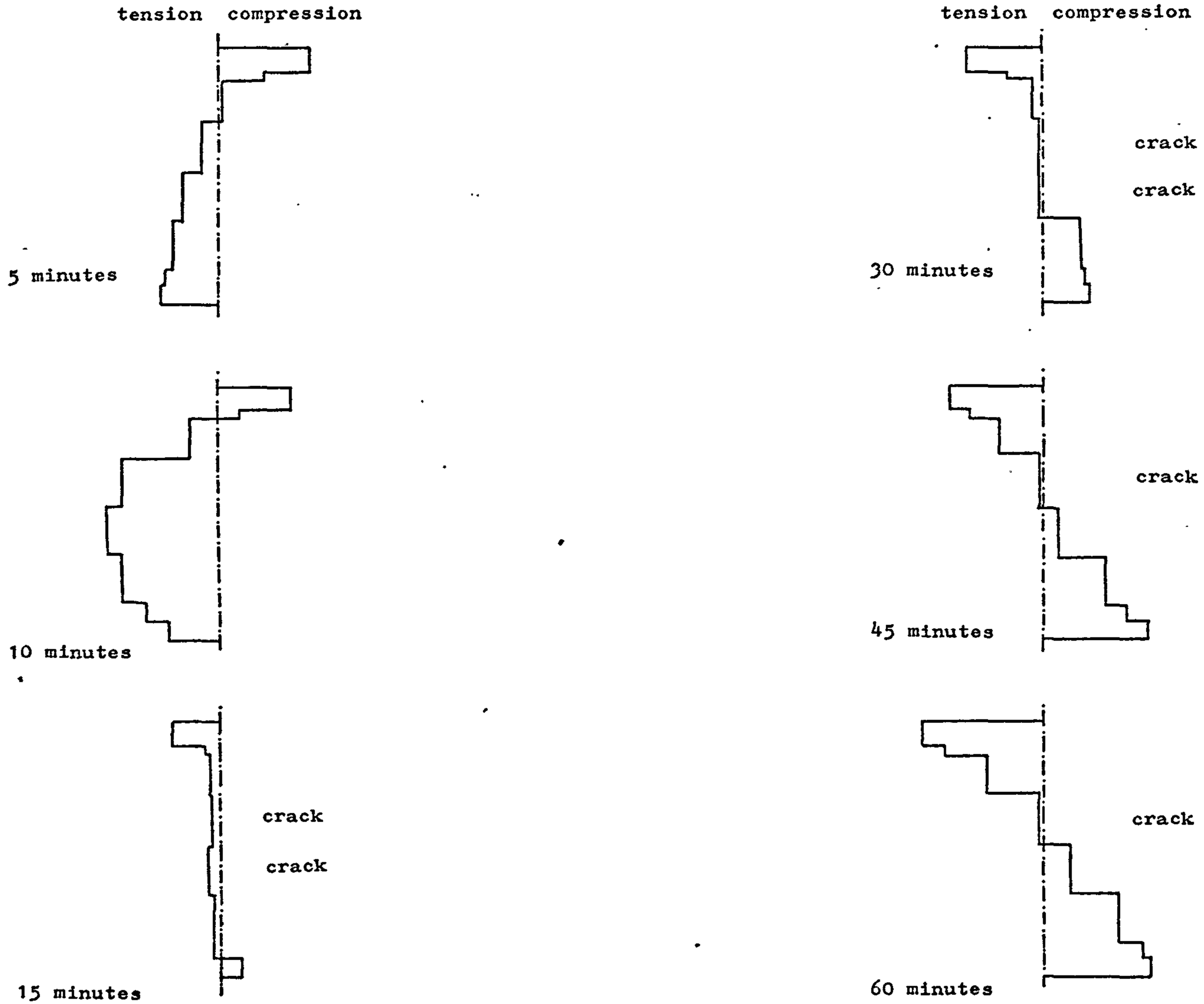

Fig.7.41- Distribution of stress throughout the height of the unreinforced and unloaded beam within the internal layers at the middle of the body during the heating.

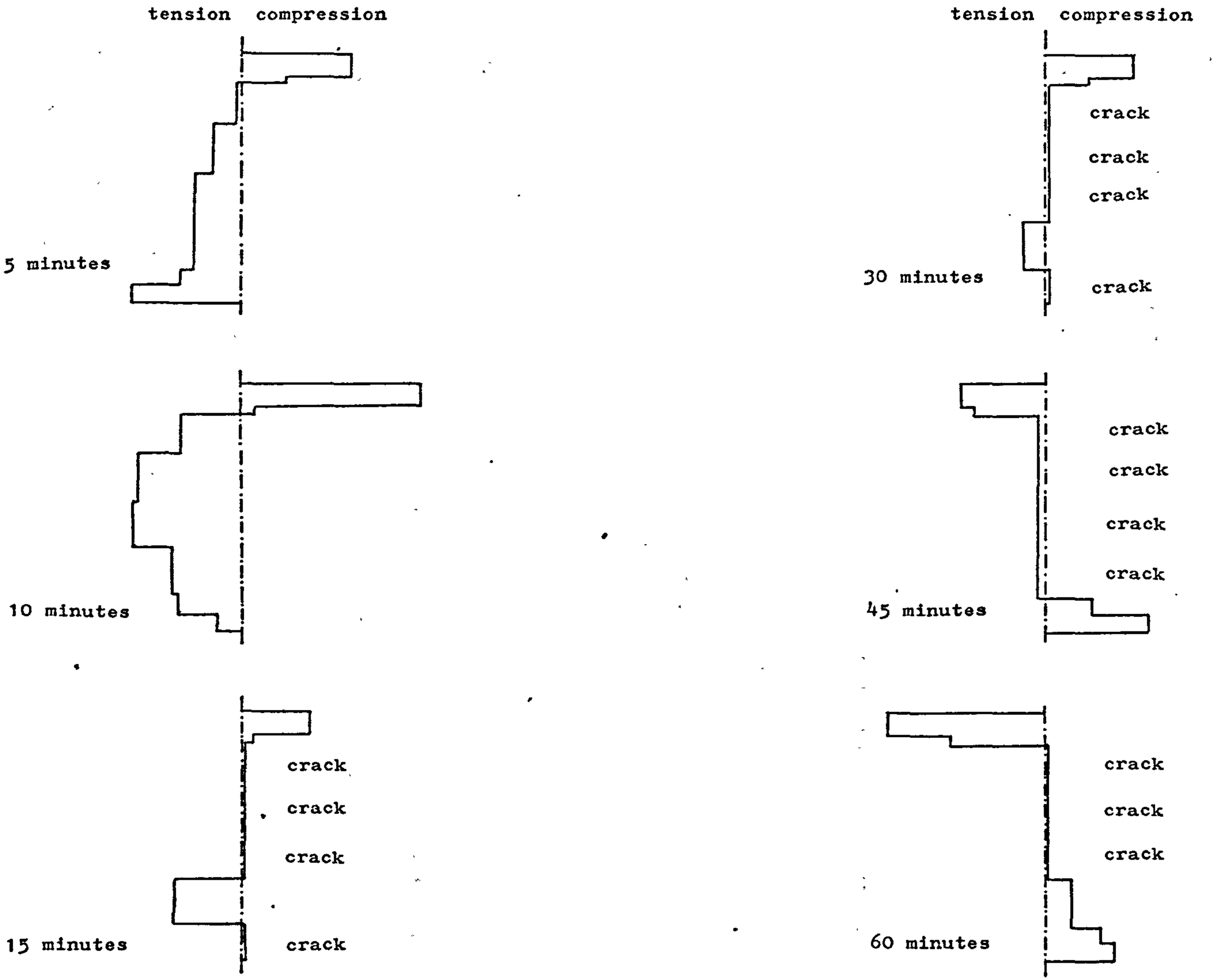

Fig.7.42- Distribution of stress throughout the height of the unreinforced and unloaded beam at section A-A 50 cm from the middle of the beam within the internal layers during heating

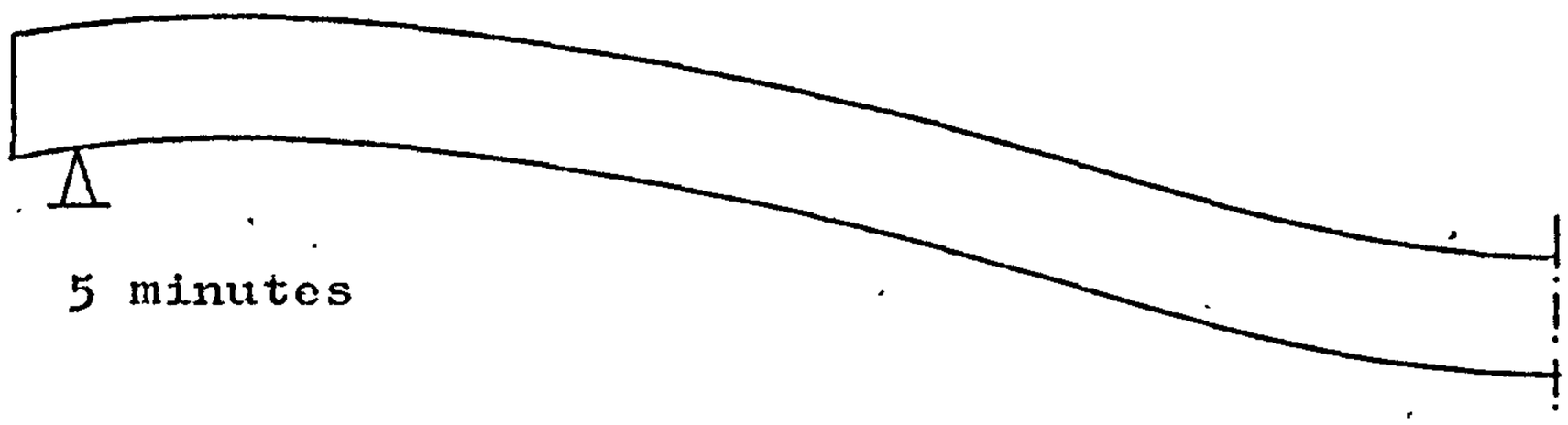

Fig. 7.43- Deflection of the unreinforced and unloaded beam subjected to fire (not to scale).

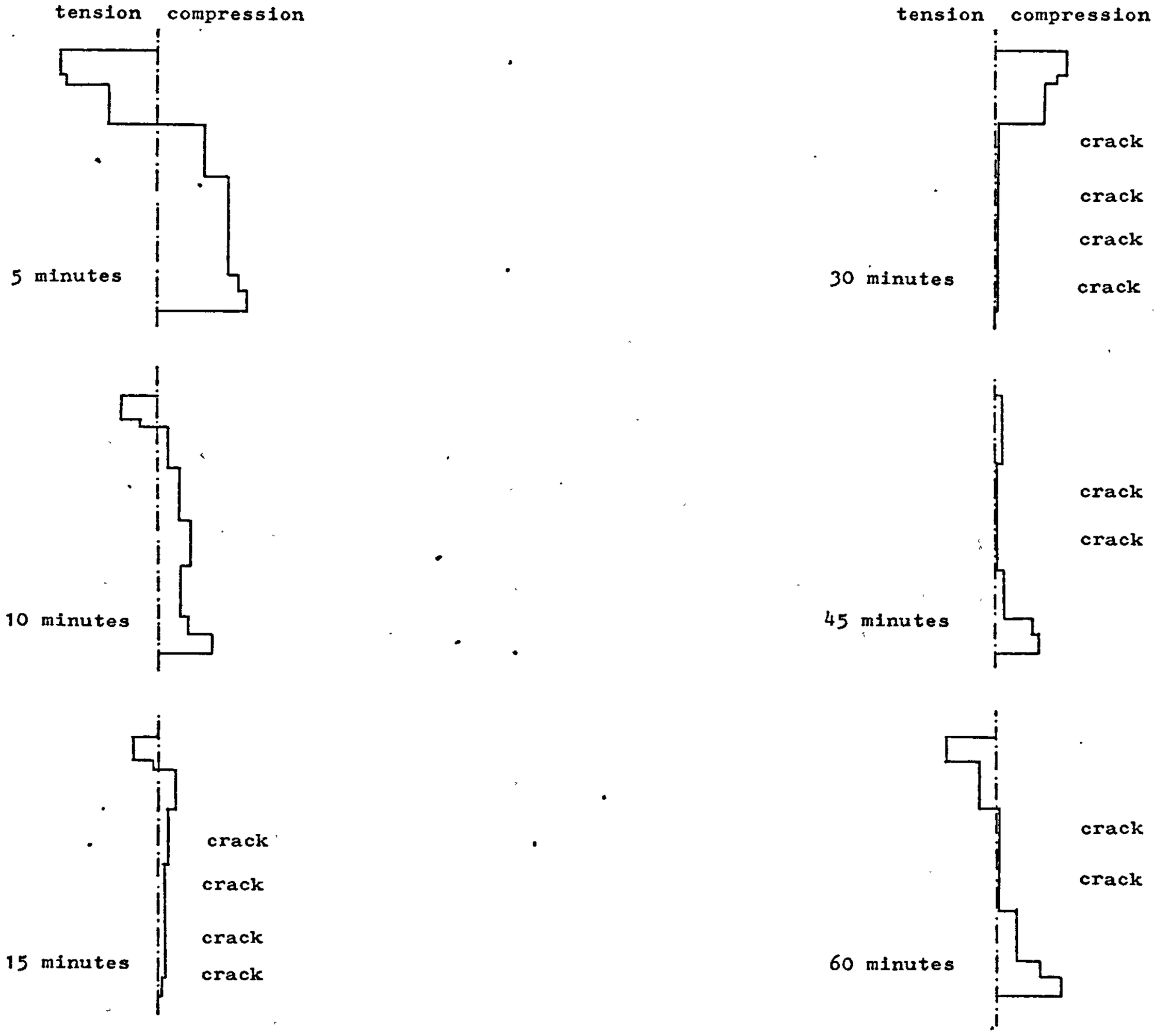

Fig. 7.44- Distribution of stress throughout the height of the unreinforced and unloaded concrete beam within the outer layers at the middle of the body during the heating.

CHAPTER EIGHT

IIX- Analysis Of Slabs

8.1- Object And Scope

The purpose of this chapter is to obtain analytically the behaviour of reinforced concrete slabs under uniform distributed load and high temperature. A rectangular slab, simply supported along all edges and subjected to a uniform distributed load was designed, and the analytical model of this slab was loaded incrementally up to the design load, followed by an increase in temperature similar to the condition applied to the analytical models of beams in chapter seven. The distribution of temperature within the body was calculated with the help of equation (6.52), with the difference that, the surface temperature at the edges of the slab was assumed to be $\frac{3}{4}$ of the maximum value of surface temperature which appeared at the centre of the boundary.

Since no experimental evidence of loads deflections etc. at elevated temperature was available, the SLAB program was checked by introducing an input suitable for a long narrow slab and then using the BEAM program with the same input. The output for both examples gave very similar results.

The SLAB program is capable of analysing rectangular reinforced or unreinforced concrete slabs with any boundary restraints and surface temperature as described in chapter five and six.

8.2- Analytical Model Of The Slab

A rectangular slab with a length of 500 cm., width of 360 cm. and depth of 12.5 cm. i.e. a span/depth ratio of 40 was used as the model.

The weight of concrete was taken as 2400 kg/m^3 giving a self weight of 3 kN/m^2. Taking a characteristic live load of 7.5 kN/m^2 with a live load factor of 1.6 and the dead load factor of 1.4, the ultimate design load (w) is calculated as;

$$w = 1.4\ w_d + 1.6\ w_l = 16.2\ kN/m^2$$

By reinforcing the slab orthotropically the steel area in the two orthogonal directions, for the average effective depths of 10.75 cm. and 10.50 cm. were A_1 = 1539 mm^2 and A_2 = 794 mm^2, respectively. A good structural grade of 30 N/mm^2 was used for the concrete and a high tensile strength for the steel reinforcement of 420 N/mm^2.

The slab was divided into eight layers throughout the thickness as shown in figure (8.1). Since symmetrical conditions exist for the slab in two orthogonal directions,only one quarter of the plate was required for analysis. This was divided into 104 rectangular elements with 14 nodes in the x-direction (along the largest side) and 9 nodes in the y-direction as shown in figure (8.2), with the largest elements appearing near the free boundary of the slab and the smallest elements and layers at the vicinity of the symmetrical axes and reinforcing bars. To economize in computer storage and usage the nodes of the structure were numbered along the smallest side in the y-direction of the body. In spite of

these measures the mesh contained 832 of steel or concrete layers. Tensile reinforcement was idealised as 7 reinforcing bars (layers) parallel to the x-direction overlying 12 reinforcing bars (layers) in the y-direction as in figure (8.3), providing areas of steel of 840 mm^2 and 1582 mm^2 as compared to the calculated design values of 794 mm^2 and 1539 mm^2 respectively.

In this simply supported slab, all nodes along the two edges of quarter of the structure were assumed to be free horizontally and fixed in a vertical position (in z-direction) except for node No. 9 which was fixed in the y-direction and node No. 118 which was fixed in the x-direction arising from the geometric and loading symmetries. The rotations of nodes No. 1 to No. 9 about the x-axis were assumed to be zero throughout the loading and heating the body. Also the rotations of nodes along the other edge of the quarter slab, on the x-axis, about the y-axis were zero during the loading and heating the structure again due to the geometric and loading symmetries. Because of the symmetrical conditions of the slab all the nodal points on the axis parallel to the y-direction (nodes No. 119 to No. 126) were fixed in the x-direction and had zero rotations about the y-axis. They were however free in the z-direction. Similarly all nodal points on the other symmetrical axis (nodes No. 18, 27, 36, 45, 54, 63, 72, 81, 90, 99, 108, 117 and 126) were free in a vertical position and fixed in the y-direction with zero rotations about the x-axis.

Finally it must be mentioned here that, the physical

and mechanical properties of the slab were assumed to be similar to the values adopted in chapter seven which were also used for the analysis of the reinforced concrete beams.

8.3- Behaviour Of The Slab Under

The External Load

The design load ($w_d + w_l = 10.50$ kN/m^2), was applied at five increments. The first load increment 3.0 kN/m^2 was the weight of the body itself. The live load 7.5 kN/m^2 was then applied at four equal increments of 1.875 N/m^2.

Four cracks appeared at the concrete cover (first layer) of elements No. 88, 95, 96 and 104 at the central part of the slab below the tensile reinforcing bars under the second load increment, when the load reached 4.875 kN/m^2. The orientations of cracks were in a direction parallel to the x-direction. These cracks propagated under the third load increment within the concrete cover and a series of new cracks initiated and propagated within the second layer of the slab. The propagations of cracks within the first and second layers which appeared under the third load increment are shown in figure (8.4). The distributions of tensile stresses within the reinforcing bars at the second and third layers of the body at the end of the third load increment are shown in figure (8.5).

The original cracks propagated under the 4th and 5th load increments through part of the concrete cover (1st layer) and also propagated through the second layer of the member.

The crack patterns within the first and second layers of the structure under the 4th and 5th load increments are shown in figures (8.6) and (8.7), respectively. Also further cracks initiated within the third layer under the 4th load increment and propagated under the 5th load increment as shown in figure (8.8). Three cracks initiated within the 4th layers of the elements No. 80, 96 and 104 under the 5th load increment (design load). The tensile stresses in the reinforcing bars increased considerably when the 4th and 5th incremental loads were applied as indicated in figure (8.9).

While all the nodal points of the slab deflected downwards under the first and second load increments, they moved horizontally towards the central point of the slab with the maximum horizontal movements in x and y-directions appearing at points No. 9 and No. 118 respectively. Node No. 1 started to move outwards in the x-direction after the second load increment and nodes No. 2 and 3 moved outwards in the x-direction under the third load increment and continued moving under the 4th and 5th load increments in the same direction. Node No. 10 moved outwards in the x and y-directions after the third load increment and node No. 4 started to move outwards in the x-direction under the design load. As the foregoing movements were taking place nodal points No. 1, 2, 3 and 4 moved outwards in the y-direction. These deformations were calculated as the horizontal displacements of the nodes on the middle surface (reference surface) of the slab which is different to the horizontal movements of the upper and lower edges of the body. By considering that all straight

lines of the body perpendicular to the middle surface remain straight and perpendicular to the middle surface after deformation (under external load) and also with the help of the rotations of nodal points the deformations of the upper and lower edges of the slab can be found. The horizontal shapes of the upper edge, lower edge and middle surface edge of the deformed body are shown in figure (8.19) under different conditions of loading and heating.

8.4- Behaviour Of The Slab

Subjected To Fire

The first incremental surface temperature 100°C corresponded to a time interval of 30 seconds which was applied to the slab had only a slight effect on the member with two new cracks appearing within the concrete cover. The member expanded slightly under the second temperature increment at 1.5 minutes heating when the surface temperature was 200 °C. The maximum horizontal movement appeared at nodal point No. 1 which moved about 1.0 mm in the x-direction. A few double cracks appeared within the concrete cover which were single cracks under design load. The third incremental surface temperature 440 °C which corresponded to a time interval five minutes expanded the slab horizontally and the additional horizontal movement of nodal point No. 1 in the x-direction reached about 2.4 mm. The additional horizontal displacement of nodal point No. 1 in the y-direction was only 0.17 mm. While the maximum horizontal movement in the x-direction appeared at nodal point No. 1, the maximum horizontal displace-

ment of approximately 1.33 mm in the y-direction appeared at nodal point No. 118. The nodal numbering of the analytical model of the structure is shown in figure (8.2).

Generally all the nodal points of the slab deflected downwards during the first ten minutes heating and the maximum deflection which was about 37 mm appeared at the central point of the member i.e node No. 126. The deflection of this point under the design load was about 33.5 mm. A series of new cracks appeared within the concrete layers at the first and second levels during the fifth minute of heating and the maximum tensile stress of around 210 N/mm^2 within the reinforcing bars appeared at the second layer of element No. 95. All the crack branches propagated through the first, second and third concrete layers of the structure under the fourth temperature increment and a series of new crack branches initiated within the 4th layer. The surface temperature of 500 ^{o}C in this increment corresponding to 10 minutes time interval produced a crack pattern within the first and second layers of the slab as shown in figure (8.10).

The tensile stresses within the reinforcing bars of the member reduced considerably after ten minutes heating especially at the central part of the body when the slab was heated for 20 minutes and the distributions of stresses within the reinforcing bars are shown in figure (8.11). All nodal points of the slab deflected downwards and the maximum vertical displacement of 47.5 mm appeared at nodal point No. 126, the centre of the member. The member also expanded horizontally, reaching a maximum movement of 4.1mm

in the x-direction at point No. 1. In the meantime the maximum horizontal displacement in the y-direction appeared at point No. 118 which was about 2.2 mm.

More cracks appeared within the first four concrete layers, particularly within the fourth layer of the member after 20 minutes heating, as shown in figure (8.12). Certain areas of the slab (marked I in figure 8.13) at the vicinity of the corners of the slab showed very small deflection during the first half an hour heating, and the deflections of nodal points on this part of the slab remained approximately constant during the second half hour heating.

All the nodal points of the slab deflected downwards during 30 and 45 minutes heating and the maximum deflection of the central point at these time intervals reached about 68 mm and 80 mm, respectively. The cracks propagated within the concrete layers and through the thickness of the slab and the first crack within the 5th layer appeared at the 45 minute of heating. Ten cracks appearing within elements No. 10, 12, 26, 28, 44, 46, 78, 80, 94 and 96 propagated at the 8th temperature increment corresponding to one hour time interval. Figure (8.14) illustrates the distributions of stresses within the reinforcing bars at the second and third layers of the structure after one hour heating.

All nodal points deflected downwards during this 60 minutes heating, except an area of the body (marked II in figure 8.13) which slightly deflected upwards. This part of the body included the nodal points No. 101, 110, 111, 119, 120 and 121. The deflections of nodal points on a section

A-A (see figure 8.2) under the design load and during the heating of the body are shown in figure (8.15).

Twelve double cracks appeared within the concrete layers when the slab was under the 9th temperature increment corresponded to 90 minutes time interval and the total number of doubly cracked layers reached 242. The maximum vertical displacement of the centre point of the slab reached about 94 mm which increased about 13 mm under the next incremental temperature corresponded to 105 minutes and eight doubly cracked layers appeared.

The vertical displacements of nodal points in the vicinity of the corner of the slab (part I in figure 8.13) were approximately constant during the heating up to 105 minutes heating but deflected considerably after two hours heating, as shown in figure (8.15). While the central part of the structure deflected downwards it pushed an area of the body (marked II in figure 8.13) upwards, during the heating the body, especially at the 60th and 90th minutes.

The first crack within the upper layer of the slab appeared after two hours heating and the body became weaker at the central part of the slab and all cracks propagated gradually within the upper layer of the structure after $2\frac{1}{4}$, $2\frac{1}{2}$ and $2\frac{3}{4}$ hours heating. The slab finally collapsed a few minutes after $2\frac{3}{4}$ hours heating before reaching the next surface temperature increment corresponded to 170 minutes. The maximum deflection of the centre of the slab at $2\frac{3}{4}$ hours heating reached about 150 mm. The upper layers of five elements No. 18, 26, 27, 28 and 34 crushed during the $2\frac{3}{4}$

hours heating. The displacements of nodal points on the symmetrical axes of the slab duringheating are shown in figures (8.16) and (8.17). Also the time-deflection curve of the nodal point No. 126 at the centre of the slab during heating is given in figure (8.18).

The horizontal shape of the slab (upper, lower and middle surface edges) under the design load and also horizontal shape of the middle surface edge of the body after two hours heating are shown in figure (8.19).

8.5- Effect Of External Load On The Behaviour Of The Slab Subjected To Fire

The effect of different intensities of external load and temperature applied independently were investigated for the slab as designed previously and also with extra steel reinforcement added to the slab. The behaviour of each case is described below;

Case 1. Slab Loaded With 3/5 Design Load Prior To Heating.

After five increments of load were applied up to a maximum of 3/5 design load, the maximum vertical deflection recorded was only 14 mm. All nodal points moved towards the central part of the body except a few nodes in the vicinity of the corners which moved outwards under the 4th and 5th load increments. As the bottom surface of the slab began to increase in temperature the slab deflected generally downwards during the first half an hour. The central area of the body

continued to move downwards during further heating but a part of the slab which was slightly larger than the area marked I in figure (8.13) started to move upwards. A slight upward movement was also noticed after $2\frac{1}{2}$ hours heating in the central point of the structure marked II in figure (8.13).

Finally the slab collapsed a few minutes after three hours heating before reaching the next incremental temperature corresponded to 190 minutes. The time-deflection curve of the nodal point No. 126 as compared with the time deflection curve of this point when the design load was applied to the slab before subjected to fire is shown in figure (8.20).

Case 2. Heating Of Slab With No Applied Load

The maximum deflection of the nodal point No. 126 under the weight of the body was about 3.4 mm. The slab deflected downwards during the first half hour heating. The maximum compressive stress appeared within the concrete cover at the central part of the body and this compressive stress reduced towards the upper layer and tensile stress appeared within and around the upper layer of the member. The compressive stress at the bottom and the tensile stress at the top of the slab increased with increasing the surface temperature up to 90 minutes heating, and reduced considerably thereafter some single cracks which previously opened at the central part of the top layer of the body closed after $1\frac{1}{2}$ hours heating.

The central part of the slab started to deflect upwards after about half an hour heating, reaching a maximum upward deflection at the centre of the slab of about 65 mm after $1\frac{1}{2}$ hours. The body started to deflect downwards again

after $1\frac{1}{2}$ hours and tensile stresses appeared at the bottom causing cracks to branch within the concrete cover at the central part of the body. In the meantime the upper layers of the slab became compressive and some further cracks in this area closed during the 90th, 105th and 120th minutes. The slab continued to deflect downwards and finally collapsed a few minutes after $3\frac{1}{2}$ heating. The time-deflection curve of the the nodal point No. 126 at the centre of the slab is given in figure (8.20).

Case 3. Application Of Overload Prior To Heating

For continuity the effect of the external overload equal to 120% and 140% of the design load was applied seperately prior to heating. The maximum deflection of the nodal point No. 126 under these external loads alone became 44 mm and 92 mm, respectively. The slab deflected downwards rapidly during heating in both the above conditions and finally collapsed after $1\frac{3}{4}$ and $1\frac{1}{4}$ hours heating, respectively. The time-deflection curves of these two examples are shown in figure (8.20).

The distributions of tensile stresses within the reinforcing bars at the second and third levels of the slab under the 120% of the design load are shown in figure (8.21). The crack patterns at the first and second layers of the slab under the 120% of the design load are given in figure (8.22) and the crack propagation within various layers under overload conditions are shown in figures (8.23) and (8.24).

Case 4. Extra Reinforcement Added To Slab And Heated At No Load

To study the effect of the magnitude and location of the tensile reinforcing bars, extra reinforcement areas were added to the reinforcing bars of the slab. For this reason the thickness of the second and third layers of the slab increased to 2.5 mm and 2.0 mm, respectively, and the thickness of the 4th layer reduced by 2.4 mm to keep the middle surface of the slab in the same position as before.

The maximum deflection at the centre of the body reached about 1.5 mm under the self weight. The slab deflected nearly uniformly downwards during heating for $1\frac{3}{4}$ hours. The deflection rate reduced considerably between 2 hours and $2\frac{1}{2}$ hours heating. The deflection rate increased beyond this time and finally collapsed after 6 hours heating when the maximum downward deflection at the centre of the slab exceeded 285 mm. The bottom layers of the slab were in tension during all the heating while compressive stress appeared at the top layers of the slab.

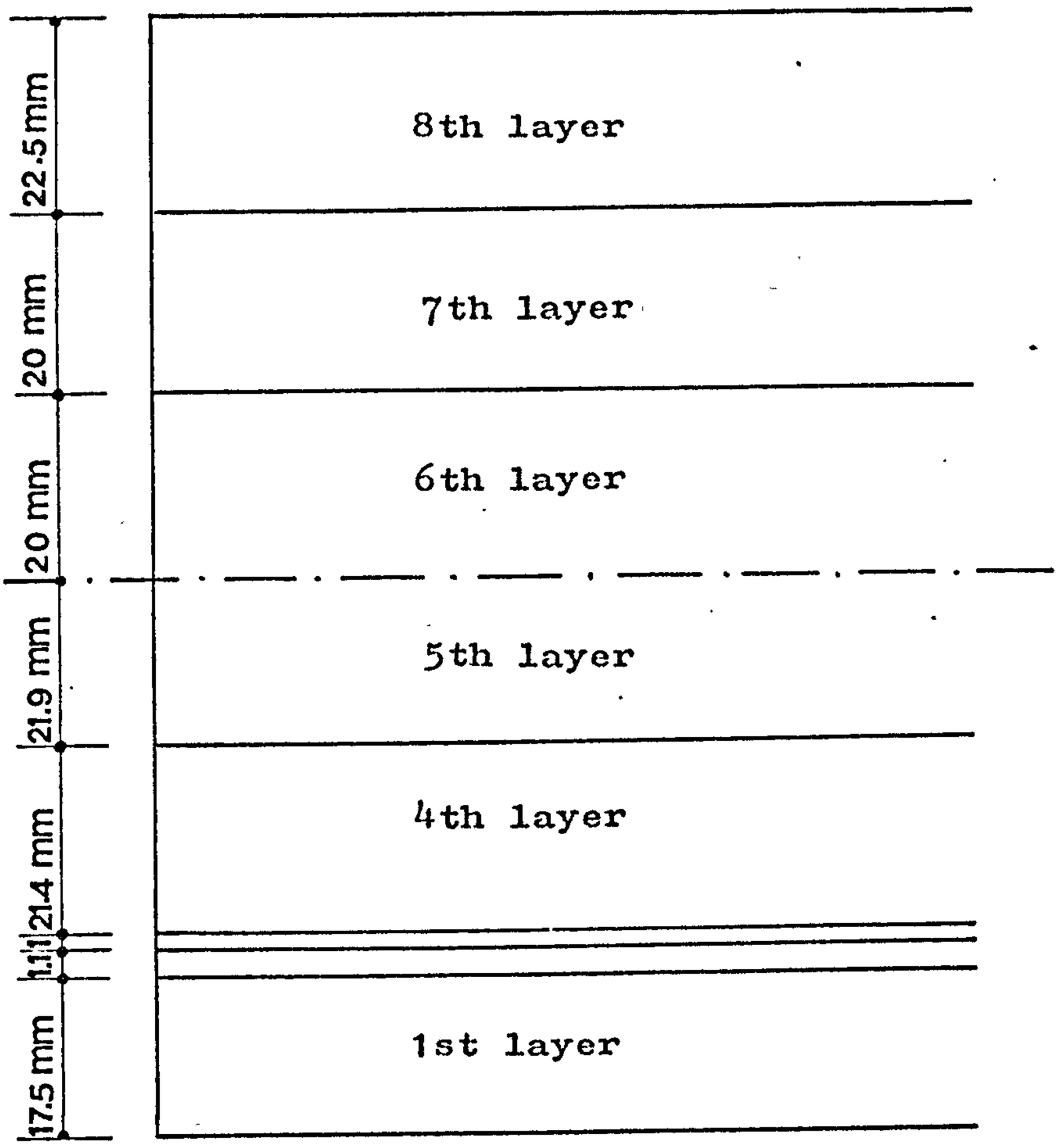

Fig. 8.1- A cross-section of the analytical model of the slab.

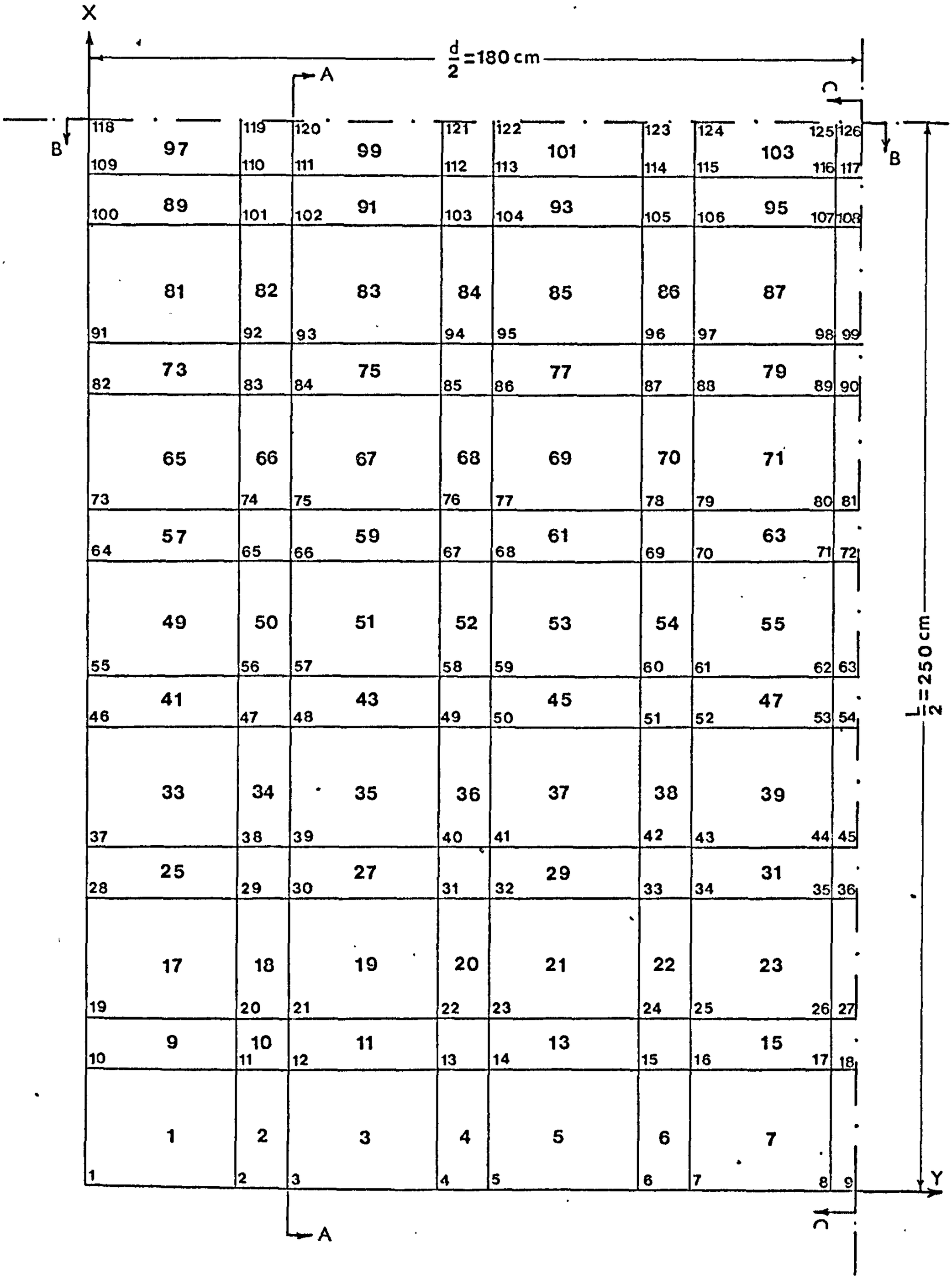

Fig. 8.2- A quarter of analytical model of the slab with 832 layers, and 104 elements.

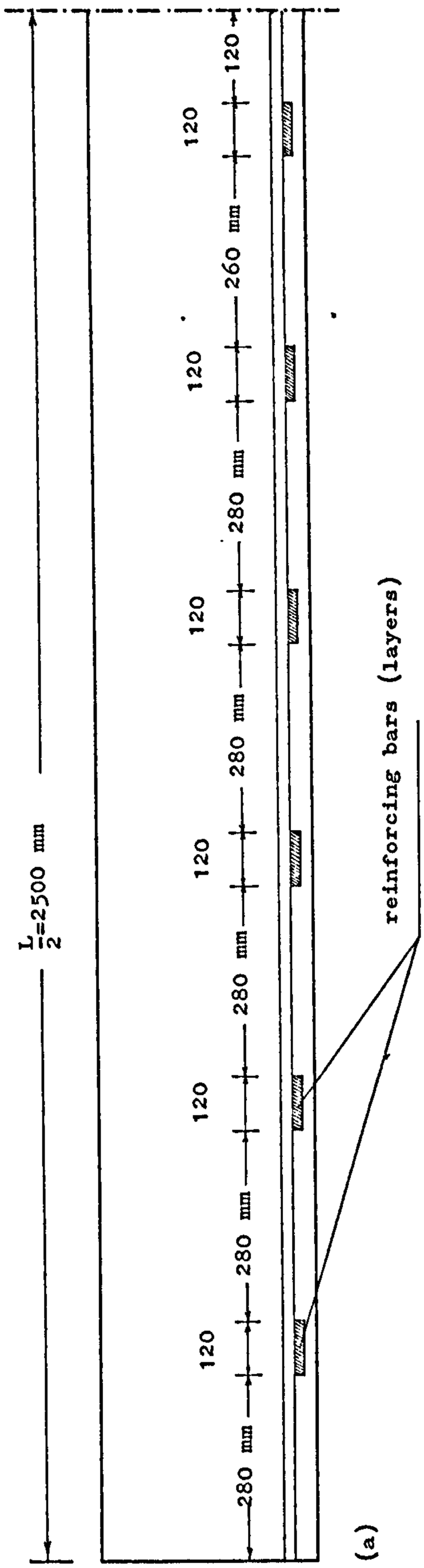

Fig. 8.3- Cross-sections of the slab parallel with X and Y-directions.

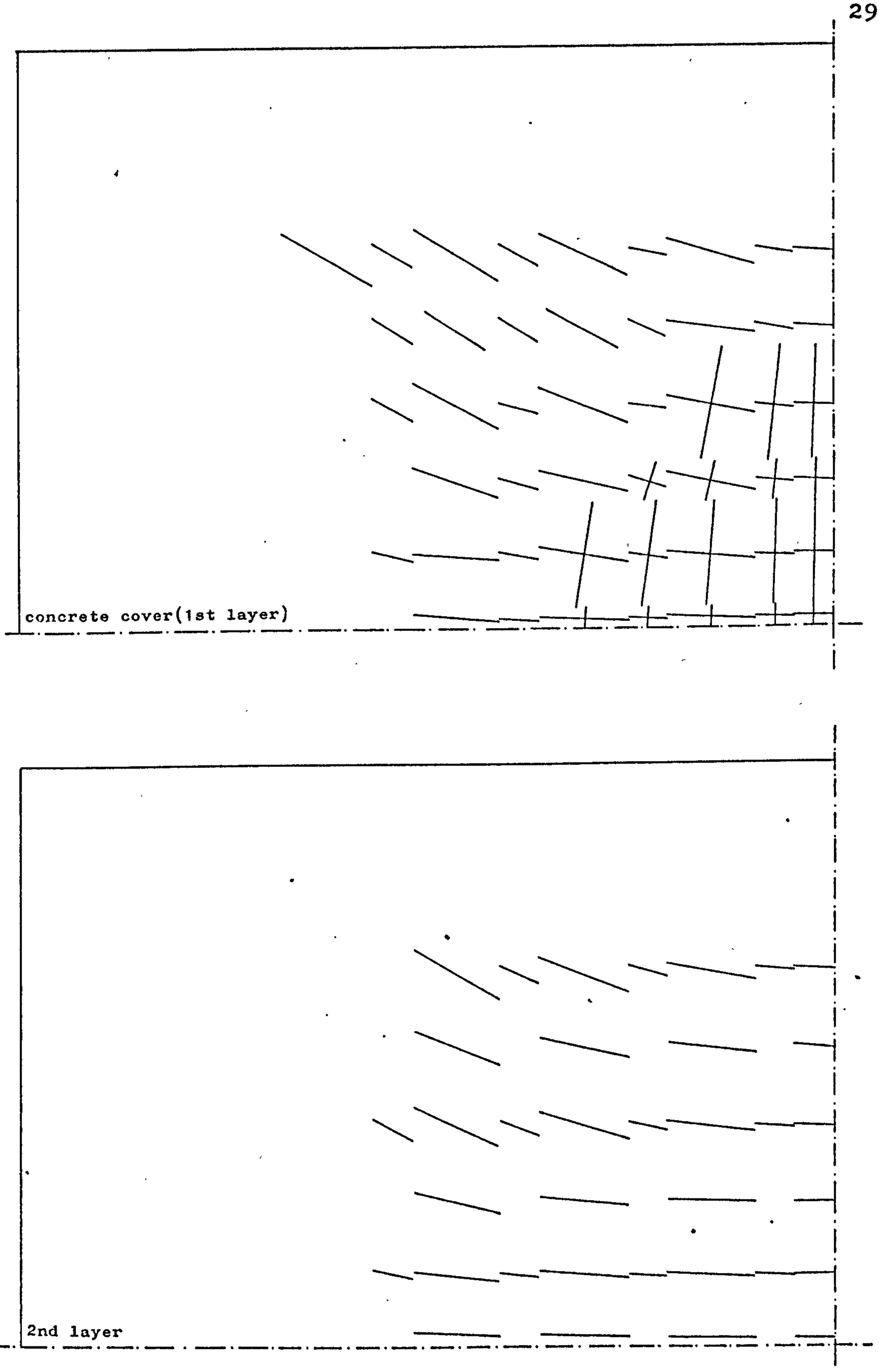

Fig. 8.4- Propagations of cracks at the first layor (concrete cover) and at the second layer of the slab under the third load increment.

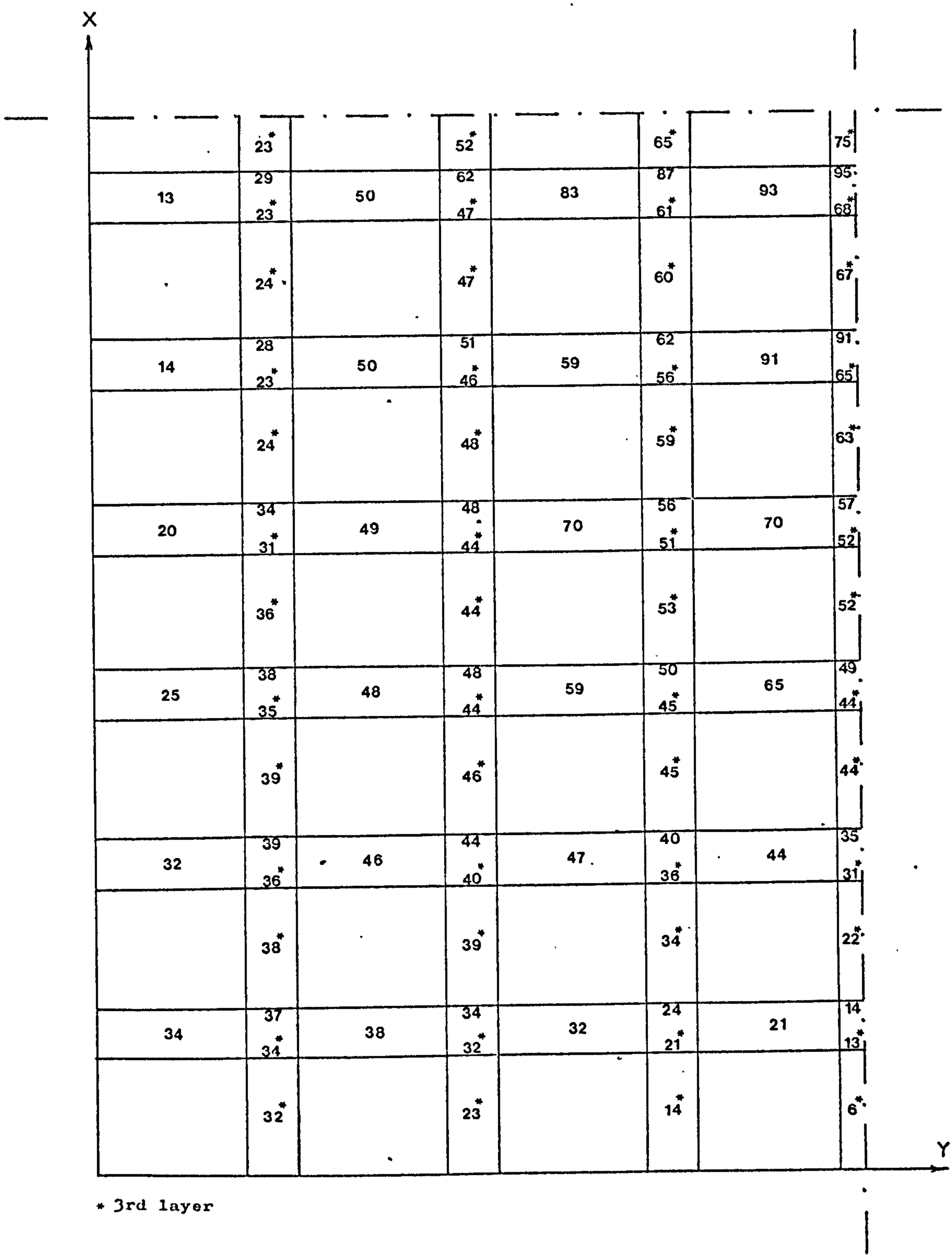

* 3rd layer

Fig. 8.5- Distribution of stress within the tensile reinforcing bars at 2nd and 3rd layers of the slab after third load increment. N./mm^2

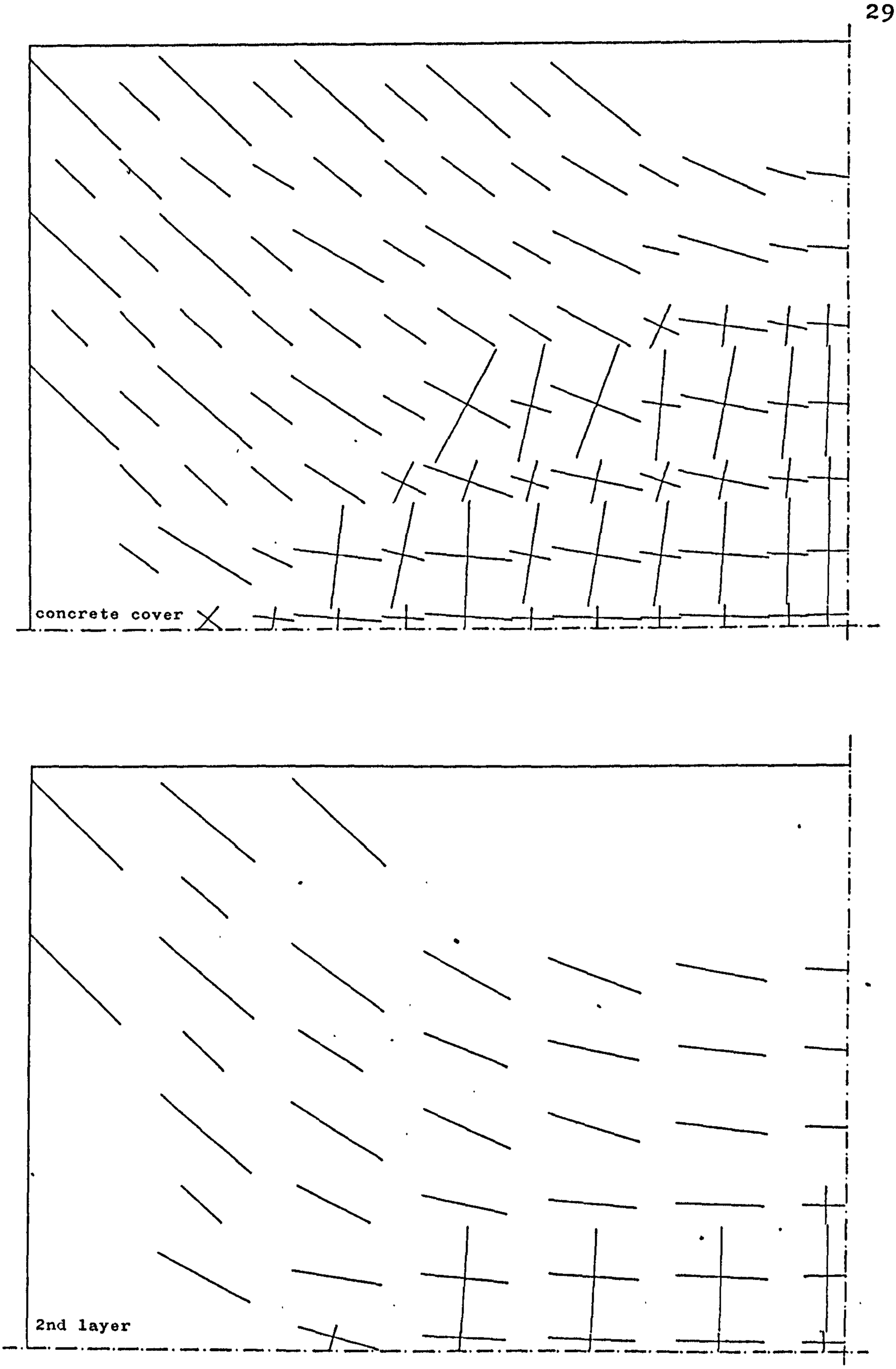

Fig. 8.6- propagation of cracks within the concrete cover (1st layer) and within the 2nd layer of the slab under the 4th load increment.

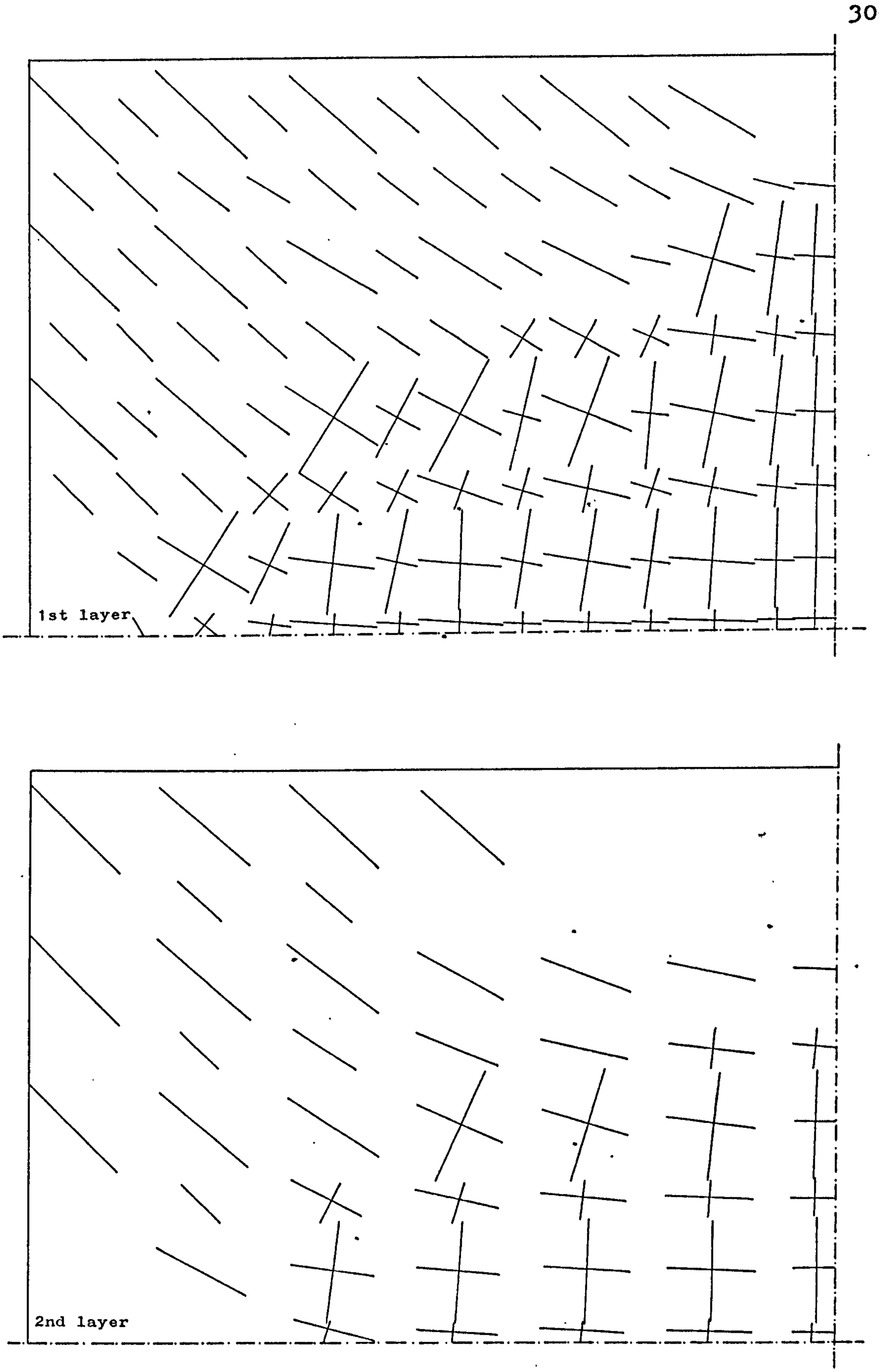

Fig. 8.7- Propagations of cracks within the concrete cover (1st layer) and within the second layer of the slab under the 5th load increment.

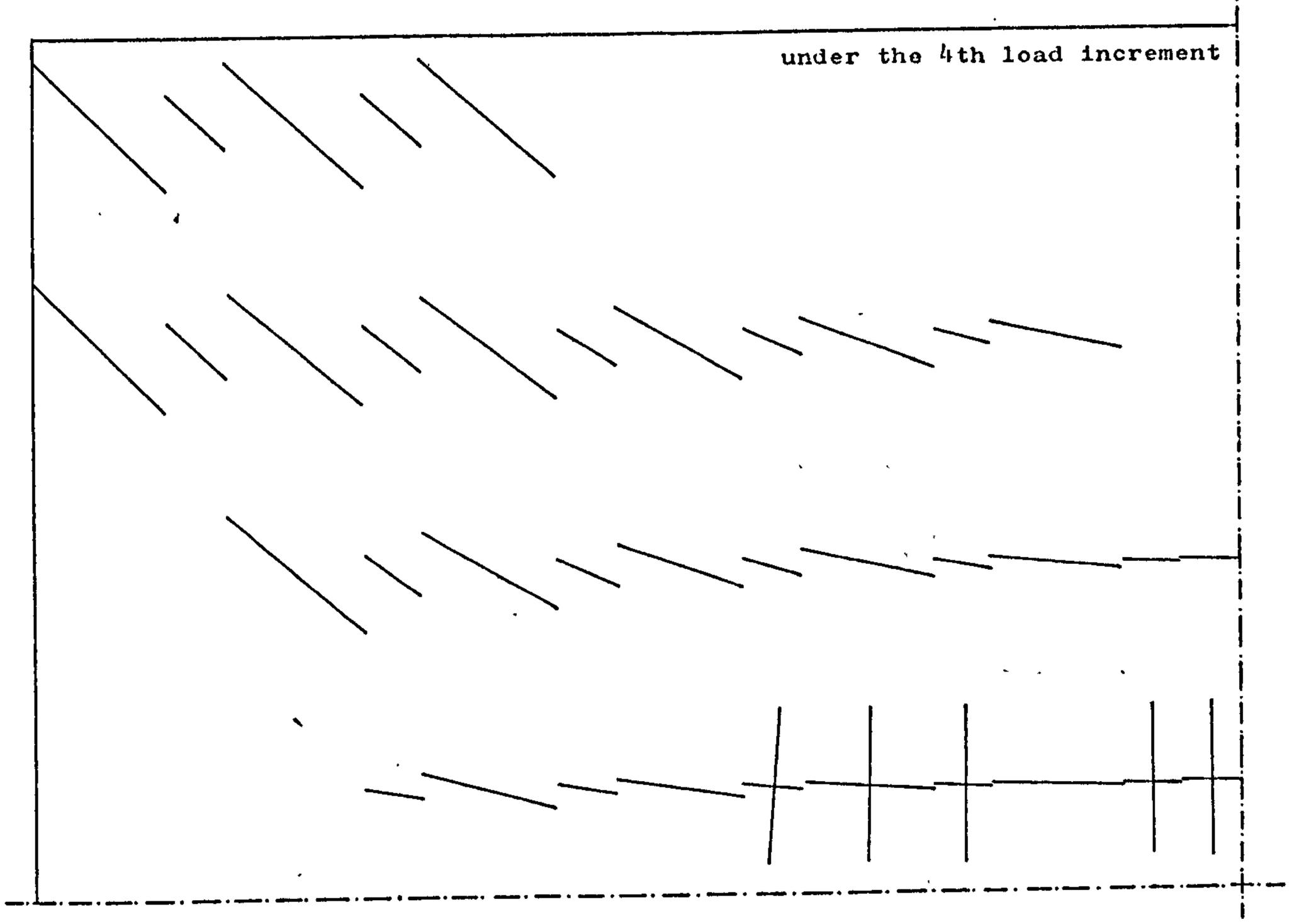

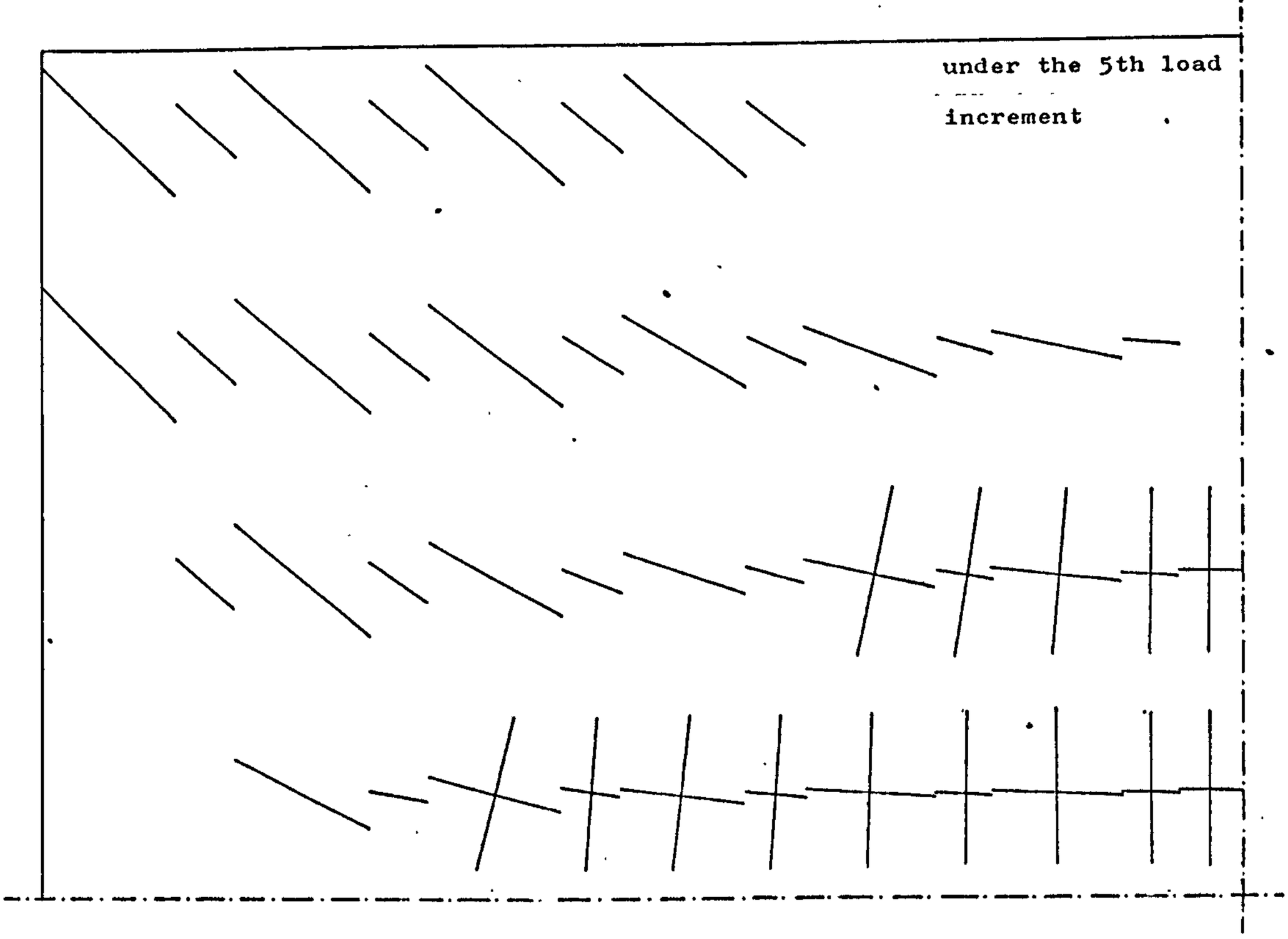

Fig. 8.8- Propagations of cracks within the third layer of the slab under the 4th and 5th load increments.

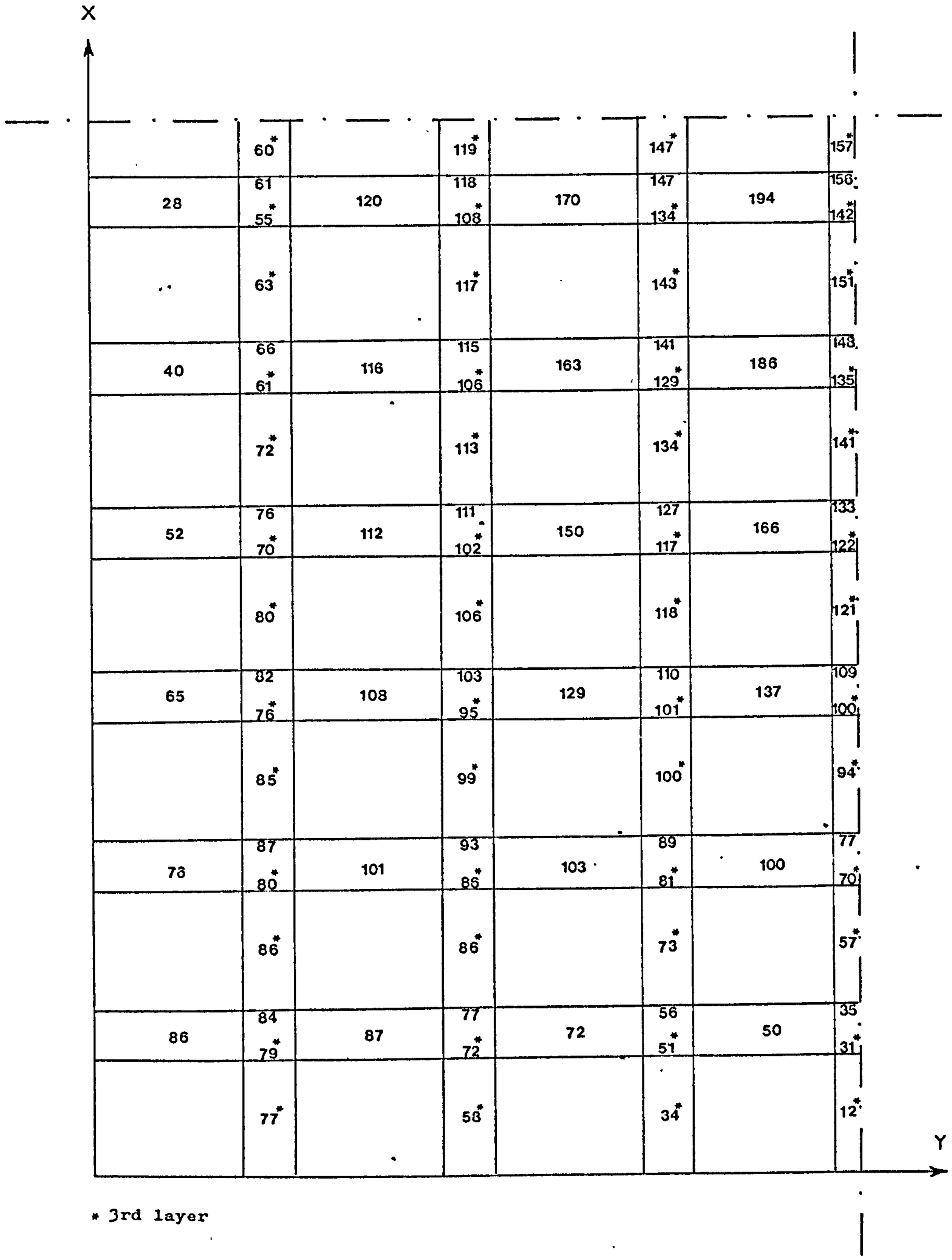

* 3rd layer

Fig. 8.9- Distribution of stress within the tensile reinforcing bars at the second and third layers of the slab under the design load, N./mm^2

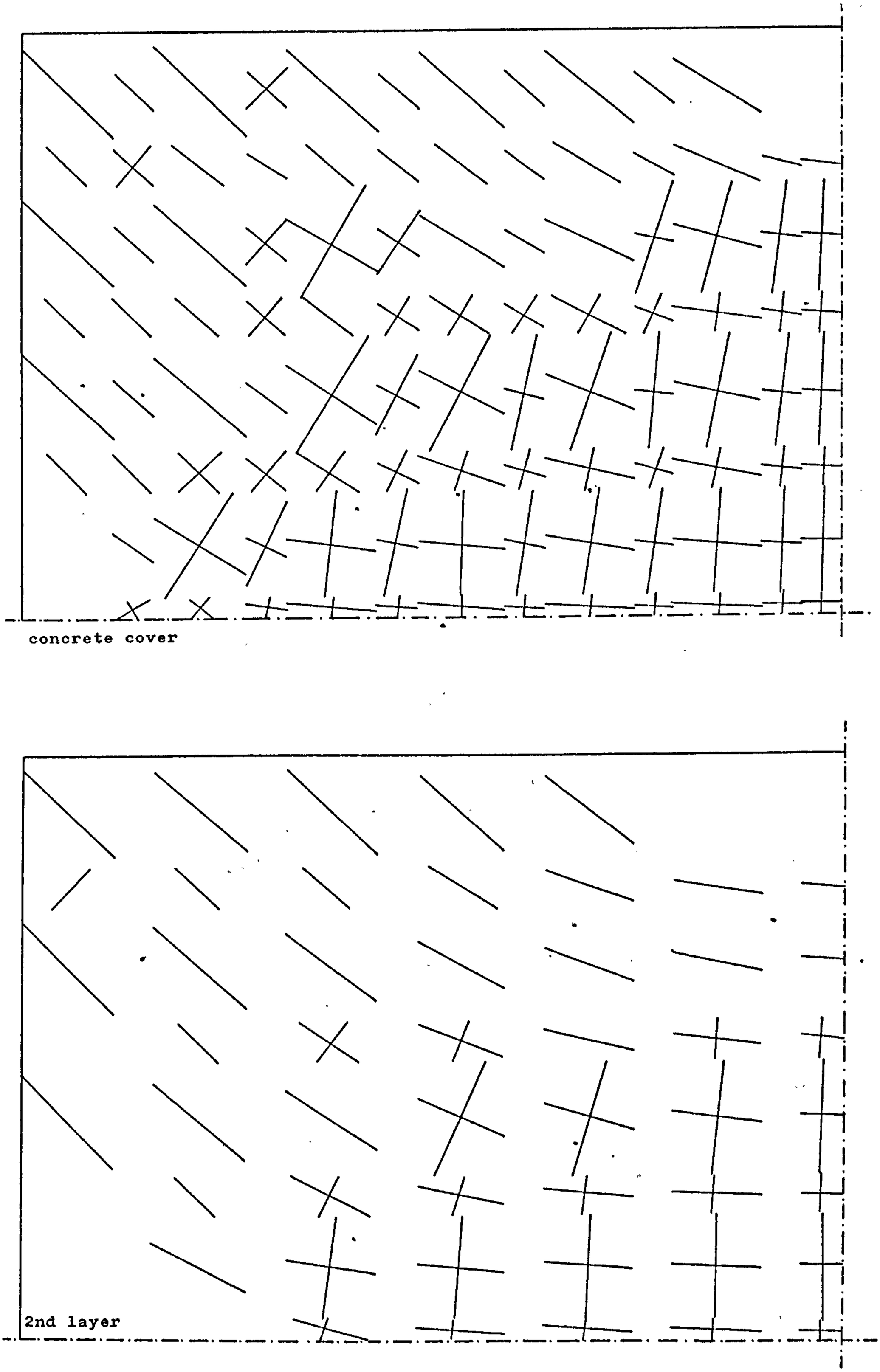

Fig. 8.10- Propagations of cracks within the first and second layers of the slab after ten minutes heating.

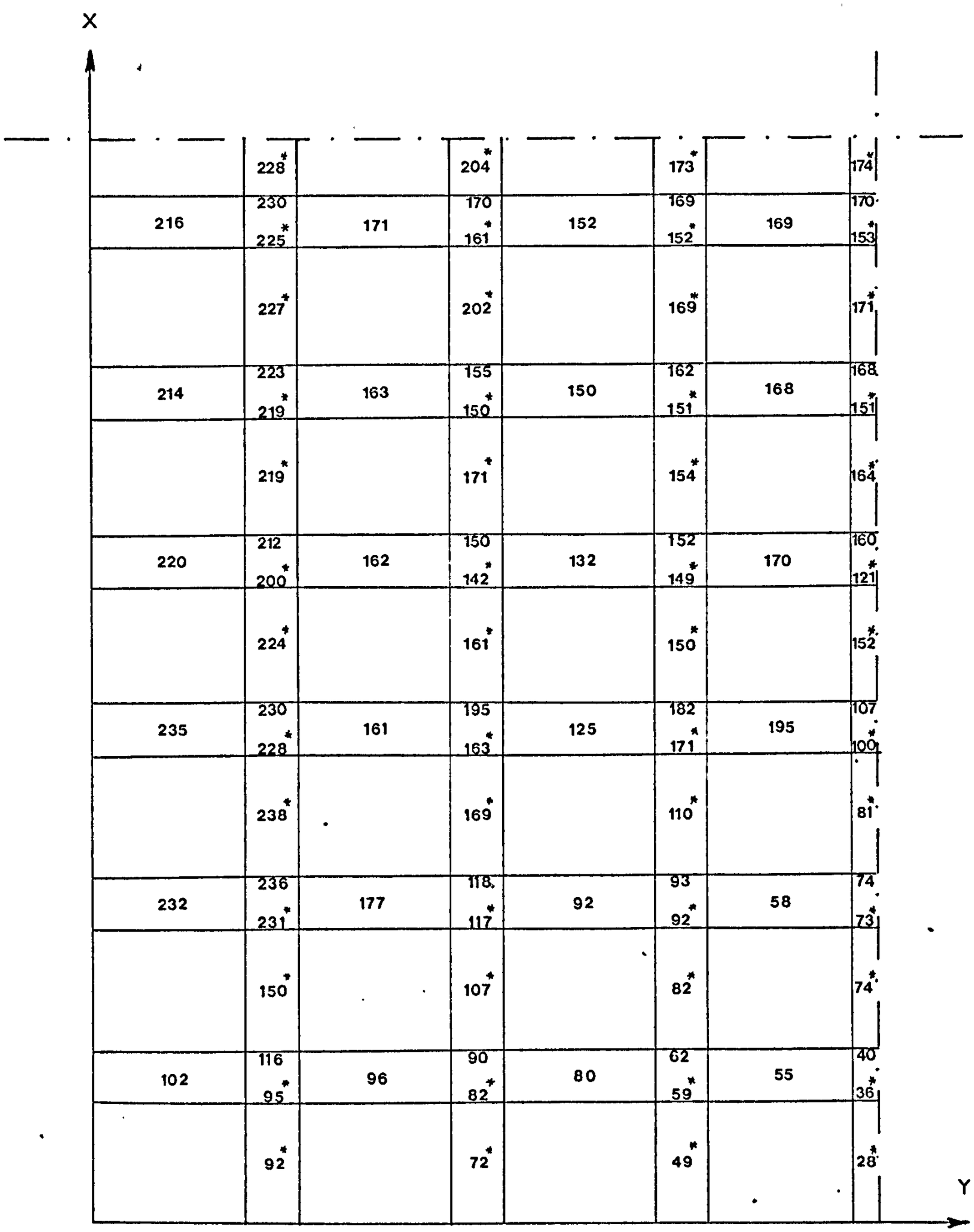

* 3rd layer

Fig. 8.11- Distribution of stress within the tensile reinforcing bars at the second and third layers of the slab after 20 minutes heating.

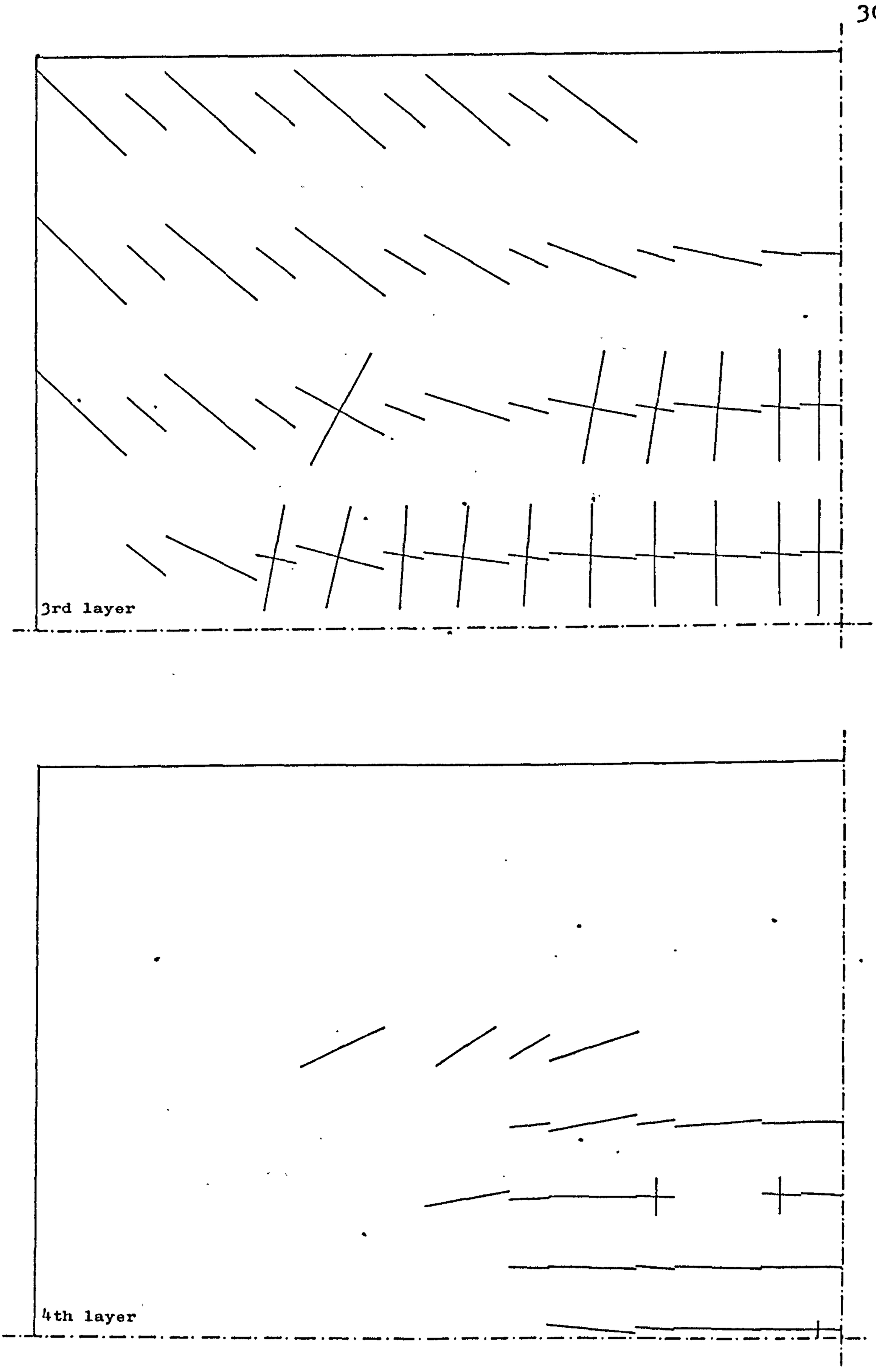

Fig. 8.12- Propagations of cracks within the third and fourth layers of the reinforced concrete slab under 20 minutes heating.

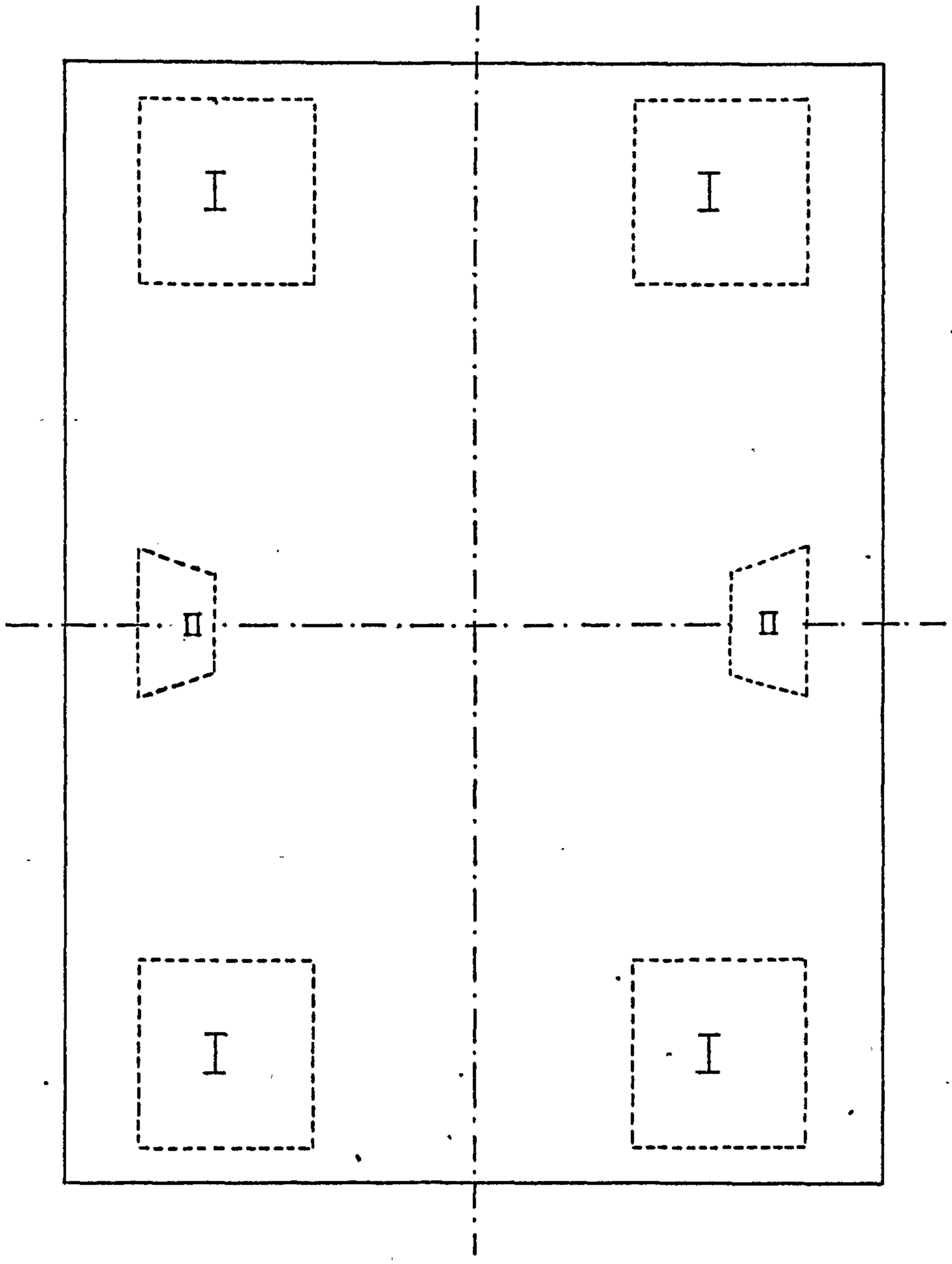

Fig. 8.13- Two special parts of the slab during the deflection of the body.

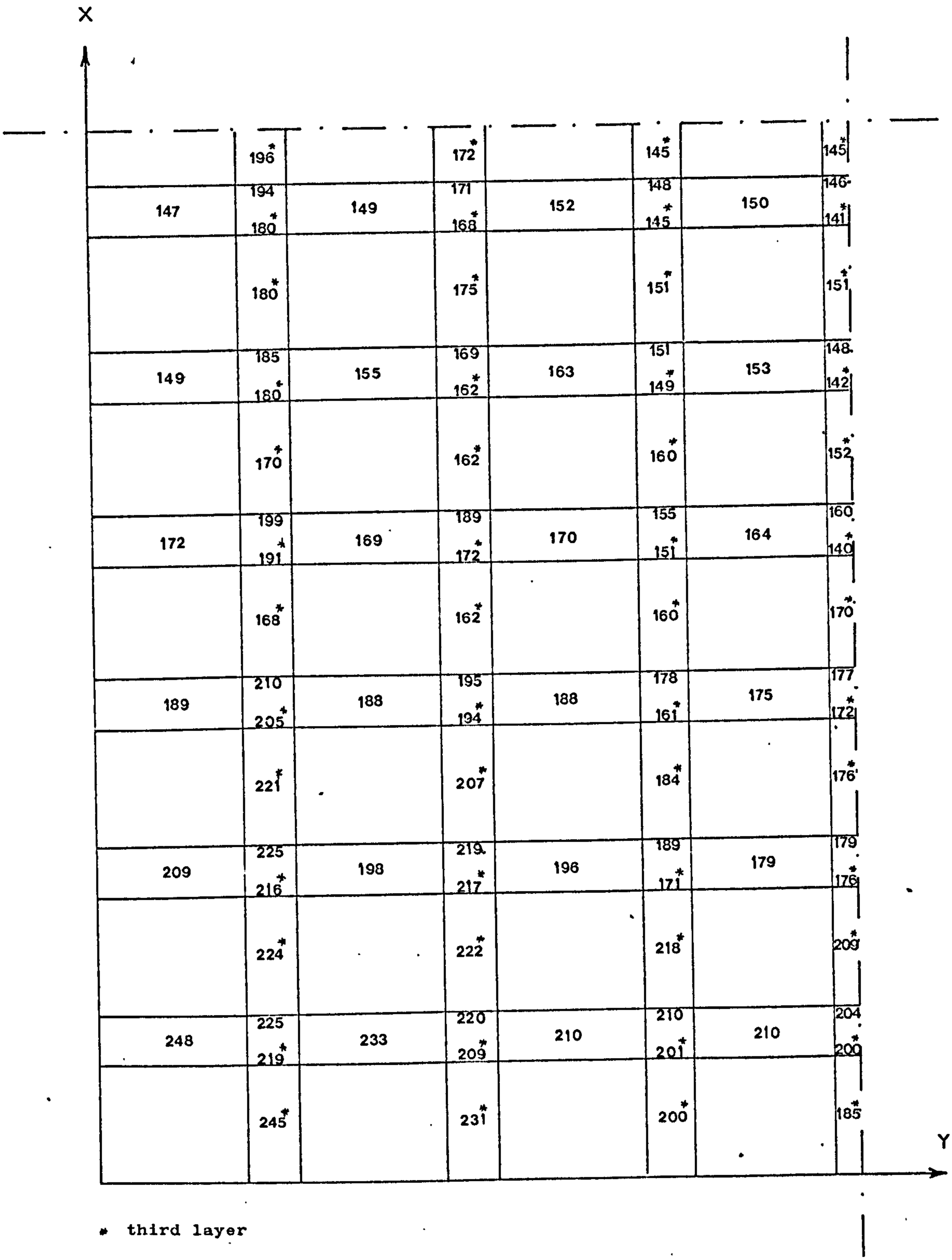

* third layer

Fig. 8.14- Distributions of tensile stress within the tensile reinforcing bars of the slab after one hour heating.

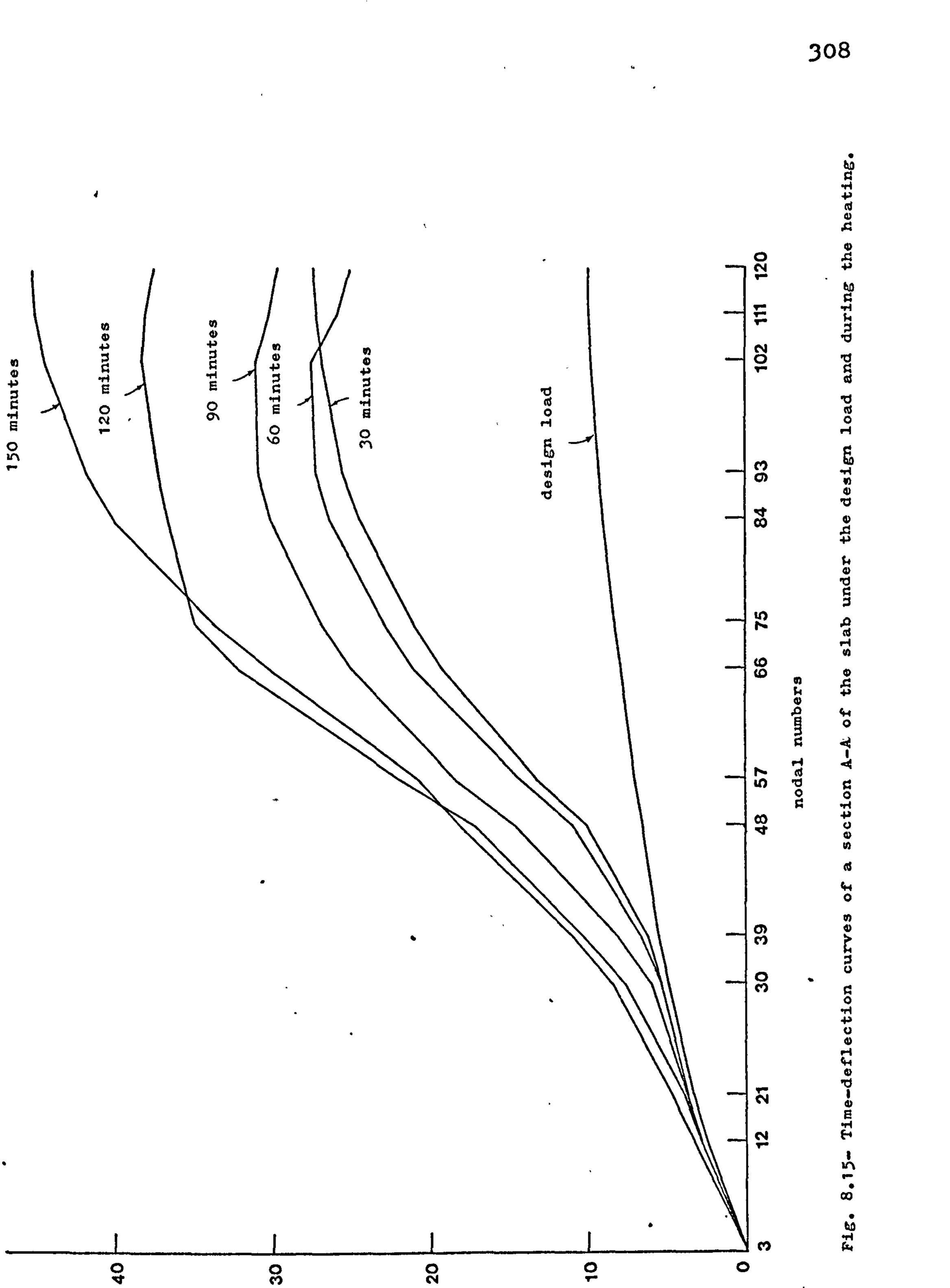

Fig. 8.15- Time-deflection curves of a section A-A of the slab under the design load and during the heating.

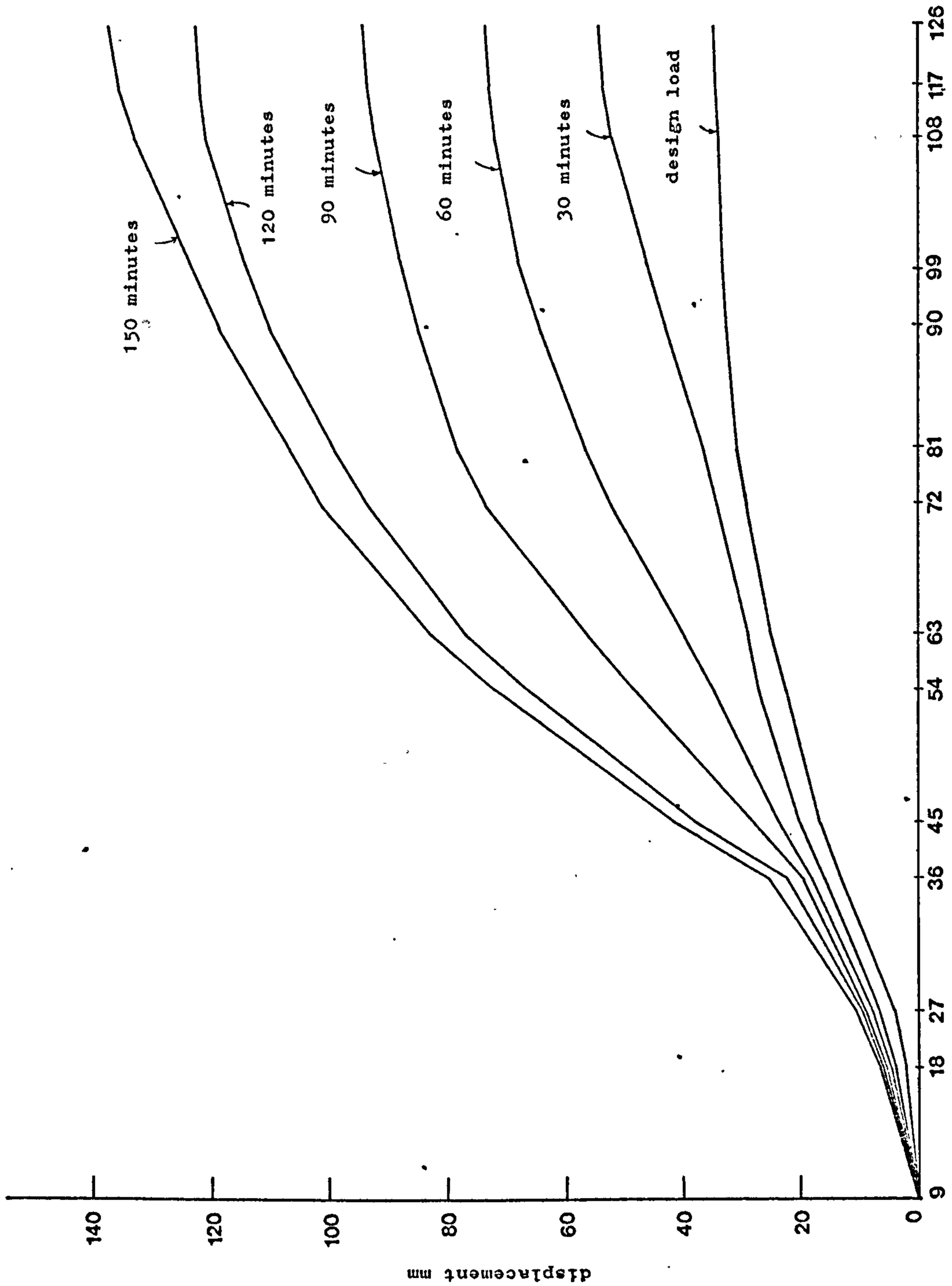

Fig. 8.16- Time-deflection curves of a section C-C of the slab during heating

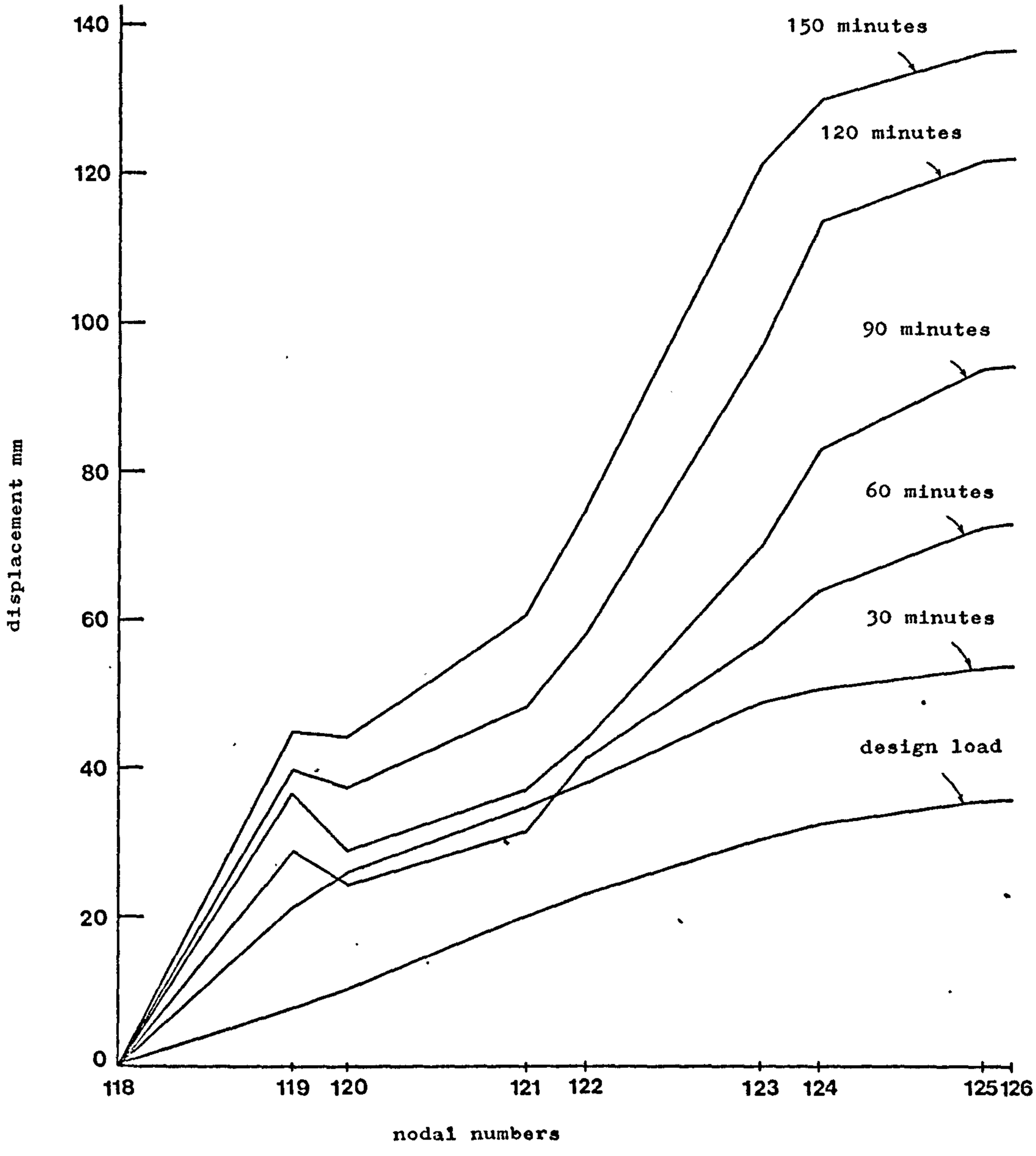

Fig. 8.17- Time-deflection curves of a section B-B of the slab during heating

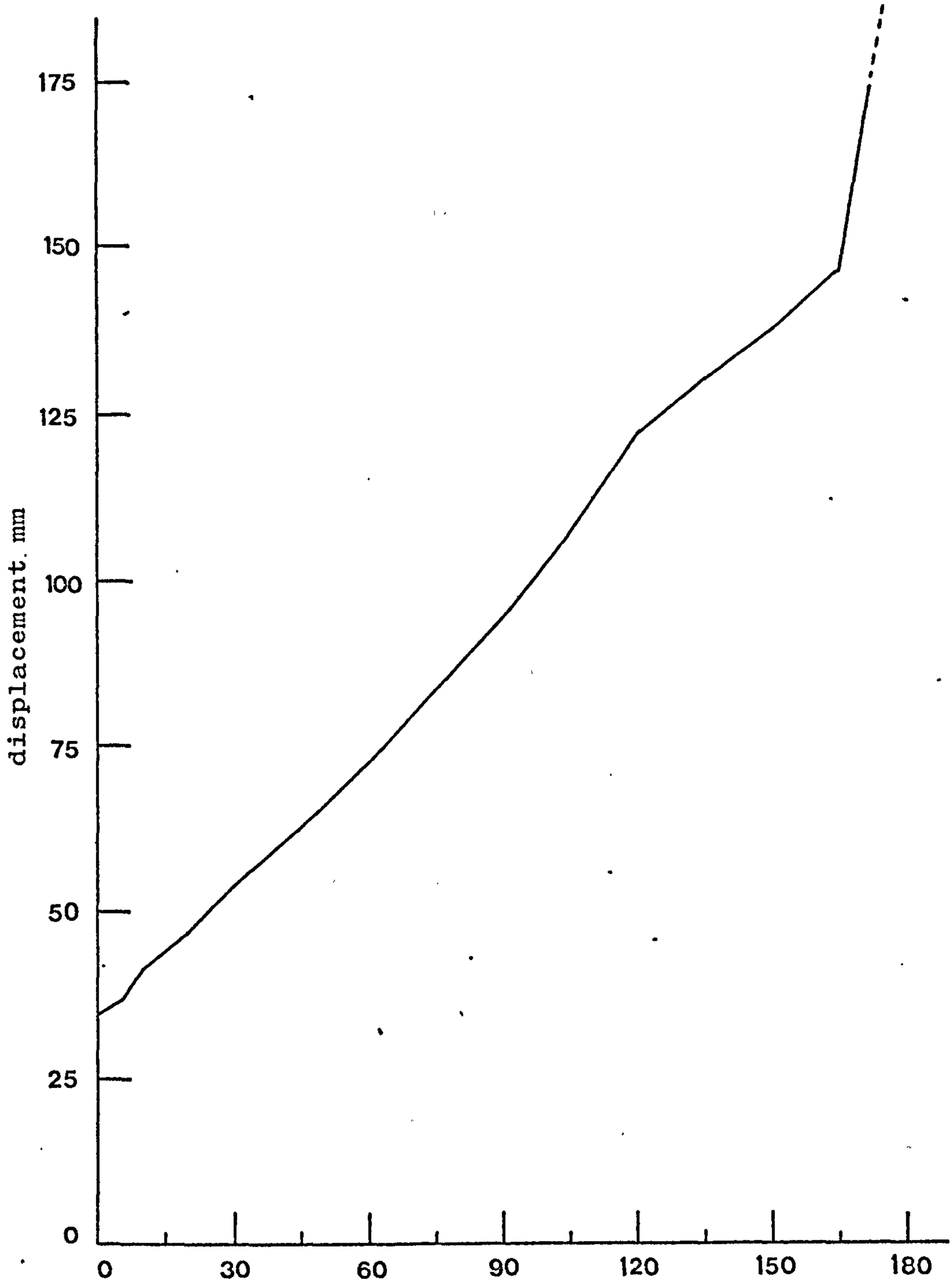

Fig. 8.18- Time-deflection curve of node No. 126 at the centre of the slab.

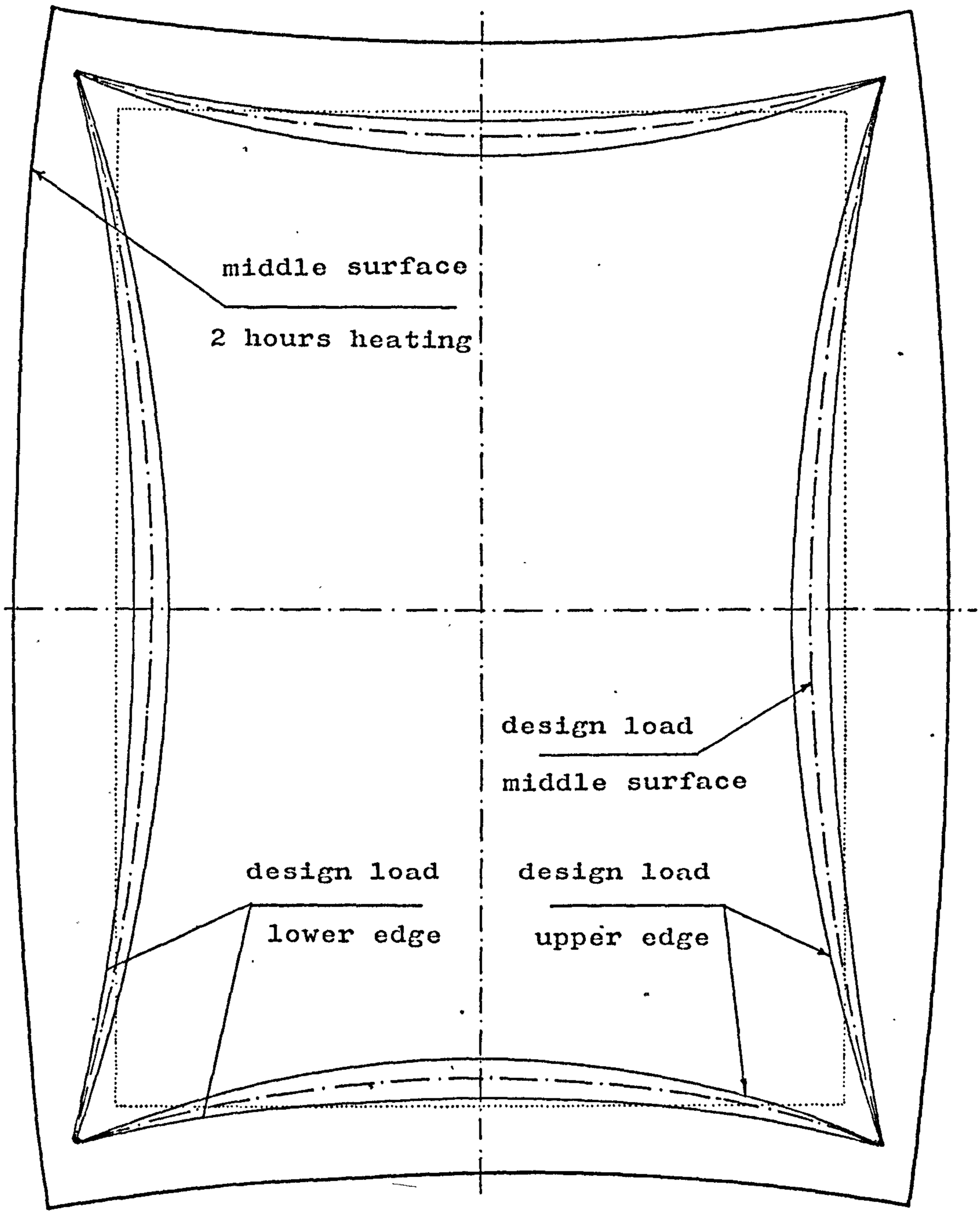

Fig. 8.19- Horizontal shapes of the slab under design load and after two hours heating.

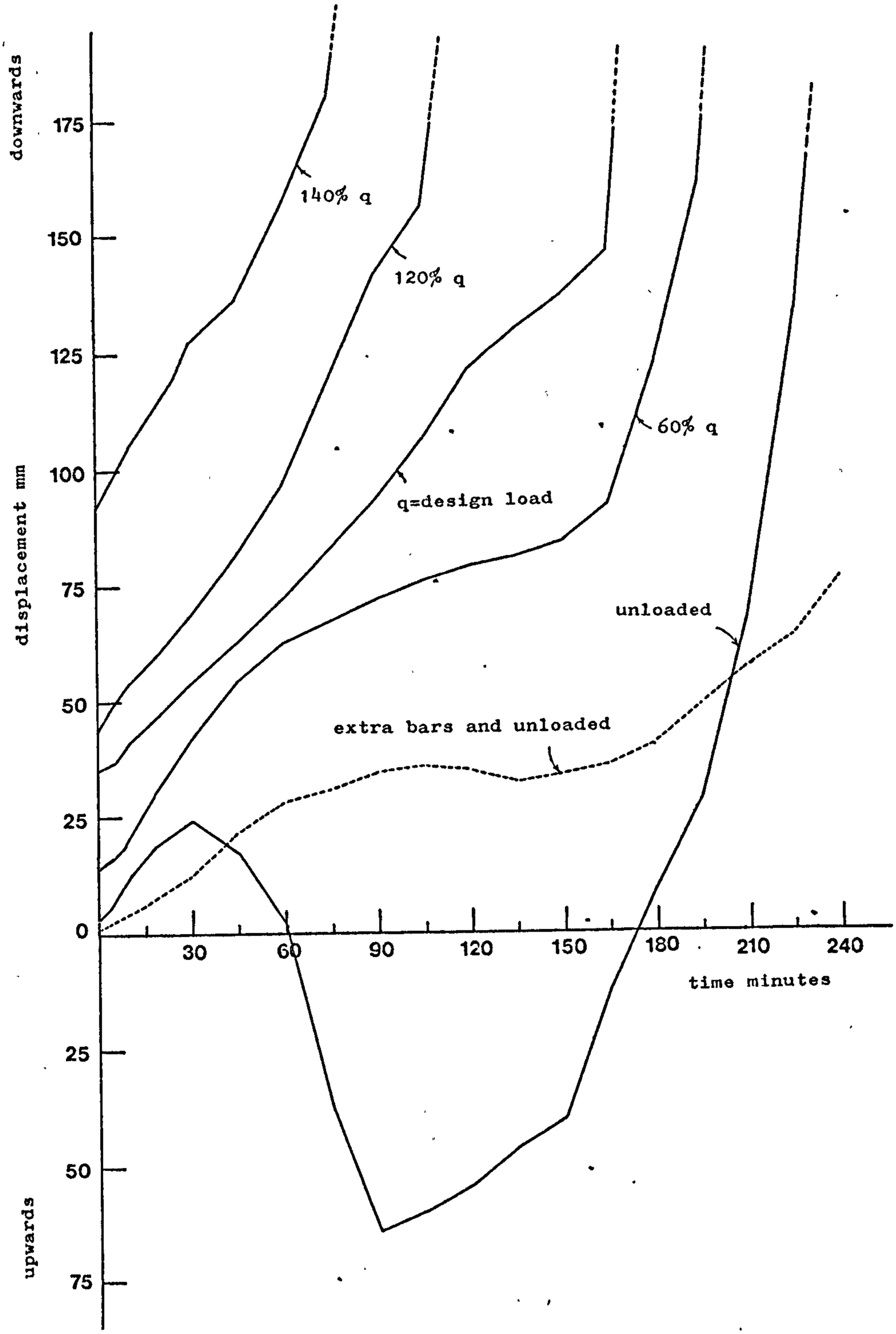

Fig. 8.20- Time-deflection curves of the nodal point No. 126 at the centre of the slab during heating for different external loads.

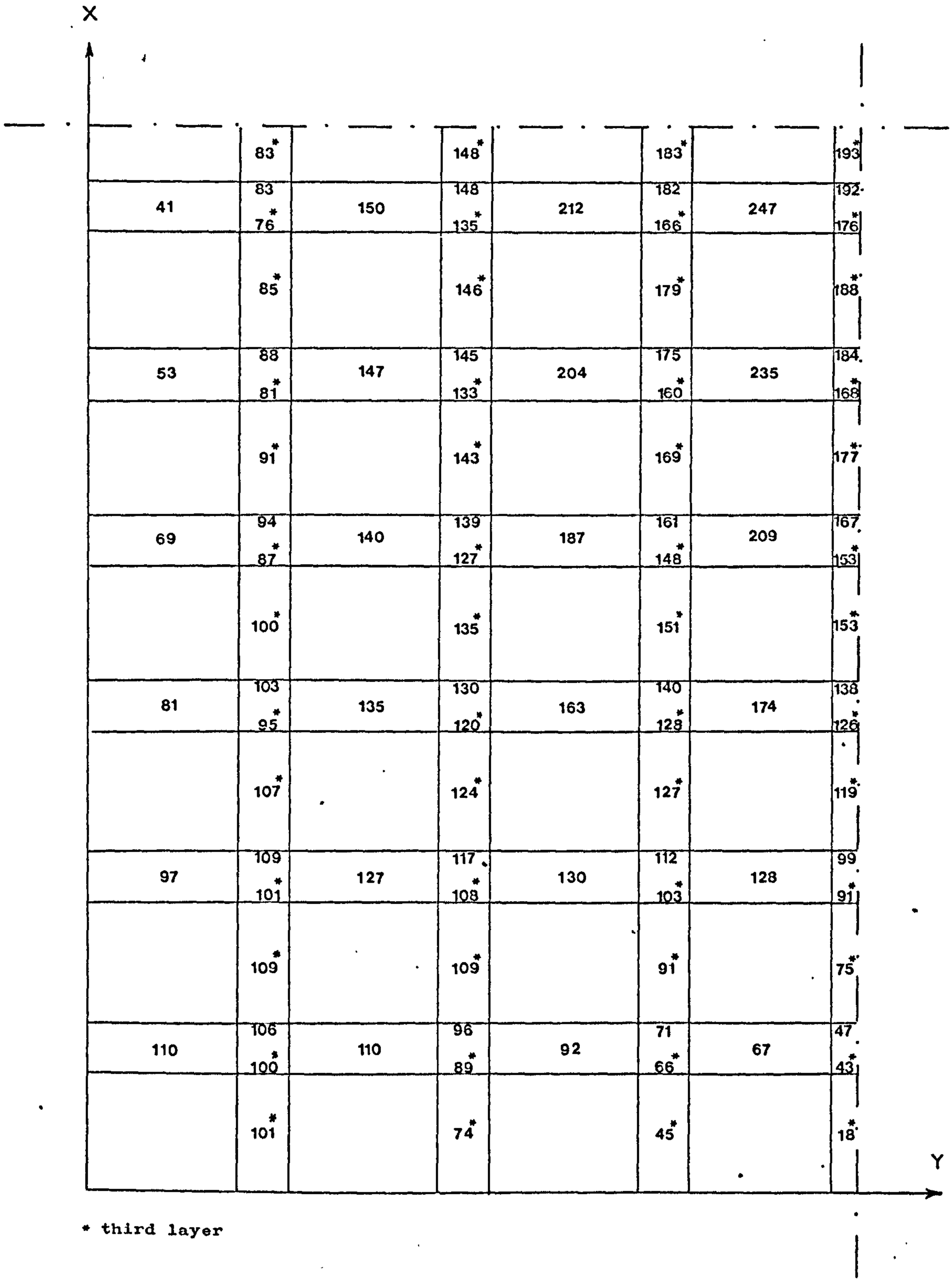

* third layer

Fig. 8.21- Distribution of tensile stress within the tensile reinforcement bars at the second and third layers of the slab under 120% of the design load

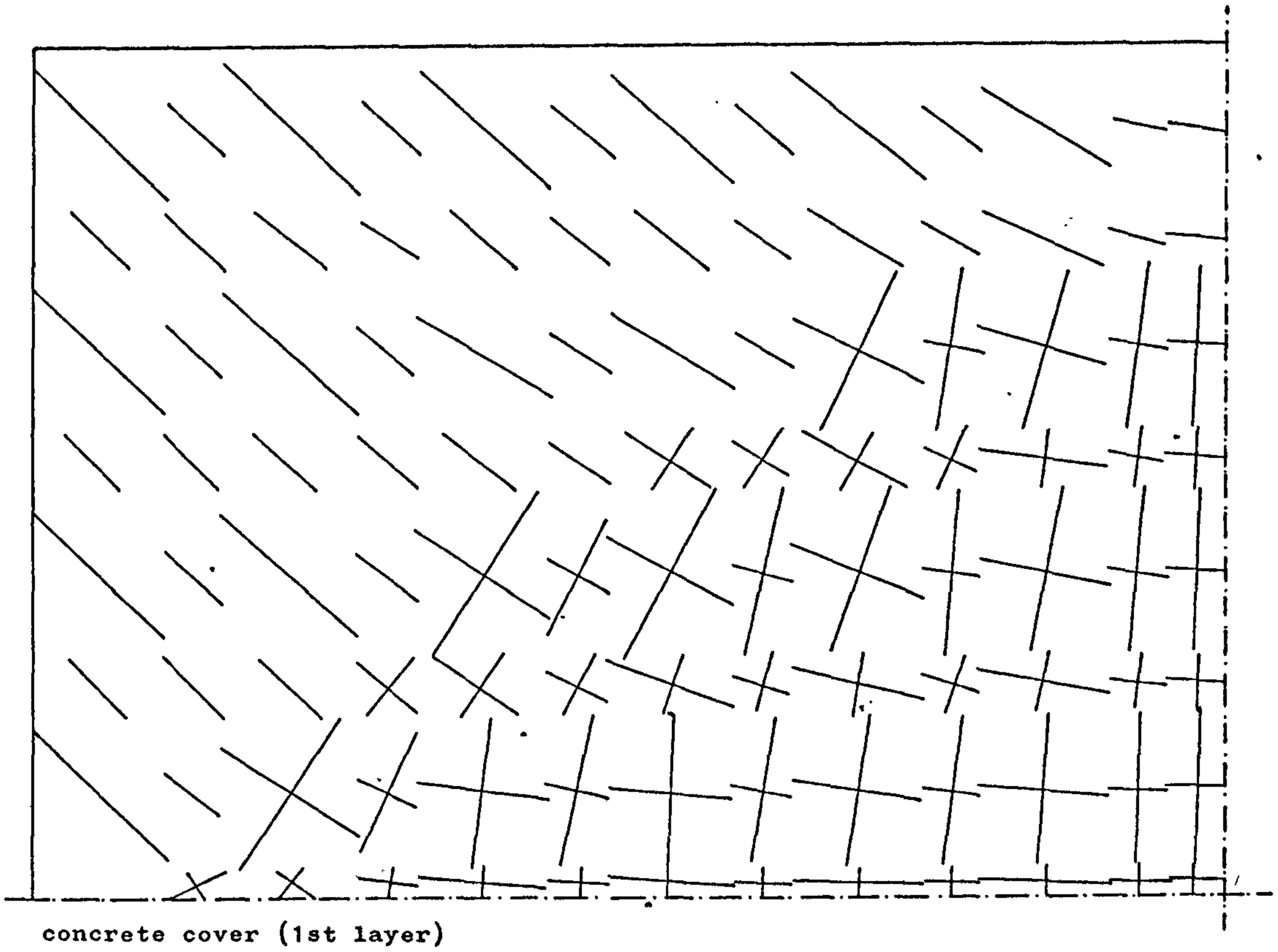

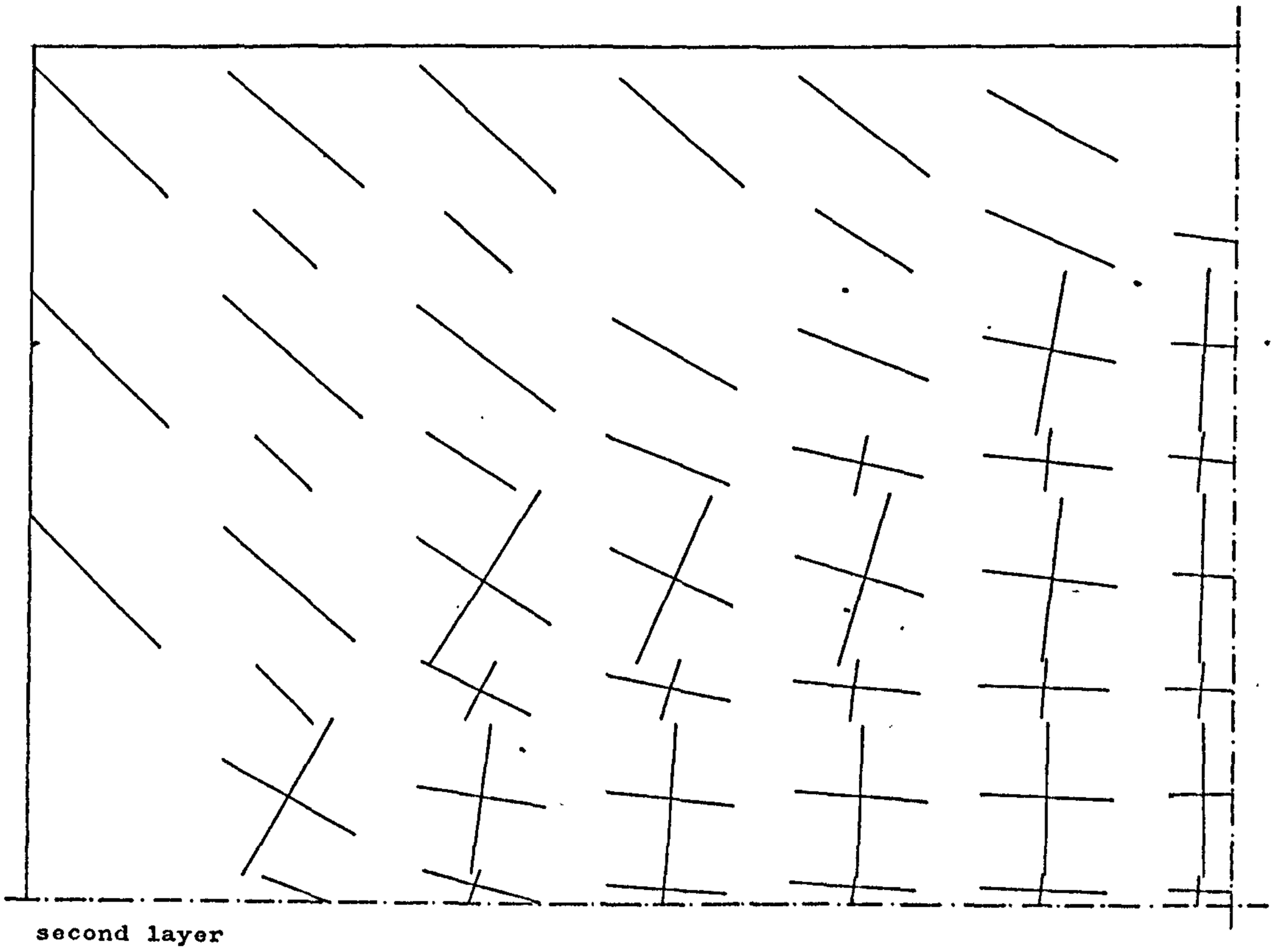

Fig. 8.22- Propagations of cracks within the first and second layers of the slab under 120% of the design load.

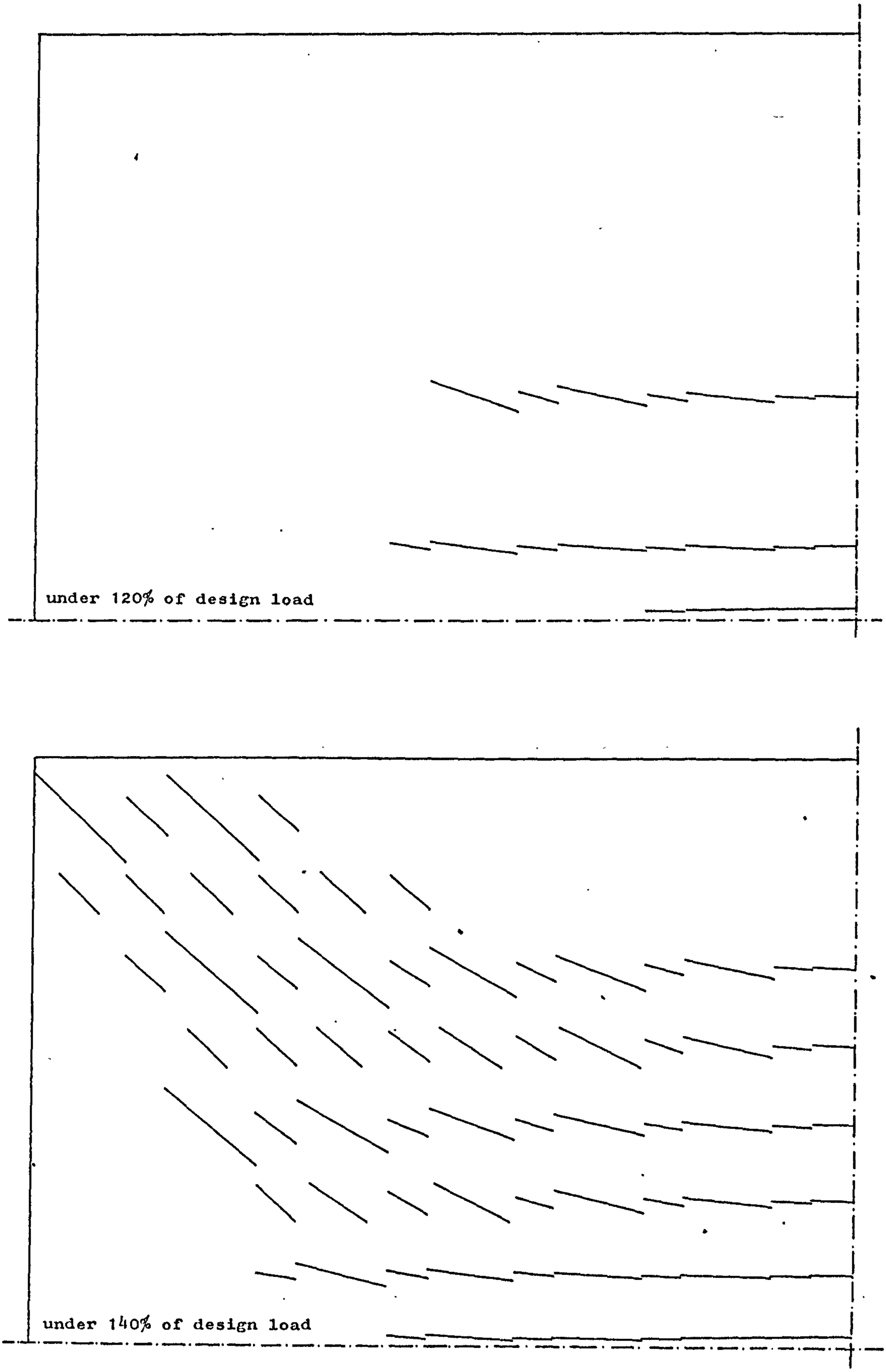

Fig. 8.23- Propagations of cracks within the 5th layer of the slab under 120% and 140% of the design load.

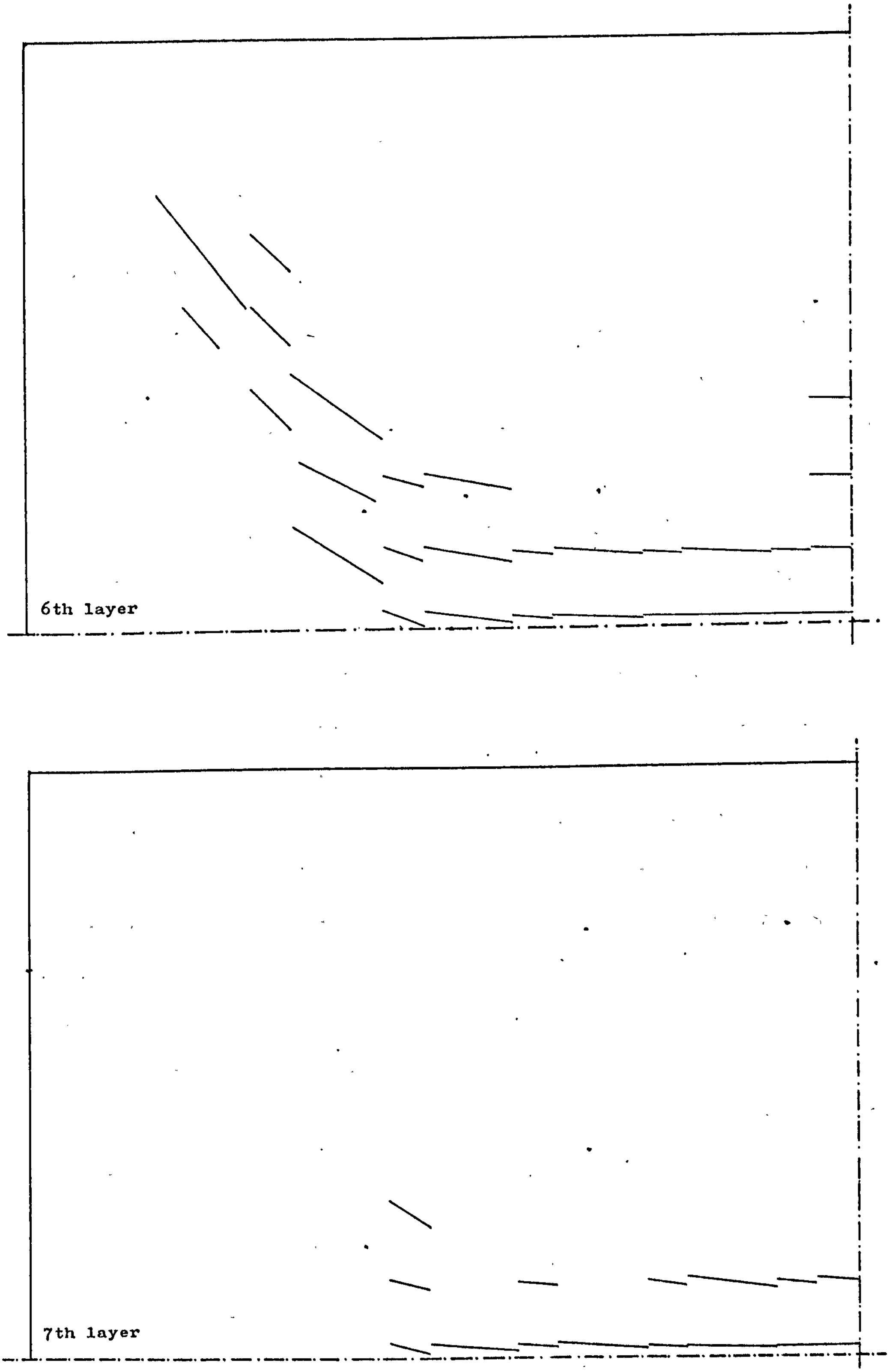

Fig. 8.24- Propagations of cracks within the 6th and 7th layers of the slab under 140% of the design load.

CHAPTER NINE

IX- Computer Programs

9.1- Introduction

Two computer programs have been developed to analyse beams and slabs under external loads and the influence of high temperature. They can, however, be used with a wide choice of options including elasto plastic solutions for plane stress and bending problems encountered in a variety of structures, unreinforced, reinforced concrete beams and slabs, I, T or box beams and can take into account the non-linear behaviour of concrete and reinforcement.The response of structures in terms of displacements, strains and stresses can be determined under gradually increasing external loads or surface temperatures and propagation of cracks can be traced up to ultimate condition. Furtheremore, it is possible to introduce any geometrical boundary conditions, external static loads and also any temperature distributions on the surface of the structures in both BEAM and SLAB programs.

These programs have been formulated by layered finite element method on the equilibrium-stiffness approach which are coded in the Fortran IV language for use on both C.D.C. 6400 and 6600 computers. The maximum size system which can be analysed is governed by the size of the computer available. With a fast core storage of 65 K, the BEAM program can analyse a member with 400 elements, 450 nodes and 2000 layers, and the SLAB program is able to analyse a member with 250 elements 300 nodes and 1500 layers.

For symmetrical configurations, boundary conditions, surface temperatures and external loads, the BEAM program analyses a quarter of the body and for symmetrical conditions of slab the corresponding program analyses a half or a quarter of the body depending on the axes of symmetry.

Distributions of temperature within beams and slabs are evaluated directly from the two or three dimensional heat equation by a classical solution considering the time variable for any type of surface temperatures, such as, uniform, linear, sinusoidal, symmetrical or any non-symmetrical boundary temperatures. These boundary temperatures can be applied on one two, three or four sides of beam structures and on one or two sides of slab structures. The surface temperatures can also be constant or time dependent. The influence of cracks, crushing of concrete layers and yielding of steel can also be taken into account.

9.2- Failure Criteria Of materials

1- Steel yields by excessive stress and a constant yield stress of the steel is, however, sustained by the steel layer and this constant yield stress itself depend on the layer's temperature value.

2- Concrete fails by cracking or crushing according to the assumed criteria of failure in biaxial state of the stress.

9.3- The Convergence Criteria

The principal stresses obtained from the analysis are compared with the actual principal stresses given from the constitutive relationship in that direction. The analytical principal stresses generally differ from the actual values except, the structure is under external load only and the material relationship is linear in the two principal directions as explained in chapter three.

To assess the accuracy of the results obtained by the analysis, the difference between the analytical and actual principal stresses are checked against the actual values. Assuming that σ'_A and σ'_B are the principal stresses of a layer in directions 1 and 2, respectively, given by the analysis, and σ'_a and σ'_b are the actual principal stresses in those directions;

$$C_1 = \left| \frac{\sigma'_A - \sigma'_a}{\sigma'_a} \right|$$

$$C_2 = \left| \frac{\sigma'_B - \sigma'_b}{\sigma'_b} \right|$$

where the ratios C_1 and C_2 define the coefficients of convergency in the two principal directions of the layer. These ratios are clearly zero in case of elastic and non-heating structures. For the present non-linear behaviour, the constitutive relationship is assumed to be satisfied, if the above ratios reduced to negligible values In order to obtain the solution of a particular load increment, the material nonlinearity of

the layers should be satisfied.

The following values are assumed as the crireia of convergency of material nonlinearities;

1- Concrete in biaxial state of stress;

$$C_1 \leq 0.05, \quad C_2 \leq 0.05$$

2- For steel layers as a rectangular layers;

$$C_1 \leq 0.02, \quad C_2 \leq 0.02$$

in which the behaviour was assumed to be elastic-plastic.

3- For a cracked concrete layer the convergence criteria is given along and perpendicular to the crack diec-tions. If a concrete layer cracks the stress perpendicular to the crack direction must be zero, i.e,

$$\sigma'_a = 0,$$

and the material relationship is assumed to converge when;

$$\left|\sigma'_A - \sigma'_a\right| \leq 0.2 \quad N./mm^2$$

4- For the crack in the second direction or crush of a concrete layer, the following condition is added to the above relation;

$$\left|\sigma'_B - \sigma'_b\right| \leq 0.2 \quad N./mm^2$$

9.4- The main Sequence Of Operations

Each program consists of the main program which reads the input data and writes the required results and calculates characteristics of the whole structural stiffness matrix and

calls various sub-routines to calculate the necessary physical and mechanical properties of layers in every particular load or time increment. The assemblage of element stiffness matrices gives the whole structural stiffness matrix, which becomes non-singular by introducing the geometrical boundary conditions, and is then inverted to obtain the nodal incremental displacements. The strains and stresses of layers are calculated in both global and principal directions in a particular load or temperature increment. The principal strains and stresses of each layer are compared and checked with the individual stress-strain relationship which is available as data and the excess stresses are released in terms of nodal forces. This procedure gives the nodal residual forces in the principal directions which are then transformed to global coordinates. Generally the principal directions of strains do not coincide with the principal directions of stresses, but as the principal stresses are important to find direction of cracking the strains and stresses are compared along the principal directions of stresses.

The above procedure is also used to calculate the nodal release forces due to temperature increasing within the layers with the following difference. The initial strains are first calculated by incremental temperature and then the nodal forces are evaluated from the layers incremental stresses corresponding to the initial strains.

If some concrete layers develop tension in their principal direction in excess of the ultimate tensile strength of concrete they are labelled as cracked layers, and the

programs release all the tensile stresses of the cracked layers in the direction perpendicular to the cracks in terms of the nodal forces. Some layers may have two cracks in two different directions. The number of cracked layers in each incremental load or temperature depends on the magnitude of incremental load or temperature.

To obtain an accurate result the number of cracked layers should be kept to a minimum and this can be achieved by reducing the magnitude of incremental load or temperature to as small a value as compatible with computer space and time. To avoid an increase in computer time the programs select the first (n) cracked layers, whose tensile stresses are greater than the rest of cracked layers, where n is given in data. The same technique is applied for yielding of the steel with the difference that, steel can carry the yield stress, and all stresses in excess of this yield stress are released. Actually the yield stress of steel and ultimate tensile stress of concrete are not constant and vary with temperature and these relationships are given in data.

However, when the nodal release forces due to initial stresses or strains are calculated, their corresponding nodal incremental displacements are obtained directly by multiplying the released forces with the inverse of the whole structural stiffness matrix, which is already available, from the previous steps. The iteration continues until all released layers reach the initial values. This process is repeated for the next increment of load or temperature.

The whole stiffness matrix of structure is updated

according to the following criteria;

1- When the number of internal iterations exceeds a prescribed number.

2- When the number of cracked layers exceeds a given number.

Updating the structural stiffness matrix is, however, quite arbitrary, i.e. with more internal iteration convergence of the results to the actual solution may be possible.

The speed of convergence of a particular solution depends on many factors namely;

1- The geometrical shape of the constitutive relation of an individual material (steel and concrete). A smooth curve representing this relationship results in a rapid convergence.

2- The magnitude of the load or temperature increment. the smaller the magnitude of the load or temperature the more rapid is the convergence for the solution of this increment.

3- Progressive cracking of concrete layers in a particular load stage. If a concrete layer cracks the stresses perpendicular to the crack directions are converted into nodal forces and distributed to the surrounding layers and elements. In order to obtain an equilibrium state of the structure with larger number of these cracks, more internal iterations are necessary.

However, it should be noted that the stiffness matrix of the structure is not necessarily updated for a new load or temperature increment.

The structure is assumed to fail in any one of the

following modes.

A- Failure by the mechanism, when enough layers or elements crack or crush so that the structural stiffness matrix becomes nearly singular, yielding large residual errors in the solution of the resulting equations.

B- Failure due to all layers and elements surrounding a node being cracked, crushed or yielding, so that the displacement of this node becomes large, which in the view point of computer is infinity.

C- Failure due to release of the unbalanced forces (caused by material non-linearities) which do not converge in a specified number of iterations.

The flow chart of the main programs is given first, followed by a brief description of the subroutines. A brief description of the main programs is given in appendix III.

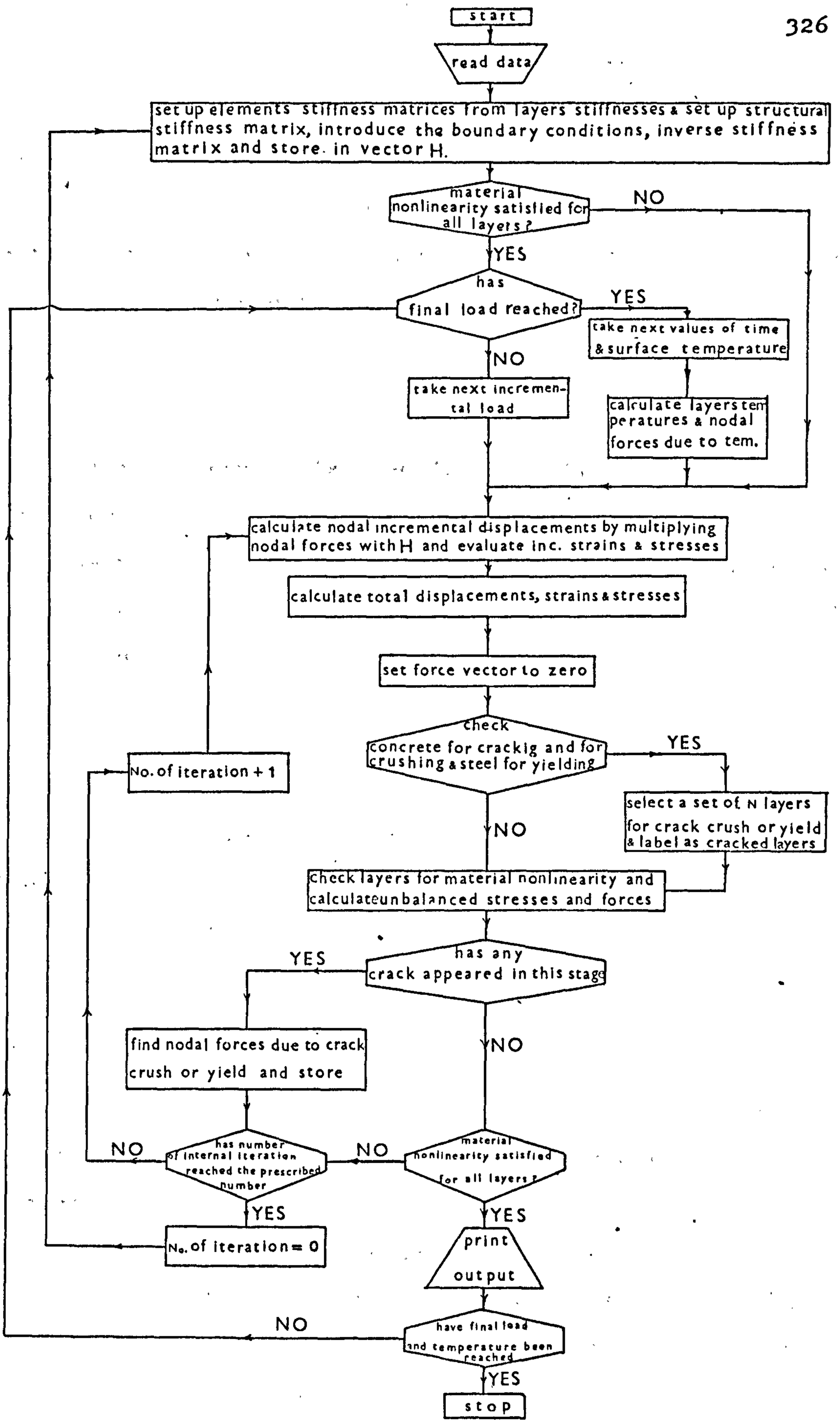
start
read data
set up elements stiffness matrices from layers stiffnesses & set up structural stiffness matrix, introduce the boundary conditions, inverse stiffness matrix and store in vector H.
material nonlinearity satisfied for all layers?
NO
YES
has final load reached?
YES
take next values of time & surface temperature
calculate layers temperatures & nodal forces due to tem.
NO
take next incremental load
calculate nodal incremental displacements by multiplying nodal forces with H and evaluate inc. strains & stresses
calculate total displacements, strains & stresses
set force vector to zero
check concrete for crackig and for crushing & steel for yielding
YES
select a set of N layers for crack crush or yield & label as cracked layers
NO
check layers for material nonlinearity and calculateunbalanced stresses and forces
has any crack appeared in this stage
YES
NO
find nodal forces due to crack crush or yield and store
No. of iteration + 1
has number of internal iteration reached the prescribed number
NO
YES
No. of iteration = 0
material nonlinearity satisfied for all layers?
NO
YES
print output
have final load and temperature been reached
NO
YES
stop

9.5- A Brief Description Of The Subroutines

There are seventeen sub-routines, either called from the main programs or from other sub-routines. A brief descriptions of these sub-routines are given here.

1- Subroutine STIFF

This subroutin is used in both the main programs and calculates directly the members of upper triangle of the 8×8 stiffness matrix of plane stress rectangular layers, in which, the equation (4.28) is used for BEAM program and the equation (4.30) is used for SLAB program.

2- Subroutine NESS

This subroutine appears in SLAB program and calculates the additional stiffness matrices of rectangular layers of slab structure given by equations (4.62) and (4.63).

3- Subroutine PIJK

The subroutine PIJK generates the nodal numbers of each element in a economical pattern. In the BEAM program it takes the nodal numbers anticlockwise, while in the SLAB program it takes the element nodal numbers clockwise. In both programs the structure is numbered in the direction of the smallest dimension by this subroutine to obtain the smallest bandwith of the structural stiffness matrix.

4- Subroutine ANGLE

This subroutine calculates the principal direction of stress of uncracked layers and gives the positive angle between the global x-axis and the first principal direction. This subroutine also evaluates the principal stresses of the uncracked layers and stors in two seperate vectors.

5- Subroutine ACTUAL

This subroutine substitutes the strains values in principal directions of stresses into the stress-strain relationship and finds the actual values of principal stresses for each layer, then calculates the residual stresses by comparing these stresses with computer results. This sub-routine also adds the residual stresses to the total stresses in principal directions for equilibrium state.

6- Subroutine EVALUE

The subroutine EVALUE first calculates the strains of the layers in principal directions of the stresses from the strain values in x and y-directions, then calculates the corresponding values of modulus of elasticity for steel or concrete material by considering the strain ratio, initial modulus, peak stress and corresponding strain and the layer;s temperature value as explained in chapter three.

This sub-routine also calculates the ultimate tensile strength of concrete material for the correspondingvalue of

temperature and also gives the yield stress of steel. The calculated yield and ultimate tensile stresses are returned to the main program to check for yielding or cracking of corresponding layer.

7- Subroutine COEF

The subroutine COEF calculates the coefficient of thermal expansion of the layer's material for a particular model which has been given in chapter three.

8- Subroutine STEADY

This subroutine calculates the first term of temperature equation in the first incremental temperature when the surface temperature distribution is constant during the time increasing and stores in vector TS(I), and in the next incremental temperature calculates the new term of the temperature by;

$$\frac{T_{i+1}}{T_i}.TS(I)$$

where T_{i+1} is the surface temperature of the next increment. When the surface temperature distribution varies with time, the sub-routine STEADY is called by the main program for every incremental temperature to evaluate the first term of the temperature equation. The characteristics of boundary temperature distribution are given in data.

9- Subroutine TEMP

The second term of temperature value is calculated by this subroutine and is called by the main program in each incremental time.

10- Subroutine DIFU

Calculates the diffusivity of the layers for a particular model of steel and concrete materials which has been given in chapter three.

11- Subroutine STRAIN

The layers incremental strains in global coordinates are evaluated in this subroutine by multiplying the incrememtal displacements with the strain matrix.

12- Subroutine DMATRX

The subroutine DMATRX constructs first the elasticity matrix in the principal direction for uncracked, cracked or layer which have yielding, then transforms into global co-ordinates by equation (4.26).

13- Subroutine UNSTRS

This subroutine transforms the unbalanced stresses due to incremental temperature strains, residual stresses or released stresses of cracked, crushed of concrete layers or

which have yielded steel, into the global coordinates. This subroutine also adds the unbalanced stresses (initial values) to the totat stresses of the layer.

14- Subroutine UNFORC

The nodal release forces of elements due to stresses of cracked layers are calculated in this subroutine and then substituted into the incremental displacement vector in the BEAM program.

15- Subroutine RELEAS

The nodal forces due to incremental temperature strains are calculated and stored in incremental displacement vector in this subroutine.

16- Function JKW

This function takes the number of row and column of the element stiffness matrix and calculate the local number of corresponding term in structural stiffness matrix in a vector form.

17- Subroutine SOLVE

The subroutine SOLVE is a standard subroutine which calculates the inverse of any non-singular and symmetrical matrix written in the upper or lower triangular terms

in a vector form by well known Choleski method with the difference that, in the present programs the inverse of the stuctural stiffness matrix is stored in stiffness matrix itself to use in next iteration.

The Choleski method of matrix inversion depends upon the properties of triangular matrices. The basis of this method is that any squar matrix can be expressed as the product of an upper and a lower triangular matrices. The actual inversion of the matrix is then reduced to the inversion of the two triangular matrices, which is very simple procedure.

In the present problems the structural stiffness matrices that to be inverted are symmetric, and for these cases only one triangular matrix need be inverted.

It is assumed first that the nonsingular matrix $\underline{H}$ can be expressed as the product of a lower triangular matrix $\underline{L}$ and a unit upper triangular matrix $\underline{U}$, which all the diagonal elements of matrix $\underline{U}$ are units, so that;

$$\underline{H} = \underline{L} \cdot \underline{U} \qquad (9.i)$$

By multiplying out the triangular matrices in the above equation and equating the corresponding matrix elements all terms of triangular matrices are obtained one after each other. Once the two triangular matrices $\underline{L}$ and $\underline{U}$ have been calculated, the inverse of the matrix $\underline{H}$ is determined from;

$$\underline{H}^{-1} = \underline{U}^{-1} \cdot \underline{L}^{-1}$$

To determine the inverse of lower triangular matrix

the following relationship is used;

$$\underline{L} \cdot \underline{L}^{-1} = \underline{I} \qquad (9.2)$$

where $\underline{I}$ is the identity matrix, and the members of matrix $\underline{L}^{-1}$ must be calculated. By multiplying the triangular matrix $\underline{L}$ with its inverse in equation (9.2) and equating corresponding identity matrix $\underline{I}$ the terms of matrix $\underline{L}^{-1}$ are evaluated one after each other. The inverse of the lower triangular matrix also becomes a lower triangular matrix. Finally, the inverse of the unit upper triangular matrix $\underline{U}$ is calculated, which becomes an upper triangular matrix.

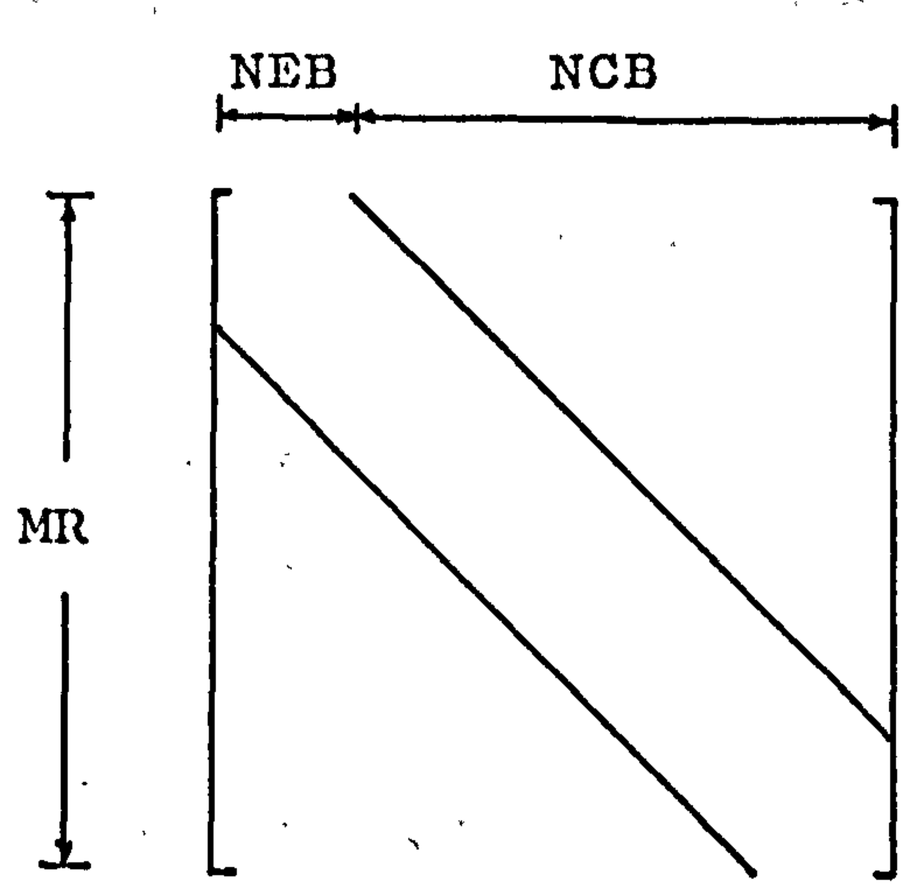

Fig. 9.1- Characteristics of structural stiffness matrix.

CHAPTER TEN

X- Conclusions

10.1- General Conclusions

1- The temperature equations derived from the classical solution of the heat conduction equation can be efficiently utilized to calculate the distribution of temperature within two or three dimensional rectangular bodies for a given distribution of surface temperature (constant or time variable).

2- The layered finite element models developed for reinforced concrete beams and slabs is realistic in that the steel reinforcement simulates very closely to the designed slab and can therefore be usefully employed to simulate other structural members with different boundary conditions and geometrical configurations. The programs have facilities which allow the use of concrete and/or steel members under load and fire temperatures to be analysed, which to the authors knowledge is not available in the literature.

3- The technique used to deal with material non-linearities can be modified to include geometrical nonlinearity of the members which may arise due to the large displacements.

4- The crack patterns in slabs can be traced under increasing loads and temperature. A pattern results which although is more detailed than the yield line analysis for slabs under loading alone is still compatible with it. The final pattern that emerges therefore can be considered as the

true yield lines of a slab under loading.

5- In addition the effect of temperature is to distort the slab in a complicated manner and cracks propagate not necessarily in the same direction as those of the load. Thus the analysis can be considered to have derived a 'yield line' crack pattern under temperature condition. This shows clearly that the effect of the cracking due to heat can only be superimposed vectorially.

10.2- Conclusions From The Analytical Results Of The Beams And Slabs

From the analysis of the simply supported beams, heated from three surfaces (bottom and two side faces), the following conclusions may be drawn;

1. The Unloaded Unreinforced Concrete Beam

The behaviour of this member when subjected to fire deflects downwards near the mid-span and upwards around the supports at early stages of heating. Compressive stresses exist at the sides near the bottom increasing towards the bottom face. These compressive stresses, however, decrease towards the inner sections of the member and become tensile near the mid-section.

As the temperature increases on the boundaries, the member moves upwards until a maximum upward deflection is reached at a section somewhat closer to the mid-span than to the supports. With further increase of temperature a

reversal of stress distribution takes place around the top and the bottom faces of the member. The member starts to deflect downwards rapidly until failure occurs.

2. Reinforced Concrete Beams

These members deflect downwards at all stages of heating, whether they are loaded (four equal point loads at 1/8 and 3/8 of the span from the supports) or unloaded before subjected to fire. The magnitude of deflection depends on the amount of the applied load prior to heating, percentage of the reinforcement and particularly the location of the tensile reinforcing bars.

a-When a small load is applied (such as self weight), compressive stresses may exist around the bottom face. This stress distribution, however, varies depending on the amount of the load and percentage and location of tensile reinfoecement.

b-When the magnitude of the load is appreciable in comparison with the design load, tensile stresses around the bottom face and compressive stresses at the top appear in the members. The tensile stress in the reinforcement decreases with an increase of temperature on the member surfaces.

3. Reinforced Concrete Slabs

The following conclusions may be drawn from the analytical study of uniformly loaded rectangular reinforced concrete slabs simply supported along all sides and subjected to a temperature distribution at the bottom face, which has

a maximum at the centre and decreases to $\frac{1}{4}$ of the maximum value towards the supports.

a- When the load is small the member deflects downwards during the early stages of heating causing compressive stresses at the bottom face and tensile stresses at the top. The magnitudes of these stresses depend on the design and detailing of the member i.e. the percentage and the position of the tensile reinforcing bars. This can be seen in the example of the designed slab which contained 1.5% reinforcement as compared with the example when the steel reinforcement was increased to as much as 5%. As temperature increases on the bottom suface of the slab, the direction of deflection depends on the percentage of reinforcement. In the case where no reinforcement is provided the slab deflects away from the hot surface. When 1.5% reinforcement is provided the deflection may be in either direction depending on its location. In the case described, there was an initial downward deflection followed by a slight hogging and final downward deflection. When 5% reinforcement was included the deflection was always towards the hot surface.

b- When the magnitude of the load is close to the design load the member deflects downwards throughout the heating. Tensile stresses exist at the bottom face and compressive stresses around the top of the member prior to failure.

10.3- Recommendation For Future Work

1- A parametric study can be under taken using the designed reinforced concrete models to study the effect in greater detail of the load magnitude prior to heating and percentage of reinforcement on the behaviour of beams and slabs when subjected to fire.

2- The present models can, with the appropriate modification, include the effect of creep on the behaviour of reinforced concrete beams and slabs, which from the analytical view is similar to the effect of temperature (initial strain method).

3- These models can also be used as subroutine of a general frame analysis to study the effect of local fire in two or three dimensional frame system.

REFERENCES

1- POPOVICS, S. "A Review of Stress-Strain Relationships for Concrete" ACI Jouunal, Vol. 67, No. 14, March 1970, PP. 243-248.

2- HOGNESTAD, E. "A Study of Combined Bending and Axial Load in Reinforced Concrete Members" Bulletin No. 399, Engineering Experiment Station, University of Illinois, Urbana, Illinois, Nov. 1951, PP. 128.

3- HOGNESTAD, E., HANSON, N.W. and McHENRY, D. "Concrete Stress Distribution in Ultimate Strength Design" ACI Journal, Proceedings Vol. 52, No. 4, Dec. 1955, PP. 455-479.

4- SMITH, R.G. "The Determination of Compressive Stress-Strain Properties of Concrete in Flexure" Magazine of Concrete Research, Vol. 12, No. 36, London, Nov. 1960, PP. 165-170.

5- BROCK, G. "Concrete: Complete Stress-Strain Curves" Engineering, Vol. 109, London, May 1962, PP. 1606-1608.

6- KIRTZ, L.B. and LEE, S.L. "Ultimate Strength of Over Reinforced Beams" Journal of the Engineering Mechanics Division, ASCE, Vol. 86, No. EM3, Proc. Paper 2502, June 1960, PP. 95-105.

7- RUSCH, H. "Researches Toward a General Flexural Theory for Structural Concrete" ACI Journal, Proceedings Vol. 57,

No. 1, July 1960, PP. 1-28.

8- DESAYI, P. and KRISHNAN, S. "Equation for the Stress-Strain Curve of Concrete" ACI Journal, Vol. 61, No. 3, March 1964, PP. 345-350.

9- SAENZ, L.P., Discussion of "Equation for the Stress-Strain Curve of Concrete" by DESAYI KRISHNAN, ACI Journal, Vol. 61, Sept. 1964, PP. 1229-1235.

10- STURMAN, G.M., SHAH, S.P. and WINTER, G. "Effect of Flexural Strain Gradient on Microcracking and Stress-Strain Behaviour of Concrete" ACI Journal, Proc. Vol. 62, No. 7, July 1965, PP. 805-822.

11- KUPFER, H., HILSDORF, H.K. and RUSCH, H. "Behaviour of Concrete Under Biaxial Stresses" ACI Journal, Vol. 66, No. 8, Aug. 1969, PP. 656-666.

12- BRESLER, B. and PISTER, K.S. "Strength of Concrete Under Combined Stresses" ACI Journal, Vol. 55, No. 3, Sep. 1958, PP. 321-345.

13- GOODE, C.D. and HELMY, M.A. "The Strength of Concrete Under Combined Shear and Direct Stress" Magazine of Concrete Research, Vol. 19, No. 59, June 1967, PP. 105-112.

14- McHENRY, D. and KARNI, J. "Strength of Concrete Under Combined Tensile and Compressive Stress" ACI Journal, Proceedings Vol. 54, No. 10, April 1958, PP. 829-840.

15- NEWMAN, K. and NEWMAN, J.B. "Failure Theories and Design Criteria for Plain Concrete" International Conference on Structures, Solid Mechanics and Energy. Design in Civil Engineering, Southampton University, April 1969, Paper 83.

16- KUPFER, H. "Das Verhalten des Betons unter mehrachsiger Kurzzeitbelastung unter besonderer Berucksichtigung der Zweiachsigen Beanspruchung" Deutscher Ausschuss Fur Stahlbeton, HEFT 229, Berlin 1973.

17- HILSDORF, H. "The Specification of Biaxial Strength in Concrete" (Die Bestimmung der Zweiachsigen Festigkeit von Betons), Proceedings, Vol. 173, Deutscher Ausschuss fur Stahlbeton, Berlin, 1965.

18- BUYUKOZTURK, O., NILSON, A.H. and SLATE, F.O. Stress-Strain Response and Fracture of a Concrete Model in Biaxial Loading" ACI Journal, Proceedings Vol. 68, No. 8, Aug. 1971, PP. 590-599.

19- TIMOSHENKO, S. and WOINOWSKY-KRIEGER, S. "Theory of Plates and Shells" 2nd Edition, McGraw-Hill Book Company, 1959.

20- LIU, T.C.Y., NILSON, A.H. and SLATE, F.O. "Stress-Strain Response and Fracture of Concrete in Uniaxial and Biaxial Compression" ACI Journal, Vol. 69, No. 5, May 1972, PP. 291-295.

21- LIU, T.C.Y., NILSON, A.H. and SLATE, F.O. "Biaxial Stress-Strain Relations for Concrete" Journal of the Structural Division, ASCE, Vol. 98, May 1972, PP. 1025-1034.

22- WILLIS, T.F. and DEREUS, M.E. "Thermal Value Change of Aggregates and Their Effects on Concrete" Proc. ASTM. Vol. 39, PP. 1919-1939.

23- MALHOTRA, H.L. "The Effect of Temperature on Compressive Strength of Concrete" Magazine of Concrete Research, Vol. 8, No. 23, Aug. 1956, PP. 85-94.

24- HARMATHY, T.Z. and BRENDT, J.E. "Hydrate Portland Cement and Light Weight Concrete at Elevated Temperature" Proc. ACI Vol. 63, PP. 93-112, 1966.

25- FURUMURA, F. "The Stress-Strain Curve of Concrete at High Temperature (No. 1)" Report for Annual Meeting or Architectural Inistitute of Japan, 1966.

26- SULLIVAN, P.J. and PUCHER, M.P. "The Influence of Temperature on the Physical Properties of Concrete and Mortar in the Range of 20 to 400 ^{o}C" ACI SP-25, "Temperature and Concrete" 1968, PP. 103-135.

27- TAKEDA, J. "Strength, Elasticity and Thermal Properties of Concrete Subjected to Elevated Temperature" ACI Seminar on Concrete for Nuclear Reactors, West Berlin, 1970.

28- BIZRI, H. "Structural Capacity of Reinforced Concrete Columns Subjected to Fire Induced Thermal Gradients" Report No. UC SESM 73-1, Structural Engineering Laboratory, University of California, Berkeley, California, Tanuary 1973.

29- AKHTARUZZAMAN, A.A. The Effect Of Transient and Steady Temperature on Concrete" Thesis Submitted for Ph.D. of University of London, January 1973.

30- CAMPBELL-ALLEN, D. and THORNE, C.P. "The Thermal Conductivity of Concrete" Magazine of Concrete Research, Vol. 15, No. 43, March 1963, Cement and Concrete Association, PP. 39-48.

31- HARADA, T. "The Variation of Thermal Conductivity of Cement Mortar and Concrete Under High Temperature" Transaction of the Architectural Inistitute of Japan, No. 49, September 1954.

32- HARADA, T., SHIINA, T. and TANAKA, T. "Results of Measuring the Thermal Properties of Steam-Curing Concrete at High temperature" Report for Meeting of Architectural Inistitute of Japan, 1966, PP. 145-148.

33- ODEEN, K. "Calculation of the Fire Endurance of P.C. and P.S.V. Beams" Division of Building Construction, Royal Institute of Technology, Bulletin 1970, Stockholm, PP.74.

34- PHILLEO, R. "Some Physical Properties of Concrete at High Temperature" ACI Journal, Vol. 54, April 1958, PP. 857.

35- HARMATHY, T.Z. "Thermal Properties of Concrete at Elevated Temperature" ASTM, Journal of Materials, March 1960, PP. 47-74.

36- HARMATHY, T.Z. "Effect of Moisture of the Fire Endurance of Building Element" ASTM STP-385, Moisture in Materials in Relations to Fire Tests 1965.

37- KISHITANI, K. "Material Properties at Elevated Temperature" Encyclopedia of Architecture, Vol. 21, Shokokusha Ltd., Fire Protection of Buildings, Tokyo, 1970, PP.203.

38- HARMADA, M. "Light weight Concrete Structure" Maruzen Ltd., 1956.

39- ORCHARD, D.F. "Concrete Technology" Vol. 1, 1958.

40- The British Iron and Steel Research Association, "Physical Constants of some Commercial Steels of Elevated Temperature" Butterworths Scientific Publications, London, 1953.

41- SIMMONS, W.F. and CROSS, H.C. "Elevated Temperature Properties of Carbon Steel" ASTM STP 180, 1955.

42- The British Iron and Steel Research Association and the Iron and Steel Institute "High-Temperature Properties of Steels" April 1966.

43- JOHNSON, R.F., GLEN, J., MAY, M.J., THURSTON, H.G. and ROSE, B.H. "The analysis and Assessment of Elevated-Temperature Lower Yield or Proof Stress, Creep and

stress-Rupture Data" The British Iron and Steel Research Association and the Iron and Steel Institute, PP.61-77.

44- TODESCHINI, C.E., BIANCHINI, A.C. and KESLER, C.E. "Behaviour of Concrete Columns Reinforced with High Strength Steels" ACI Journal Proc. Vol. 61, No. 6, June 1964, PP. 701-716.

45- PFRANG, E.O., SIESS, C.P. and SOGEN, M.A. "Load Moment Curvature Characteristics of Reinforced Concrete Cross-Sections" ACI Journal Proc. Vol. 61, No. 7, July 1964, PP. 763-777.

46- SARGIN, M. "Stress-strain Relationship for Concrete and the Analysis of Structural Concrete Sections" Study No. 4, Solid Mechanics Division, University of Waterloo, Ontario, Canada, 1971.

47- ODEN, J.T. "Finite Element Applications in Nonlinear Structural Analysis" Proceedings of the Symposium on Application of Finite Element Method in Civil Enginner-ing, ASCE, Nashville, Nov. 1969, PP. 419-456.

48- ARGYRIS, J.H. "Elasto-Plastic Matrix Displacement Analysis of Three Dimensional Continua" Journal of Royal Aero-nautical Society, Vol. 69, Sept. 1965, PP. 633-636.

49- NILSON, A.H. "Finite Element Analysis of Reinforced Concrete" Ph.D Thesis, University of California, Berkeley, California, 1967.

50- FRANKLIN, H.A. "Nonlinear Analysis of Reinforced Concrete Frames and Panels" Report No. SESM-70-5, Department of Civil Engineering, University of California, Berkeley, March 1970.

51- MARCAL, P.V. and KING, I.P. "Elastic-Plastic Analysis of Two Dimensional Stress System by the Finite Element Method" Int. Journal Mech. Sci., Vol. 9, No. 3, 1967, PP. 143-155.

52- ZIENKIEWICZ, O.C., VALLIAPPAN, S. and KING, I.P. "Stress Analysis of Rock as a 'No Tension' Material" Geotechnique, Vol. 18, No. 1, 1968, PP. 56-66.

53- ZIENKIEWICZ, O.C., VALLIAPPAN, S. and KING, I.P. "Elasto-Plastic Solutions of Engineering Problems, Initial Stress, Finite Element Approach" International Journal for Numerical Method in Engineering, Vol. 1, Jan. 1969, PP. 75-100.

54- ZIENKIEWICZ, O.C. and VALLIAPPAN, S. "Analysis of Real Structures for Creep, Plasticity and othe Complex Constitutive Laws" Conf. on Materials in Civil Eng.,. University of Southampton, 1969.

55- HRENNIKOFF, A. "Plane Stress and Bending of Plates by Method of Articulated Framework" Doctoral Thesis, Massachusetts Institute of Technology, Boston, U.S.A., May 1940.

56- HRENNIKOFF, A. "Solution of Problems in Elasticity by the Framework Method" Journal of Applied Mechanics, Vol. 8, 1941.

57- HRENNIKOFF, A. "Framework Method and its Technique for Solving Plane Stress Problems" International Association for Bridge and Structural Engg. Zurich 1949.

58- McHENRY, D. "A Lattice Analogy of the Solution of Stress Problems" Journal of the Institution of Civil Engineers, Vol. 21, No. 2, 1943-1944, PP. 59-82.

59- PESTEL, E.C. "Investigation of Plate and Shell Models by Matrix" Technische Hochschule, Hannover, Report No. 434846 to European Office, Aerospace, U.S. Air Force, Brussels, Belgium.

60- PARIKH, E.S. and MORRIS, C.H. "Analysis of Shells using Framework Analogy" Proceegings, World Conference on Shell Structures, San Francisco, California, U.S.A., Oct. 1962.

61- McCORMIC, C.W. "Plane Stress Analysis" Journal of Structural Division, American Society of Civil Engineers, Proc. Paper No. 3581, Vol. 89, ST. 4, Aug. 1963.

62- ARGYRIS, J.H. "Energy Theorems and Structural Analysis" Aircraft Engg., 26, 1954-Aircraft Engg. 27, 1955.

63- TURNER, M.J., CLOUGH, R.W., MARTIN, H.C. and TOPP, L.J. "Stiffness and Deflection Analysis of Complex Structures" Journal Aeronaut. Sci. 23, No. 9, 1956.

64- PRZEMIENIECKI, J.S. "Theory of Matrix Structural Analysis" McGraw Hill, 1968.

65- SINGHAL, A.C. "775 Selected References of The Finite Element Method of Structural Analysis" Report S-12, Civil Engineering Dept., Laval Unive., Quebec, Jan. 1969.

66- GALLAGHER, R.H. "Analysis of Plate and Shell Structures" Proceedings of the Symposium on Application of Finite Element Method in Civil Engineering, Nashville, Tennessee, Nov. 13-14, 1969.

67- CLOUGH, R.W. "The Finite Element Method in Plane Stress Analysis" 2nd Conference on Electronic Computer, ASCE, Pittsburgh, Sept., 1960, PP. 345-378.

68- WILSON, E.L. "Matrix Analysis of Non-linear Structures" 2nd Conference on Electronic Computation, ASCE, Pittsburgh, Sept., 1960, PP. 415-428.

69- DOHERTY, W.P., WILSON, E.L. and TAYLOR, R.L. "Stress Analysis of Axisymmetric Solids Utilizing Higher Order Quadrilateral Finite Elements" SESM Depart 69-3, Struct. Eng. Lab., University of California, Berkeley, 1969.

70- WILSON, E.L., TAYLOR, R.L., DOHERTY, W.P. and GHABOUSSI, J. "Incompatible Displacement Methods" Proc. O.N.R. Conf. on Numerical Methods, Urbana, Illinois, Sept, 1971, PP. 43-57.

71- WILSON, E.L. "Finite Element Analysis of Two Dimensional Structures" A Thesis, Structural and Materials Research Report No. 63-2, Dept. of Civil Engineering, University of California, Berkeley, June 1963.

72- MALLETT, R.H. "Mathematical Models for Structural Discrete Elements" Unpoblished Lecture Notes, Cornell University, Fall 1966.

73- ZIENKIEWICZ, O.C. "The finite Element Method in Engineering Sciences" 2nd Edition, McGrow Hill Book Co. Inc., London, England, 1971.

74- FENVES, S.J., PERRONE, N., ROBINSON, A.R. and SCHNOBRICH, W.C. "Numerical and Computer Method in Structural Mechanics" Academic Press, New York and London, 1973.

75- NGO, D. and SCORDELIS, A.C. "Finite Element Analysis of Reinforced Concrete Beams" ACI Journal, Vol. 64, No. 3, March 1967, PP. 153-163.

76- NGO, D., FRANKLIN, H.A. and SCORDELIS, A.C. "Finite Element Study of Reinforced Concrete Beams with Diagonal Tension Crack" Report No. UC SESM 70-19, Dept., Civil Eng., University of California, Berkeley, Dec. 1970.

77- TAYLOR, M.A. and BROMS, B. "Shear Bond Strength Between Coarse Aggregate and Cement Paste or Mortar" ACI Journal Proceedings Vol. 61, No. 8, Aug. 1964, PP. 939-957.

78- VILLIAPPAN, S. and NATH, P. "Tensile Crack Propagation in Reinforced Concrete Beams by Finite Element Technique" International Conference on Shear Tension and Bond in Reinforced Concrete, India, Jan. 1969.

79- CERVENKA, V. "Inelastic Finite Element Analysis of Reinforced Concrete Panels under In-plane Loads" Ph.D. Thesis University of California, 1970.

80- VALLIAPPAN, S. and DOOLAN, T.F. "Nonlinear Stress Analysis of Reinforced Concrete" Journal of the Structural Division, ASCE, Vol. 98, No. ST4, Proc. Paper 8845, April 1972, PP. 885-898.

81- SCHNOBRICH, C., SALEM, M.H., PECKNOLD, D. and MOHRAZ, B., Discussion on "Nonlinear Stress Analysis of Reinforced Concrete" Journal of the Structural Division, ASCE, Vol. 98, No. ST10, Oct. 1972, PP. 2327-2328.

82- NAM, C.H. and SALMAN, C.G. "Finite Element Analysis of Concrete Beams" Journal of the Structural Division, ASCE, ST12, Dec. 1974, PP. 2419-2432.

83- HAND, F.R., PECKNOLD, D.A. and SCHNOBRICH, W.C. "Nonlinear Layered Analysis of RC. Plates and Shells" Journal of the Structural Division ASCE, ST7, July 1973, PP. 1491-1505.

84- SUIDAN, M. and SCHNOBRICH, W.C. "Finite Element Analysis of Reinforced Concrete" Journal of the Structural Division, ASCE, ST10, Oct. 1973, PP. 2109-2122.

85- COLVILLE, J. and ABBASI, J. "Plane Stress Reinforced Concrete Finite Element" Journal of the Structural Division, ASCE, ST5, May 1974, PP. 1067-1083.

86- LIN, C. and SCORDELIS, A.C. "Nonlinear Analysis of RC. Shells of General Form" Journal of the Structural Division, ASCE, ST3, March 1975, PP. 523-538.

87- SHAH, S.P. and WINTER, G. "Inelastic Behaviour and Fracture of Concrete" ACI journal, Vol. 63, No. 9, Sept. 1966, PP. 925-930.

88- BROMS, B. "Crack width and Crack Spacing in Reinforced Concrete Members, Part 1" ACI Journal Proceedings Vol. 62, No. 10, Oct. 1965, PP. 1237-1255.

89- BROMS, B. "Stress Distribution in Reinforced Concrete Members with Tension Cracks, Part 2" Supplement, ACI Journal 1965.

90- BROMS, B. "Crack Width and Crack Spacing in Reinforced Concrete Members, Part 2" Supplement, ACI Jounal 1965.

91- CEDOLIN, L. and DEI POLI, S. "Finite Element Nonlinear Analysis of Reinforced Concrete Bidimensional Structures" Technical Report No. 40, I.S.T.C., Polytechnic Milano, Sept. 1974, PP. 66.

92- COOK, R.D. "Concepts and Applications of Finite Element Analysis" John Wiley & Sons Book Co. Inc., New York, London, Sydney and Toronto, 1974.

93- MALHOTRA, H.L. "Fire Resistance of Structural Concrete Beams" Report No. 741, Fire Research Station, May 1969.

94- NEWMAN, J.B. "Criteria for Concrete Strength" Ph.D. Thesis, University of London, Dec. 1973.

95- KOTOSOVOS, M. "Failure Criteria Under Generalized Stress States" Ph.D. Thesis, University of London 1974.

96- HSU, T.T.C., SLATE, F.O. STURMAN, G.M. and WINTER, G., "Microcracking of Plain Concrete and the Shape of the Stress-Strain Curve" ACI Journal, Proceedings Vol. 60, No. 2, Feb. 1963, PP. 209-224.

97- ROSENTHAL, L. and GLUCKICH, J. "Strength of Plain Concrete Under Biaxial Stress" ACI Journal, Proceedings Vol. 67, No. 11, Nov. 1970, PP. 903-914.

98- VILE, G.W.D. "Strength of Concrete Under Short-time Static Biaxial Stress" International Conference on the Structure of Concrete, Paper F2, Sept. 1965.

99- ROBINSON, G.S. "Behaviour of Concrete in Biaxial Compression" Proceedings, ASCE, Vol. 93, ST1, Feb. 1967, PP. 71-86.

100- CARSLAW, H.S. and JAEGER, J.C. "Conduction of Heat in Solids" 2nd Edition, Oxford at the Clarendon Press, Oxford, England, 1971.

101- ODEEN, K. "Experimental and Theoretical Studies on Fire Resistance of Double-T Units" Report 23, Stockholm, 1968.

102- PETTERSON, O. "Fire Engineering Research Today and in Future" Division of Building Construction, KTH, Bulletin 11, Stockholm, 1964.

103- KOLLBRUNNER, C.F. "Beurteilung der Feuersicherheit von Stahlhochbauten" Internationale Vereinigung fur Bruckenban and Hochban, Sechster Kongress, Schlussbericht, Stockholm, 1960.

104- TIMOSHENKO, S. and GOODIER, J.N. "Theory of Elasticity" 3rd Edition, McGraw-Hill Book Company, 1970.

105- "Fire tests on building materials and structures" BS 476 Part 8, 1972.

APPENDIX I

$$\frac{1}{6} = \int_0^1 (1-\bar{x})(1-2\bar{x}).d\bar{x} = \int_0^1 \bar{x}(1-\bar{x}).d\bar{x} = \int_0^1 (1-\bar{x})(1-2\bar{x})(1-3\bar{x}).d\bar{x}$$

$$\frac{1}{2} = \int_0^1 (1-2\bar{x})(2-3\bar{x}).d\bar{x} = \int_0^1 (1-\bar{x})(2-3\bar{x}).d\bar{x} = \int_0^1 (1-3\bar{x})(2-3\bar{x}).d\bar{x}$$

$$\frac{1}{2} = \int_0^1 (1-2\bar{x})(1-3\bar{x}).d\bar{x} = -\int_0^1 \bar{x}(1-3\bar{x}).d\bar{x} = -3\int_0^1 \bar{x}(1-2\bar{x}).d\bar{x}$$

$$\frac{1}{4} = \int_0^1 \bar{x}(2-3\bar{x})^2.d\bar{x} = \int_0^1 (1-\bar{x})(1-3\bar{x})^2.d\bar{x} = \int_0^1 \bar{x}(1-3\bar{x})(2-3\bar{x}).d\bar{x}$$

$$\frac{2}{15} = \int_0^1 \bar{x}^2(2-3\bar{x}).d\bar{x} = \int_0^1 (1-\bar{x})^2(1-3\bar{x})^2.d\bar{x}$$

$$\frac{1}{12} = \int_0^1 (1-\bar{x})^2(1-3\bar{x}).d\bar{x} = \int_0^1 \bar{x}(1-\bar{x})(2-3\bar{x}).d\bar{x} = -\int_0^1 \bar{x}^2(2-3\bar{x}).d\bar{x}$$

$$\frac{1}{6} = \int_0^1 \bar{x}(1-2\bar{x})(2-3\bar{x}).d\bar{x} = -2\int_0^1 \bar{x}(1-\bar{x})(1-3\bar{x}).d\bar{x}$$

$$\frac{1}{3} = \int_0^1 (1-2\bar{x})^2.d\bar{x} = 10\int_0^1 \bar{x}(1-\bar{x})(1-3\bar{x})(2-3\bar{x}).d\bar{x}$$

$$0 = \int_0^1 \bar{x}(2-3\bar{x}).d\bar{x} = \int_0^1 (1-\bar{x}).d\bar{x}\int_0^1 (1-2\bar{y})\left[1-6(\bar{x}+\bar{y})+6(\bar{x}^2+\bar{y}^2)\right].d\bar{y}$$

$$\frac{1}{4} = \int_0^1 (1-\bar{x})1-3\bar{x})(2-3\bar{x}).d\bar{x} = -\tfrac{1}{2}\int_0^1 d\bar{y}\int_0^1 \bar{x}\left[1-6(\bar{x}+\bar{y})+6(\bar{x}^2+\bar{y}^2)\right].d\bar{x}$$

$$1 = \int_0^1 (2-3\bar{x})^2.d\bar{x} = \int_0^1 (1-3\bar{x})^2.d\bar{x}$$

$$\frac{1}{10} = \int_0^1 (1-\bar{x})(1-3\bar{x}).d\bar{x}\int_0^1 \left[1-6(\bar{x}+\bar{y})+(\bar{x}^2+\bar{y}^2)\right].d\bar{y}$$

$$\frac{1}{4} = \int_0^1 (1-\bar{x}).d\bar{x}\int_0^1 (1-3\bar{y})\left[1-6(\bar{x}+\bar{y})+6(\bar{x}^2+\bar{y}^2)\right].d\bar{y}$$

$$-\tfrac{1}{2} = \int_0^1 (1-\bar{x}).d\bar{x} \int_0^1 [1-6(\bar{x}+\bar{y})+6(\bar{x}^2+\bar{y}^2)].d\bar{y}$$

$$-\frac{1}{10} = \int_0^1 \bar{x}(2-3\bar{x}).d\bar{x} \int_0^1 [1-6(\bar{x}+\bar{y})+6(\bar{x}^2+\bar{y}^2)].d\bar{y}$$

$$-\tfrac{1}{4} = \int_0^1 (1-\bar{x}).d\bar{x} \int_0^1 (2-3\bar{y})[1-6(\bar{x}+\bar{y})+6(\bar{x}^2+\bar{y}^2)].d\bar{y}$$

$$0 = \int_0^1 (1-2\bar{x}).d\bar{x} \int_0^1 \bar{y}[1-6(\bar{x}+\bar{y})+6(\bar{x}^2+\bar{y}^2)].d\bar{y}$$

$$-\tfrac{1}{4} = \int_0^1 (2-3\bar{x}).d\bar{x} \int_0^1 \bar{y}[1-6(\bar{x}+\bar{y})+6(\bar{x}^2+\bar{y}^2)].d\bar{y}$$

$$-\tfrac{1}{4} = \int_0^1 (1-3\bar{x}).d\bar{x} \int_0^1 \bar{y}[1-6(\bar{x}+\bar{y})+6(\bar{x}^2+\bar{y}^2)].d\bar{y}$$

$$\frac{7}{5} = \int_0^1 d\bar{x} \int_0^1 [1-6(\bar{x}+\bar{y})+6(\bar{x}^2+\bar{y}^2)].d\bar{y}$$

APPENDIX II

Part One

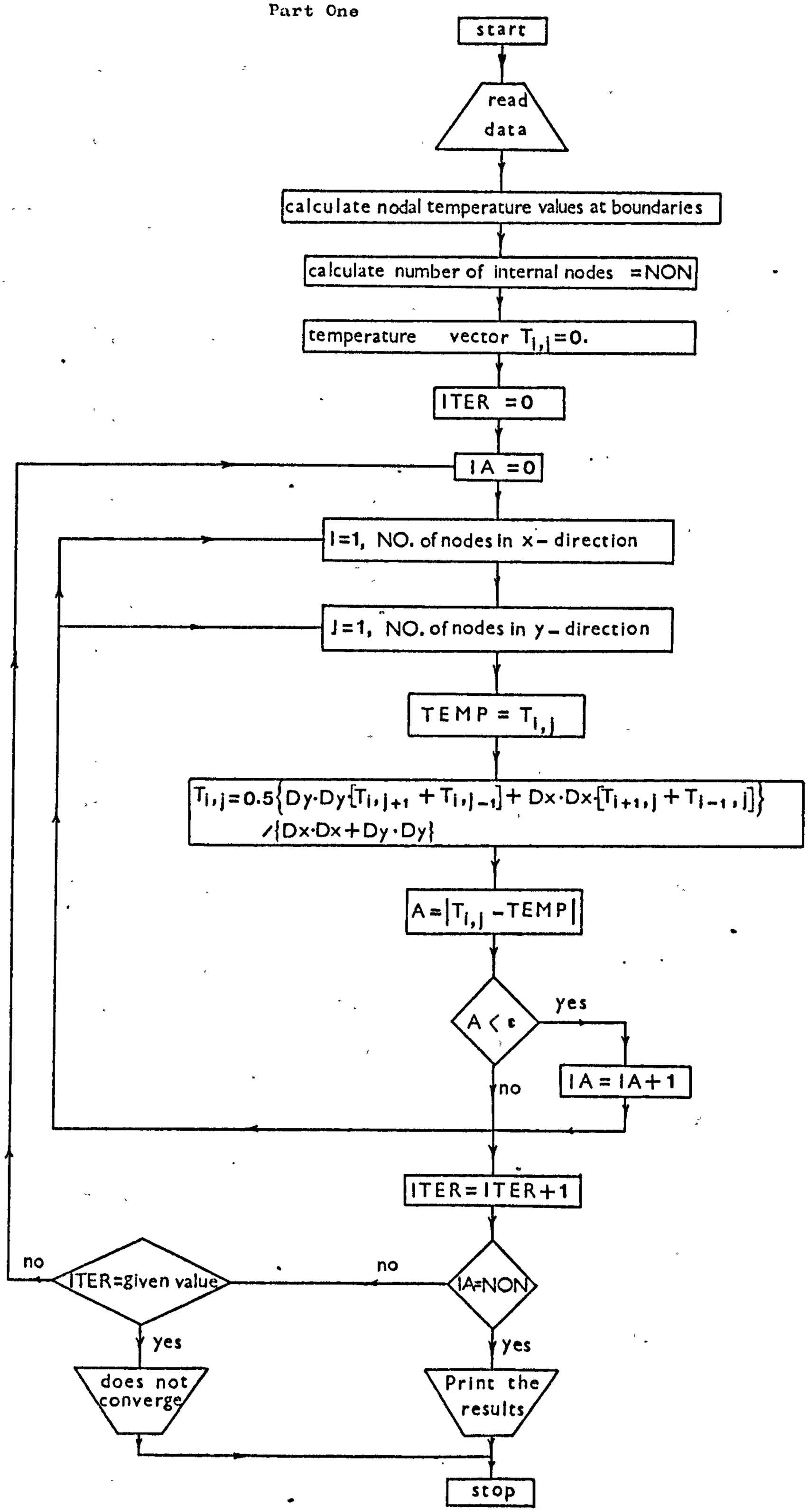

2- Comparison The Classical And Numerical Solution Of Heat Conduction Equation.

Point	Coordinates		Temperature Value		differ-
No.	X	Y	Numer.	Class.	ence %
1	5.0	2.5	71.8	72.0	0.27%
2	5.0	5.0	48.9	49.0	0.20%
3	5.0	7.5	35.8	36.1	0.83%
4	5.0	10.0	27.7	28.0	1.07%
5	5.0	12.5	22.2	22.5	1.33%
6	5.0	15.0	18.2	18.5	1.62%
7	5.0	17.5	15.4	15.8	2.53%
8	5.0	20.0	12.9	13.4	3.73%
9	5.0	22.5	10.9	11.5	5.22%
10	10.0	2.5	80.2	80.4	0.25%
11	10.0	5.0	67.3	67.5	0.29%
12	10.0	7.5	55.7	55.9	0.35%
13	10.0	10.0	46.3	46.6	0.64%
14	10.0	12.5	38.8	39.2	1.02%
15	10.0	15.0	32.9	33.4	1.50%
16	10.0	17.5	28.0	28.5	1.75%
17	10.0	20.0	24.0	24.6	2.44%
18	10.0	22.5	20.7	21.4	3.27%
19	15.0	2.5	87.2	87.4	0.23%
20	15.0	5.0	75.5	75.7	0.26%
21	15.0	7.5	65.7	65.9	0.30%
22	15.0	10.0	57.1	57.4	0.52%
23	15.0	12.5	49.6	50.0	0.80%
24	15.0	15.0	43.2	43.6	0.92%
25	15.0	17.5	37.6	38.0	1.05%
26	15.0	20.0	32.8	33.3	1.50%
27	15.0	22.5	28.6	29.2	2.04%

Point	Coordinates		Temperature Value		differ-
No.	X.	Y	Numer.	Class.	ence %
28	20.0	2.5	88.1	88.3	0.22%
29	20.0	5.0	80.4	80.6	0.25%
30	20.0	7.5	73.2	73.4	0.27%
31	20.0	10.0	66.5	66.8	0.45%
32	20.0	12.5	60.5	60.9	0.66%
33	20.0	15.0	55.1	55.5	0.72%
34	20.0	17.5	50.3	50.8	0.98%
35	20.0	20.0	46.0	46.6	1.29%
36	20.0	22.5	42.3	43.0	1.63%
37	25.0	2.5	90.0	90.2	0.22%
38	25.0	5.0	82.5	82.7	0.24%
39	25.0	7.5	76.5	76.7	0.26%
40	25.0	10.0	70.8	71.1	0.42%
41	25.0	12.5	65.5	65.8	0.46%
42	25.0	15.0	60.7	61.1	0.65%
43	25.0	17.5	56.2	56.7	0.88%
44	25.0	20.0	52.2	52.7	0.95%
45	25.0	22.5	48.5	49.1	1.22%
46	30.0	2.5	91.6	91.8	0.22%
47	30.0	5.0	84.0	84.2	0.24%
48	30.0	7.5	77.6	77.8	0.26%
49	30.0	10.0	71.8	72.1	0.41%
50	30.0	12.5	66.9	67.2	0.45%
51	30.0	15.0	62.0	62.4	0.64%
52	30.0	17.5	57.8	58.2	0.69%
53	30.0	20.0	53.0	53.4	0.75%
54	30.0	22.5	50.1	50.6	1.00%

APPENDIX III

Description Of The Main Programs

1- Read the necessary data, such as geometrical characteristics, boundary conditions, external loads and characteristics of surface temperature.

2- Initialize the necessary vectors, matrices and required variables.

3- Calculate the initial values of modulus of the elasticity for concrete and steel materials at given room temperature.

4- Calculate the nodal coordinates of the structure and store in vectors X(I) and y(I).

5- Calculate the characteristics of structural stiffness matrix such as, matrix rank (MR), number of terms in band (NEB), number of complete band (NCB) and number of terms in bandwith (NEM), as shown in figure (9.1).

6- Calculate the nodal forces due to the material weight and substitute them in incremental displacement vector W(I).

7- Set up the structural stiffness matrix in a vector form H(I). The program is continued by the following steps to construct this vector.

7.1- Initialize the stiffness matrix, H(I) = 0.

7.2- Take an element and generate the nodal numbers of the element economically to obtain the smallest bandwith of the structural stiffness matrix, by calling the subroutine PIJK, then calculate the dimensions and area of the element.

7.3- Take a layer of the element and follow the following steps;

7.3.1- Substract 1 from the number of availabe layers if the layer has been collapsed or doubly cracked in the previous incremental loads or temperature, then take the next layer.

7.3.2- If it is the first incremental load go to step 7.3.4.

7.3.3- Calculate the total strains in principal directions of stresses and then calculate the values of modulus of elasticity in these directions by the stress-strain and temperature relationship, by calling the sub-routine EVALUE.

7.3.4- Calculate the elasticity matrix of the layer in principal direction and transform it into global co-ordinates by calling the subroutine DMATRX and then write the transformed elasticity matrix in TAPE 3.

7.3.5- Calculate the thickness of the layer. In SLAB program also calculate the distance of the middle surface of the layer from the middle surface of the element.

7.3.6- Calculate the upper triangular part of layer stiffness matrix and add to the previous layer stiffness matrix by calling the subroutine STIF. For SLAB program also call the subroutine NESS to complete the stiffness matrix of the layer and add to the previous layer stiffness matrix.

7.3.7- If the layer is not the last layer of the element go to step 7.3.

7.4- Complete the element stiffness matrix by equating the lower triangular part of the element stiffness matrix with the upper part.

7.5- Substitute the terms of the element stiffness matrix into the structural stiffness matrix in a vector form by calling the function JKW.

7.6- If the element is not the last element of the structure go to step 7.2.

8- Introduce the boundary conditions into the structural stiffness matrix, which may be one of the following form;

i- If a node is fixed in u-direction the corresponding stiffness value on the diagonal of the structural stiffness matrix is multiplied by a large number (10^{15}).

ii- If there is an initial displacement in u-direction at a node, the initial displacement is multiplied by the corresponding stiffness value and the resulting force is added to the force vector and also all corresponding terms of the stiffness matrix to the initial displacement are reduced to zero except the diagonal term which is substituted by unit.

9- If all layers have not been satisfied in the previous incremental load or temperature which was needed to update the stiffness matrix go to step 14.

10- If all external loads have been applied go to step 12.

11- Take the next incremental load which has been given in data, then go to step 14.

12- Take a new time value and the corresponding value of surface temperature which have been given in data.

13- Calculate if necessary the characteristics of surface temperature and follow the following steps, to calculate the temperature distribution and corresponding properties.

13.1- Take an element and calculate the area and dimensions of this element and generate the nodal numbers.

13.2- Take a layer of the element and if it has been collapsed or doubly cracked or, if it does not exist take the next layer.

13.2.1- Calculate the thickness of the layer (in the SLAB program also calculate the distance of the middle surface of the layer from the middle surface of the element) and calculate the coordinates of the centroid of the layer, (x, y, z).

13.2.2- Read the elasicity matrix from TAPE 3 which is available from step 7.3.4.

13.2.3- Evaluate the first term of temperature value of the centroid of the layer by calling the subroutine STEADY.

13.2.4- Calculate the diffusivity of the layer (DIF), corresponding to the previous value of the layer's temperature by calling the subroutine DIFU.

13.2.5- Calculate the second term of temperature value T_n^* by inserting the new value of diffusivity (DIF) by calling the subroutine TEMP and evaluate the new value of the layer's temperature by;

$$T_{i+1}^{j+1} = T_s - T_n^*$$

and store in vector $T_{i+1}(I)$.

13.2.6- If;

$$\left| T_{i+1}^{j+1} - T_{i+1}^{j} \right| > \lambda \cdot T_{i+1}^{j}$$

go to step 13.2.4, where λ is a small positive value given in data.

13.2.7- Calculate the incremental temperature of the layer by;

$$T_{i+1}(I) - T_i(I)$$

and store in vector TT(I).

13.2.8- Evaluate the coefficient of thermal expansion of the layer corresponding to the temperature of the layer by calling the subroutine COEF.

13.2.9- Calculate the incremental initial strain due to the incremental temperature by multiplying the coefficient of thermal expansion (CO) with the incremental temperature of the layer by the following statement;

TT(I) = CO×TT(I)

13.2.10- Calculate the nodal release forces due to the initial strain TT(I) in global coordinates, by calling the subroutine RELEAS.

13.2.11- Add the nodal released forces to the previous residual forces into the incremental displacement vector W(I).

13.2.12- If the layer is not the last layer of the element go to step 13.2.

13.3- If the element is not the last element of the structure go to step 13.1.

14- Call the subroutine SOLVE to find the incremental displacements. If the structural stiffness matrix is newly updated, this subroutine calculates the inverse of the stiffness matrix H(I) and stores in vector H(I), but if not the inverse of stiffness matrix is already available in vector H(I) from the previous iteration. Multiply the force vector W(I) by the inverse of the stiffness matrix yields the incremental displacements which are stored in vector W(I).

15- Calculate the total displacements of nodal points by adding the evaluated incremental nodal displacements to the previous values and store in vector WW(I).

16- Calculate the layers strains by the following operations;

16.1- Take an element and generate the nodal numbers.

16.2- Calculate the first term of the incremental strains of the element due to incremental displacements by calling the subroutine STRAIN. In the SLAB program these strains are the strains of the reference surface.

16.2.1- Take a layer of the element and if the layer has been collapsed or doubly cracked or does not exist.take the next layer.

16.2.2- In the case of the SLAB program, calculate the first terms of the layer's incremental strains by the Kirshhoff assumption.

16.2.3- Add the initial strains due to the incremental temperature to the layer's incremental strains to obtain the incremental strain values of the layer.

16.2.4- Read the elasticity matrix of the layer from

TAPE 3 which is available from step 7.3.4.

16.2.5- Calculate the incremental stresses of the layer by multiplying the incremental strains by elasticity matrix.

16.2.6- Calculate the total strains and stresses in global coordinates by adding the incremental values to the previous corresponding values.

16.2.7- If the layer is not the last layer of the element go to step 16.2.1.

16.3- If the element is not the last element of the structure go to step 16.1.

17- Initialize the incremental displacement vector, W(I) = 0.

18- To check the equilibrium of layers follow the following steps;

18.1- Take an element and calculate the dimensions of the element and generate the nodal numbers.

18.1.1- Take a layer of the element. If this layer does not exist or doubly cracked or collapsed take the next layer.

18.1.2- Calculate the angle of the principal direction of stresses by calling the subroutine ANGLE.

18.1.3- Transform the global strains to the principal directions of the stresses to find the corresponding strains and also ultimate stress(tensile strength of concrete or yield stress of steel), by calling the subroutine EVALUE.

18.1.4- Read the elasticity matrix of the layer from TAPE 3 which is available from step 7.3.4.

18.1.5- Calculate the actual principal stresses of the layer corresponding to principal strains of the analysis from stress-strain relationship explained in chapter three. Compare and check these stresses with the computer results and calculate the unbalanced stresses in principal directions by calling the subroutine ACTUAL. If the layer is a concrete material and developed tension in the major principal direction in excess of the ultimate tensile strength of concrete calculate the unbalanced stress in that direction and repeat the same statement for the second direction if the layer is doubly cracked. If it is a concrete layer, and developed compressive stress in the minor principal direction, or the layer is steel and developed tensile principal stress in excess of ultimate or yield stress calculate the unbalanced stresses, i.e, the difference of the computer results and the ultimate values.

18.1.6- Transform the unbalanced stresses into global coordinates by calling subroutine UNSTRS.

18.1.7- Calculate the nodal forces by calling the subroutine UNFORC. These nodal forces are calculated due to the unbalanced stresses in global coordinates.

18.1.8- Check if the layer's stresses are satisfied by statements explained in section (9.3) of chapter nine.

18.1.9- If the layer is not the last layer of the element go to step 18.1.1.

18.2- Substitute the nodal released forces into the incremental nodal displacement vector W(I) by calling the subroutine RELEAS.

18.3- If the element is not the last element of the structure go to step 18.1.

19- If all layers have been satisfied in both principal directions go to step 22.

20- If number of iterations is less than the given number go to step 14.

21- Go to step 7 to update the stiffness matrix of the structure.

22- If there are new cracked or collapsed layers go to step 24.

23- Write all required results. Calculate the positions of neutral axes of the elements (in SLAB program only) if the structure is under the temperature increments, and write as an output. If the applied load is equal with the given load and the time value is equal with the maximum value of the time which is given in data, STOP, if not go to step 10 to apply the next incremental load or temperature.

24- Check the stresses of the collapsed or cracked layers to find the first (n) cracked or collapsed layers, whose stresses are larger than the others and label these layers as the cracked or crushed layers.

25- Check the stresses of cracked or crushed layers and release the unbalanced forces as explained above.